OCS Study
BOEM 2013-222

IMPROVING THE PREDICTIVE CAPABILITY OF 3-D SEISMIC SURFACE AMPLITUDE DATA FOR IDENTIFYING CHEMOSYNTHETIC COMMUNITIES

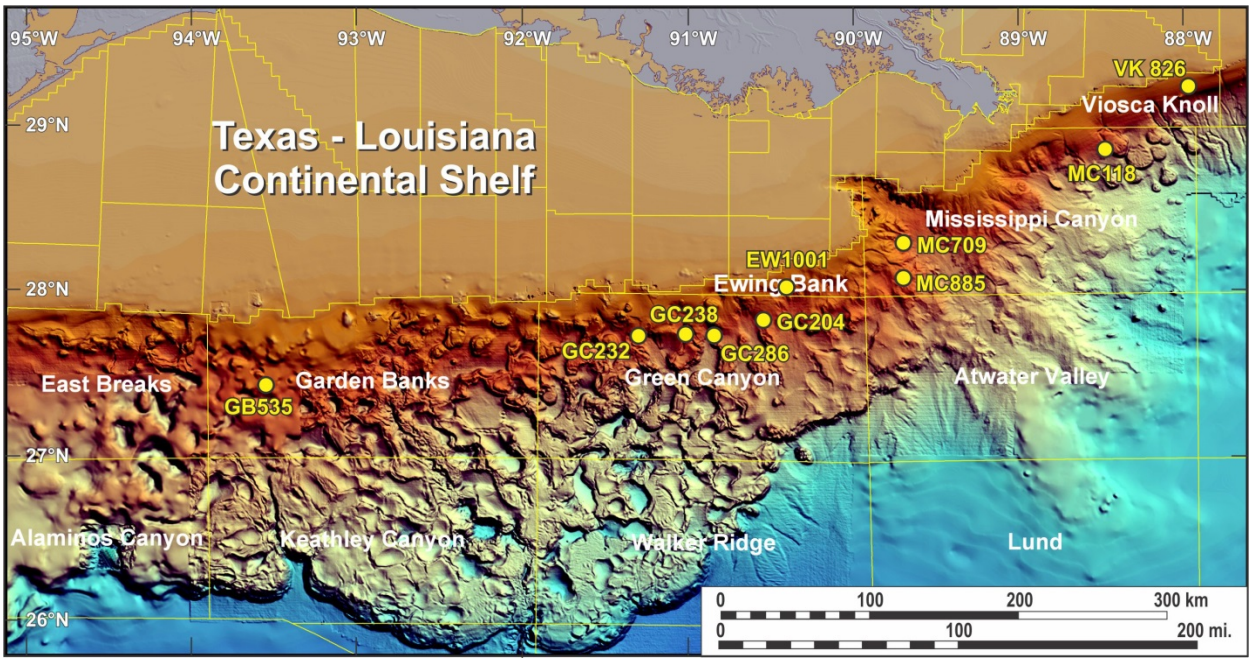

US Department of the Interior
Bureau of Ocean Energy Management
Gulf of Mexico Region
December 2013

OCS Study
BOEM 2013-222

IMPROVING THE PREDICTIVE CAPABILITY OF 3-D SEISMIC SURFACE AMPLITUDE DATA FOR IDENTIFYING CHEMOSYNTHETIC COMMUNITIES

Author

Harry H. Roberts

Prepared under BOEM Cooperative Agreement
14-01-99-CA-30951-17801
by
Louisiana State University
Coastal Studies Institute
School of the Coast and Environment
Baton Rouge, LA 70803

US Department of the Interior
Bureau of Ocean Energy Management
Gulf of Mexico Region
December 2013

DISCLAIMER

Study collaboration and funding were provided by the US Department of the Interior, Bureau of Ocean Energy Management, Environmental Studies Program, Washington, DC, under Agreement Number 14-01-99-CA-30951-17801. This report has been technically reviewed by BOEM and it has been approved for publication. The views and conclusions contained in this document are those of the authors and should not be interpreted as representing the opinions or policies of the US Government, nor does mention of trade names or commercial products constitute endorsement or recommendation for use.

REPORT AVAILABILITY

To download a PDF file of this Gulf of Mexico OCS Region report, go to the US Department of the Interior, Bureau of Ocean Energy Management, Environmental Studies Program Information System website and search on OCS Study BOEM 2013-222.

This report can be viewed at select Federal Depository Libraries. It can also be obtained from the National Technical Information Service; the contact information is below.

US Department of Commerce
National Technical Information Service
5301 Shawnee Rd.
Springfield, VA 22312
Phone: (703) 605-6000, 1(800)553-6847
Fax: (703) 605-6900
Website: http://www.ntis.gov/

CITATION

Roberts, H.H. 2013. Improving the Predictive Capability of 3-D Seismic Surface Amplitude Data For Identifying Chemosynthetic Communities. US Dept. of the Interior, Bureau of Ocean Energy Management, Gulf of Mexico Region, New Orleans, LA. OCS Study BOEM 2013-222. 190 pp.

PREFACE

This research project, entitled "Improving the Predictive Capability of 3-D Seismic Surface Amplitude Data For Identifying Chemosynthetic Communities", was undertaken to provide a scientific basis for making better interpretations of sea floor geology and biology from remotely sensed data. The following report is a summary of research sponsored by the U.S. Department of Interior Minerals Management Service, Gulf of Mexico Region OCS through the Coastal Marine Institute at Louisiana State University (Cooperative Agreement No. 1435-01-99-CA-30951, Task Order No. 17801).

The Bureau of Ocean Energy Management (BOEM), formerly the Minerals Management Service (MMS), is tasked not only with leasing and assessing risks in the hydrocarbon-rich deepwater slope environment of the northern Gulf of Mexico, but also with protecting sensitive benthic communities (particularly chemosynthetic communities) from the impacts of operational activities. In order to carry out this regulatory function, BOEM personnel must know where these communities are located. However, the confident prediction of chemosynthetic sites from seismic data alone has been an allusive goal. Their existence is usually confirmed by direct observations using submersibles, ROVs, or bottom cameras, all of which are expensive and time-consuming. Data collected over the last decade from studies using manned submersibles suggest that these unusual communities are direct products of their geologic setting. Although they have been associated with acoustic wipe-out zones on seismic profiles, we now realize that there are exceptions to this association. Manned submersible observations indicate that wide-spread chemosynthetic communities appear to be closely linked to surface or near-surface gas hydrates. Gas hydrates apparently contain the unique requirements to sustain chemosynthetic communities over long periods of time. In the Gulf, we know through repeated observations and studying, the subsurface geology of gas hydrate sites, that faults are common conduits for bringing gas, crude oil, and formation water to the slope surface or shallow subsurface. Learning to recognize the combination of features that characterize a chemosynthetic community site on a slope-wide remotely sensed data base, like 3-D seismic data, can certainly be of enormous value to BOEM as a predictive tool.

This project was designed both to improve the predictive use of 3-D seismic surface reflectivity or amplitude data and directly expose critical BOEM decision makers to the variabilities of sea floor geology and biology represented in amplitude data of varying intensity. The study was conducted as both a field and laboratory investigation. The field data consisted of video and 35 mm photographic surveys, core samples, grab samples of sediment and elements of biological communities, samples of lithified substrates, gas samples, and gas hydrate samples. In all but one site discussed in this report, the field observation and sampling program was carried out using Harbor Branch Oceanographic Institute's manned submersible, the Johnson Sea-Link. Laboratory work consisted of analyzing 3-D seismic data with BOEM geoscientists for dive site selection and later seismic-ground truth calibrations. Other laboratory work related to processing and analyzing samples collected from selected sites. The end result of these activities is a much better understanding of sea floor characteristics as reflected in remotely sensed 3-D seismic surface amplitude and profile data. The report is accompanied by appendices of detailed dive logs.

ACKNOWLEDGMENTS

This research would not have been possible without the scientific foundation created from the long history of previous northern Gulf of Mexico studies of hydrocarbon seep communities that started in the mid-1980s. Several previous studies by the PI also provided valuable input to the use of 3-D seismic data for the confident interpretation of sites likely to support chemosynthetic communities. The BOEM (MMS)-sponsored study related to the use of high resolution acoustic data for sea floor interpretation helped frame the questions addressed in the study outlined in this report. This study was funded through the Coastal Marine Institute at Louisiana State University (Contract Number 14-35-0001-30660). Extremely valuable direct observations and samples used to relate real-world bottom characteristics to remotely sensed acoustic data were funded in a number of projects by the NOAA National Underseas Research Center, University of North Carolina at Wilmington, NC (Contracts Numbers NA 80AA-8-00081, NA88AA-D-UR004, and NA 36 RU0060). The crew members of the Johnson Sea-Link and support ships, Harbor Branch Oceanographic Institution, are gratefully acknowledged for their professionalism in helping us collect the observations and other data sets related to understanding the northern Gulf of Mexico's hydrocarbon seep environments. We are also indebted to the Louisiana State University, Coastal Studies Institute Field Support Group for their help with preparation for field projects, sampling, and other field-related activities. Mike Kaluza of Geoscience, Earth, and Marine Sciences, Inc. of Houston, Texas is acknowledge for providing the multibeam image of the continental slope with lease blocks superimposed on it, which we used throughout this report. Mr. Bill Shedd of the BOEM is gratefully acknowledged for his constant help throughout the project regarding accessing the 3-D seismic database and creating products used to identify and collect ground truth data from numerous surface amplitude anomalies from the northern Gulf's continental slope. Stephan Palmes of the New Orleans BOEM office is acknowledged for his help with interpreting the structural complexities of each case presented in this report. This project would not have been possible without access to the vast 3-D seismic database archived by BOEM in their New Orleans office. Sincere thanks to to Western Geco for their permission to use the examples presented in this report.

TABLE OF CONTENTS

PAGE

PREFACE i

ACKNOWLEDGMENTS ii

TABLE OF CONTENTS iii

LIST OF FIGURES vi

LIST OF TABLES xi

1.0 INTRODUCTION AND PROJECT RATIONALE 1

2.0 A COMPLEX SALT-SEDIMENT FRAMEWORK FOR THE CONTINENTAL SLOPE 3

3.0 STRUCTURAL SETTING: UPPER CONTINENTAL SLOPE 5

3.1 Extensional Faults 6
3.1.1 Peripheral Faults 6
3.1.2 Crestal Faults 6
3.1.3 Keystone Faults 8
3.1.4 Roller Faults 8
3.1.5 Ramp Faults 8
3.1.6 Shale-Detachment Faults 8
3.1.7 Asymmetric Counterregional Faults 8
3.1.8 Flap Faults 8
3.1.9 Rollover Faults 8
3.2 Contractual Faults 9
3.2.1 Toe-Thrust Faults 9
3.2.2 Break-Thrust Faults 9
3.3 Strike-Slip Faults 9
3.4 Salt Welds 9

4.0 GEOLOGIC EXPRESSION OF FLUID AND GAS EXPULSION SITES 10

4.1 Background for our Present Understanding 10
4.2 Distribution of Hydrocarbon Seepage and Venting Sites 11
4.3 Sea Floor Responses to the Expulsion Process 13
4.3.1 Mud-Prone Rapid Delivery response 14
4.3.2 Mineral-Prone Slow Delivery Response 16
4.3.3. Intermediate Delivery Response 17

5.0 TECHNOLOGY DEVELOPMENT: A CRITICAL STEP IN UNDERSTANDING GULF GEOLOGY 21

6.0 DATA SETS AND METHODOLOGY 24

6.1 Introduction 24
6.2 Available Data Sets 25
6.3 Methodology 25

7.0 CASE INVESTIGATIONS 26

7.1 Garden Banks 535 (GB 535) 27
7.1.1 Location and Geologic Setting 27
7.1.2 Sea Floor Amplitudes and Surface Geology 28
7.1.3 Interpretation of 3-D Seismic Sea Floor Amplitudes Using "Ground Truth" Data 28
7.1.4 Summary 29

7.2 Green Canyon 232 (GC 232) 35
7.2.1 Location and Geologic Setting 35
7.2.2 Sea Floor Amplitudes and Surface Geology 35
7.2.3 Interpretation of 3-D Seismic Sea Floor Amplitudes Using "Ground Truth" Data 35
7.2.4 Summary 36

7.3 Green Canyon 238 (GC 238) 42
7.3.1 Location and Geologic Setting 42
7.3.2 Sea Floor Amplitudes and Surface Geology 42
7.3.3 Interpretation of 3-D Seismic Sea Floor Amplitudes Using "Ground Truth" Data 42
7.3.4 Summary 43

7.4 Green Canyon 286 (GC 286) 50
7.4.1 Location and Geologic Setting 50
7.4.2 Sea Floor Amplitudes and Surface Geology 50
7.4.3 Interpretation of 3-D Seismic Sea Floor Amplitudes Using "Ground Truth" Data 51
7.4.4 Summary 52

7.5 Green Canyon 204 (GC 204) 59
7.5.1 Location and Geologic Setting 59
7.5.2 Sea Floor Amplitudes and Surface Geology 59
7.5.3 Interpretation of 3-D Seismic Sea Floor Amplitudes Using "Ground Truth" Data 60
7.5.4 Summary 61

7.6 Ewing Bank 1001 (EW 1001) 68
7.6.1 Location and Geologic Setting.....68
7.6.2 Sea Floor Amplitudes and Surface Geology.....68
7.6.3 Interpretation of 3-D Seismic Sea Floor Amplitudes Using "Ground Truth" Data 68
7.6.4 Summary.....70

7.7 Mississippi Canyon 885 (MC 885) 77
7.7.1 Location and Geologic Setting.....77
7.7.2 Sea Floor Amplitudes and Surface Geology.....77
7.7.3 Interpretation of 3-D Seismic Sea Floor Amplitudes Using "Ground Truth" Data 78
7.7.4 Summary.....80

7.8 Mississippi Canyon 709 (MC 709) 87
7.8.1 Location and Geologic Setting.....87
7.8.2 Sea Floor Amplitudes and Surface Geology.....87
7.8.3 Interpretation of 3-D Seismic Sea Floor Amplitudes Using "Ground Truth" Data 88
7.8.4 Summary.....88

7.9 Mississippi Canyon 118 (MC 118) 95
7.9.1 Location and Geologic Setting.....95
7.9.2 Sea Floor Amplitudes and Surface Geology.....95
7.9.3 Interpretation of 3-D Seismic Sea Floor Amplitudes Using "Ground Truth" Data 96
7.9.4 Summary.....97

7.10 Vioska Knoll 826 (VK 826) 104
7.10.1 Location and Geologic Setting.....104
7.10.2 Sea Floor Amplitudes and Surface Geology.....104
7.10.3 Interpretation of 3-D Seismic Sea Floor Amplitudes Using "Ground Truth" Data 105
7.10.4 Summary.....106

8.0 SUMMARY AND CONCLUSIONS 113

9.0 REFERENCES.....118

10.0 APPENDIX A Dive Log Summary 2000 125

11.0 APPENDIX B Dive Log Summary 2002 141

LIST OF FIGURES

PAGE

Figure 1. Map of 3-D seismic coverage of the northern Gulf of Mexico continental slope ····· 3

Figure 2. The geologic cross section across the central part of the northern Gulf of Mexico by Peel et al. (1995) ····· 4

Figure 3. Shaded relief image of the northern Gulf's continental slope as constructed from multibeam bathymetry data ····· 5

Figure 4. Block diagrams illustrating the structural complexity N-S across the continental shelf and slope (Rowan et al., 1999) ····· 7

Figure 5. A diagram that illustrates the relationship between (a) surface amplitude anomalies derived from 3-D seismic data collected in the Mississippi Canyon lease blocks and (b) subsurface relationships between intraslope basin sediments, salt, fluid-gas migration pathways, and sea floor mound in MC 929 ····· 12

Figure 6. A summary of relationships between flux rate of fluids-gases to the sea floor and general geologic-biologic responses (modified from Roberts, 2001b) ····· 14

Figure 7. Mud volcano from GC 143 ····· 15

Figure 8. This 3-D seismic (a) surface amplitude map and (b) profile across the Green Canyon Block 140 dome display high positive acoustic amplitudes from the sea floor ····· 18

Figure 9. A sea floor exposure of gas hydrate and associated chemosynthetic community ····· 20

Figure 10. The side-scan sonar mosaic illustrates the high level of sea floor variability in seep-related areas ····· 21

Figure 11. Shaded relief maps of the northern Gulf of Mexico continental slope showing the location of GB 535 ····· 30

Figure 12. Combined bathymetric and 3-D seismic surface amplitude map of GB 535 and surrounding area ····· 31

Figure 13. A seismic profile across the GB 535 area of interest. Location of the profile is shown on Figure 12 ····· 31

Figure 14. Combined bathymetric and 3-D seismic surface amplitude map of GB 535. The red line illustrates a Johnson Sea-Link submersible transect along which "ground truth" observations and samples were collected ····· 32

Figure 15. Photographs of the seabed along the submersible transect illustrated in Figure 14 ····· 33

Figure 16. Shaded relief maps of the northern Gulf of Mexico continental slope showing the location of GB 232 ····· 37

Figure 17. Combined bathymetric and 3-D seismic surface amplitude map of GB 232 and surrounding area ····· 38

Figure 18. A seismic profile across the GB 232 area of interest. Location of the profile is shown on Figure 17 ····· 38

Figure 19. Combined bathymetric and 3-D seismic surface amplitude map of GB 232. The red line illustrates a Johnson Sea-Link submersible transect along which "ground truth" observations and samples were collected ····· 39

Figure 20. Photographs of the seabed along the submersible transect illustrated in Figure 19 ····· 40

Figure 21. Shaded relief maps of the northern Gulf of Mexico continental slope showing the location of GB 238 ····· 45

Figure 22. Combined bathymetric and 3-D seismic surface amplitude map of GB 238 and surrounding area ····· 46

Figure 23. A seismic profile across the GB 238 area of interest. Location of the profile is shown on Figure 22 ····· 46

Figure 24. Combined bathymetric and 3-D seismic surface amplitude map of GB 238. The red line illustrates a Johnson Sea-Link submersible transect along which "ground truth" observations and samples were collected ····· 47

Figure 25. Photographs of the seabed along the submersible transect illustrated in Figure 24 ····· 48

Figure 26. Shaded relief maps of the northern Gulf of Mexico continental slope showing the location of GB 286 ····· 53

Figure 27. Combined bathymetric and 3-D seismic surface amplitude map of

GB 286 and surrounding area·····54

Figure 28. Two seismic profiles across the GB 286 area of interest. Locations of the profiles are shown on Figure 27·····55

Figure 29. Combined bathymetric and 3-D seismic surface amplitude map of GB 286. The red lines illustrates a Johnson Sea-Link submersible transect along which "ground truth" observations and samples were collected·····56

Figure 30. Photographs of the seabed along the submersible transect illustrated in Figure 29·····57

Figure 31. Shaded relief maps of the northern Gulf of Mexico continental slope showing the location of GB 204·····62

Figure 32. Combined bathymetric and 3-D seismic surface amplitude map of GB 204 and surrounding area·····63

Figure 33. Two seismic profiles across the GB 204 area of interest. Locations of the profiles are shown on Figure 32·····64

Figure 34. Combined bathymetric and 3-D seismic surface amplitude map of GB 204. The red lines illustrates a Johnson Sea-Link submersible transect along which "ground truth" observations and samples were collected·····65

Figure 35. Photographs of the seabed along the submersible transect illustrated in Figure 34·····66

Figure 36. Shaded relief maps of the northern Gulf of Mexico continental slope showing the location of EW 1001·····71

Figure 37. Combined bathymetric and 3-D seismic surface amplitude map of EW 1001 and surrounding area·····72

Figure 38. Two seismic profiles across the EW 1001 area of interest. Locations of the profiles are shown on Figure 37·····73

Figure 39. Combined bathymetric and 3-D seismic surface amplitude map of EW 1001. The red lines illustrates a Johnson Sea-Link submersible transect along which "ground truth" observations and samples were collected·····74

Figure 40. Photographs of the seabed along the submersible transect illustrated in Figure 39·····75

Figure 41. Shaded relief maps of the northern Gulf of Mexico continental slope

showing the location of MC 885 81

Figure 42. Combined bathymetric and 3-D seismic surface amplitude map of MC 885 and surrounding area 82

Figure 43. Three seismic profiles across the MC 885 area of interest. Locations of the profiles are shown on Figure 42 83

Figure 44. Combined bathymetric and 3-D seismic surface amplitude map of MC 885. The red lines illustrates a Johnson Sea-Link submersible transect along which "ground truth" observations and samples were collected 84

Figure 45. Photographs of the seabed along the submersible transect illustrated in Figure 44 85

Figure 46. Shaded relief maps of the northern Gulf of Mexico continental slope showing the location of MC 709 90

Figure 47. Combined bathymetric and 3-D seismic surface amplitude map of MC 709 and surrounding area 91

Figure 48. A seismic profile across the MC 709 area of interest. Location of the profile is shown on Figure 47 91

Figure 49. Combined bathymetric and 3-D seismic surface amplitude map of MC 709. The red line illustrates a Johnson Sea-Link submersible transect along which "ground truth" observations and samples were collected 92

Figure 50. Photographs of the seabed along the submersible transect illustrated in Figure 49 93

Figure 51. Shaded relief maps of the northern Gulf of Mexico continental slope showing the location of MC 118 98

Figure 52. Combined bathymetric and 3-D seismic surface amplitude map of MC 118 and surrounding area 99

Figure 53. Two seismic profiles across the MC 118 area of interest. Locations of the profiles are shown on Figure 52 100

Figure 54. Combined bathymetric and 3-D seismic surface amplitude map of MC 118. The red lines illustrates a Johnson Sea-Link submersible transect along which "ground truth" observations and samples were collected 101

Figure 55. Photographs of the seabed along the submersible transect illustrated

in Figure 54 102

Figure 56. Shaded relief maps of the northern Gulf of Mexico continental slope showing the location of VK 826 107

Figure 57. Combined bathymetric and 3-D seismic surface amplitude map of VK 826 and surrounding area 108

Figure 58. Two seismic profiles across the VK 826 area of interest. Locations of the profiles are shown on Figure 57 109

Figure 59. Combined bathymetric and 3-D seismic surface amplitude map of VK 826. The red lines illustrates a Johnson Sea-Link submersible transect along which "ground truth" observations and samples were collected 110

Figure 60. Photographs of the seabed along the submersible transect illustrated in Figure 59 111

LIST OF TABLES

Table 1. Summary of Hydrocarbon Concentrations in Core Samples (MC 885) ·····79

Table 2. Structural Summary·····114

Table 3. Summary of Acoustic Amplitude Response and Sea Floor Characteristics·····116

I. INTRODUCTION AND PROJECT RATIONALE

Within the BOEM divisions that use geological data for the purposes of resource evaluations, leasing, geohazards assessments, and protection of sensitive biological communities there is a significant need to optimize the use of high quality 3-D seismic data for improving interpretations of the modern sea floor. Exploration has pushed oil and gas activity to the deepest parts of the continental slope and onto the adjacent deep basin floor where acquisition of traditional high resolution acoustic data sets previously used for sea floor evaluations are costly and sometimes very difficult to collect. Because of this situation and the vastness of the northern and northwestern Gulf of Mexico continental slope province, more and more reliance is being placed on 3-D seismic data to provide accurate and insightful appraisals of the sea floor and shallow subsurface. In addition to important geohazards evaluations, 3-D seismic data are being relied upon more frequently by BOEM for regulatory purposes regarding the protection of sensitive benthic communities such as deep water corals and, most importantly, to this study, hydrocarbon seep-related chemosynthetic communities. To date, over 190 large 3-D seismic survey datasets image most of the Louisiana-Texas continental slope. The data are currently being evaluated by BOEM personnel in an effort to produce more useful interpretation of the slope's modern sea floor and the hydrocarbon-productive subsurface beneath it. A primary driving force for analysis of the sea floor is to identify areas where hydrocarbons are seeping or being vented into surficial sediments. These areas may provide the basic trophic resources for densely populated and lawfully protected chemosynthetic communities. Knowledge of the existence of these communities started with their appearance in dredge samples associated with regional biological and geochemical sampling (Kennicutt et al. 1985). Over a couple of decades of direct observation and sampling of these communities, using a variety of manned submersibles has been supported by a variety of both applied and basic science projects (MacDonald et al. 1995, 2002; Roberts, 2001a). Although these in situ and direct observational studies have produced a new and more detailed appraisal of the effects of natural hydrocarbon seepage on the geology of the modern sea floor and resulting biological responses, studies have been largely site-specific. The identification of reliable criteria for prediction of sea floor conditions from regional remotely sensed data, particularly 3-D seismic data, has been largely missing. Use of 3-D seismic data as a means of predicting sea floor geology and associated biology has become a need for government regulatory agencies as well as industry as leasing has progressed into deeper and deeper water.

A very promising approach for utilizing regional 3-D seismic data for enhanced predictability of the sea floor and shallow subsurface is application of surface reflectivity or surface amplitude mapping. This process involves mapping the reflection strength associated with a narrow window of data centered on the sea floor. An interval of about 10 ms is commonly used. This technique is valuable for quickly mapping large areas of sea floor and identifying those local zones which differ in reflection strength from ambient conditions. However, a variety of conditions can account for reflectivity or amplitude that deviates from the "norm." These conditions range from hard bottoms associated with rock outcrops, (mineralized mounds, hardgrounds, other cemented bottom types, as well as, surface-to-shallow subsurface gas hydrate) to very soft bottoms that are charged with gas (biogenic, thermogenic, or a combination of the two). The hard bottom areas constitute a medium through which acoustic energy travels slightly faster than the surrounding sea floor while gas-charged sediment have just

the opposite response of slower velocities. Therefore, the identification of these slightly different velocities of seismic energy moving through the surface sediment can help discriminate hard and soft bottoms. This classification can be accomplished through phase analysis, phase being a product of velocity of the acoustic energy and density of the medium. Results of this analysis which identifies a polarity shift in the data can help distinguish one end-member bottom type from another. These techniques have previously been used to help interpret site-specific sea floor conditions and features, particularly those that are associated with hydrocarbon seepage or more rapid venting of fluids and gases to the modern sea floor (Roberts et al., 1992a, Roberts, 2001a). Amplitude mapping has also been employed successfully in a broader range of geohazards assessments (Hill 1996). However, for the project described in this report, the emphasis is placed on improving the use of 3-D seismic data, particularly surface amplitude or reflectivity data, for predicting sea floor geology and biology, that can be used in the regulatory framework. The project specifically focuses on developing links between surface reflectivity data and areas that support chemosynthetic communities. Accomplishing this overall project objective is a non-trivial task even though numerous surface amplitude anomalies have been identified from the enormous continental slope 3-D seismic database by BOEM personnel (Figure 1). This project contributes to field verification of 3-D seismic surface reflectivity signatures. This step is absolutely crucial to developing reliable predictors of sea floor characteristics from remotely sensed data. Because of the high degree of geologic complexity of the northern Gulf of Mexico continental slope, understanding the range of sea floor geologic/biologic features and areas that give rise to 3-D seismic amplitude anomalies is a challenging task that has required a determined effort on the part of both academic and BOEM personnel associated with this project. The hypothesis that was tested by this project can be stated as follows:

Approach – Analysis of 3-D seismic surface reflectivity or amplitude data coupled with direct field verification data in a matrix of known geologic configurations will lead to the development of a scheme for predicting the sites of various hydrocarbon seep-vent features and particularly the probable sites for occurrence of chemosynthetic communities. The presence or absence of chemosynthetic communities is directly dependent on delivery of hydrocarbons to the sea floor. This delivery system is a product of the continental slope's geologic framework. Therefore, understanding the geology of hydrocarbon seep-venting sites is viewed in this study as fundamental to being able to predict general biologic response.

The following five sections of this report set the stage for interpreting datasets and results of the case histories for individual sites for fluid-gas expulsion that were analyzed remotely using 3-D seismic data and then verified with direct observation sampling using manned submersibles. These five sections provide geologic framework summary information on the sash-sediment relationships that create a unique structural framework that promotes fluid and gas expulsion and associated seafloor responses. In addition, the evolution of technology advances that currently allow us to interpret seafloor geology with a high degree of confidence as well as the methodologies directly applied to this project are also discussed.

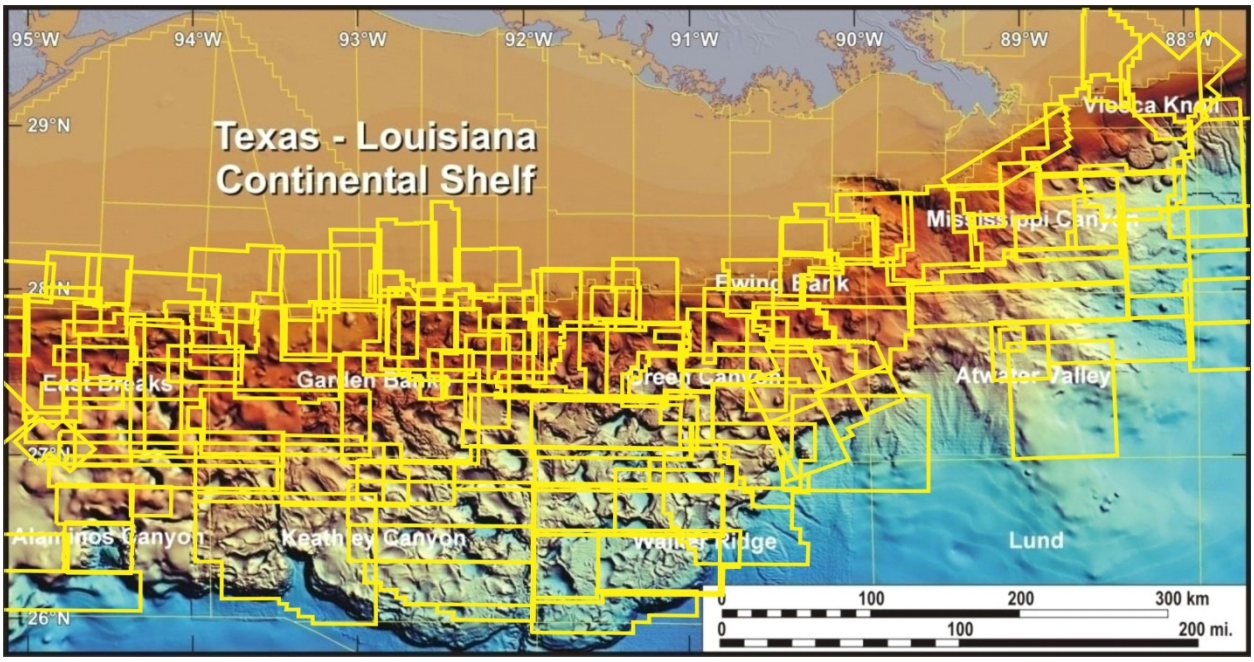

Figure 1. This map illustrates the 3-D seismic coverage of the northern Gulf of Mexico continental slope. Some areas have several generations of seismic data. These data are held by the Bureau of Ocean Energy Management (BOEM) formerly Minerals Management Service for leasing and other regulatory purposes.

2.0 A COMPLEX SALT-SEDIMENT FRAMEWORK FOR THE CONTINENTAL SLOPE

Coincident with the advances in seismic technology, the shift from analog-to-digital data acquisition, and rapid evolution of computing power and software development our view of the subsurface and its salt-sediment relationships have dramatically changed. Prior to the mid-1980s, it was generally believed by geologists and geophysicists that the northern Gulf of Mexico Basin was dominated by deeply rooted salt stocks and massifs with associated growth faults (Buffler and Sawyer, 1985). This concept has now been replaced by a geologic framework that incorporates more horizontally mobile salt sheets and canopies. Diegel et al. (1995), Rowan (1995), and McBride et al. (1998a) have published summaries of this next quantum jump in our understanding of the slope's structure and salt-sediment relationships. Figure 2, constructed by Peel et al. (1995), is a highly summarized dip-oriented profile across the northern Gulf's shelf and continental slope illustrating sediment thicknesses and simplified salt geometries typical of onshore Louisiana to the deep Gulf floor. The improved understanding of salt-sediment relationships has developed from better acoustic imaging of allochthonous salt, particularly through development and constant improvement of 3-D seismic data, new data processing software, and the use of quantitative palinspastic reconstructions (Rowan 1994; McBride 1998; McBride et al. 1998b).

Historically, the realization that the Sigsbee Escarpment was a product of Jurassic salt being thrust over much younger sediments (DeJong 1968; Amery 1969) triggered research

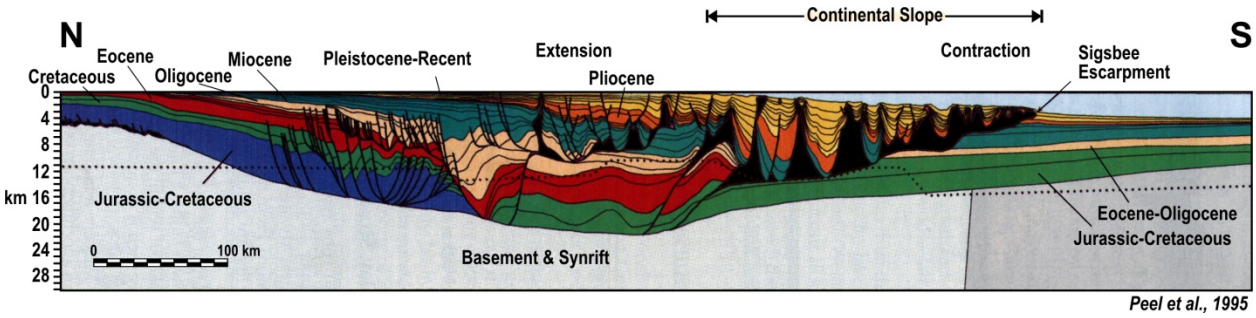

Figure 2. The geologic cross section across the central part of the northern Gulf of Mexico by Peel et al. (1995) illustrates the relationships of sediment and salt (black) from onshore Louisiana to beyond the Sigsbee Escarpment. The thick sedimentary sequences, various salt geometries, and numerous faults make this hydrocarbon-prone geologic framework ideal for fluid-gas migration and trapping.

leading to our present appreciation of the mobility of allochthonous salt and the impact of salt on the geologic complexity of the continental slope. Humphries (1978) also made the observation that salt thrusting at the toe of the slope was a product of sedimentary loading updip. By the late 1980s, industry geoscientists, with the aid of 3-D seismic, were clearly imaging allochthonous salt sheets and canopies where salt stocks were interpreted from earlier generation 2D-seismic profiles. A review of the Cenozoic evolution of the northern Gulf of Mexico Basin by Worrall and Snelson (1989) emphasized the basinward movement of salt and growth faulting as sediments were applied updip. By the early 1990s researchers, primarily from the oil and gas industry, were recognizing linked sediment, salt, and structural systems, and that minibasins on the continental slope were the results of evacuation of allochthonous salt (Sumner et al. 1990). Talbot (1993) and Vandeville and Jackson (1993) showed that variations in the rate of sediment application affect the deformation of salt bodies, which in turn exerts a strong control on the locations and orientations of minibasins and associated faults. The research also prompted a new understanding of the northern Gulf of Mexico's sea floor and its geomorphic characteristics. High quality multibeam bathymetry of the slope clearly identified salt-related features from intraslope sedimentary basins (Figure 3). Since the mid-1990s, there has been a wealth of scientific papers, special publications, and sessions at professional meetings that focused both industry and academic research on the rapidly evolving understanding of allochthonous salt systems (Vendeville and Jackson 1992; Weimer et al. 1994; Rowan 1994; Rowan 1995; Peel et al. 1995; Schuster 1995; Diegel et al. 1995; Travis et al. 1995; McBride 1998; McBride et al. 1998a; Rowan and Weimer 1998; Rowan et al. 1999; Post et al. 2004, and many more). This body of information has provided the framework for the much improved understanding that petroleum systems, for any given region of the northern Gulf's continental slope, are directly affected by the evolution of allochthonous salt. Both oil generation and migration are critically tied to overlying sediments and the time-dependent changes in the geometries of salt bodies. The impermeable nature of salt prevents vertical migration in given areas. Therefore, hydrocarbon migration may be deflected laterally updip at the base of salt. The edges of salt bodies and their associated faults commonly function to focus migration to the modern sea floor. Rowan et al. (1999) summarized salt-related fault families that potentially function as conduits along which fluids and gases may be transported to the modern sea floor.

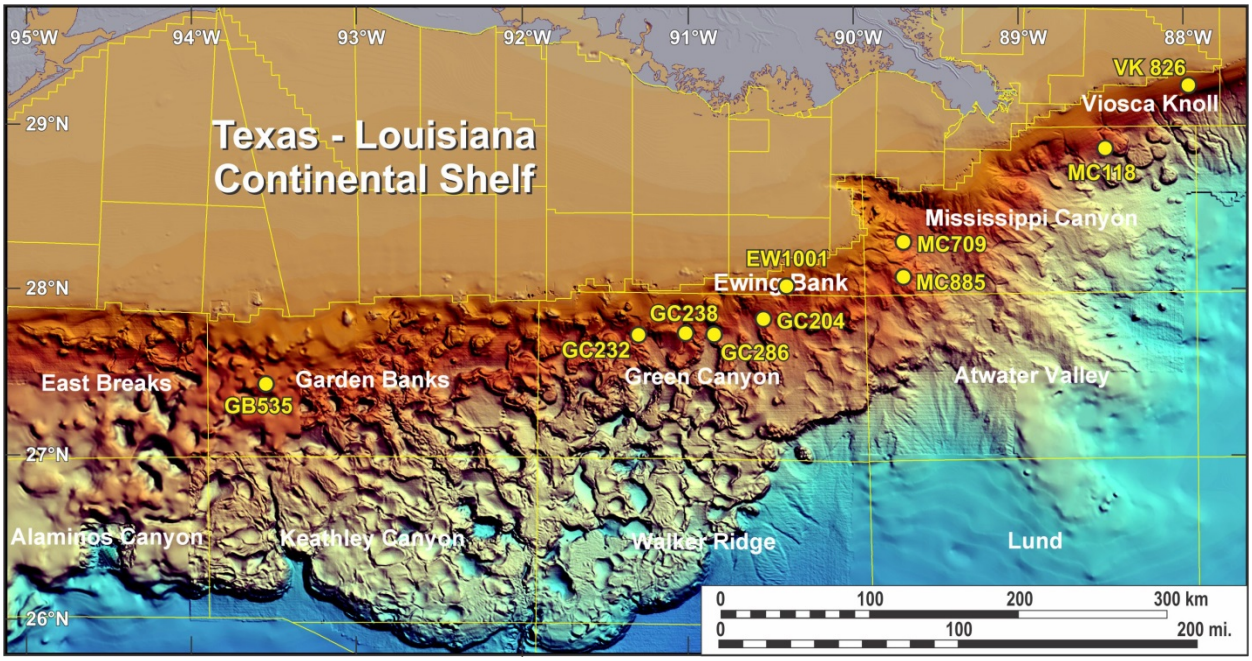

Figure 3. This shaded relief image of the northern Gulf's continental slope was constructed from multibeam bathymetry data. The complex sea floor morphology reflects an even more complex subsurface relationship between sediment and salt bodies. Sub rounded smooth areas represent intraslope basins while the rough and higher relief basin margins and generally supported by salt in the shallow subsurface. These margins are the locations of numerous faults that function as migration pathways for fluids and gas to the modern sea floor. The ten 3-D seismic sea floor amplitude areas discussed in this report are identified by oil and gas lease area and block numbers.

3.0 STRUCTURAL SETTING: UPPER CONTINENTAL SLOPE

Seismic data from the northern Gulf of Mexico indicate that faults, which function as migration pathways for hydrocarbons, are numerous and of various types. It is generally accepted by prominent geoscientists who study the region (Diegel et al. 1995; McBride et al. 1998b; Peel et al. 1995; Rowan et al. 1999; and others) that most faults are related to deformation of the Jurassic Louann Salt. Although extensional faulting is common to the upper slope, strike-slip and contractional faults can occur. Studies conducted before the widespread acquisition of 3-D seismic data in deep water indicate that the slopes structural framework is a product of gravity driven salt deformation as a massive sedimentary overburden thickness, spreads seaward, and slides basinward on salt detachments (Jackson and Galloway 1984; Worrall and Snelson 1989; Wu et. al. 1990). The sedimentary sections below the continental shelf extending to the mid-slope are generally characterized by extension, while contraction usually occurs at the base of the slope. However, linked gravitational systems occur on many scales and extension is characteristic of the landward and middle parts of these linked systems, while contraction occurs near the basinward limits and strike-slip deformation may connect the two. Where contraction does not occur toward the basinward limits, downslope movement is reconciled by salt extrusion, (Jackson and Cramez 1989; Worrall and Snelson 1989).

Recently, Rowan et al. (1999) have classified salt-related faults and fault welds based on the 3-D geometry of the faults on welds, deformed strata, and associated salt. They define six types of extensional faults (peripheral faults, crestal faults, keystone faults, roller faults, ramp faults, and shale detachment faults), along with counterregional faults, and contractional faults, Figure 4. In addition, six types of salt welds are defined (primary welds, roho welds, counterregional welds, bowl welds, thrust welds, and wrench welds).

To explain the relationships between salt and associated sediment, Jackson et al. (1994) used the concept of a salt system comprised of a source layer of salt, plus its overburden and subsalt strata. Every salt system is defined by distinct salt-sediment geometries, evolutionary patterns, and structural styles. As autochthonous salt is mobilized, evacuation structures are created. Resulting allochthonous salt, in turn, forms salt tongues, salt stocks, and nappes (Rowan 1997). The structural styles, salt geometries, and salt welds typical of the northern Gulf of Mexico outer continental shelf and continental slope are illustrated in the block diagrams of Figure 4. Salt tongues are subhorizontal sheets of salt that evolve with stepped counterregional or roho evacuation systems (Schuster, 1995). The salt stocks consist primarily of isolated salt masses of various shapes that can coalesce into salt canopies (Jackson and Talbot 1989). Salt nappes translate basinward as thick sheets and generally climb in the stratigraphic section. This salt geometry is typical of salt that has moved a long distance from its original source area.

The classification proposed by Rowan et al. (1999) for fault families and salt welds for the northern Gulf of Mexico, is a geometric classification. They state that "fault form is in response to vertical movement (caused by downward salt withdrawal or upward diapirism) and to lateral translation above salt." Sedimentary loading drives salt displacement and ultimately the structural style. The authors emphasize that this classification is not perfect and that it simply defines end member fault types. However, for the purpose of relating hydrocarbon seeps and vents to styles of faulting, this classification is more than adequate.

The following discussion briefly outlines the various fault types summarized under three fault-type families: (1) extensional faults, (2) contractional faults, and (3) strike-slip faults.

3.1 Extensional Faults: This family of fault types result in bed-parallel elongation which gives rise to thinning of the stratigraphic section. This summary presents nine types of extensional faults.

3.1.1 Peripheral Faults: Are faults at the landward periphery of an autochthonous salt basin, the updip limit of tectonic activity related to salt. The Maxia-Talco fault system of eastern Texas-western Louisiana is an example of this fault type. This fault type is not present in the modern continental slope study area.

3.1.2 Crestal faults are planar growth faults that originate from the crests of triangular shaped salt masses. Rather symmetric linear-to-curvilinear grabens form from this faulting style. Crestal faults and associated grabens characteristically occur over reactive diapirs and form due to basinward movement of the overburden where the faults roughly parallel the shelf edge.

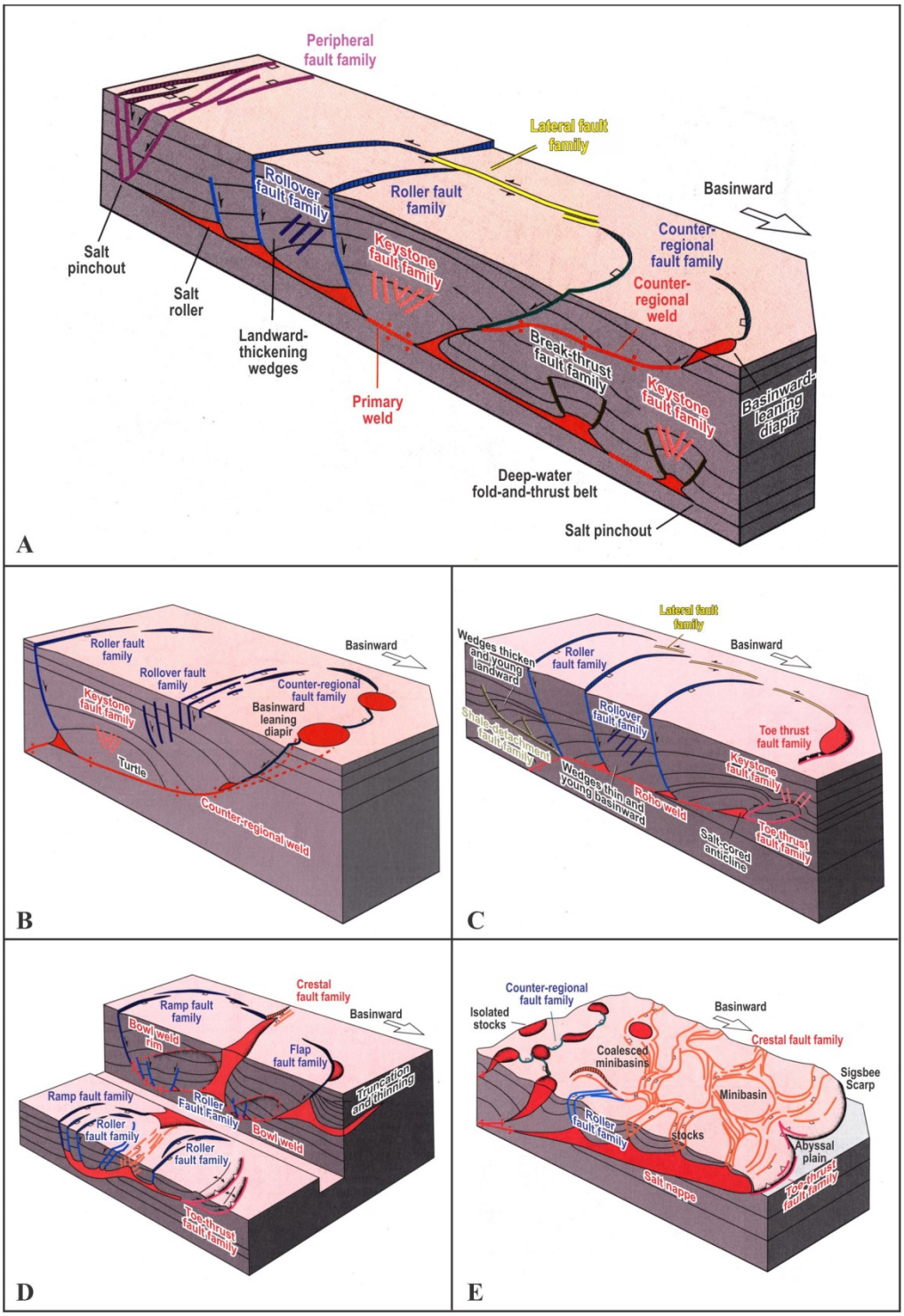

Figure 4. Block diagrams organized from north to south across the continental shelf and slope illustrate (a) typical northern Gulf fault families and salt/fault welds, (b) faults in counterregional allochthonous salt systems, (c) faults and welds of a roho salt systems, (d) faults and welds in a salt stock canopy setting, and (e) fault families of a salt nappe system (modified from Rowan et al. 1999).

3.1.3 Keystone faults occur where stratigraphic units are most highly curved, at the hinge zones or crests of anticlinal structures. These faults are linear-to-curvilinear in plan-view and are associated with symmetric grabens. Keystone faults don't extend from a salt mass and are not growth faults (Figure 4A).

3.1.4 Roller faults are basinward dipping, listric growth faults that sole out in a salt layer or salt weld (Figure 4A). These faults may have a triangular salt rollers in their footwalls, if salt has been evacuated. The hanging walls of roller faults generally display rollover into the fault with expanded growth sections. These faults generally strike in the direction of the strike of the continental slope. Rowen et al. (1999) indicate that roller faults are the dominant fault style in the northern Gulf of Mexico and they typically occur above autochthonous salt or allochthonous salt tongues or sheets. They also develop over bulbous salt diapirs. These roller faults can dip in all directions but only affect the immediate overburden and commonly do not extend to the modern sea floor.

3.1.5 Ramp faults are slightly listric growth faults that form where the base of salt or a salt weld cut up through the stratigraphic section (Jackson and Talbot 1991). These are highly arcuate faults that follow the perimeter of a salt body. These faults intersect the bowl-shaped base of salt.

3.1.6 Shale-detachment faults are listric and basinward dipping growth faults that sole out into a shale detachment. Most of these faults are located updip of the landward rim of allochthonous salt sheets. These faults periodically back-step creating landward-thickening growth wedges associated with the hanging wall young landward. This association is unlike roller faults where the wedges become younger in a basinward direction.

3.1.7 Asymmetric counterregional faults are defined by Diegel et al. (1995) as landward-dipping listric growth faults associated with basinward-leaning and roughly cylindrical salt stocks. In map view, counterregional faults are arcuate. They link two salt bodies or extend from a single salt stock. On seismic profiles, these faults merge at depth with inclined-to-subhorizontal salt welds.

3.1.8 Flap faults are normal faults which have a footwall that contains a salt diapir with a rotate roof that is commonly eroded and uplifted above the regional datum. This family of faults can dip in any direction, but a landward dip is most common in the northern Gulf. Strata associated with the hanging wall thicken toward the salt diapir. The geometry of these fault systems and associated strata suggests that the diapir is active and thereby displaces strata above it. Flap faults form primarily on the landward edges of elongated salt diapirs and accommodate active diapiric activity. Counterregional faults derive from polygonal salt masses and form due to subsidence.

3.1.9 Rollover faults occur in strata that rollover into the hanging wall of some other fault type such as a counterregional fault. These faults are antithetic to the main bounding fault (e.g. counterregional fault) and they dip in the same direction as the strata that roll over into the main bounding fault. These are not growth faults and they generally disappear before reaching the modern sea floor. These fault families are similar to keystone faults in that they both occur

where strata sharply bend. However, rollover faults form asymmetric fault groups while keystone faults form symmetrical graben structures.

3.2 Contractional faults: This fault family is comprised of faults along which there has been bed-shortening resulting in thickening of the stratigraphic section. Two types, toe-thrust faults and break-thrust faults are given.

3.2.1 Toe-thrust faults are reverse faults that dip landward near the downdip toes of allochthonous salt masses or where allochthonous salt has been evacuated. These faults extends up-section in a basinward direction and tend to have an arcuate shape in plan-view. Reverse displacement is common to these faults and they die out upward into contractional folds. Rowen et al. (1999) suggest that the downward translation of the overburden above the allochthonous salt body causes the toe thrusts to form. Because these faults usually die out before they reach the sea floor, they are not fault types that commonly form migration routes that result in hydrocarbon seeps and vents.

3.2.2 Break-thrust faults are both landward-and basinward-dipping reverse faults that cut salt-cored detachment folds. These types of faults are very steep and they don't flatten into stratigraphically higher detachments. Displacement decreases to zero upward at which point the fault dies out. In plan-view, break thrust faults are curvilinear. Break thrust faults are common to the Perdido Fold Belt at the basinward limit of the continental slope. These faults and the folds associated with them are the products of massive updip sedimentary loading.

3.3 Strike-Slip Faults: This fault type is characterized by movement that is parallel to the fault: strike. Lateral strike-slip faults are rooted in either autochthonous or allochthonous salt and are oriented roughly parallel to the regional dip. In plan-view the faults are either linear or form en echelon groups. In profile-view on seismic lines these faults are steep individual faults or flower structures. Lateral faults can be either reverse or normal faults that commonly intersect the sea floor and therefore are candidates for being hydrocarbon migration pathways. These faults can form at the edges of allochthonous salt bodies, at the dip-oriented junctions between different types of allochthonous salt systems, or they can separate extensional compartments that have downslope movement over salt.

3.4 Salt Welds: Even thought it is not clearly established that salt welds can function as migration pathways for fluids and gases (Rowan et al. 1999.), they will be briefly discussed here because they are so intricately associated with many of the faults discussed above. Many faults sole out in welds and probably continue to accommodate movement as updip sedimentary loading continues. Welds are the linkage between fault systems of different types.

Primary salt welds are those that have formed on the autochthonous salt layer (Jackson and Cramez 1989). These welds link updip extension to downdip salt extrusion.

Roho salt welds are defined as any weld into which roller faults detach. Roho welds accommodate significant basinward translation of the overlying stratigraphic section above allochthonous salt. Counterregional salt welds are composed of both landward-dipping and

subhorizontal parts below large basinward-dipping wedges of sediment. Parts of the weld that are landward-dipping represent evacuated, basin-leaning salt diapirs. The subhorizontal parts represent evacuated salt sheets or salt tongues (Rowan et al. 1999). This weld type transitions upward into a counterregional fault and the transition from one to the other is difficult to pick on a seismic line. Bowl welds have an upward concave shape and represent the evacuated margins of bulb-shaped salt stocks. Thrust welds dip landward and may form when rejuvenated salt diapirs are squeezed shut by compression (Rowan 1995). In the process of shortening, stratigraphic units on the landward side of the diapir will be thrust over similar strata on the basinward side. Wrench welds develop when a diapir is located along a lateral fault. As differential movement of strata on either side of the diapir occurs, the diapir is welded shut and a wrench weld which accommodates strike-slip movement results.

The fault systems and associated welds discussed above occur in related groups as one moves across the continental shelf to the bottom of the continental slope. Autochthonous salt systems, stepped counterregional systems, and roho salt systems are found primarily beneath the modern continental shelf. In contrast, salt-stock canopy systems and salt-nappe systems are more typical of the continental slope province.

Figure 4 illustrates that the fault systems discussed above do not occur randomly, but are part of a structural system that has evolved since the Jurassic Louanne Salt was deposited and then progressively loaded with sediments since Cretaceous times. The updip peripheral and roller fault systems accommodate extension within the basin. Extension is accommodated by salt extrusion and contractional deformation at the downdip limit of salt. The part of this structural and salt deformational spectrum that is most relevant to the study documented in this report is the salt-stock canopy system of the present middle-to-upper continental slope as identified in Figure 4. Complex fault systems can provide migration routes for hydrocarbons and other fluids and gases in the context shown in Figure 4D. A fault system can develop and be linked to remnant allochthonous salt and bowl welds. Ramp fault families can occur at the landward margins of these systems while flap faults occur on the basinward sides. Roller fault families may occur in the central regions. Crestal fault families and reactive diapirs can occur where the canopy feeds a salt tongue. These and toe-thrust and lateral fault families are all parts of the salt-stock canopy system which dominates the upper slope setting. Migration pathways to seep sites identified later in this report will be discussed with regard to salt geometries and fault families reviewed above.

4.0 GEOLOGIC EXPRESSION OF FLUID AND GAS EXPULSION SITES

4.1 Background for our Present Understanding

Following the shift in hydrocarbon exploration and production from the continental shelf to the continental slope in the 1970s, supporting data sets revealed the existence of a higher order of sea floor features superimposed on the domes, ridges, and to a lesser extent the intraslope basins. This unexpected array of bottom features ranged from submarine landslides and other products of slope instability to reef-like mounds, hardgrounds, mud volcanoes, mudflows, and brine pools and lakes. Starting in the mid-1980s, direct observation and sampling of these

features determined that many were the products of fluid and gas expulsion at the modern sea floor.

Drilling in the continental slope environment quickly established that intraslope basins contain geopressured sediments. Under these conditions, interstitial fluid pressures exceed hydrostatic values. Episodic breaches in overlying seals by faulting and salt adjustments result in the release of fluids and gases into shallower stratigraphic units or to the sea floor. This process is ongoing and takes place as sediments are added to intraslope basins and underlying allochthonous salt is systematically evacuated (Hunt 1990). High subsurface fluid pressures are thought to develop by rapid sedimentation (Harrison and Summa, 1991), aquathermal pressuring (Baker 1972), clay diagenesis (Barber et al. 1986), and hydrocarbon generation at depth (Hedberg 1974). Release of this pressure results in charging of reservoirs (Anderson 1983), creation of thermal and saline anomalies in the subsurface (Bennett and Hanor 1987), and delivery of hydrocarbons to the modern sea floor (Anderson et al. 1983). At present, data are insufficient to determine the frequency of expulsion events on the continental slope. However, it seems reasonable that breaches in the overpressure zone are probably maximized following significant sedimentary loading events. It is well known, at least for most of the Neogene Period, that most sediments were delivered to the slope during periods of lowered sea level when fluvial systems migrated across the shelf and built deltas at the shelf edge (e.g. Suter and Berryhill 1985; Sydow and Roberts 1994). As suggested by Roberts and Carney (1997), it therefore seems reasonable to assume that seepage and venting of hydrocarbons, formation fluids, and fluidized sediment from the subsurface is modulated by sea level, a proxy for sediment loading of the continental slope. In addition, there is growing support for the process of gas hydrate-related release of methane and other thermogenic gases from continental margins (Kennett et al. 2002). This theory relates to the decomposition of gas hydrate as hydrostatic pressure decreases and warm surface waters come in contact with the hydrate stability zone during a fall of sea level. Kennett et al. (2002) present compelling evidence that during the late falling stage and early rise of the + 100,000 years sea level cycles typical of the late Pleistocene, decomposing marine gas hydrates loaded the ocean and atmosphere with methane causing global warming and sea level rise. Although these gas releases from continental margins may have apparently been catastrophic at times, leading to slope failures and rapid flux hydrocarbon venting, the catastrophic gas venting associated with decomposing gas hydrates is not a factor now when sea level is high and the continental margin is once again within the hydrate stability zone. However, seepage and venting of hydrocarbons is still an on-going process, but perhaps at a scaled down intensity as compared to periods of lowered sea level when both sedimentary loading and decomposing hydrates impacted the upper continental slope. So, where are today's active hydrocarbon seeps and vents located on the northern Gulf's continental slope?

4.2 Distribution of Hydrocarbon Seepage and Venting Sites

The enormous database from 3-D seismic surveys conducted on the northern Gulf of Mexico continental slope (Figure 1) has provided a means of determining the locations and numbers of hydrocarbon seep sites throughout the slope province. Methodologies outlined in this report and published by Roberts et al. (2006) were used by BOEM personnel to analyze vast areas of 3-D seismic surface amplitude data and map the slope-wide distribution of seepage and venting sites using the data base illustrated in Figure 1. Migration pathways for fluid and gas to

the modern sea floor are largely determined by the presence of salt in the subsurface, salt geometries, and associated faulting, Figure 3 displays the intraslope basins as “smooth” or featureless areas surrounded with regions of elevated and bathymetrically “rough” sea floor. These complex areas that form the boundaries of the salt-withdrawal mini-basins are generally salt-supported, faulted, and the sites of fluid and gas migrations Figure 5 illustrates the relationships between intraslope basins, salt, and vertical migration of fluids and gases. Starting in the mid-1980s, “ground-truth” surveys of venting and seeping areas of the upper continental slope using manned submersibles provided a clear correlation between surface amplitude anomalies derived from 3-D seismic data (Figure 5) and areas of seepage (Roberts et al. 1992a). The data emphasized that venting and seepage is primarily confined to the margins of intraslope basins. As a surface amplitude map of Mississippi Canyon blocks (Figure 5) illustrates, large areas of sea floor are impacted by fluid and gas expulsion.

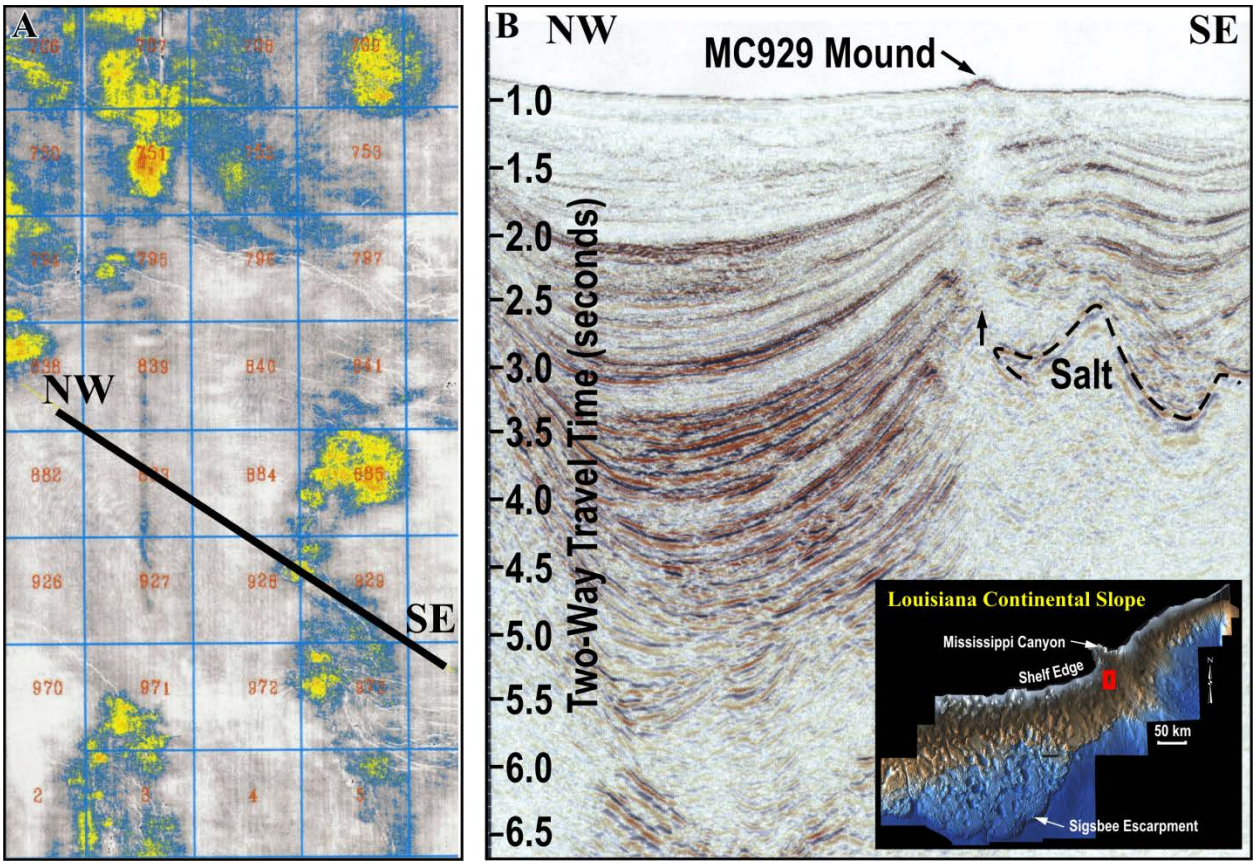

Figure 5. This diagram illustrates the relationship between (a) surface amplitude anomalies derived from 3-D seismic data collected in the Mississippi Canyon lease blocks and (b) subsurface relationships between intraslope basin sediments, salt, fluid-gas migration pathways, and sea floor mound in MC 929.

Figure 2 by Peel et al. (1995) clearly shows the geologic framework of the continental slope changes from a growth fault dominated extensional regime with isolated salt masses and canopies on the upper slope to a contractual setting with salt thrust sheets on the lower slope. From the present seismic database, the frequency of occurrences of fluid and gas expulsion sites decreases downslope. However, it is clear that the deep and ultra deep slope sea floor is affected by expulsion processes. Expulsion occurs where sedimentary basins, "perched" on the salt thrust sheets, are not completely salt-floored or where salt sheets incompletely merge and salt welds appear to be permeable. Also, expulsion occurs in areas at the base of the slope where compressional folds are breached and do not have overlying salt. At this writing, scientific interest and resources are being focused on the deep parts of the northern and western Gulf's continental slope to develop a better understanding of the role that fluid and gas expulsion plays in shaping deep sea floor geology and biology (Roberts et al. 2010a, b; Garcia-Peneda et al. 2010; Orcutt et al. 2010, and others).

4.3 Sea Floor Responses to the Expulsion Process

When high resolution seismic and side-scan sonar data became widely used by industry for geohazards assessments, pipeline surveys, and evaluation of drilling sites, it became apparent that the slope sea floor was much more geologically complex than previously envisioned from low frequency exploration-scale seismic profiles. Even though abundant historical records of oil slicks, tar on beaches, and bubbling gas existed from the Gulf of Mexico (Geyer and Giammons, 1980), it wasn't until the early-to-mid 1980s that the abundance of seeps and vents on the continental slope was fully realized. During this time, many industry supported coring projects revealed oil stained sediments, gas hydrates, authigenic carbonates, and chemosynthetic organisms with some regularity (Brooks et al. 1984; Kennicutt et al. 1985; Brooks et al. 1986; Childress et al, 1986; Kennicutt et al. 1988; Roberts et al. 1989; Neurauter and Roberts 1992; and others). With the advent of Gulf of Mexico manned submersible and ROV research, investigators were finally able to confidently "calibrate" images provided by acoustic data to actual sea floor conditions and characteristics. The use of manned submersibles and ROVs allowed researchers to start developing an understanding of the spatial relationships between fluid and gas expulsion at the sea floor and the associated geological and biological responses.

The impact of the fluid-gas expulsion process is related both to the composition of products being delivered to the sea floor as well as the rate of delivery. The products being delivered are primarily hydrocarbons (biogenic and thermogenic gas and crude oil), formation fluids, and fluidized sediment. Qualitatively, rates of delivery range from slow "seepage" to rapid "venting." The corresponding range of sea floor responses to these qualitative delivery rates was first explained by Roberts and Carney (1997) and Roberts (2001b). Later Roberts et al. (2006) described how 3-D seismic surface reflectivity is used to interpret sea floor responses to the fluid-gas expulsion process. The biological and geological sea floor responses to end-member and intermediate hydrocarbon delivery rates are summarized in Figure 6 and briefly explained in the following sections.

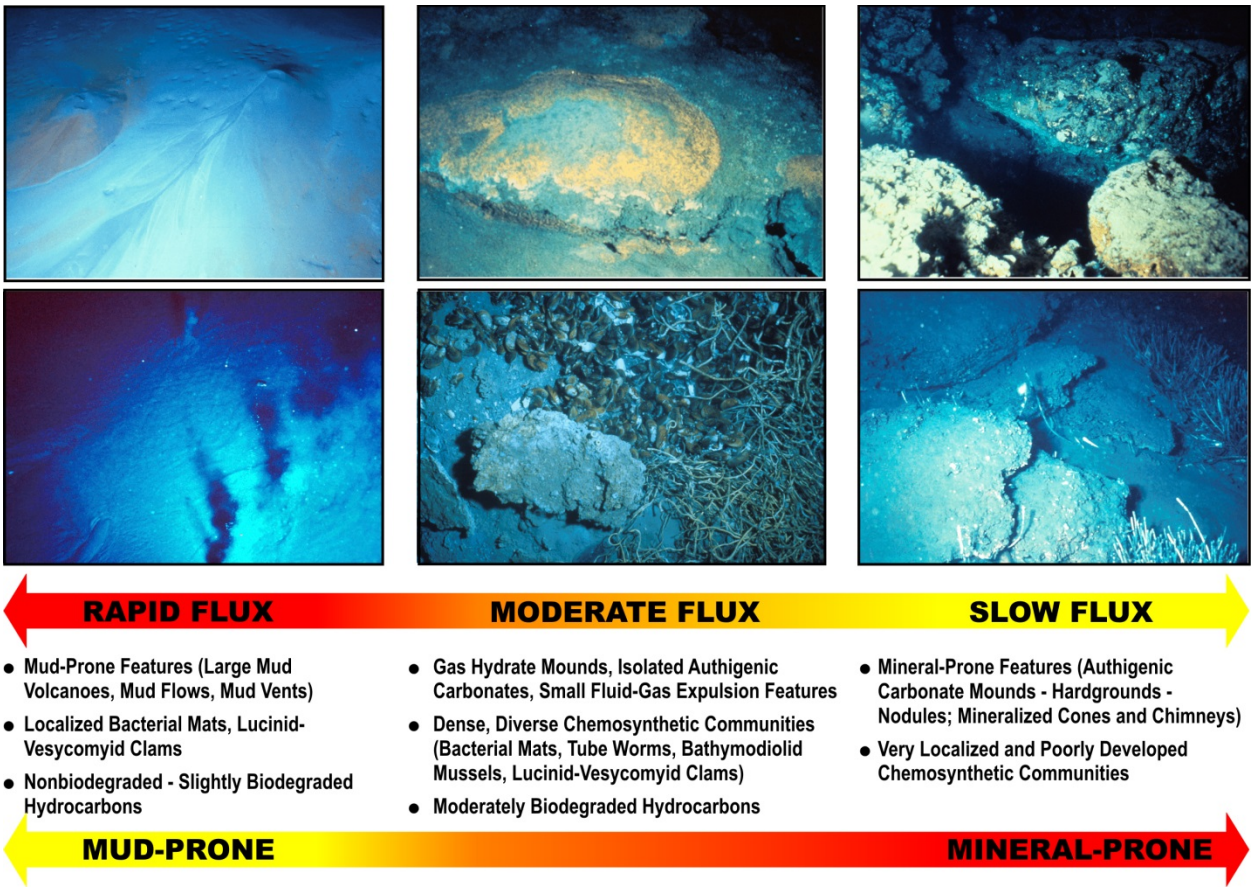

Figure 6. A summary of relationships between flux rate of fluids-gases to the sea floor and general geologic-biologic responses (modified from Roberts 2001b).

4.3.1 Mud-Prone Rapid Delivery Response

Fluidized sediment is commonly transported to the modern sea floor in rapid delivery settings. Mud volcanoes (Figure 7) are found on the northern Gulf of Mexico continental slope and in other deep water locations throughout the world (Hovland and Judd 1988). Barber et al. (1986) attributed the formation of shale diapirs and mud volcanoes to a variety of processes including (a) sedimentary loading, (b) tectonic loading, (c) abnormally high pore pressures, (d) hydrocarbon generation, (e) diagenesis of clays, (f) density inversions in stratigraphic units, and (g) faulting and seismic activity. In the Gulf, it has long been recognized that sediments fluidized by gas and liquids are primarily ejected from geopressured subsurface settings as a slurry onto the modern sea floor (Hedberg 1974; 1980). Manned submersible research in the slope province of the northern Gulf has verified the occurrence of mud volcanoes ranging in size from below the resolution of high resolution seismic and side scan sonar data to those with a diameter greater than 1 km (Newton et al. 1980; Neurauter and Bryant 1990; Neurauter and Roberts 1994; Kohl and Roberts 1994, 1995; Samuel 2004).

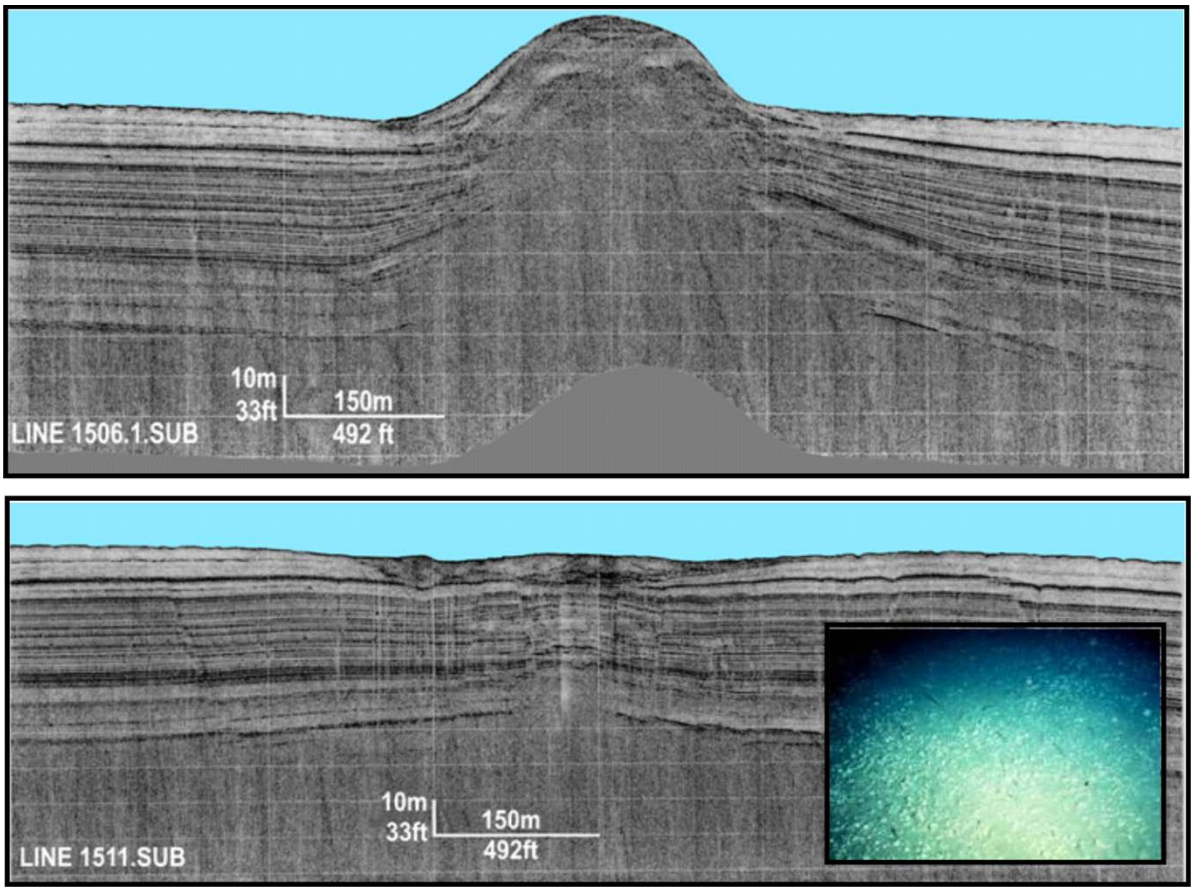

Figure 7. This mud volcano from GC 143 exhibits the shape and other morphological characteristics typical of mud volcanoes found scattered over the continental slope of the northern Gulf of Mexico. Lucinid-vesycomyid clams like those illustrated in the inset picture, commonly inhabit flows from mud volcanoes that contain hydrocarbons. The clams exploit the hydrogen sulfide in these deposits and once depleted the clams die and leave a field of shells as shown in this picture.

On seismic records, mud volcanoes usually have acoustically opaque central interiors that define the migration pathway from the subsurface in the ocean floor. This seismic response is generally interpreted as bubble phase gas along the sediment transport route from the deep subsurface. However, Roberts et al. (1999) and Roberts (2001a) indicate that a composite mound-like expulsion feature in GB 161 has an acoustically opaque interior, but coring and foundation borings indicate that gas is not present. The present opaque signature of this feature is largely attributed to the thorough mixing of sediments during the vertical transport process. A resulting lack of reflection horizons within the migration pathway creates as acoustically opaque character. So, the acoustic blanking in the GB 161 is probably a combination of both thorough sediment mixing and the occurrence of bubble phase gas along the transport pathway.

Active mud volcanoes visited in manned submersibles usually have central vents filled with fluidized sediment laced with crude oil and escaping gas. The surface of the fluidized sediment is usually colonized by white or orange bacteria (*Beggiatoa sp.*). During energetic

expulsion events, mud is forced over the lip of the central vent and runs down the side of the cone-like buildup of sediment to create a thin mudflow. In addition, active out gassing in the central vent entrains sediments into the water column where it is carried away from the mud volcano by ambient currents. Ejected sediments can be sand-sized, but they are usually in the mud range. Kohl and Roberts (1994) and Roberts et al. (1999) indicate that sediments expelled from mud volcanoes may contain displaced microfossils from deep subsurface horizons, shale clasts, and exotic grains of salt, calcite, dolomite, and other particles.

Active expulsion and deposition of sediment, either through suspensions or flows, create conditions that are hostile to most benthic organisms, especially filter feeders. Also, high deposition rates preclude sulfide-producing anaerobic oxidation of hydrocarbons contained within the extruded sediment. However, once mud flows containing hydrocarbons are deposited, mats of *Beggiatoa sp.* bacteria may colonize the sediment surface. Later lucinid-vesycomyid clams colonize the flows to exploit the sulfide produced by microbial degradation of the hydrocarbons. After this source of sulfide is depleted, the clam population perishes leaving a field of disarticulated clam shells (Figure 7). These shells eventually blanket the mud flow deposit, which directly after deposition, has an acoustically "soft" surface. With the shells at the surface and buried a few centimeters below the surface, the acoustic character of this originally "soft" deposit changes to an acoustically "harder" surface return.

Additional reflectivity can be added to a mudflow deposit by early diagenetic processes. Because these sediments are laced with hydrocarbons, authigenic carbonates form as nodular masses and cemented crusts as by-products of microbial activity related to sulfate reduction and anaerobic hydrocarbon oxidation (Ritger et al. 1987; Roberts and Aharon 1994; Neurauter and Roberts 1994; and Roberts and Feng 2010). These reactions of sulfate reduction and anaerobic hydrocarbon oxidation increase alkalinity by production of bicarbonate, which stimulates Mg-Ca carbonate precipitation. Such authigenic carbonates have distinctive $\delta\ ^{13}C$ values because ^{12}C from the hydrocarbons is incorporated into the Mg-Ca carbonate molecules, giving them a characteristic ^{13}C-depleted isotope signature.

4.3.2 Mineral-Prone Slow Delivery Response

There are areas throughout the continental slope province characterized by very slow seepage of hydrocarbons to the ocean bottom. At these sites, the trophic resources for supporting diverse and highly populated chemosynthetic communities are not present. Bacterial mats (*Beggiatoa sp.*) and scattered lucinid-vesycomyid clams are most common in slow seepage rate environments. Slow seepage settings can result from a low-level primary source of hydrocarbons or a change from active delivery to a much slower rate. Rapid delivery systems, resulting in feature like mud volcanoes, may experience long periods of quiescence. When that happens, sea floor lithification by carbonate precipitation usually occurs. Both anaerobic oxidation of hydrocarbons in the sediments or sulfate reduction reactions cause the pore fluid dissolved inorganic carbon content and carbonate alkalinity to rise, resulting in supersaturation and precipitation of Ca-Mg carbonates (Aharon 2000). These carbonates sequester large volumes of CO_2, provide physical stability to the sea floor (Roberts and Aharon 1994), and make available hard substrates for development of hard-bottom invertebrate communities (Sassen et al. 2004). Many of the knolls along the shelf-slope transition in the northern and northwestern Gulf

have known gas seeps. The biogenic veneers of these features are likely seated on authigenic carbonates formed as a by-product of microbially mediated hydrocarbon oxidation (Roberts 1992c, Aloisi et al. 2002).

Hydrocarbon seep-related authigenic carbonates, produced by microbially mediated processes, have diagnostic ^{13}C-depleted $\delta\ ^{13}C$ values as discussed above. Sassen et al. 2004 suggest that the range of $\delta\ ^{13}C$ values observed in carbonates from different sites may reflect parent hydrocarbon sources from methane to crude oil. The mineralogy of authigenic carbonates at seep sites is also variable and much more complex than those described by Paull et al. (1992) from the Florida Escarpment. Studies by Roberts and Aharon (1994) and Ferrell and Aharon (1994) indicate that the most common authigenic carbonate mineral phase at northern Gulf of Mexico seep sites is Mg-calcite. Ferrell and Aharon (1994) determined that most Mg-rich carbonates range between 10-15 mol % $MgCO_3$. Other common carbonate mineral phases are aragonite and dolomite. Sea floor lithification by authigenic carbonates occurs as isolated nodular masses in near-surface sediments, slabs and other hardgrounds, and mounds-chimneys of various sizes. Carbonate cements associated with these various sea floor lithification types vary from microcrystalline dolomite and Mg-calcites to void-filling and circurrgranular acicular aragonites. Some botryoidal splays of aragonite cement have also been found (Roberts and Feng 2010). Figure 8 is a 3-D seismic surface amplitude map and profile across a dome on the upper continental slope illustrating the very irregular and reflective surface of the dome crest. The inset of side-scan sonar data shows that the irregularities are mounded buildups, probably exposed by physical erosion. Manned submersible observations at this site determined that the mounds were composed of authigenic carbonates and analysis of samples of these mounds determined they were composed of Mg-calcite and dolomite (Roberts and Aharon 1994; Roberts 2001b). A general lack of observed chemosynthetic communities associated with these mounds and no remains of chemosynthetic organisms in the carbonates matched the general absence of active seepage in the slow delivery rate setting. Although authigenic carbonates can be found at sites representing all three major delivery rate environments, by far the most authigenic carbonates are associated with slow fluid-gas delivery rate settings.

4.3.3 Intermediate Delivery Response

Somewhere between the extremes of very slow delivery of hydrocarbons to the modern ocean floor and rapid venting of fluidized sediment containing hydrocarbons, conditions are met to support densely populated and diverse chemosynthetic communities. It has been observed from manned submersible dives, ROV work, and further supported with piston coring, that these sites of chemosynthetic community occurrence are frequently associated with gas hydrate deposits exposed at the sea floor or in the very shallow subsurface. Carney (1994) suggests that continental slope areas with gas hydrate present at or near the sediment-water interface have the unique requirements of methane and sulfide chemistry to support densely populated chemosynthetic communities. Gas hydrates, frozen water and gas, will form where the boundary conditions of temperature and hydrostatic pressure are met. This frozen substance is comprised of a cage of water molecules surrounding a gas molecule, usually methane (clathrate structure). Although methane is the most common gas, other higher molecular weight thermogenic gases are usually present in hydrates of the northern Gulf of Mexico continental slope. Depending on gas composition, hydrate could be stable at water depths as shallow as 300 m (984 ft). This

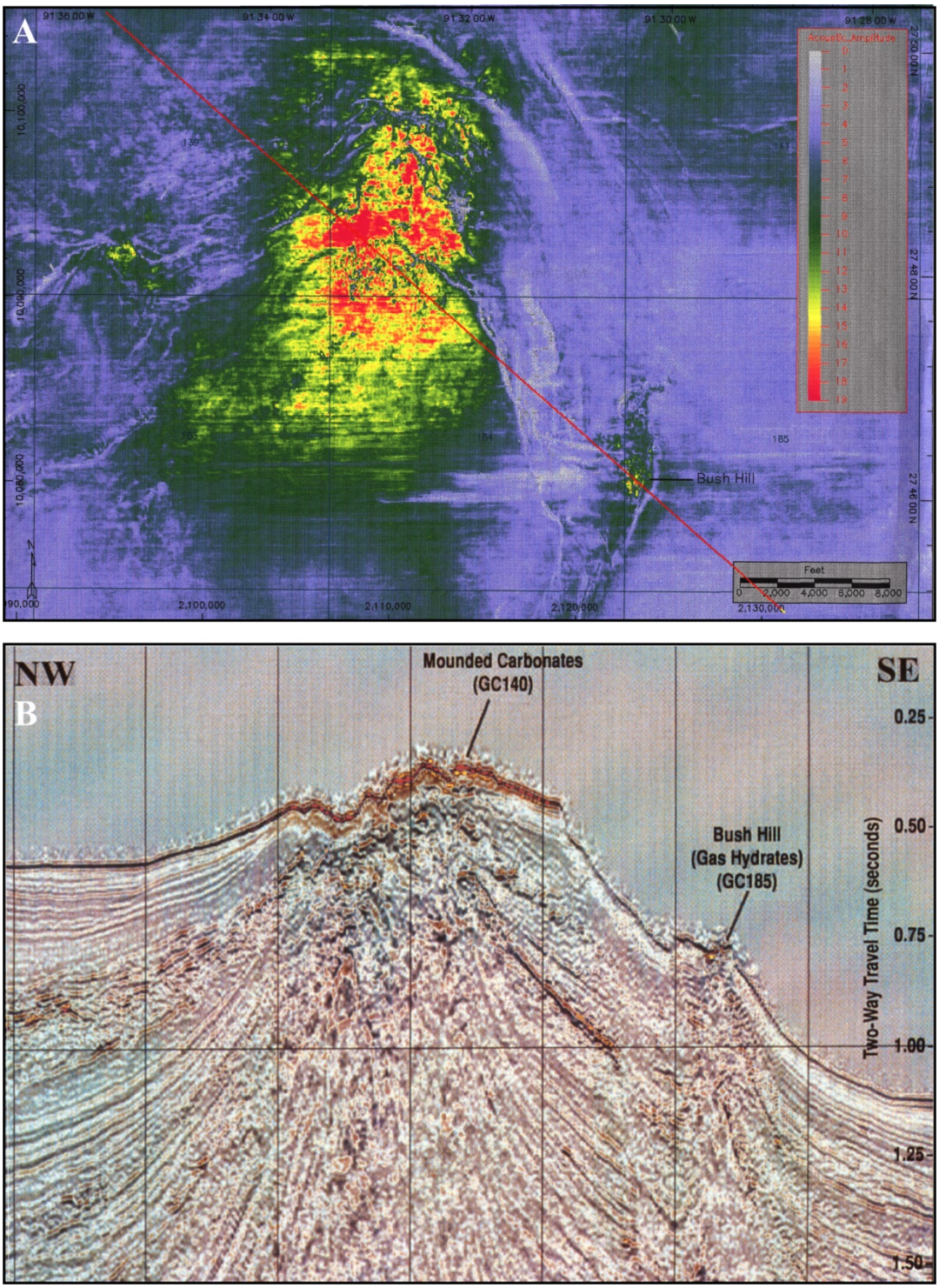

Figure 8. This 3-D seismic (a) surface amplitude map and (b) profile across the Green Canyon Block 140 dome display high positive acoustic amplitudes from the sea floor. Note the highly reflective surface of the dome on both the surface amplitude map and on the profile. The side-scan sonar inset associated with the seismic profile identifies this hard bottom reflectivity as related to mounded carbonates.

depth roughly corresponds to the shallowest occurrence of chemosynthetic organisms in the Gulf at Green Canyon Block 140 (GC140) (Roberts et al. 1992a). However, observational data suggest that most hydrate in the northern Gulf starts appearing at water depths of about 500 m (1640 ft).

Gas hydrate can have a complex relationship with surrounding sediment. It can occur in disseminated, nodular, layered, or massive form (Sloan 1990). But, if gas is fluxed to the surface at a rather constant and critical rate, gas hydrate forms and is frequently exposed at the sea floor. Figure 9A illustrates the first outcrop of gas hydrate observed in the Gulf and perhaps anywhere else in the marine environment. It was observed and sampled in 1991 in Green Canyon Block 232 (GC232). Since this initial discovery, numerous exposures of gas hydrate have been found using manned submersibles and ROVs (MacDonald et al. 1994). Most sites of exposed gas hydrate are geologically and biologically diverse with regard to surface conditions. Within a small spatial framework dark anoxic sediment, authigenic carbonates, and chemosynthetic organisms can usually be found in conjunction with exposed gas hydrate (Figure 9). These sites are always leaking gas which is detectable on high frequency acoustic profilers as plumes rising in the water column above the sea floor (Roberts 2001b). Observations from manned submersibles indicate that most bubble streams exiting the sediment are small and require patience on the observers part to see them. However, at sites of exposed gas hydrate bubble streams are usually obvious and bubble size tends to be larger than at most sites where gas hydrate is in the shallow subsurface or occurs in low-relief mound-like structures that rise slightly above the surrounding sediment surface.

Many sites do not conveniently fit the sea floor response spectrum that qualitatively responds to a wide range of fluid-gas expulsion rates (Figure 6). Variations in the simple qualitative relationships between flux rate and geological-biologic response can arise from a number of factors including: (1) variations in the chemistry of fluids and gases transported to the modern sea floor, (2) frequency of expulsion events, (3) duration of expulsion events and length of associated quiescent periods, (4) the strength of expulsion events, (5) the spatial relationship between expulsion sites, and perhaps other variables. For example, in the case of mud volcanoes if the venting activity ceases, extruded mud flows may undergo surface lithification, a characteristic of slow flux settings. Figure 10 illustrates an area of the northern central Gulf's continental slope that emphasizes the variability of fluid-gas expulsion features that can occur within a relatively small area (Samuel 2004). In this image, a mud volcano (rapid flux feature) is surrounded by patches of lithified sea floor (products of a slow flux setting). If the mud volcano remains inactive, given enough time, the surface of the mud volcano may also become lithified. Highly reflective (dark) areas on the flanks of this feature may indicate that this process is currently well underway.

A comprehensive study by Fillon (2007) utilizing data from 250,000 oil and gas wells in the northern Gulf of Mexico Basin illustrates that over the last 1.35 ma, the highest sediment deposition rates have been on the upper-to-middle continental slope. This study also indicates that the focus of deposition has generally shifted from west to east over this time interval, basically a shift from the Garden Bank lease area to the Green Canyon area. This most recent depositional focus suggests a strong response in salt deformation and movement on associated faults. This sedimentary loading is therefore interpreted as a driver of hydrocarbon seepage and

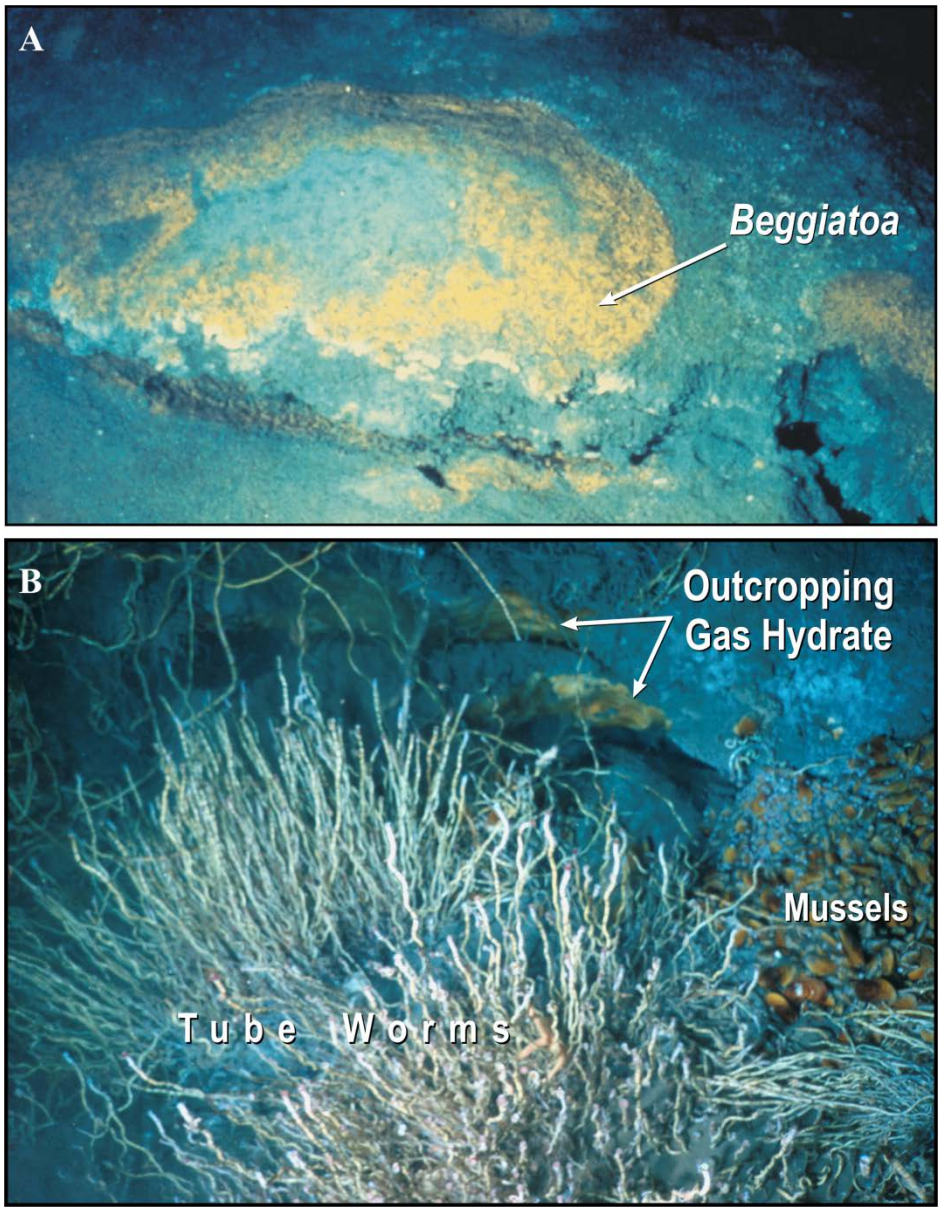

Figure 9. The first recognized sea floor exposure of gas hydrate (a) was discovered in 1991 in Green Canyon Block 232. Gas hydrates at or near the sea floor commonly are associated with well-developed chemosynthetic communities (b).

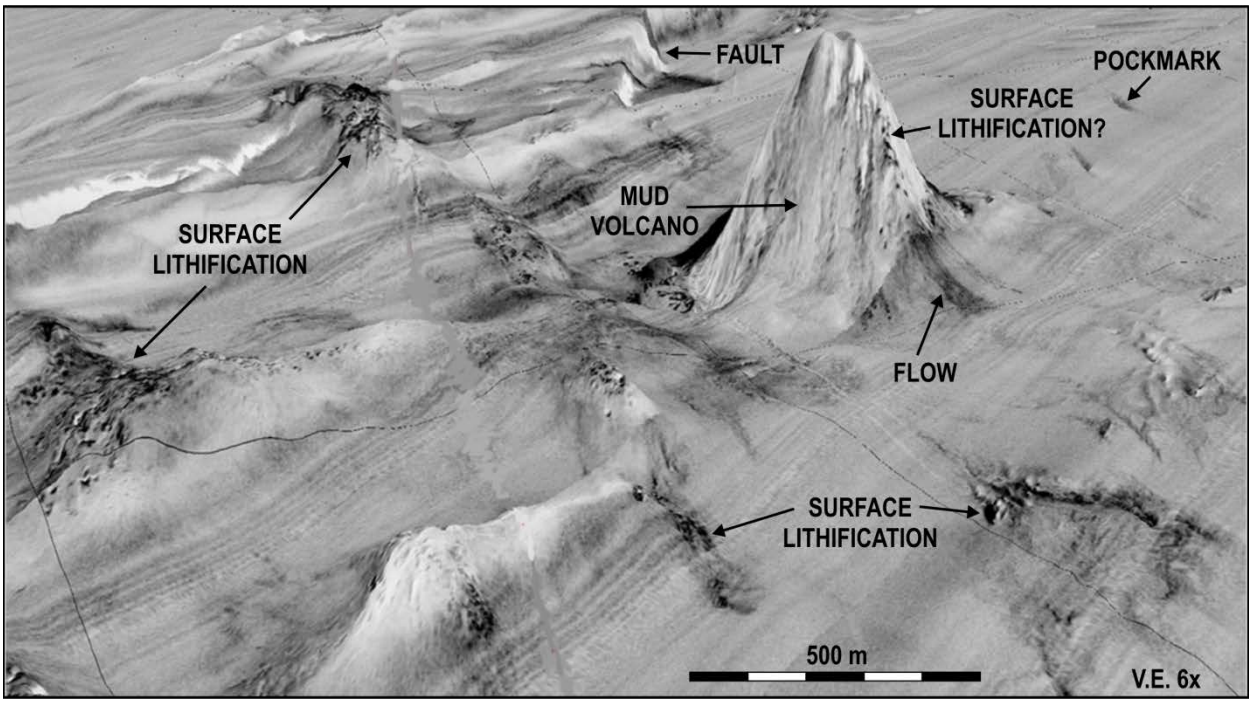

Figure 10. This side-scan sonar mosaic illustrates the high level of sea floor variability in seep-related areas. Faults, hardgrounds, mud vent/flows, and a mud volcano all occur in this area (adapted from Samuel, 2004).

more rapid vent that persists today. Both seismic studies (Roberts 2001b), manned submersible dives (MacDonald et al. 1995), and surface oil slicks (MacDonald et al. 1999; MacDoanld et al. 2002; DeBeukelaer et al. 2003)) suggest that hydrocarbon seepage on the northern Gulf's continental slope is highly concentrated in the Garden Banks and Green Canyon lease areas, with fluid-gas expulsion most common in the Green Canyon lease blocks where sedimentary loading has been most recently concentrated.

5.0 TECHNOLOGY DEVELOPMENT: A CRITICAL STEP IN UNDERSTANDING GULF GEOLOGY

In order to be able to undertake a regional study of the continental slope as outlined in this report, the technology of acquiring and analyzing high quality remotely sensed data of the ocean floor and subsurface had to exist. The advent of 3-D seismic dramatically changed our view of the northern Gulf of Mexico continental slope. Not only did this technology give us the ability to view salt-sediment relationships in 3-D, but "horizon slicing" provided a means of looking at thin stratigraphic intervals in plan-view using amplitude variability as an imaging tool. This methodology produces time-synchronous views that can result in imaging such things as channels, deltas, and other depositional systems, in plan-view, much like the surface reflectivity or surface amplitude images of hydrocarbon seep sites used in this study. Because of the importance of rapid technology advancements to our present ability to study fluid-gas expulsion sites with high quality remotely sensed data, a brief history of the evolution of 3-D seismic technology and navigation is included in this report.

Less than a decade after World War II, seismic data were starting to be routinely acquired from marine settings and attention was focused on the Gulf of Mexico because it was a proven hydrocarbon producing province. Salvador (1991) indicates that the first offshore seismic reflection survey was in 1944. Since then, the petroleum industry, government (U.S. Geological Survey), and academic groups (particularly the Institute for Geophysics, University of Texas) have acquired seismic reflection data from throughout the Gulf. These surveys have been instrumental in establishing the geologic framework for the Gulf basin since little direct geological data were available for most of the deep Gulf. It wasn't until the 1960s to 1970s until adequate seismic reflection and refraction data became available to define the geology of the deep Gulf as a thick sedimentary wedge overlying an acoustic basement consisting of oceanic crust or transitional crust (Buffler 1991). However, our present understanding of the northern and northwestern Gulf's continental slope comes primarily from the geological and geophysical data collected in support of the exploration for and production of oil and gas. Our present concepts of structure, stratigraphy, sedimentology, and surficial geomorphology of the continental slope have evolved largely because of technological advances in data collection systems.

Understanding Gulf of Mexico geology is directly linked to advances in seismic imaging of the subsurface. This statement is particularly true of our current understanding of the northern Gulf's continental slope geology. Since the transition from refraction to reflection technology in the 1930s, the seismic industry has undergone a number of major technological advances. Perhaps the most important advance was the shift from analogue-to-digital data acquisition systems that occurred in the late 1960s with the parallel development of computers. The digital revolution not only improved seismic data acquisition, but the shift to digital data encouraged major advances in post-processing. At the same time, major improvements in seismic sources and receiver systems were being made. Explosive charges were steadily replaced by vibrators (onshore), sparkers, air guns, and water guns for lower frequency exploration-scale seismic acquired at sea. Higher frequency sparkers, boomers, sleeve-guns, transducer-based subbottom profiles and side-scan sonar followed (Bouma 1981). Rapid improvements from the electronics industry steadily improved collection of seismic reflection data. As the analogue-to-digital transition was taking place, offshore exploration for oil and gas was moving across the continental shelf to deep water of the shelf edge and upper continental slope.

Following the analogue-to-digital transition, the most significant advance in seismic technology was the development of 3-D seismic. The first 3-D seismic data acquisition was carried out onshore in New Mexico in 1972 (Graebner et al. 2002). By the 1980s, the acquisition of 3-D seismic data had moved offshore and was being used by the petroleum industry for exploration of the northern Gulf of Mexico continental slope. New and more versatile 3-D seismic data sets quickly replaced 2-D seismic profiles as the preferred data for exploration. Models and concepts derived from 2-D data were quickly revised when 3-D data became available. In 1982 and early 1983, EXXON successfully used 3-D seismic in Mississippi Canyon Block 438 in support of their Alabaster Prospect (Greenlee et al. 1994). This project was part of a significant escalation in the acquisition of 3-D seismic data that took place in the 1980-83 periods. In addition to data acquisition, Shell and other companies made major software improvements in 3-D seismic imaging (Nestvold 1992). Steady advances in computer technology led to the development of seismic interpretation systems (work stations) with

associated software applications. The 3-D seismic data acquisition business grew slowly until the late 1980s when the petroleum industry universally recognized the substantial benefits of 3-D over 2-D data. After about 1987 to 1988, 3-D seismic data became the standard for the offshore industry. Both the use and acquisition of 3-D seismic data experience rapid growth after the late 1980s, a trend that continues today (Graebner et al. 2002). Now over 98% of the northern and northwestern Gulf of Mexico continental slope is covered with high quality 3-D seismic data sets. In some areas of the slope province, multiple generations of 3-D seismic surveys have been acquired. According to Aylor (1998), one of the greatest contributions of 3-D seismic to the petroleum industry is the reduction of risk in prospect identification and evaluation. For example, AMOCO's success rate for exploration wells increased from 13% in 1991 to 44% in 1996 (Aylor 1998). The increase in success rate is attributed to use of 3-D seismic data. Sandia National Laboratories, a group not affiliated with the petroleum industry, stated in a report commissioned by the U.S. Department of Energy that 3-D seismic reduced the cost of finding new oil and gas by 47% (Graebner et al. 2002). On the production side, repeated 3-D seismic surveys over the same field (so called 4D-seismic) was found to provide insight into production efficiency, reservoir character, infill drilling strategies, and secondary recovery strategies and efficiency.

Advances in seismic technology could not have been made without parallel improvements in navigation and offshore positioning. In the 1940s and early 1950s when the petroleum industry was moving offshore, surveyors with theodolites were stationed at known positions onshore and line-of-sight positions were radioed to a survey vessel as it moved from one predetermined position to another. Later, radio direction finding was developed from World War II technology for surveys beyond line-of-sight. However, this methodology had poor accuracy. To solve the accuracy problem, Seismic Service Corporation established a survey method in 1952 that involved three synchronized radio transmitters positioned along the northern Gulf coast, using this system, a survey vessel offshore could plot a position relative to the three onshore transmitter stations by measuring phase differences rather than time differences, as used in earlier radio navigation systems like Loran A. This system, Lorac, was accurate to about 30 m, but could only be used during the day because of sky wave effects at night. Because the offshore industry thrust was centered around Morgan City, Louisiana, this is where the original Lorac systems were deployed. However, by 1960, a Lorac net covered the entire northern Gulf from Brownsville, Texas to Key West, Florida. A new method of navigation was started in 1965 when the U.S. Navy launched a navigation satellite and made it available for one-to-two hours daily. The satellite data could be used to "calibrate" other navigation data such as data from Lorac. A small computer was needed to acquire and process the satellite navigation data. This combination of a navigation satellite and computer marked the beginning of a new era of offshore positioning.

After the first navigation satellite was put in place, the science of positioning took three distinct paths: (a) steady improvement of radio-based techniques, (b) development and use of microwave transponders, and (c) improvement of satellite-based navigation technologies. Today, satellite navigation and positioning is the standard. The visionary, John Chance of Lafayette, Louisiana, pioneered the development of software and hardware to utilize geostationary satellites for accurate marine positioning. His system, STARFIX, became operational in 1985 and operated for about a decade before differential Global Positioning

System (GPS) became widely available and cost effective. Before the onset of GPS, STARFIX had an important impact on the offshore oil and gas business. It was quickly accepted as the standard for use by seismic data acquisition companies, for positioning drilling vessels, and siting production facilities. Accurate and rapidly acquired navigation data was an essential part of rapid evolution of 3-D seismic to the industry standard. Therefore, the exploration for hydrocarbons during the parallel development of a satellite-based positioning system and steadily improving 3-D seismic acquisition technologies, as well as data processing software, has created a deep water data base unmatched for any continental slope in the world.

6.0 DATA SETS AND METHODOLOGY

6.1 Introduction

Research conducted in the early 1990s (e.g. Roberts et al. 1992a) demonstrated that the strength or amplitude of the sea floor reflector and its plan-view pattern as derived from 3-D seismic data can be powerful methodologies for making informed interpretations of surficial geology and benthic community habitat characteristics. Sheriff (2002) defines amplitude as "the maximum departure of a wave from its average value." Reflection is defined as the energy or wave from a seismic source that has been reflected (returned) from an acoustic impedance contrast (reflector) or series of contrasts within the earth. The objective of most reflection seismic work is to determine the locations and altitudes of reflectors from measurements of the travel time of primary reflections and to infer geologic structure and stratigraphy from these relationships. In the study reported here, interpretation of subsurface geology is certainly important for determining location and characteristics of hydrocarbon migration pathways to the modern sea floor. Conditions at the sediment-water interface, however, are critical to determining settings that are likely to support diverse and well-populated communities of chemosynthetic organisms.

In the 3-D seismic analysis used in this study, reflection strength (amplitude) and phase were determined from approximately a 10 millisecond window starting at the sediment-water interface and progressing into the shallow subsurface. This window translates into a stratigraphic interval approximately 7.6 m (25 ft) thick. Phase is defined by Sheriff (2002) as "the angle or lag or lead of a sign wave with respect to a reference." Phase is a seismic attribute related to amplitude and has a sawtooth appearance resulting from amplitude maxima and minima. Phase can be both positive and negative with values from 180° to -180° depending on the amplitude trace. A zero phase value corresponds to amplitude maxima, where as a minimal amplitude value causes a phase reversal (Tanner and Sheriff 1977). Phase reversals may help identify gas contained in near-surface sediments. As applied in the study, phase helps define "fast" (usually hard bottom) and "slow" (usually soft, gas charge bottom). Early appraisals of surface reflectivity (amplitude) from regional 3-D seismic data sets indicated that the continental slope of the northern Gulf of Mexico was punctuated with sea floor bright spots (Roberts et al. 2006). Research conducted since the early 1990s indicates that sea floor bright spots can be correlated to localized surface areas of fluid-gas expulsion where carbonates have been precipitated as a by-product of microbial oxidation of hydrocarbons and to some degree gas hydrate occurrence. Seismic reflectivity and phase are used to interpret sea floor responses to the fluid-gas expulsion process, as discussed in a previous section of this report.

6.2 Available Data Sets

The basic data sets used in this study consisted of 186 3-D seismic surveys acquired over 76,000 mi^2 (196.850 km^2) across the upper, middle, and lower continental slope of the northern and northwestern Gulf of Mexico (Figure 1). These surveys represent data collected by oil and gas companies as well as speculative acquisitions by survey companies. The data are held proprietary by the BOEM in their New Orleans, Louisiana office where they are used in the lease evaluation process. Because support for the study discussed in this report originated from BOEM and the study is designed to help BOEM fulfill its regulatory mission, selected 3-D seismic data sets were made available. The proprietary guidelines for access and use of the data have been followed throughout the study and report preparation process.

6.3 Methodology

Depth data were sparse at the beginning of the study and the decision was made to use only the extensive and, in many cases overlapping, time data. In most 3-D seismic data sets, the sea floor reflector was strong and well suited to the automatic picking programs on the BOEM new Orleans Office Sun Workstation using Geoquest's "Autopix" and "ASAP" in "IESX". The sea floor horizon was given a unique, consistent name for each survey (wb_survey permit name) to avoid amplitude display problems caused by the wide variation in amplitude scaling between surveys. Due to time and data storage constraints, the sea floor amplitude interpretations were not normalized. Every sea floor horizon was defined as a positive (compressional) event in the horizon settings. (As many seed lines were interpreted by hand as the interpreter deemed necessary for each survey, depending on the complexity and rugosity of the sea floor bathymetry and the highly variable amplitude response.) The automatic picking program was then started and let run overnight. Upon completion, the interpreter then quality-checked the resulting interpretation for bad picks and gaps. Hand picking after autopicking was necessary in some high dip and complex areas to "clean up" the interpretation.

Upon completion of the picking process, the interpreters posted the amplitude interpretation of each survey and identified potential seep sites. Those that were high positive amplitudes were (outlined with red fault polygons) and interpreted as areas with extensive authigenic carbonates, hydrates, and chemosynthetic communities that should have anomalously strong positive reflection coefficients. Those areas with low positive responses or negative responses (phase reversals from peak to trough), often embedded within the high positive areas, were outlined with polygons and interpreted as areas of very high flux rates with gas saturated muds that should have weak positive-to-negative reflection coefficients. Mud volcanoes, with rapid but intermittent flux rates fall into this category and often display weak amplitude response. However, they have characteristic conical shapes on the time display and seismic cross sections.

Care was taken not to outline amplitude anomalies that did not show direct evidence of migration pathways for seepage on the seismic cross sections but showed strong positive acoustic amplitude response. These areas were clearly identified as either 1) flows of sediments from active seeps nearby caused by a change in lithology of the flow from the surrounding

hemipelagic mud or cementation by authigenic carbonate due to high oil and gas saturations in the flow sediments, or 2) turbidite flows of sand rich sediments over the hemipelagic mud, or 3) exposure of salt or dense saline brines on the sea floor.

7.0 CASE INVESTIGATIONS

The remainder of this report is devoted to the explanation of ten case investigations where both field and data are combined for making informed identifications of hydrocarbon seep and vent sites that impact the modern sea floor. As stated in the introductory sections of this report, the primary objective of this study is to improve the predictive use of 3-D seismic surface reflectivity or surface amplitude data for enhanced interpretation of sea floor geology and biology associated with sites where fluid and gas expulsion is taking place. The laboratory data consist of industry-acquired 3-D seismic data analyzed under proprietary guidelines at the Bureau of Ocean Energy Management (BOEM) office in New Orleans, Louisiana. In conjunction with BOEM geoscientists, each site was geophysically characterized using both surface attributes and stratigraphic-structural properties of the shallow subsurface interpreted from 3-D seismic data. Interpretations about the character of the sea floor derived from these data were field "calibrated" using observational data (video tape and 35mm photographs) from the Harbor Branch Oceanographic Institute's Johnson Sea-Link (JSL) submersible and sea floor sampling (grab samples and short cores).

The case investigations discussed here are but a few of the hydrocarbon seep-vent sites identified and studied using the 3-D seismic surface reflectivity-amplitude methodology. The case investigations selected for discussion in this report are all from the northern Gulf of Mexico upper continental slope (< 3000 ft or 915 m water depth). The site selection technique which involves analysis of the sea floor return from exploration-scale 3-D seismic data, acquired for the oil and gas industry, is applicable over the entire depth range of the continental slope. However, during this study only the Johnson Sea-Link submersible was available for collecting "ground truth" data for calibrating the seismic data to actual sea floor conditions and characteristics. The maximum diving depth for the Johnson Sea-Link was 3000 ft. (915 m). Therefore, sites were restricted to the upper continental slope, but are geographically spread from the Garden Banks lease area in the western part of the depth-restricted zone to the Vioska Knoll lease area in the eastern sector. Later work (Roberts et al. 2010a) demonstrated that the 3-D seismic surface reflectivity-amplitude methodology for sea floor analysis was applicable to the evaluation of hydrocarbon seeps-vents over the full depth range of the continental slope.

Observational data (video, 35mm photographs, and visual observations) and samples were collected along transects established for ground truth testing of the 3-D seismic surface reflectivity-amplitude variations of each site. Dives were designed to start in "background" amplitude areas and move to the highest and lowest reflectivity or surface amplitude localities within each site. The intent was to determine if certain types of sea floor correlated to various reflectivity-amplitude strengths and patterns. During each dive a surface log was kept that recorded navigational data as well as basic activities during the dive. Appendix 1 is a duplicate of the surface log for the dives highlighted in this report and others over two dive seasons. The observers in the submersible also kept notes on each dive. These notes were placed in a master

file for each cruise and archived at the Coastal Studies Institute at Louisiana State University. They were used along with the surface log for preparation of this report.

Associated with the description of each case investigation are combined 3-D seismic surface amplitude and bathymetry maps. The bathymetry is derived from seismic data. Although generally close to actual depths recorded by the submersible (e.g. in the dive logs of Appendices A and B) there may be differences of a few feet (meters) between the two. These differences derive from both the time-to-depth conversion of the sea floor reflector from 3-D seismic data as well as the actual position of the submersible on or slightly above the bottom. Local sea floor relief can introduce a difference between seismic-derived depth and actual measured depth in the submersible.

Both video and 35mm color photography were used to record images of the sea floor during each dive. Individual images extracted from the video as well as 35mm film are used in this report to illustrate sea floor types representative of various 3-D seismic surface amplitude strengths and patterns. The images extracted from video do not have the resolution of those on 35mm film. However, the video images provide a valuable record of each dive and most images include a header containing dive site information (e.g. water depth, temperature, etc.). Each dive site description contains video and/or 35 mm images to illustrate the relationship between remotely sensed seismic surface reflection-amplitude data and characteristics of the deep ocean floor.

Each of the following 10 case investigations will be discussed in terms of geologic framework of the site, characteristics of the sea floor as interpreted from 3-D seismic surface reflectivity-amplitude data, and the degree of correlation of the seismic data to sea floor observational and sample data collected on Johnson Sea-Link submersible transects across each area of interest. All case investigations include a combined 3-D seismic sea floor amplitude and bathymetry map on which the transect is plotted. Navigation fix points are designated along the transect where important observations are made. The first fix point is rarely on the transect line. It is where the submersible arrives at the bottom. Calibration of the submersibles "touchdown location" as well as the transit to the predetermined transect line usually involves making several location checks (fix points). Because of this process, the transects presented with each case investigation do not start with Fix 1.

7.1 Case Investigation: Garden Banks 535 (GB 535)

7.1.1 Location and Geologic Setting

The Garden Bank lease area, Figure 11, is just below the shelf edge south of the western Louisiana chenier plain coast where during the Latest Pleistocene glacial maximum, delta-building occurred in what is now deep water of outer shelf-to-slope transition. Investigation of a large number of line miles (kilometers) of high resolution seismic acquired by the United States Geological Survey over the Louisiana shelf show incised fluvial channels on the shelf leading to deltas at the shelf edge and extending onto the upper continental slope within the northern part of the Garden Banks lease area (Berryhill et al. 1986). Water depths in the area of interest within GB 535 range roughly from 1850 ft. (564 m) to 2000 ft (610 m).

The area displaying interesting 3-D seismic sea floor amplitude anomalies within GB 535 is located in a graben bounded by two regional NE-SW trending faults (Figure 12). An elongate intraslope basin oriented NW-SE is located to the south of the study site and thick sedimentary sections occur over salt to the NW (Figures 12 and 13). The seismic profile of Figure 13 and the combined bathymetry and 3-D seismic surface amplitude map Figure 14, indicate that the areas of elevated sea floor amplitudes are within the graben structure and bathymetrically deeper than the faulted sides of the graben. This graben is an extensional fault of the crestal graben fault family (Rowan et al. 1999). The seismic profile (Figure 13) clearly establishes a vertical fluid-gas migration pathway from the deep subsurface to the floor of the graben where the seabed is interpreted as being very reflective. The origin of this reflectivity is not clear from the seismic data alone. Crestal collapse faults focus migration to the graben floor from a high point on subsurface salt body.

7.1.2 Sea Floor Amplitudes and Surface Geology

The bathymetry, structure, and 3-D seismic sea floor amplitude patterns of the area of interest are presented in Figure 14. Increased seabed reflectivity in this central area of GB 535 is concentrated between two well-defined faults that trend NE-SW. Between the two faults, the sea floor is depressed, forming a linear graben structure. The seismic profile plotted on the regional bathymetry and sea floor amplitude map of Figure 12 and presented in Figure 13 depicts the floor of the graben as a highly reflective area, much more reflective than the sea floor along the elevated flanks of the graben. The highest reflectivity appears as a bright zone that nearly spans the width of the graben slightly beneath the present seabed.

Faulting along the graben margins is clearly revealed as major faults and a series of minor faults down-stepping to the graben floor. As discussed above, the acoustic blanking beneath the graben floor defines a vertical migration pathway from deep within the subsurface to the seabed. Fluids and gases that originate deep within the sedimentary column are probably steered into the migration pathway to the graben floor by a subsurface salt mass defined by two strong reflectors that are clearly visible on the seismic profile of Figure 13.

7.1.3 Interpretation of 3-D Seismic Sea Floor Amplitudes Using "Ground Truth" Data

A roughly NW-SE trending transect across the graben floor and beyond the defining down-to-the NW fault to undisturbed sea floor on the shoulder of the graben is illustrated in Figure 14 fix points where specific observations from the Johnson Sea-Link were made are noted along this transect. At the beginning of the transect, Fix 6, the 3-D seismic surface amplitude map of Figure 14 indicates a highly reflective bottom. The patterns of reflectivity are scattered near Fix 6, but strong. Observations from the sea floor in this area revealed indicators of hydrocarbon seepage including white bacterial mats (*Beggiatoa* sp.), small areas of dark reducing surface sediment, scattered lucinid-vesycomyid clam shells, and nodular masses of authigenic carbonate in the surface sediments (Figure 15A). Octocorals scattered throughout the area were seated on both carbonate and clam shell substrates. However, no impressive seepage sites with densely populated seep communities were observed in the vicinity of Fix 6.

The transit across the graben floor, between Fix Points 6 and 7 (Figure 14), produced the same types of observations as discussed above regarding the area around Fix 6, but bacterial mats were less frequently encountered. At Fix 7, the sea floor shifted from being relatively flat to a series of low-relief ridges oriented roughly in a NE-SW direction. Figure 15B illustrates one of these ridges with octacorals and clam shells on and surrounding it. Fix 8 is very near Fix 7 (Figure 14). The 3-D seismic surface amplitudes near this location are very high. This reflectivity appears to be associated with a high density of lucinid-vesycomyid clam shells and nodular masses of authigenic carbonate scattered throughout the near-surface sediment. However, clear evidence of active hydrocarbon seepage or venting was not encountered.

Near the regional fault that defines the SE margin of the graben the sea floor sediments were thoroughly burrowed with impressive concentrations of sea pens (octacorals) with associated ophiuroids (Figure 15D). The octacorals were attached to pieces of authigenic carbonate and clam shells, but no clear evidence of active hydrocarbon seepage was observed.

At Fix 11 (Figure 14), distinct ridges oriented in a NE-SW direction were observed (Figure 15E). Indicators of hydrocarbon or brine seepage were not present in association with these features interpreted as being fault-derived. The surface sediments on these features were thoroughly burrowed with many visible tracks and trails. Outside the fault zone at Fix 12, the sea floor was relatively flat, but appeared thoroughly burrowed as it was at Fix 11. No seepage indicators were observed SE of the major fault defining the southern side of the graben. The 3-D seismic surface amplitude data for the area around Fix Points 11 and 12 indicated very low seabed reflectivity.

7.1.4 Summary

The area of interest in GB 535 is in a graben, bathymetrically lower than the surrounding sea floor. The 3-D seismic surface amplitude data suggest a very reflective (hard) seabed. However, ground truth observations and samples acquired from the Johnson Sea-Link indicate mostly soft, unconsolidated sediments. Only a minimal number of features were observed that identify a relationship with the flux of hydrocarbons to the sea floor. The development of reflective shell beds and limited authigenic carbonate hardgrounds suggested a low hydrocarbon flux setting. Seismic profiles across the area suggest that the highly reflective surface is in the shallow subsurface and buried by a thin veneer of sediment. Considering that the 3-D seismic has a low frequency acoustic signature tailored for deep penetration into the subsurface, this acoustic frequency for oil and gas exploration purposes, cannot resolve just the sea floor. In fact, the first reflector from the sediment-water interface actually represents approximately 20-25 ft (6-7 m) of sedimentary section. Therefore, submersible observations of the sea floor may not faithfully represent the reflectivity of seismic energy included in the first seismic return from the seabed. In most cases, the modern sea floor has characteristics that support hydrocarbon seepage and associated properties that produce high reflectivity or high positive amplitudes on 3-D seismic amplitude data. In the GB 535 case the reflective surface is largely below, the present sea floor, perhaps representing a cessation of fluid-gas flux to the seabed. This hiatus in seepage may have allowed hemipelagic sediment to be deposited over a surface once impacted by active seepage which developed authigenic carbonates and perhaps gas hydrates characteristic of such settings.

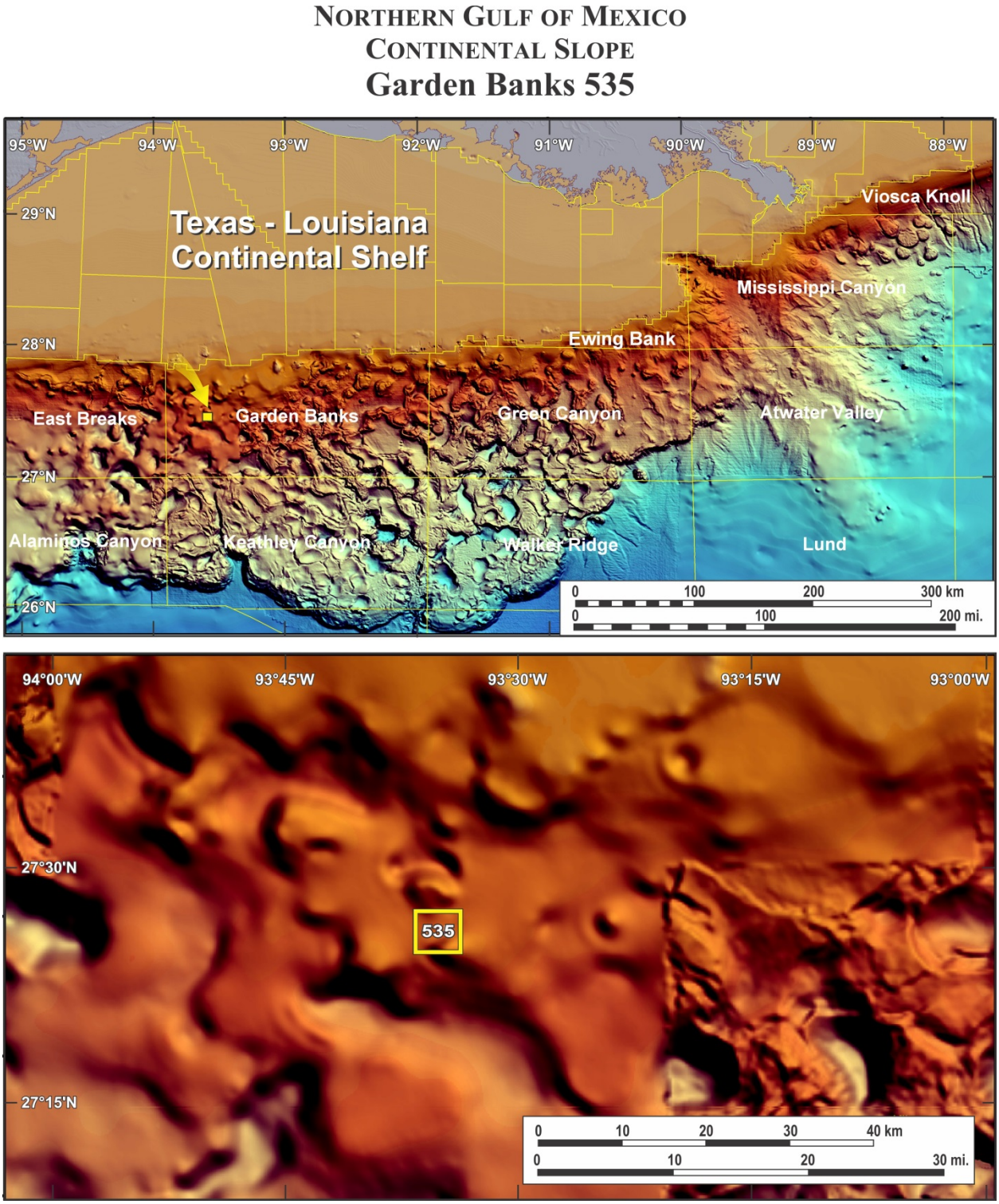

Figure 11. (A) Shaded multibeam bathymetry map of the northern Gulf of Mexico continental slope. The yellow arrow indicates the location of Garden Banks Block 535 (GB 535), (B) The enlarged area of the continental slope surrounding GB 535 illustrates the bathymetric features within and surrounding the block.

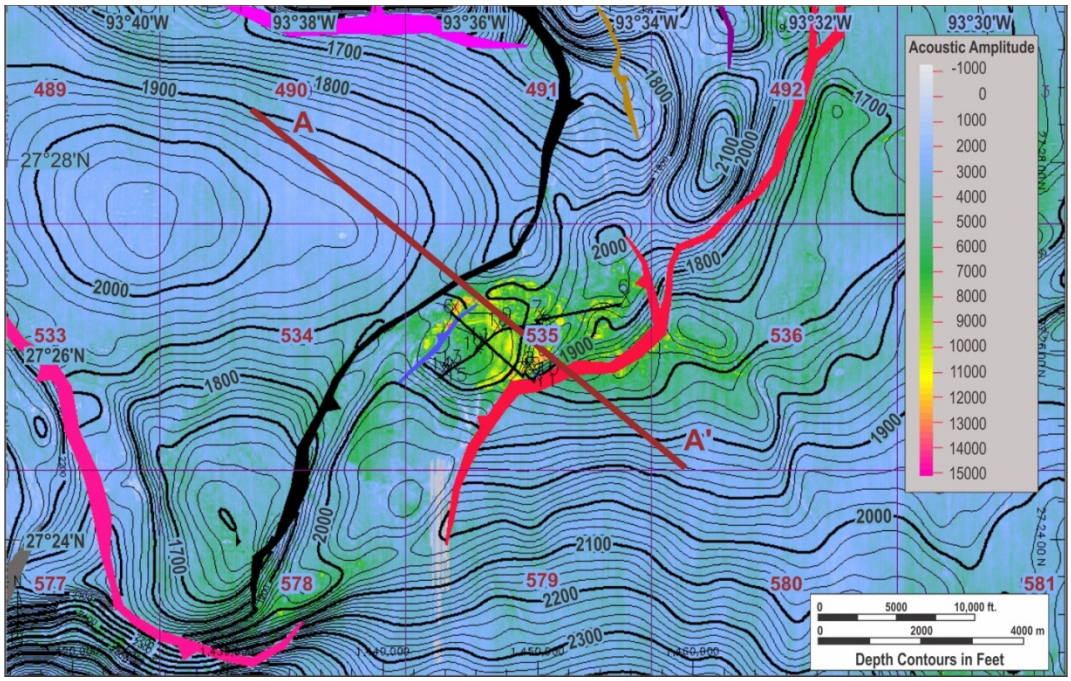

Figure 12. This combined bathymetric and 3-D seismic surface amplitude map illustrates the location of the area of interest between two NE-SW trending faults. Line A-A´ represents the location of a NW-SW oriented seismic profile through the zone of high positive surface amplitude.

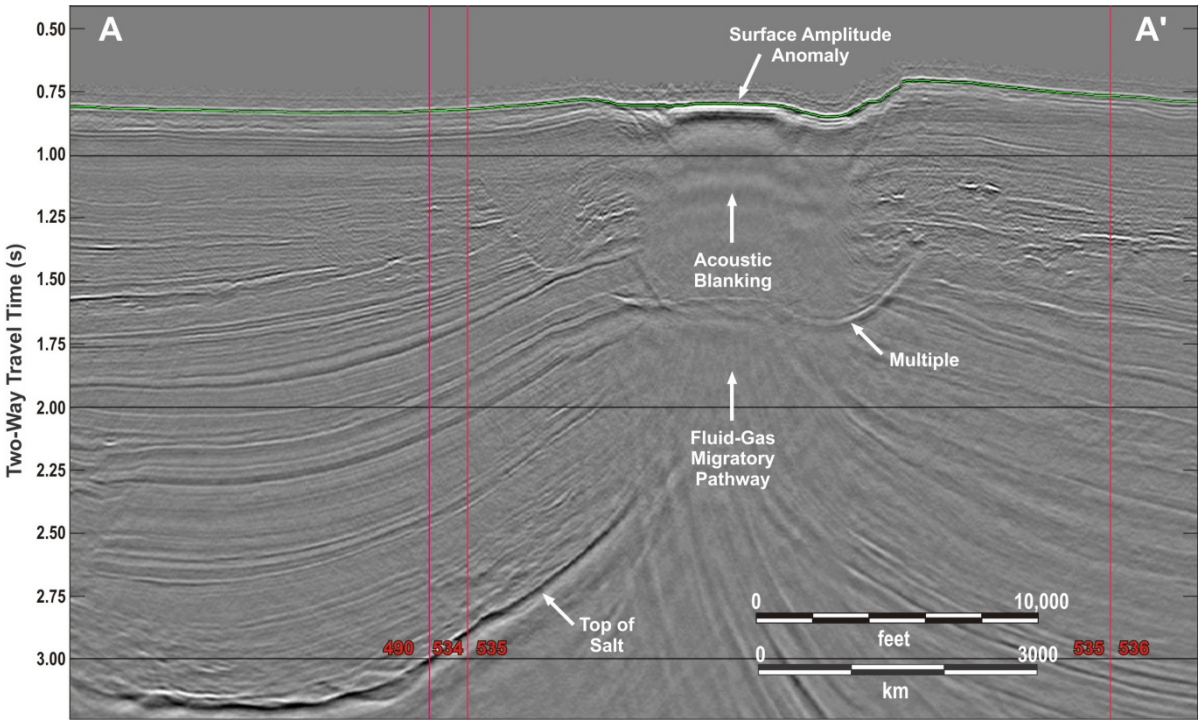

Figure 13. Seismic profile A-A´ (see Figure 12 for location) shows that the area of interest in GB 535 is a graben bound by two families of regional NE-SW trending faults (see Figure 12). A clear migration pathway for fluids and gases from the deep subsurface is indicated by a

vertically-oriented pattern of both acoustic blanking and acoustic turbidity. The surface amplitude anomaly is a bathymetric low bound by relatively higher relief seafloor on either side of the NE-SW tending regional faults. The bright amplitude anomaly just below the sea floor in the graben may represent a combination of trapped gas and base of the gas hydrate stability zone elevated in the sedimentary section by heat flow up the migration pathway.

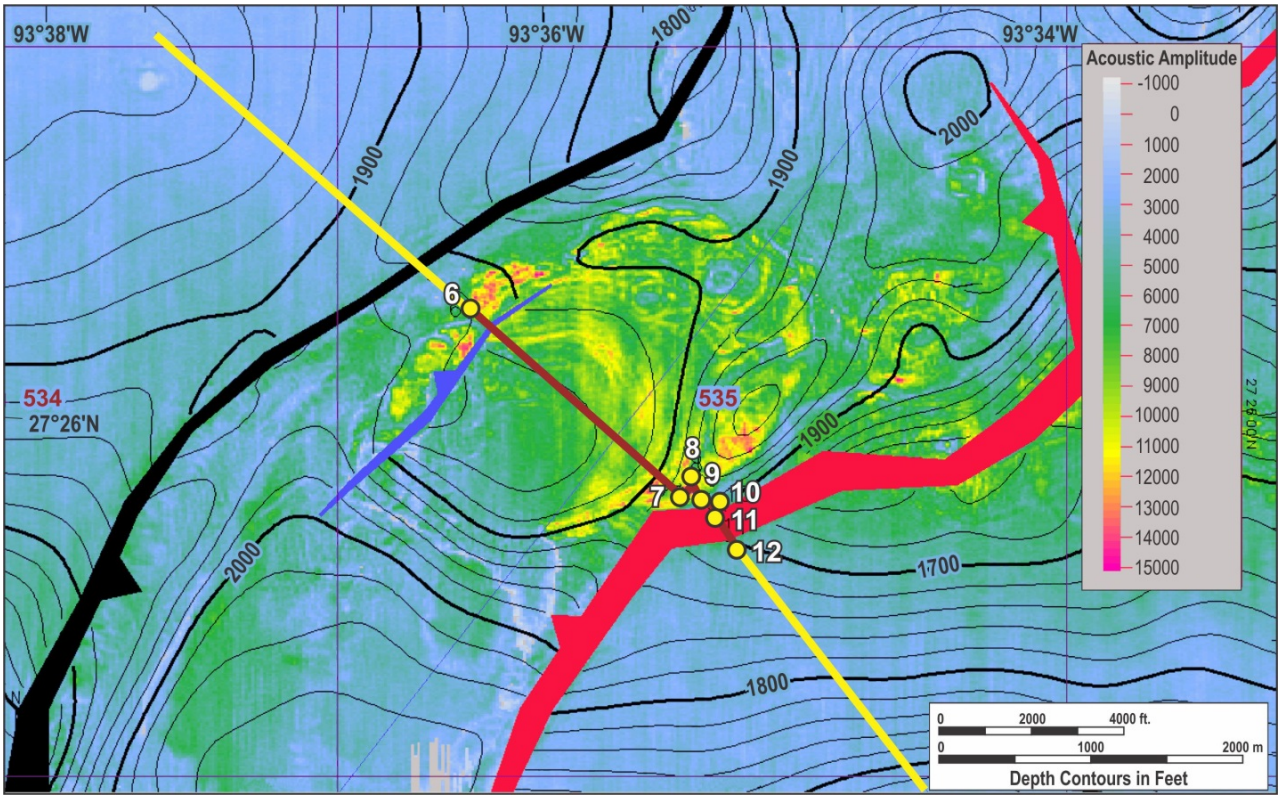

Figure 14. This combined bathymetry and 3-D seismic surface amplitude map of the area of interest in GB 535 illustrates the dive transect and the fix point locations of bottom features that are compared to 3-D seismic surface amplitude response.

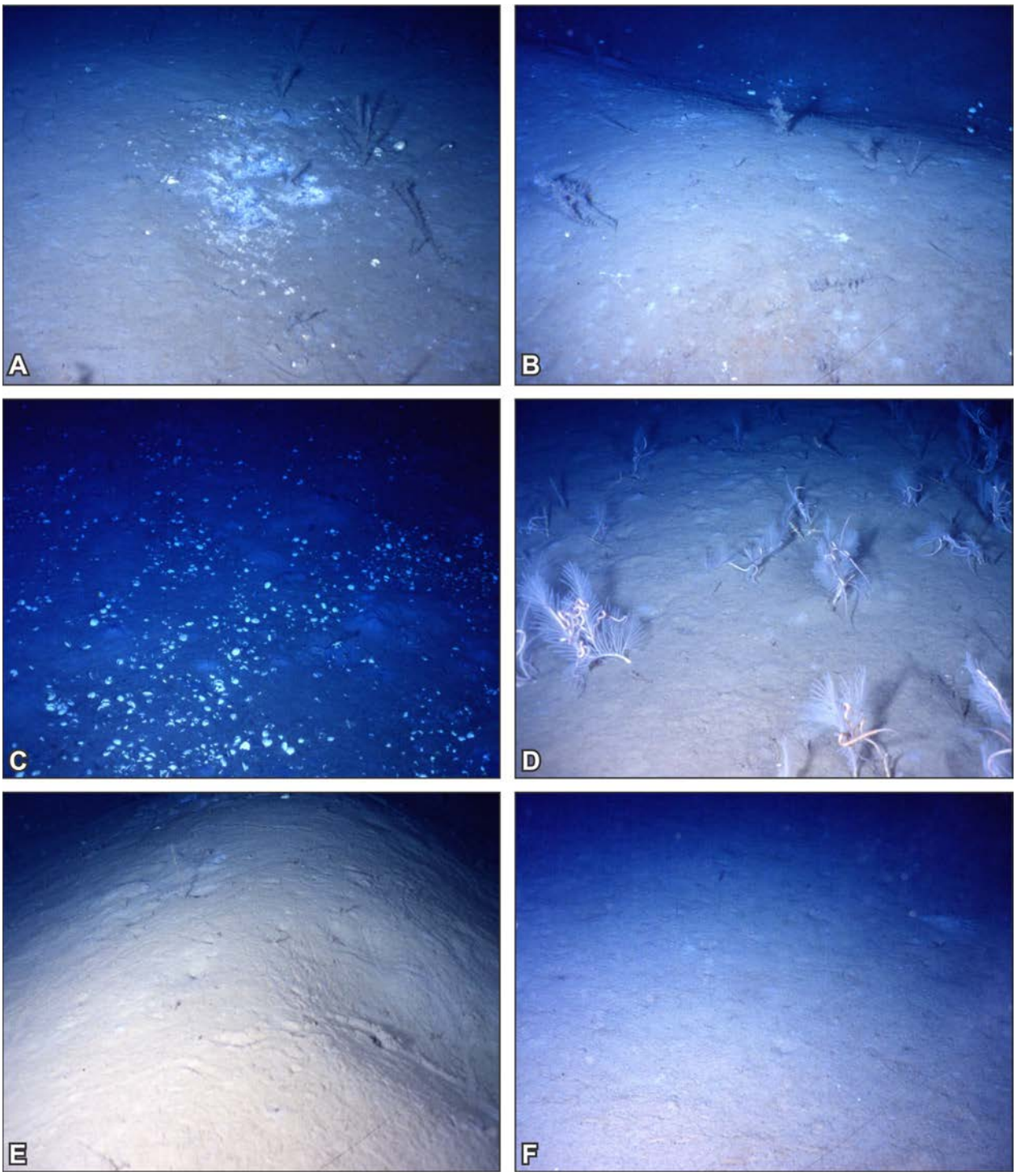

Figure 15. These photographs are typical of various sectors of the 3-D seismic surface amplitude map illustrated in Figure 14. (A) This photograph is typical of the high amplitude zone surrounding Fix Point 6. White bacterial mats, lucinid-vesycomyid clams, and nodular masses of authigenic carbonate in the fine-grained surface sediments are common to this area. Gorgonians are attached to both shells and authigenic carbonate masses distributed in the surface sediments at this site. (B) At

Fix Point 7, near the fault that functions as the eastern boundary of the high positive surface amplitude zone, the sea floor is characterized by undulating topography and scattered, occasional surface concentrations of clam shells. Scattered gorgonians indicate the presence of hard substrate (shells and authigenic carbonates). (C) The high surface amplitude at Fix Point 8 is a reflection of a hard bottom created by a high concentration of lucinid-vesycomyid clam shells. (D) Numerous sea pens hosting snake-like eels characterize Fix Point 9. The occurrence of this community indicates hard substrate beneath the fine-grained hemipelagic sediment cover. (E) In the fault zone at Fix Point 11 the bottom topography consists of a series of parallel and low relief ridges as featured in this seafloor photograph. No indicators of present or past hydrocarbon seepage are visible at the sediment-water interface. Burrows and trails are present in the surface sediments. Low background surface amplitude is typical of this site. (F) Burrowed, hemipelagic sediment characterizes this site which is well outside the zone of high positive surface amplitude response. The across-photo field of view dimensions in the above six photographs ranges from approximately 12-25 ft (4-6 m).

7.2 Case Investigation: Green Canyon 232 (GC 232)

7.2.1 Location and Geologic Setting

The Green Canyon lease area is perhaps the sector of the northern Gulf of Mexico continental slope with the highest number of active oil and gas seeps and more energetic vents. Block 232 is located on a roughly E-W trending arcuate faulted ridge that separates two upper continental slope sedimentary basins (Figure 16). Water depths within GC 232 range from approximately 2600 ft. (793 m) in the SW corner of the block to approximately 1800 ft. (549 m) in the extreme NE corner. The area of interest and the area where the Johnson Sea-Link dives were made for ground truth observations and samplings occurs near the fault illustrated in Figures 17 and 18 which offsets the sea floor in the NE corner of the block.

A seismic profile through the area of interest, Figure 18, illustrates that the highly reflective areas at or near the seabed are small and primarily located at or close to the intersection of the regional fault with the sea floor. The highly reflective sea floor areas of interest are associated with an extensional fault located at the northern boundary of a well-defined intraslope basin. This fault is obviously the oil and gas migration pathway to the sediment-water interface and is part of a crestal fault family related to a shallow salt body. The arcuate fault that cuts through GC 232 intersects a salt mass at depth that focuses migration vertically to the sea floor SW of the site where submersible-acquired observations and supporting samples were collected (Figures 17 and 18).

7.2.2 Sea Floor Amplitudes and Surface Geology

Figures 17 and 19 illustrate the 3-D seismic surface amplitude data plotted on the bathymetry and basic structure of the GC 232 area of interest. Amplitude patterns of various strengths are scattered around the fault trend and the largest pattern of surface amplitudes is to the south of the regional fault cutting across the block (Figures 17, 18, and 19). One strikingly obvious pattern in the surface amplitudes is that very low reflectivity is associated with the areas directly surrounding the fault. In fact, a narrow zone of low acoustic amplitude or low reflectivity actually defines the fault trend. Higher amplitude areas are scattered around the fault trend, but occur primarily to the south of it. Figure 18, the seismic profile through the area clearly defines several deep-cutting faults that are obvious pathways for fluid-gas migration to the modern sea floor. “Bright spots” or highly reflective areas occur in the subsurface along the major faults. These “bright spots” are mostly concentrated near or at the sea floor.

7.2.3 Interpretation of 3-D Seismic Sea Floor Amplitudes Using “Ground Truth” Data

The ground truth conducted from the Johnson Sea-Link research submersible was initiated on a transect designed to start in a zone of “background” surface reflectivity and move toward the regional fault so as to encounter the zone of low sea floor amplitudes surrounding the fault (Figure 19). As illustrated by the bottom photograph at the transect starting point, Fix 1 (Figure 19), the seabed was generally featureless except for surface sediment disturbances related to bioturbation (Figure 20A). However, moving a short distance toward the fault

produced a dramatic change in sea floor characteristics, Fix 2. Densely populated chemosynthetic communities were encountered along with impressive low-relief outcrops of orange-yellow gas hydrate (Figure 20B). Small amounts of authigenic carbonate were found associated with both the tubeworm assemblages and the mussel beds. Several bubble streams of escaping gas were observed at the edges of the gas hydrate outcrops and in association with the mussel beds. This area was not represented in the 3-D seismic surface amplitude dataset as a high amplitude or reflective zone. The relationship was quite the opposite.

Moving short distances from Fix 2 to Fix Points 3, 4, and 5 the bottom morphology was mounded and gas hydrate was observed cropping out along the mound edges and sometimes at the tops of the mounds. Small densely packed mussel beds and aggregations of tubeworm "bushes" were found at Fix Points 3 and 4 (Figures 19 and 20C and D). Figure 20E illustrates an outcrop of gas hydrate at the apex of a low-relief mound at Fix 5. These types of mounds were scattered throughout the area near the fault. White and orange bacterial mats associated with areas of dark reducing sediment were also commonly observed (Figure 20F).

7.2.4 Summary

The relationship between 3-D seismic surface amplitudes and characteristics of the sea floor in the GC 232 area seem somewhat contradictory. Hydrocarbons are clearly migrating to the ocean bottom in this region and gas hydrate deposits plus densely populated mussel and tubeworm communities have developed in a fairway that parallels the regional fault that cuts across the lease block. Instead of a highly reflective seabed as might be expected, a zone surrounding the fault has less reflectivity than the "background" area characterized by a surface cover of hemipelagic sediments that are not impacted by hydrocarbon seepage. Two possible explanations are put forward to explain this apparent contradiction.

First, numerous bubble streams of escaping gas were observed throughout the area where the Johnson Sea-Link transited the area. Numerous gas hydrate outcrops observed in the area support the observation that gas is being steadily supplied from the subsurface up the faulted zone that intersects the present sea floor. Ridge-like morphology of the sea floor near the area where the major fault is projected to encounter the seabed suggests a "fault zone" with several minor antithetic faults associated with the main fault. This setting suggests the presence of several migration pathways for fluids and gas to reach the sea floor. The presence of gas-saturated sediment would produce a low reflectivity response similar to the vent of a mud volcano. In addition, even though the area has chemosynthetic communities and gas hydrate outcrops, sizeable areas of authigenic carbonate hardgrounds and outcrops are missing.

Second, the steepness of the fault and the fact that there may be multiple faults suggests that the faults may possibly reflect a significant portion of the incident acoustic energy. Such deflection of seismic energy would certainly reduce surface amplitude values. Perhaps these unusually low reflectance areas of the seabed along the fault are a combination of these two potential mechanisms.

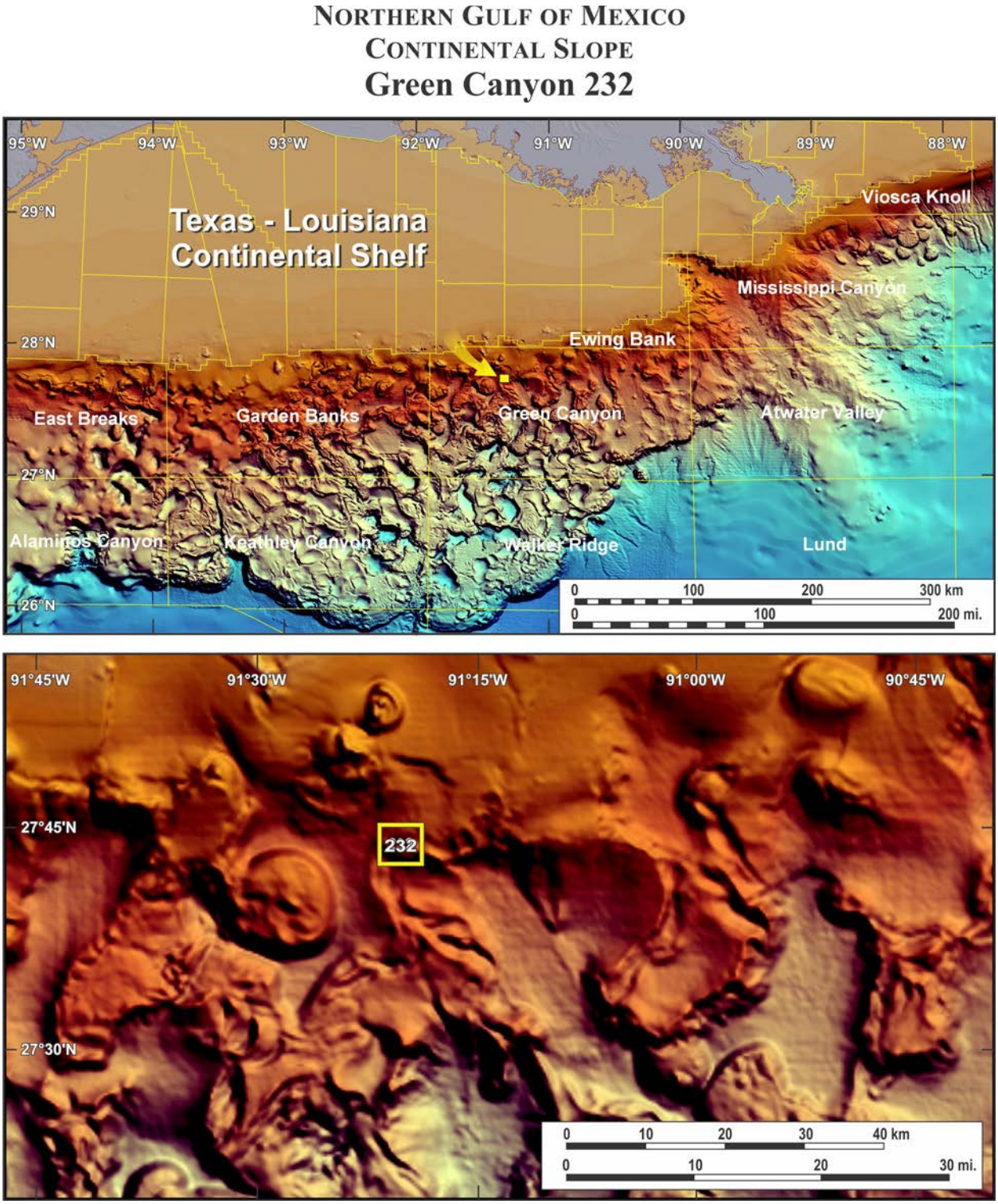

Figure 16. (A) Shaded multibeam bathymetry map of the continental slope of the northern Gulf of Mexico. The yellow arrow indicates the location of Green Canyon Block 232 (GC 232). (B) The enlarged area of the continental slope surrounding GC 232 illustrates the bathymetric features within and surrounding this block.

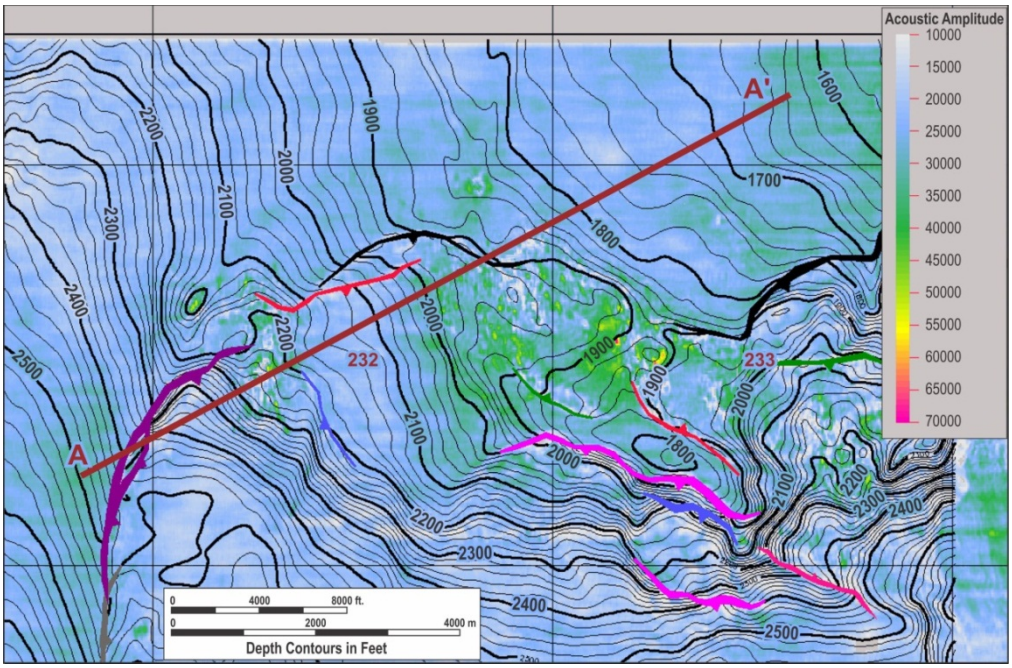

Figure 17. This combined bathymetric and 3-D seismic surface amplitude map illustrates that the area where the dive was made is essentially at the point of convergence of an E-W trending fault and the sea floor. Surface amplitudes at the dive sites constitute both small and isolated moderate positive and low positive zones. A lack of high positive 3-D seismic surface amplitudes at the dive sites may be related to the reflection of acoustic energy by the steep fault that cuts through the area of interest.

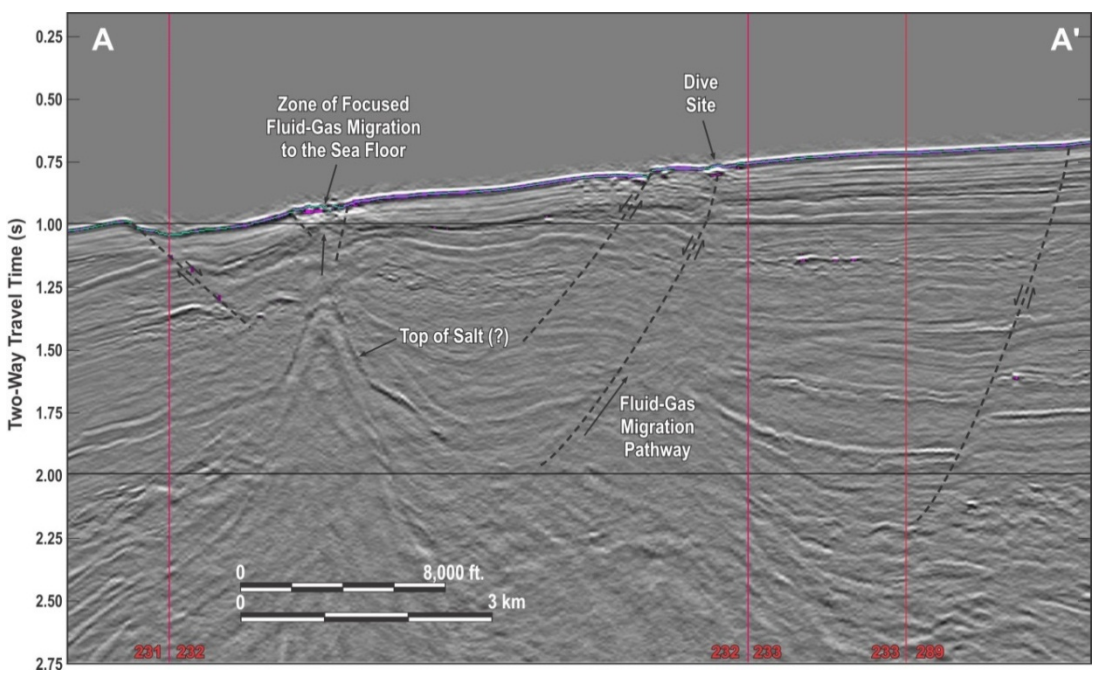

Figure 18. Seismic profile A-A´ (see Figure 17 for location) illustrates that the area of interest is essentially where the E-W trending fault intersects the seafloor. This area shows the local effects of hydrocarbon seepage to the sea floor. The regional fault is the obvious migration pathway for fluids and gases to the continental slope surface.

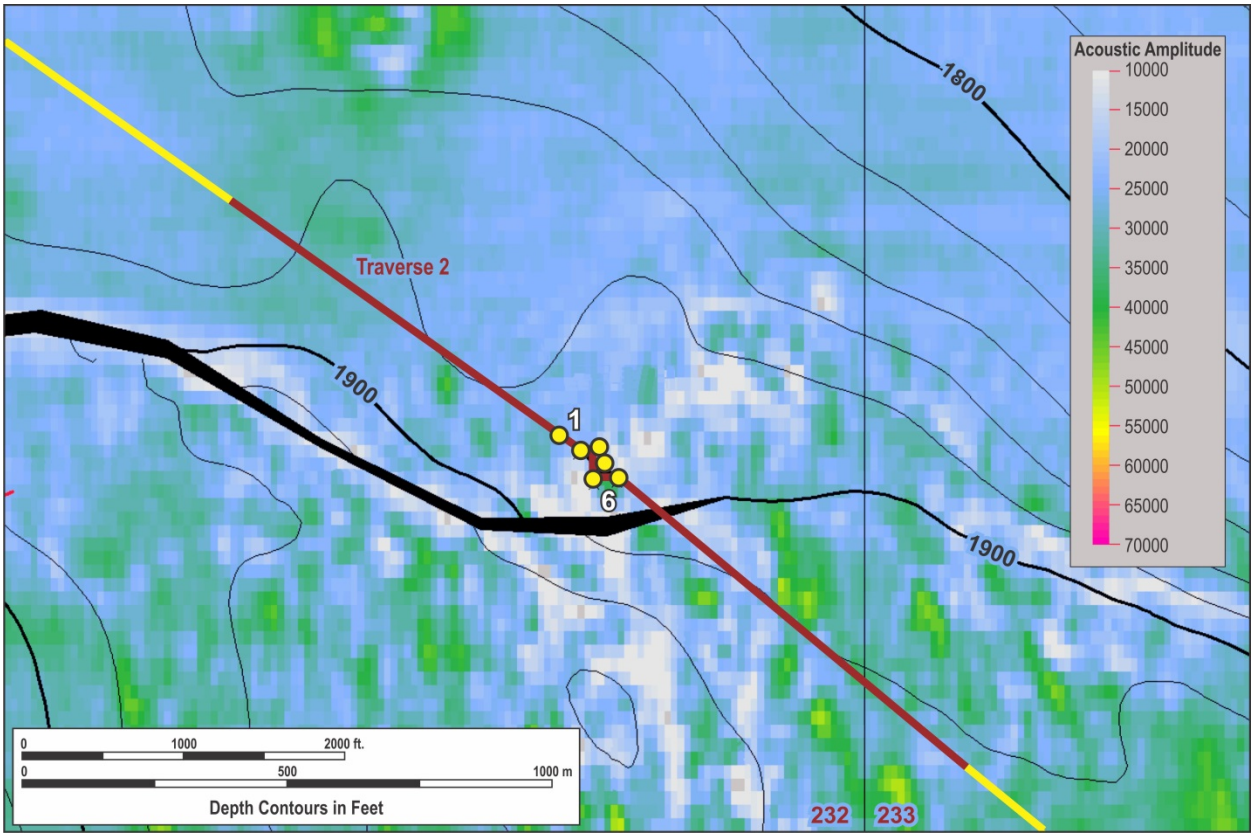

Figure 19. This combined bathymetric and 3-D seismic surface amplitude map of the area of interest in GC 232 indicates the fix points where observations were made to compare bottom features to 3-D seismic surface amplitude response.

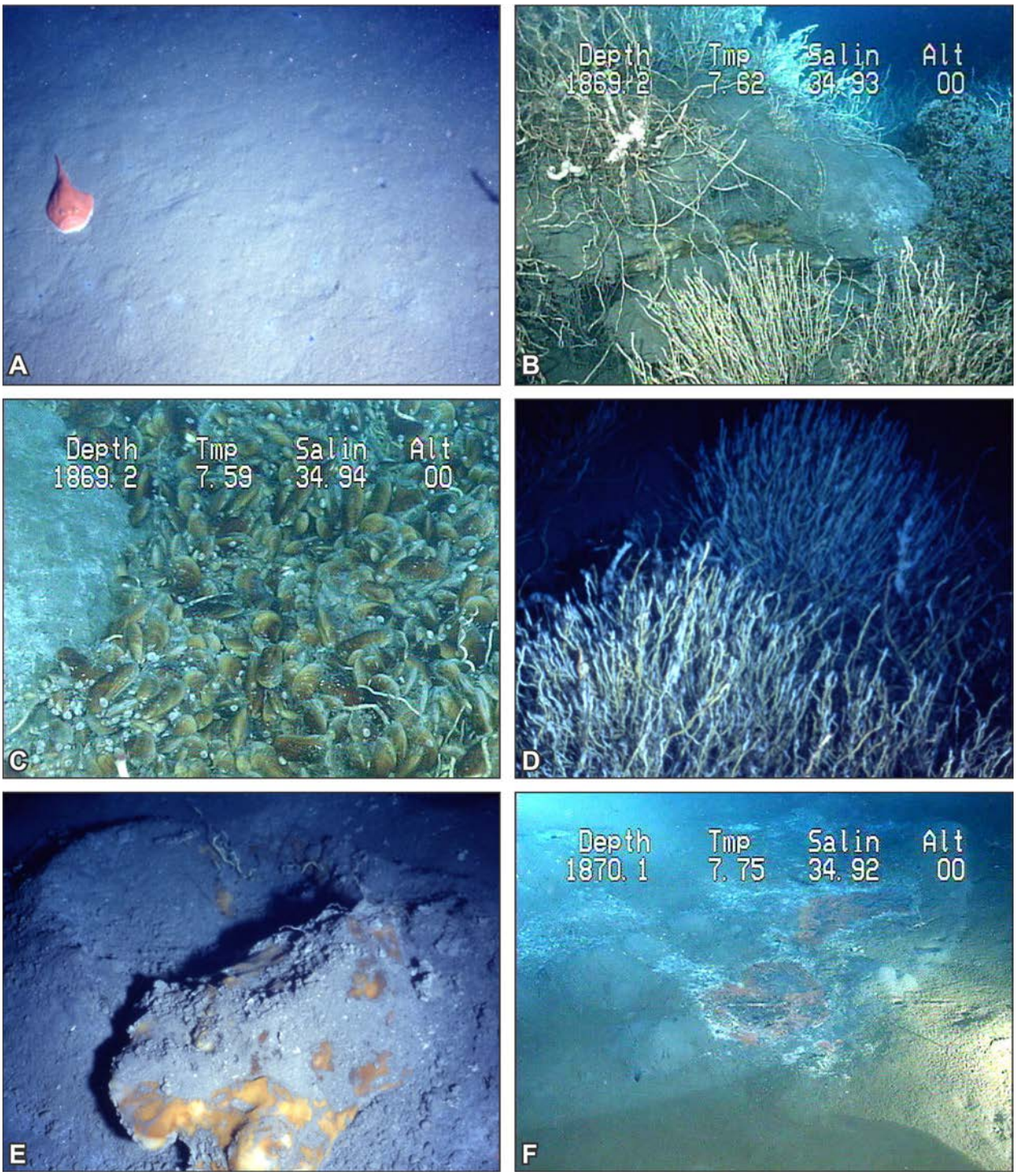

Figure 20. These photographs are typical of the sea floor at the fix points illustrated in Figure 19. (A) This picture is at Fix 1 which is outside of the zone impacted by hydrocarbon seepage. Burrowed hemipelagic sediments are illustrated in this picture. A low positive 3-D seismic surface amplitude response is characteristic of this site. (B) Once in the zone of hydrocarbon seepage, outcrops of authigenic carbonates, gas hydrates, and tubeworm-mussel communities are common. The

orange-yellow "seam" in this picture is gas hydrate. Several small gas bubble streams are visible escaping from the bottom at this site. (C) Beds of living mussels like the ones in this picture are scattered throughout the area in a narrow zone following the regional fault. (D) Multiple tubeworm "bushes" are common in the zone paralleling the E-W trending fault that runs through the area. They were observed and sampled using the Johnson Sea-Link submersible. (E) In addition to outcrops of carbonates invaded by gas hydrate, several examples of isolated gas hydrate were found at the GC 232 dive site area. This picture illustrates one example of gas hydrate exposed in a low relief mound on the sea floor. (F) Both red and white bacterial (*Beggiatoa* sp.) mats occur in the area between tubeworm aggregations and mussel beds. The across-photograph field of view dimensions for the photographs of this figure are about 6-12 ft (2-4 m) except for photographs C and E which are approximately 3 ft (1 m).

7.3 Case Investigation: Green Canyon 238 (GC 238)

7.3.1 Location and Geology Setting

Green Canyon 238 is located on the upper continental slope to the east of GC 232 on the flank of a well-defined intraslope basin SW of the block (Figure 21). This location is due south of Terrebonne Bay along the central Louisiana coast. A regional fault trending NW-SE runs through GC 238 (Figure 22). South of the fault the sea floor slopes uniformly to the S-SW with water depths changing from approximately 2000 ft (610 m) in the NW corner of the block to about 2460 ft (750 m) at the block's SW corner.

The fluid-gas migration pathway to the highly reflective area of sea floor in GC 238, as revealed by 3-D seismic data, is controlled by a vertical salt weld. A series of "step-down" faults related to the weld W-SW of the high 3-D seismic surface amplitude area is related to the salt weld. It appears that buoyancy-driven vertical migration to the sea bed originates from one of these step-down faults.

7.3.2 Sea Floor Amplitudes and Surface Geology

The major fault that cuts across GC 238 is downthrown to the north with several less significant faults paralleling its trend (Figure 22). Bathymetry of the sea floor north of the most significant fault is very complex. A distinctly mounded feature occurs in this part of the lease block and is the subject of this case investigation. The mound is bound on its SW flank by shallower sea floor and a series of faults (Figure 23). Both the seismic profile of Figure 23 and the combined bathymetry and 3-D seismic surface amplitude maps of Figures 22 and 24 indicate that the sea floor associated with the crestal part of this mound is highly reflective (high positive sea floor amplitude). The high amplitude area occurs at the crest of the low-relief mound that occurs between water depths of approximately 2320 ft (707 m) and 2275 ft (694 m).

7.3.3 Interpretation of 3-D seismic Sea Floor Amplitudes Using "Ground Truth" Data

A submersible transect oriented roughly N-NW to S-SW was conducted across the GC 238 mounded area of elevated 3-D seismic sea floor amplitude response in order to gather information about the seabed that could be compared to the remotely sensed seismic data. Observational sites along the transect started well outside of the zone of elevated sea floor amplitudes, Fix 1 on the northern flank of the mound (Figure 24). At this starting point in a region of "background" surface reflectance values (Figure 24), the sea floor was covered with hemipelagic sediments and appeared featureless except for the effects of tracks-trails and burrowing by various types of benthic fauna (Figure 25A).

As the area of increasing surface reflectivity on the 3-D seismic surface amplitude map of Figure 24 was approached (Fix 2) the character of the sea floor changed considerably. A uniform cover of hemipelagic sediments was replaced by the appearance of numerous white and orange bacterial (*Beggiatoa* sp.*)* mats (Figure 25B). These areas of bacterial mat development were associated with dark reducing sediments and numerous small gastropod shells on the

surface. These areas of obvious slow hydrocarbon flux to the seabed were also associated with scattered disarticulated lucinid-vesycomyid clam shells.

As the crest of the high reflectivity mound was approached, (Figure 24, Fix 3), the bottom developed a low-relief surface roughness which was the product of local sea floor lithification, resulting in nodular masses of authigenic carbonate in the surface sediments along with scattered clam and mussel shells (Figure 25C). White and orange bacterial mats occurred throughout this area and small beds of living mussels were scattered over the area and tended to occur in slight depressions where bacterial mats were common. On top of the mounded area between Fix Points 3 and 4 (Figure 24), an area of moderate-to-low reflectivity on the 3-D seismic amplitude map (Figure 24) with few signs of seepage to the seabed, an amazing population of brittle stars was observed (Figure 25D).

At the SE edge of the high 3-D seismic surface amplitude area of mound, near Fix 4 (Figure 24) more orange and white bacterial mats, small aggregations of mussels, and scattered clam shells were found (Figure 25E). Like other areas of the mound top, this S-SE flank of the mound displayed a sea floor covered with small-scale nodular masses of authigenic carbonate. Farther down the SE flank of the mound, near Fix 5, a large hard coral community was encountered (Figure 25F). This colony appeared to be growing on a substrate of authigenic carbonate. Small-scale carbonate debris was scattered over the sea floor in this area.

At the end of the transect, Fix 6 (Figure 24), the sea floor was blanketed by hemipelagic sediments that showed no signs of hydrocarbon seepage or hard bottom development. Figure 24 illustrates that the ocean bottom surrounding this location was not very reflective and therefore had a low-positive 3-D seismic sea floor amplitude character.

7.3.4 Summary

The GC 238 mound is a clear example of a well-defined 3-D seismic sea floor amplitude anomaly. It is faulted on the SW flank, but otherwise slopes rather uniformly away from a mound crest that is relatively flat at a water depth of approximately 2250 ft (686 m). The highest amplitudes are associated with this crestal area and upper flanks of the mound, particularly the SE part. There is no question that the crest and upper flanks of the mound display sea floor characteristics much different from start and end points of the Johnson Sea-Link transect. Both ends of the transect are in hemipelagic sediments with no indicators of hydrocarbon seepage or hard bottom conditions. However, the other sites along the transect display indicators of a slow flux setting where hydrocarbons are very slowly migrating to the seabed from deep within the subsurface. A clear migration pathway from the deep subsurface is identified to the mound by acoustic blanking on seismic profiles transecting the area of interest.

Moderate-to-high reflectivity of the mounded sea floor appears to be related primarily to nodular authigenic carbonates that have formed in the surface sediments, mussel shells, and clamshells. However, because the seabed reflector incorporates approximately 20-25 ft (6-8 m) of the uppermost sedimentary section, the “sea floor amplitude” is an integrated signal over this interval and buried hardgrounds and shell accumulations may be adding to the “surface reflectivity.”

At the NW margin of the mound a low-moderate tongue of sea floor amplitudes extends into deeper water away from the mound crest. This feature may represent the reflection of a fluidized sediment flow deposited during a period when fluid expulsion from the mound crest was active, unlike the low seepage seen today. The seismic profile of Figure 23 supports a highly reflective layer in the shallow subsurface perhaps representing a more active period of hydrocarbon seepage-to-venting. Regardless of today's low flux setting, the moderate-to-high 3-D seismic sea floor amplitudes identified the GC 238 mound as an area with "hard bottoms" and hydrocarbon seepage.

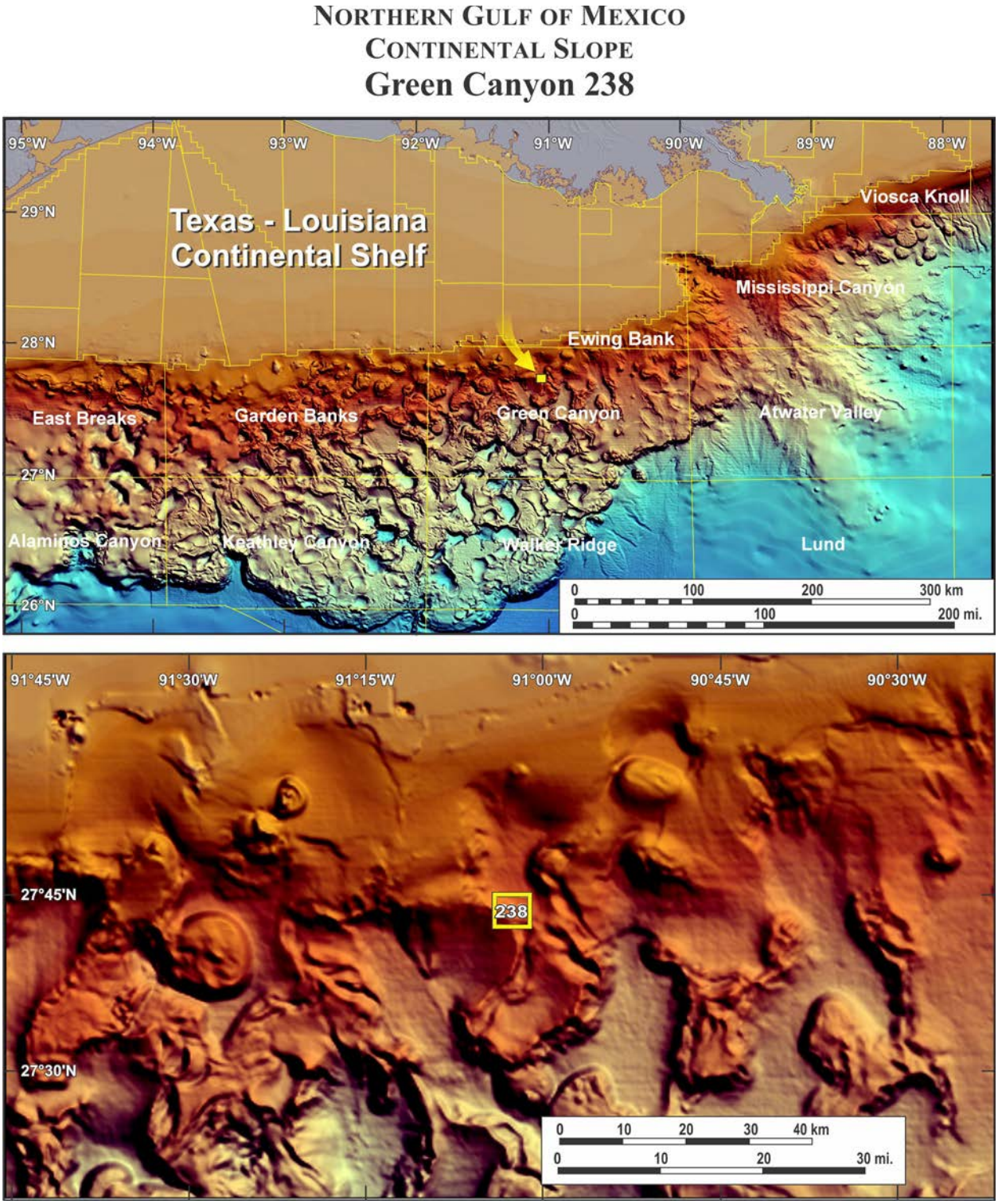

Figure 21. (A) Shaded multibeam bathymetry map of the continental slope of the northern Gulf of Mexico. The yellow arrow indicates the location of Green Canyon Block 238 (GC 238). (B) The enlarged area of the continental slope surrounding GC 238 illustrates the bathymetric features within and surrounding the block.

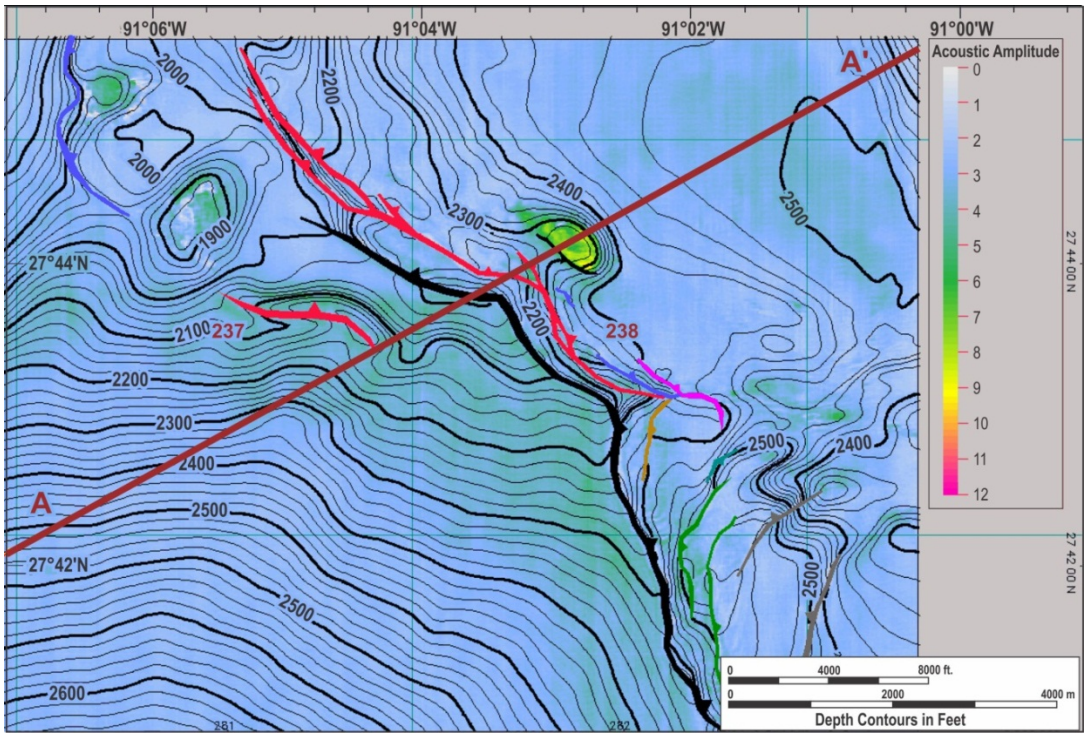

Figure 22. This combined bathymetric and 3-D surface amplitude map illustrates the location of the area of interest downthrown to the NW-SE oriented regional fault. The slightly elevated mound-like area of high surface amplitude constitutes the area of interest.

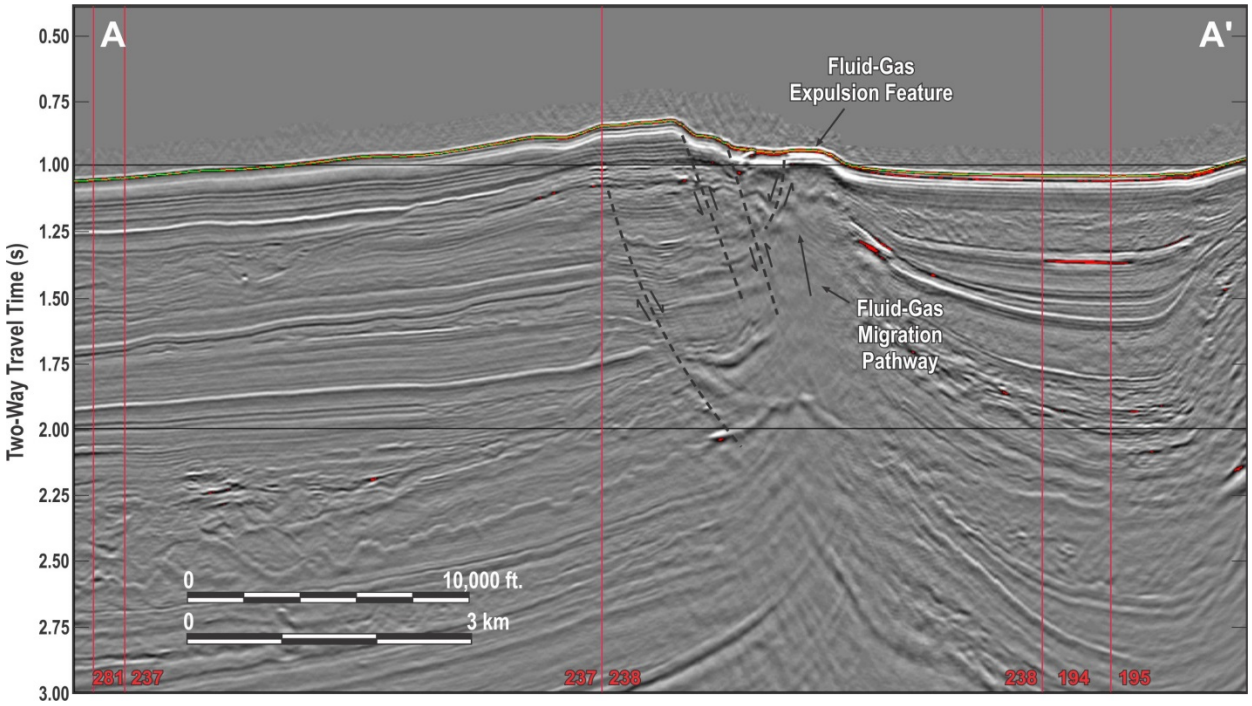

Figure 23. Seismic profile A-A´ (see Figure 22 for location) shows that the area of interest is a mounded high positive surface amplitude zone downthrown to several NW-SE trending faults. The high amplitude zone has a well-defined vertical migration pathway beneath it.

The vertical migration pathway is characterized by upturned bedding on its flanks and acoustic blanking. It appears that buoyancy-driven vertical migration of fluids-gases to the GC 238 sea bed arises from the surface of the easternmost step-down fault. No clear expression of subsurface salt is visible in this seismic profile. However, deeper penetrating data indicate that the migration pathway from the deep subsurface is along a clearly defined salt weld.

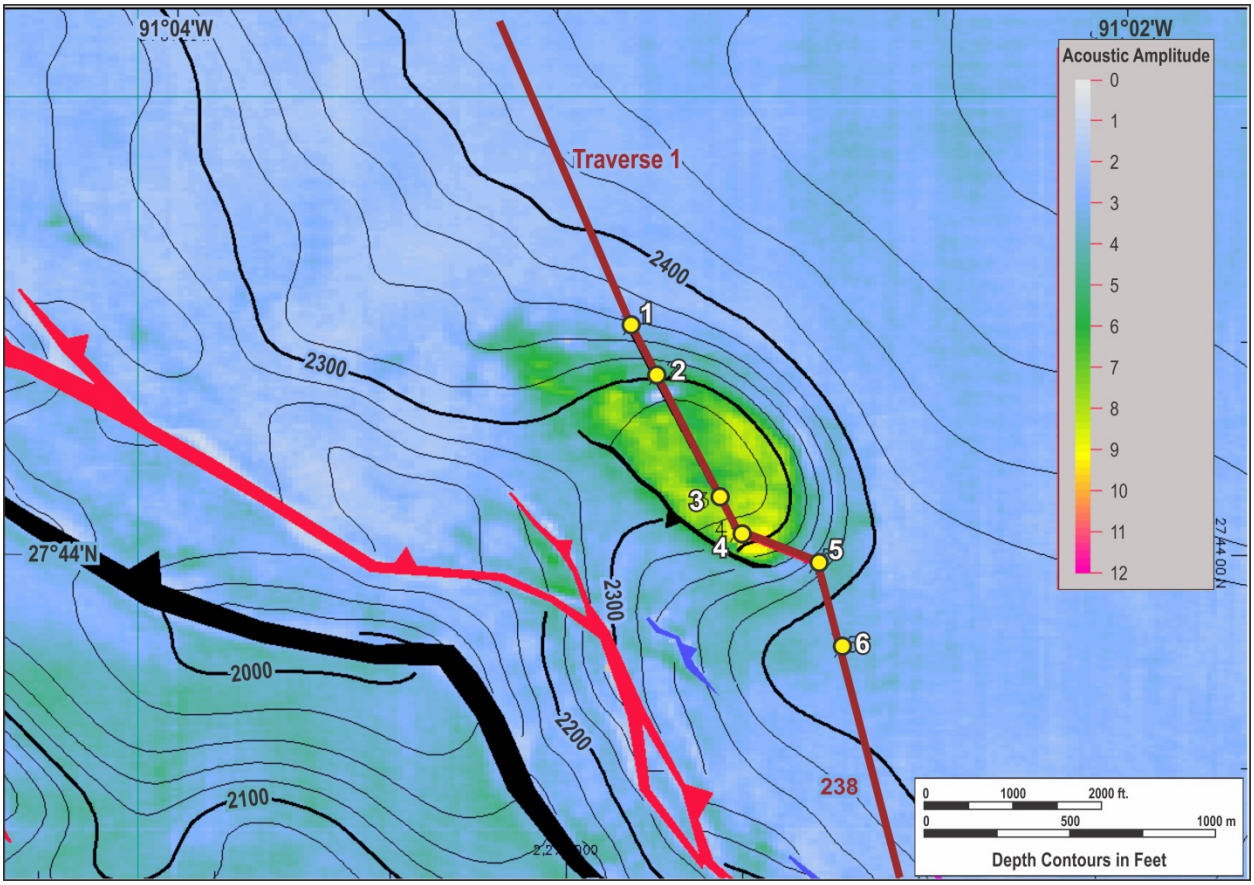

Figure 24. This combined bathymetric and 3-D seismic surface amplitude map of the area of interest in GC 238 illustrates the dive transect and fix points where bottom features are compared to 3-D seismic surface amplitude response. The low relief mounded area that has a high positive surface amplitude is clearly displayed downthrown to two well-defined NW-SE trending faults.

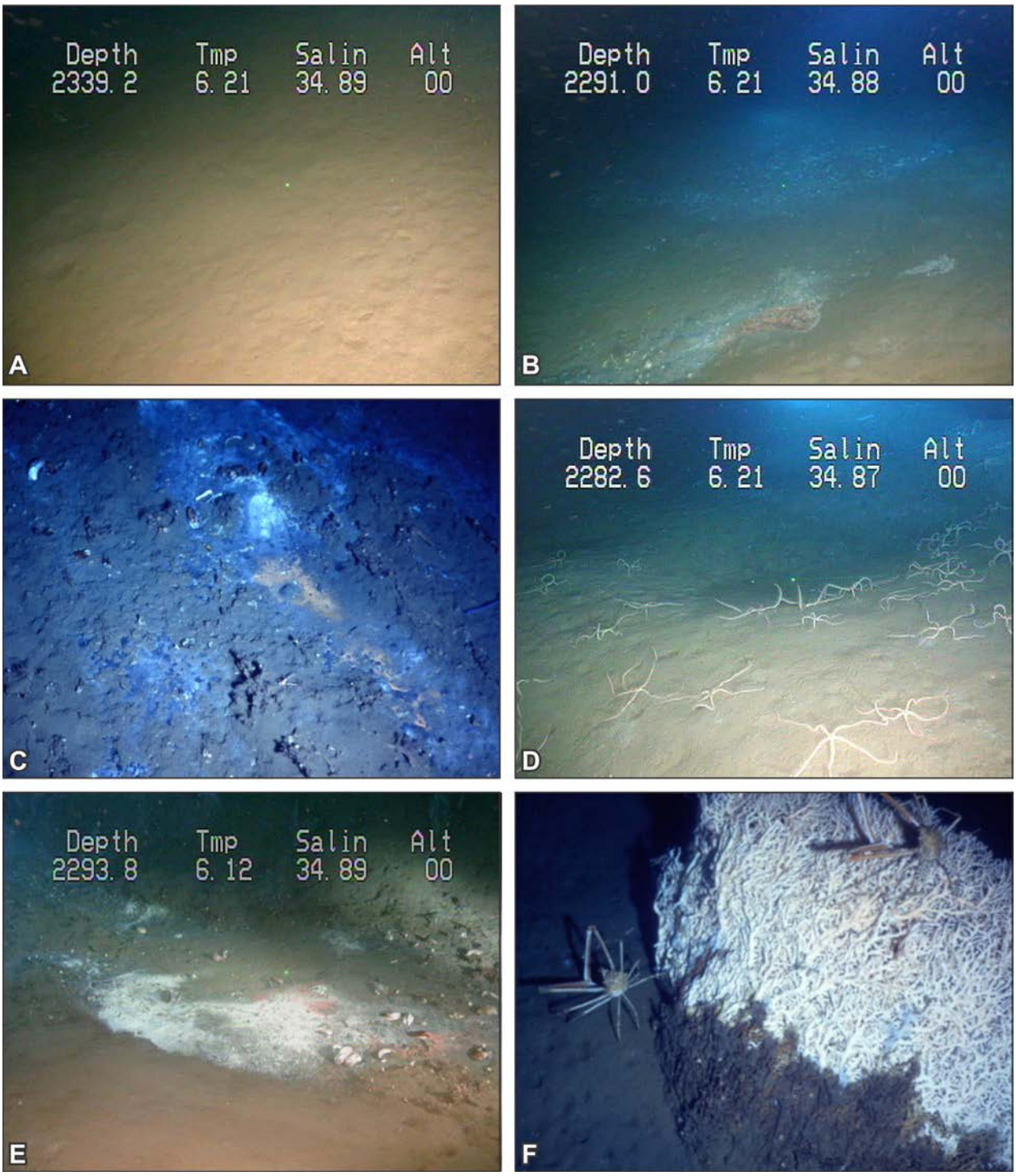

Figure 25. These photographs are related to the fix points associated with the dive transect illustrated in Figure 24. (A) At Fix Point 1 is in the zone of "background" surface amplitude response on the NW flank of the area of interest. The bottom is characterized by burrowed hemipelagic sediments with no indicators of hydrocarbon seepage. (B) At the edge of the zone of increased positive surface amplitude response the seabed shows indications of seepage in the form of both

white and orange bacterial (*Beggiatoa* sp.) mats and scattered lucinid-vesycomyid clams. (C) In the area at the mound crest between Fix Points 2 and 3, the sea floor shows signs of local lithification (nodular masses), bacterial mat development (both orange and white *Beggiatoa* sp. mats), and scattered mussel shells and living mussels. (D) Between Fix Points 3 and 4 an area with no obvious signs of seepage was found to be populated with numerous brittle stars. A moderate surface amplitude characterizes this site. (E) On the SE flank of the main area of positive surface amplitude response (near Fix Point 4), numerous lucinid-vesycomyid clams inhabit this area of slow seepage along with scattered orange and white bacterial mats. (F) A community of hard corals was discovered on the SE flank of the mounded area of interest (near Fix Point 5). The cross-photograph field of view dimensions for the seafloor photographs of this figure are approximately 6-12 ft (2-4 m).

7.4 Case Investigation: Green Canyon 286 (GC 286)

7.4.1 Location and Geologic Setting

The GC 286 area of the upper continental slope is south of the Isles Dernieres along the Terrebonne Parish coast of Louisiana. Water depths in GC 286 are generally over 3000 ft (915 m), Figure 26. The feature of interest in this area is rather large mound-like feature that extends over four lease blocks, GC 286, 287, 330, and 331. The major part of the feature is in GC 286, so to simplify the discussion the location is referred to as GC 286. Bathymetry shown in Figure 27 illustrates that the large-scale mound has over 1000 ft (305 m) of relief above the sea floor of the basin SW of the mounded feature. However, as mentioned above, the main area of interest in this case investigation is in GC 286 and slightly into GC 287 along the northern crest of the mound.

The large GC 286 mounded feature occurs on a ridge-like structure separating two well-defined intraslope sedimentary basins (Figures 26 and 27). This is an extensional setting in which the shallow salt arrived after initial basin formation and then dominated the system. Two seismic profiles A-A′ and B-B′, shown on Figure 27, cross the mound and are illustrated in Figure 28. It is clear from the seismic data that the large mounded feature is salt supported. In fact, on profile A-A′ the salt almost reaches the seabed along the mound's W-NW flank. In the western part of GC 286 and eastern part of GC 287 where seismic profiles A-A′ and B-B′ intersect (Figure 27), an acoustically opaque and vertically oriented fluid-gas migration pathway to the sea floor is apparent on the seismic profiles (Figure 28). This pathway is located at the edge of the salt body that accounts for the positive relief of the mound-like feature. The sea floor of the mounded area is very reflective above the edges of the salt body. In many places, beds are highly inclined near the salt margins and fluid-gas migration appears to be buoyance driven along the flanks of the irregular salt body.

7.4.2 Sea Floor Amplitudes and Surface Geology

The surface of the GC 286 mound displays 3-D seismic sea floor amplitudes that are generally elevated above background values, especially along the mound edges (Figure 27). A particularly reflective area occurs along the northern margin of the mound. The two seismic profiles presented in Figure 28 cross in the middle of this reflective area in west-central GC 286 near the border with GC 287. This 3-D seismic surface amplitude anomaly area occurs on a relatively flat sector of the mound top between water depths of about 2800 ft (854 m) and 2740 ft (835 m), Figures 27 and 29. As stated above, this acoustically reflective area of the mound occurs at the seabed directly above a well-defined and acoustically turbid, and vertically-oriented zone that is interpreted as a fluid-gas migration pathway (Figure 28). Within this general area of scattered surface amplitude patterns, the highest amplitude areas are on the flank of a small low-relief mound on the edge of a larger feature. This mound is located on the GC 286-287 border. The apex of the feature has a low positive amplitude (Figure 29). This mound appears to be a fluid-gas expulsion feature.

7.4.3 Interpretation of 3-D Seismic Sea Floor Amplitude Using "Ground Truth" Data

Figures 29 and 30 illustrate the Johnson Sea-Link submersible transect across the area of interest in GC 286 and associated bottom photographs at key sites. Fix 6, the transect starting point, is W-SW of the region of high 3-D seismic surface amplitude response and in a area of the GC 286 mound top with a "background" level of reflectivity. At this fix point, the observational data from the seabed indicate that the bottom was covered with thoroughly burrowed hemipelagic sediments. No indicators of hydrocarbon seepage were observed in the area around Fix 6 (Figure 29).

Moving eastward along the transect to Fix 7, the hemipelagic sediments with background 3-D seismic sea floor amplitude values start to shift to more positive values, but in a scattered pattern alternating with background values. Observations of the seabed at and near Fix 7 indicate the presence of lucinid-vesycomyid clam shells visible on the surface of a thoroughly burrowed sea floor composed of hemipelagic sediments. Small, scattered white bacterial mats are also present in the vicinity of Fix 7.

Progressing to the E-NE along the Johnson Sea-Link submersible transect to Fix Points 8 and 9 (Figure 29), the 3-D seismic surface amplitude values become more positive as acoustic reflectance of the seabed increases. Figures 30C and 30D show that the sea floor is largely lithified at these sites and the bottom is covered with disarticulated lucinid-vesycomyid clam shells. Both bottom photographs at Fix Points 8 and 9 indicate that the hard bottom outcrops of carbonate rock contain abundant clam shells. Directly to the east of these two fix points, the reflectivity of the sea floor becomes lower than background suggesting that the bottom sediments are soft and may contain bubble phase gas which scatters and absorbs acoustic energy producing lower acoustic reflectance. At Fix 10, in the vicinity of the low reflectance area, small beds of living mussels and large areas of white bacterial mats were found (Figure 30E). The mussels and extensive bacterial mats support the interpretation that hydrocarbon gas, probably methane, is migrating to the sea bed in this area.

At the final fix point on the submersible transect, Fix 11, the 3-D surface amplitude values are elevated around a low-relief mounded feature with background amplitude values at the mound. Fix 11 is on the W flank of this feature and in an area where the seabed is highly reflective. Figure 30F is a bottom photograph from this highly reflective area of the mound flank. Authigenic carbonate outcrops are common to this zone that exhibits high acoustic reflectivity. In addition to sea floor lithification, abundant disarticulated clam shells are scattered over the bottom and are part of the surface sediments. The clam shells add to the acoustic reflectivity of the low-relief mound flank. This highly reflective zone is characteristic of the upper flanks of this mound (Figure 30). The Johnson Sea-Link dive was terminated before the most reflective (highest 3-D seismic sea floor amplitude) areas of the mound flank were observed, but an area of lithified sea floor was anticipated for this area.

7.4.4 Summary

The large mounded feature of interest covers parts of four lease blocks, but is mostly in GC 286. It is salt-supported and has well-defined pathways for the migration of fluids-gases from the deep subsurface to the modern seabed, especially along the flanks of the underlying salt body. Acoustic blanking on the seismic profiles that cross the area of interest identify the interpreted hydrocarbon migration routes. Where these areas of acoustic blanking meet the sea floor moderate-to-high positive 3-D seismic surface amplitude values result.

Along the Johnson Sea-Link submersible transect, background areas of low positive values of acoustic amplitude correlated with burrowed hemipelagic muddy sediments. As acoustic amplitude values increased along the transect, indicators of hydrocarbon seepage such as bacterial mats and scattered lucinid-vesycomyid disarticulated clam shells appeared. The highest positive sea floor amplitudes correlated to areas with scattered authigenic carbonate hardgrounds and associated clam shell beds. Although some living mussels were observed in these zones of high acoustic reflectivity, clam beds and carbonates were clearly the most abundant. The carbonate hardgrounds were found to be composed of cemented clam beds, suggesting the maintenance of environmental conditions favorable to a sizeable clam population over long time periods. Two mounded sea floor features along the submersible transect had low positive acoustic amplitudes at the apex of each mound and higher amplitudes on the mound flanks. These characteristics are consistent with mounds built by sediment expulsion onto the sea floor. Extruded sediments laced with hydrocarbons are known to support sizeable lucinid-vesycomyid clam populations.

NORTHERN GULF OF MEXICO
CONTINENTAL SLOPE
Green Canyon 286-287-331

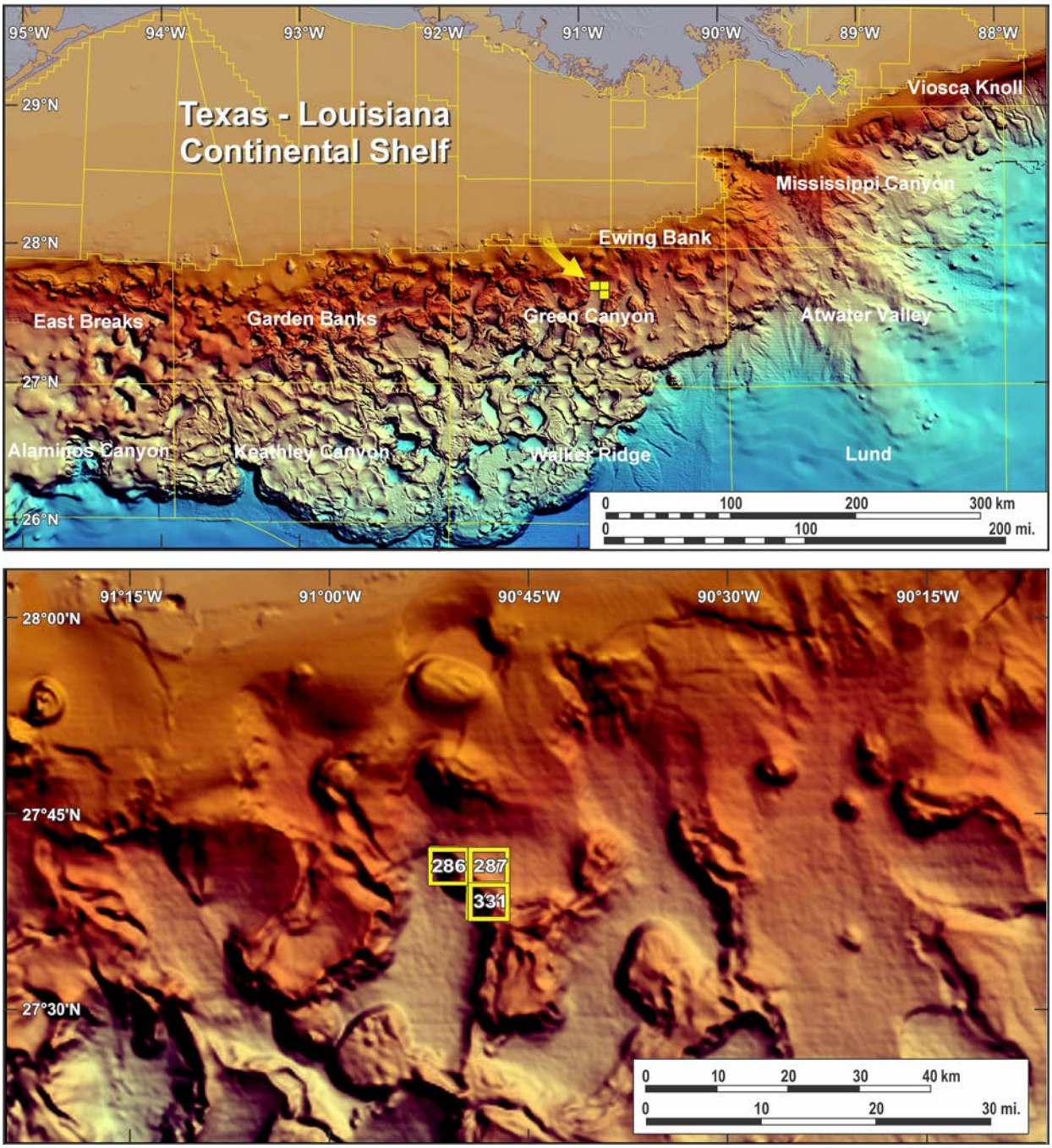

Figure 26. (A) Shaded multibeam bathymetry map of the continental slope of the northern Gulf of Mexico. The yellow arrow indicates the location of Green Canyon Block 286 (GC 286) along with adjacent blocks 287 and 331. Collectively, they constitute the area of interest. (B) The enlarged area of the continental slope in the vicinity of GC 286 illustrates the bathymetric features in this part of the continental slope.

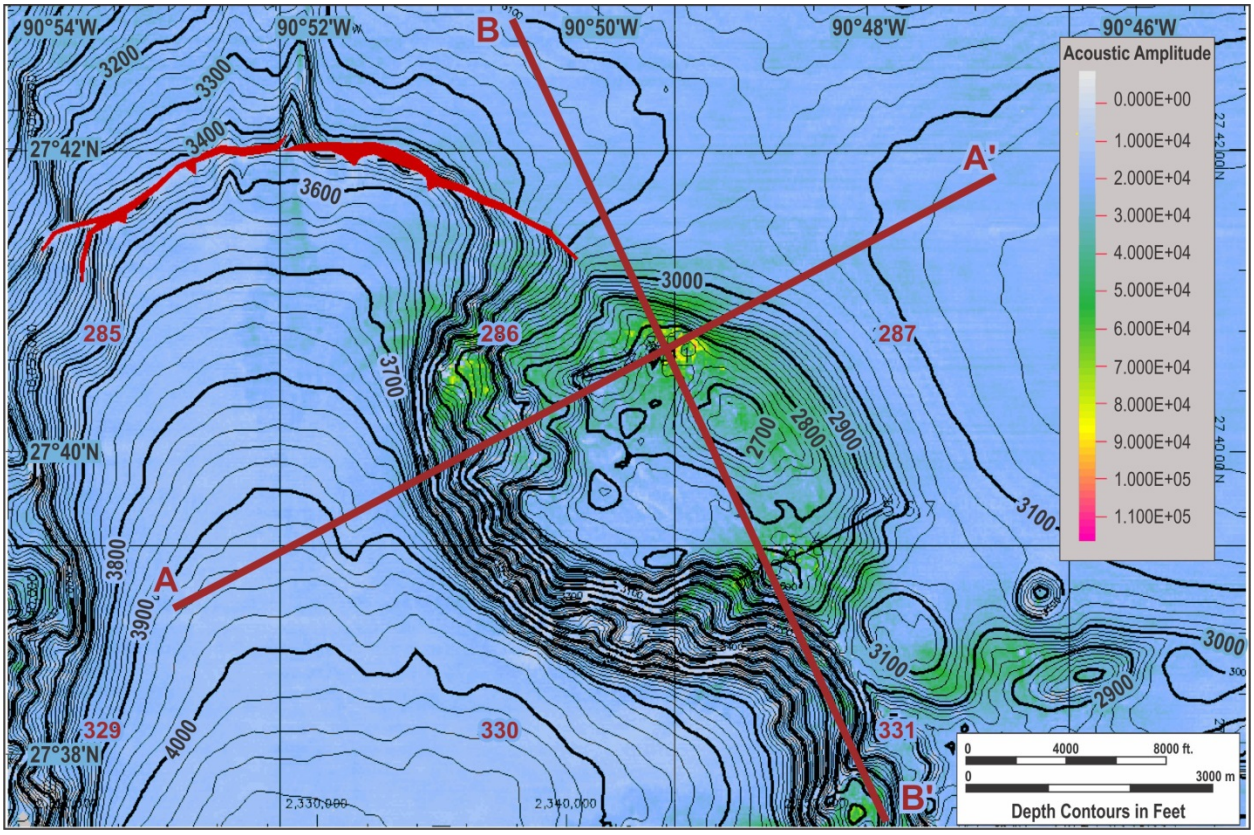

Figure 27. This combined bathymetry and 3-D seismic surface amplitude map clearly identifies the area of interest located at the northern margin of a large mounded feature supported by salt in the shallow subsurface.

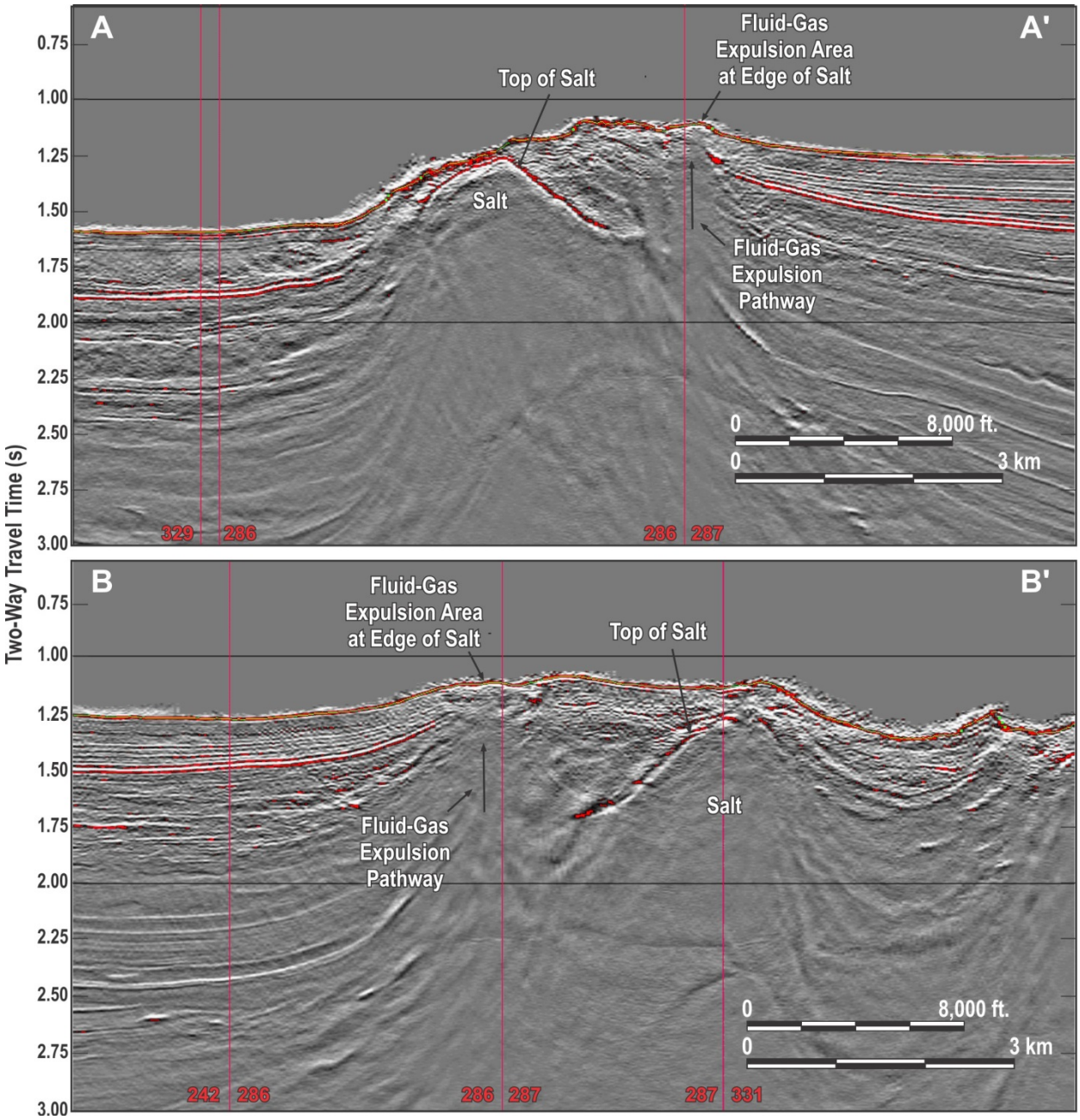

Figure 28. This figure is composed of two seismic profiles that cross the broad mounded sea floor feature that occurs mainly in GC 286, 287, and 330. Location of the two seismic profiles is given in Figure 27. (A) The SW-NE trending seismic profile (A-A´) shows the shallow position of salt on the SW flank of the mounded feature and the clear vertical migration pathway at the edge of a shallow subsurface salt body. The migration pathway intersects the sea floor along the northern margin of the feature. (B) A NW-SE trending profile (B-B´) confirms a pathway for fluid-gas migration to the sea floor along the northern flank of the large mounded feature and shows that the SE part of the mound is supported by a salt body that is located close to the seabed.

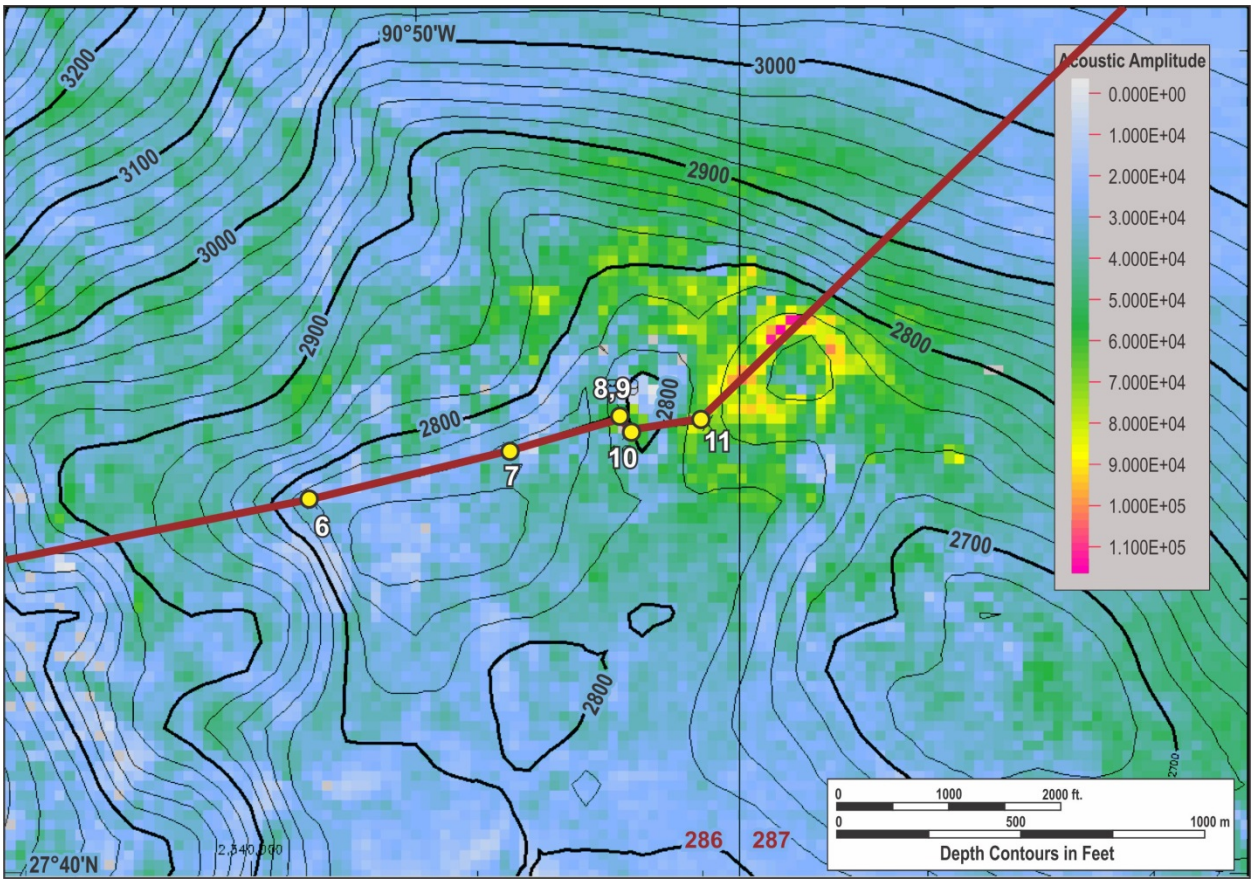

Figure 29. This enlarged map of both bathymetry and 3-D seismic surface amplitude data indicates that the area of high positive surface amplitudes span an area between GC 286-287 along the northern flank of the regional mounded feature shown in Figure 27. The dive transect is shown in red and key fix points along the transect are indicated (Fix Points 6-11).

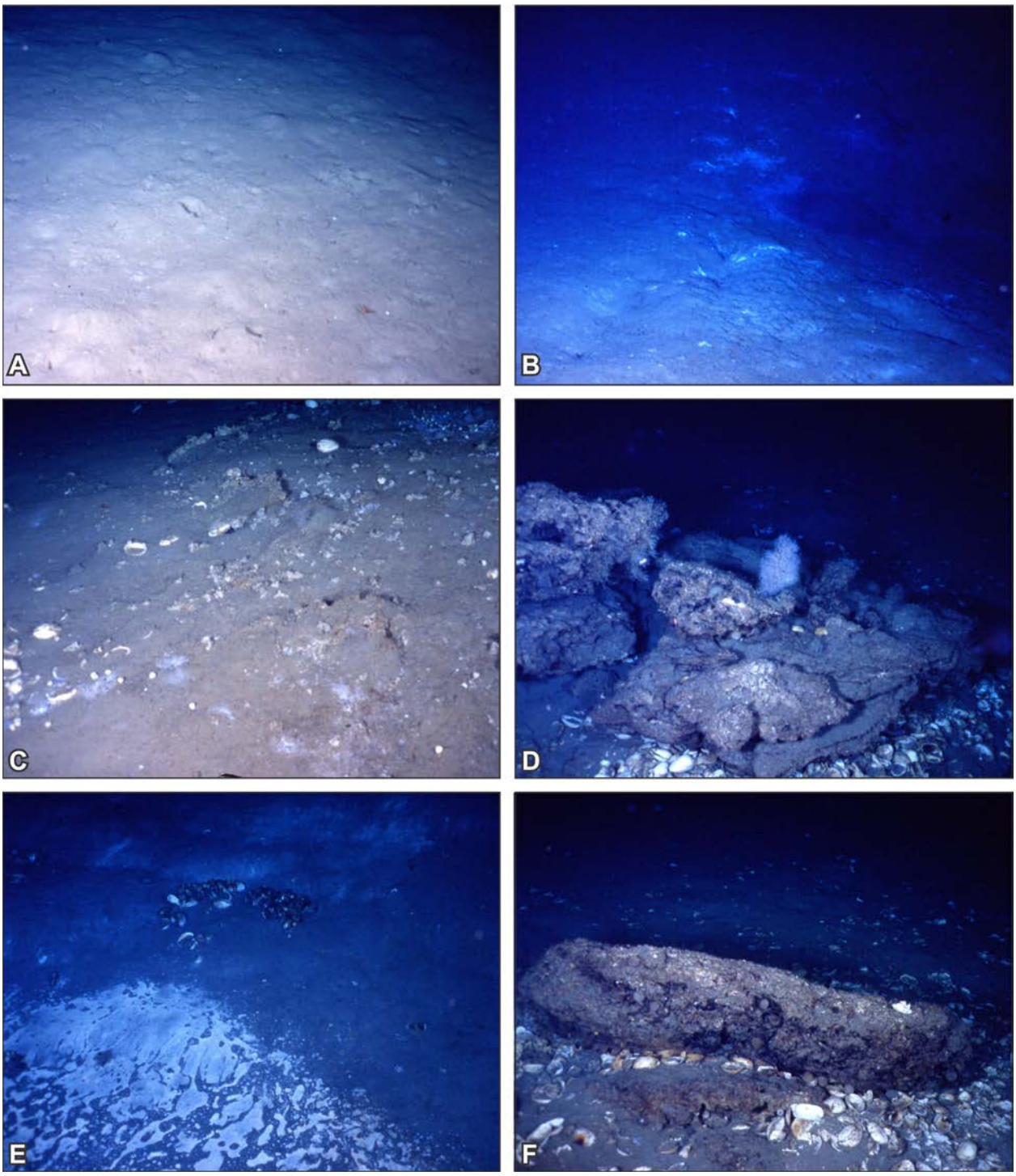

Figure 30. These photographs of the sea floor were taken at or near the fix points shown on the dive transect of Figure 29. (A) Burrowed hemipelagic mud characterizes Fix Point 6 where surface amplitudes are in the low positive "background" range. (B) At Fix Point 7 scattered moderately positive surface amplitudes occur that are slightly above background. A few lucinid-vesycomyid clam shells are scattered over the bottom at this site and appear to be responsible for the slightly higher reflectance of

the sea floor in 3-D seismic data from the area. (C) On the flank of a gentle depression as defined by the 2800 ft isobath of Figure 29, the reflectivity of the sea floor is significantly above background. The sea floor in this area (Fix Points 8 and 9) is highly lithified and clam shells and small white bacterial mats are common. A high positive 3-D seismic sea floor amplitude response occurs at this site. (D) Like the previous bottom photograph at Fix Point 8, lucinid-vesycomyid clam shells occur in great numbers. In addition, ledges and boulder-sized outcrops of authigenic carbonate containing numerous clam shells occur at this site (Fix Point 9). (E) White bacterial mats and living mussels at Fix Point 10 indicate active hydrocarbon seepage. (F) At Fix Point 11 on the flank of a low-relief mound (see Figure 29) the high positive 3-D seismic surface amplitude response correlates to a sea floor covered with clam shells and outcrops of authigenic carbonate rock. The cross-photograph field of view dimensions for the six seafloor photographs of this figure are approximately 6-14 ft (2-4 m).

7.5 Case Investigation: Green Canyon 204 (GC 204)

7.5.1 Location and Geologic Setting

The Green Canyon lease area has more active oil and gas seeps-vents than any of the other lease areas of the Gulf's northern continental slope. Lease block 204 is located near the shelf edge in the NE sector of the Green Canyon lease area (Figure 31). Water depths in GC 204 vary from over 3100 ft (945 m) in the southwest corner to a minimum of slightly over 2600 ft (793 m) in the NE part of the block at the boundary with GC 205.

The study site occurs on a NW-SE trending salt-supported ridge that separates two elongated intraslope basins (Figure 31). The ridge is bound by linear faults on both the eastern and western sides and the ridge top is characterized by numerous faults and a complex bathymetry which defines numerous mounds and depressions. In a regional perspective, the GC 204 area of interest is a complex graben-like crestal collapse feature above deep subsurface salt. Fluid-gas migration in the southern expulsion region (Figure 32) appears to be vertical from a peak on the subsurface salt mass. Fault migration pathways are clearly defined on the eastern side of the area. Other parts of this southern expulsion region are characterized by acoustic blanking, so no direct correlation to faulting can be made. Vertical migration by buoyance-driven forces are interpreted for this area as well as the large expulsion feature to the north. At the sea floor, this part of the continental slope exhibits many fluid-gas expulsion features that occur on various scales. The GC 204 site was selected for study because of the obvious occurrence of several major fluidized sediment expulsion sites that occur within this block and the wide range of 3-D seismic surface amplitudes present in this sector of the continental slope. The long downslope-oriented mudflows that are prominent feature in the 3-D seismic sea floor reflectivity data clearly identify the location of upslope expulsion centers from which these flows originated (Figure 32). This area in the Green Canyon lease area is near Chevron's Genesis Field in GC 205.

7.5.2 Sea Floor Amplitudes and Surface Geology

Figure 32, the bathymetry and 3-D seismic surface amplitude or reflectivity map of the area of interest, clearly indicates a complex sea floor geology. Both the NW and SE sectors of GC 204 have circular and mounded features, the centers of which are characterized by low reflectivity. However, the flanks of these mounded areas and the long linear features that radiate from these mounds exhibit high-to-moderate positive acoustic amplitude or reflectivity. Seismic profiles that cross the mounded features, Figure 33, reveal acoustic blanking areas beneath the mounds that are interpreted as vertical pathways for fluid and gas migration from the deep subsurface to the sea floor. On both the 3-D seismic surface amplitude map and the seismic profiles, the sea floor is highly reflective on the mound flanks and areas surrounding these features. Using only the remotely sensed data, the mounded areas with low positive acoustic amplitude or minimally reflective centers would be interpreted as expulsion centers containing soft gas-charged sediment in the central vent. Phase reversals of this sea floor reflector on seismic profiles crossing the central vent area support this interpretation. Highly reflective fluidized sediment flows originating from the expulsion centers are somewhat problematic without the aid of "ground truth" observations. Because the fluidized sediment from the

expulsion centers is normally gas-charged, a low reflectivity might be expected. Other highly reflective areas of sea floor surrounding the vents could support chemosynthetic communities and associated authigenic carbonate hardgrounds and perhaps low-relief mounded outcrops.

7.5.3 Interpretation of 3-D Seismic Sea Floor Amplitudes Using "Ground Truth" Data

The Johnson Sea-Link transect across the area of interest in GC 204 is superimposed on the bathymetry and 3-D seismic surface amplitude map of Figure 34. The very high positive acoustic amplitude and highly reflective seabed at Fix 6 is part of a curvilinear pattern of high amplitudes that start upslope at the apex of a mound and follow the deepening sea floor down-slope. This roughly circular upslope feature is clearly defined by the bathymetry of Figure 32 and 34 and both seismic profiles A-A´ and B-B´ of Figure 33. The curvilinear pattern of high amplitudes is interpreted from the 3-D seismic data, both surface amplitude map and profiles, as a fluidized sediment flow from an expulsion center at the apex of the aforementioned mound. However, one might expect a low amplitude (minimal reflectance) from a sediment flow unless it was composed of sand, but most expulsion features extrude mud.

Observations and sampling from the Johnson Sea-Link at Fix 6 (Figure 34) quickly revealed the reason for the highly reflective nature of the flow. As Figure 34A illustrates, the surface of the flow was covered with lucinid-vesycomyid clam shells, accounting for the moderate-to-high 3-D seismic sea floor amplitudes. Lucinid-vesycomyid clams exploit hydrogen sulfide produced by microbial communities that metabolize hydrocarbons incorporated in the muds. Once the hydrogen sulfide is depleted, the clams die, leaving a bed of disarticulated shells. With subsequent mud flows, new clam populations develop. It is reasonable to assume that the high reflectivity of some mud flows is caused by the accumulation of numerous stacked horizons of these shell horizons. In addition, nodular authigenic carbonates also form in the mudflows, which promote high reflectivity. Short cores of the flow sediment confirmed the presence of nodular carbonates at the GC 204 mudflow site.

At Fix 7 on the flank of the mound, clam shells scattered over the surface were less numerous than at Fix 7 and as a consequence, reflectivity on the 3-D seismic surface amplitude map was less. In contrast, however, at Fix Points 8 and 10 (Figure 34) boulder-sized outcrops of authigenic carbonate containing numerous clam shells were found. Disarticulated loose clam shells covered the seabed between the carbonate rock outcrops, living mussels were scattered throughout, and octacorals used the rocks as attachment points (Figure 35C, D, and E). Perhaps because of the steeply sloping sea floor on the expulsion mound flank, the seismic energy was scattered and only moderate amplitudes (reflectivity values) were recorded from these scattered hard bottom areas (Figure 34).

Farther eastward along the Johnson Sea-Link transect scattered hardgrounds and shell beds were encountered until a small low relief, and low positive acoustic amplitude expulsion feature was encountered at Fix Points 12 and 13 (Figure 34). At the apex of the low relief mound recently deposited fluidized mud was found. This mud was a light gray color and had not been oxidized, even though much of the surface was burrowed by a community of lucinid-

vesycomyid clams. A few disarticulated clam shells were scattered over this surface, but live clams were found harvesting the hydrogen sulfide in these recently extruded muds (Figure 35F).

7.5.4 Summary

The GC 204 area can be characterized by its fluid-gas expulsion features and the numerous fluidized sediment flows that originated from these features. The 3-D seismic surface amplitude data identified the sediment flows because of the highly reflective clam shell beds that developed on the latest flows and probably occurred in the shallow subsurface on the surfaces of older flows that are now buried.

The expulsion centers appear as low positive acoustic amplitude areas or zones of minimal surface reflectivity. On-bottom observations and samplings identify the crests of these mounded expulsion features as vents where fine-grained sediment laced with both crude oil and gas is being extruded. Surrounding the expulsion features are zones of carbonate hardgrounds and larger carbonate outcrops supporting octacorals. Clam shell beds and living mussel aggregations occupy the areas between carbonate outcrops. Although tubeworms were present, they were small and confined primarily to the edges of carbonate outcrops or in crevasses. A moderate reflectivity resulted from these diverse areas between expulsion centers. One may expect a higher reflectivity from these hard bottoms. However, the diverse and local variability of slopes related to the seabed may have scattered the 3-D seismic energy resulting in only a moderate reflectivity. Generally, the 3-D seismic surface amplitude method of interpreting the character of the seabed worked well in the GC 204 area.

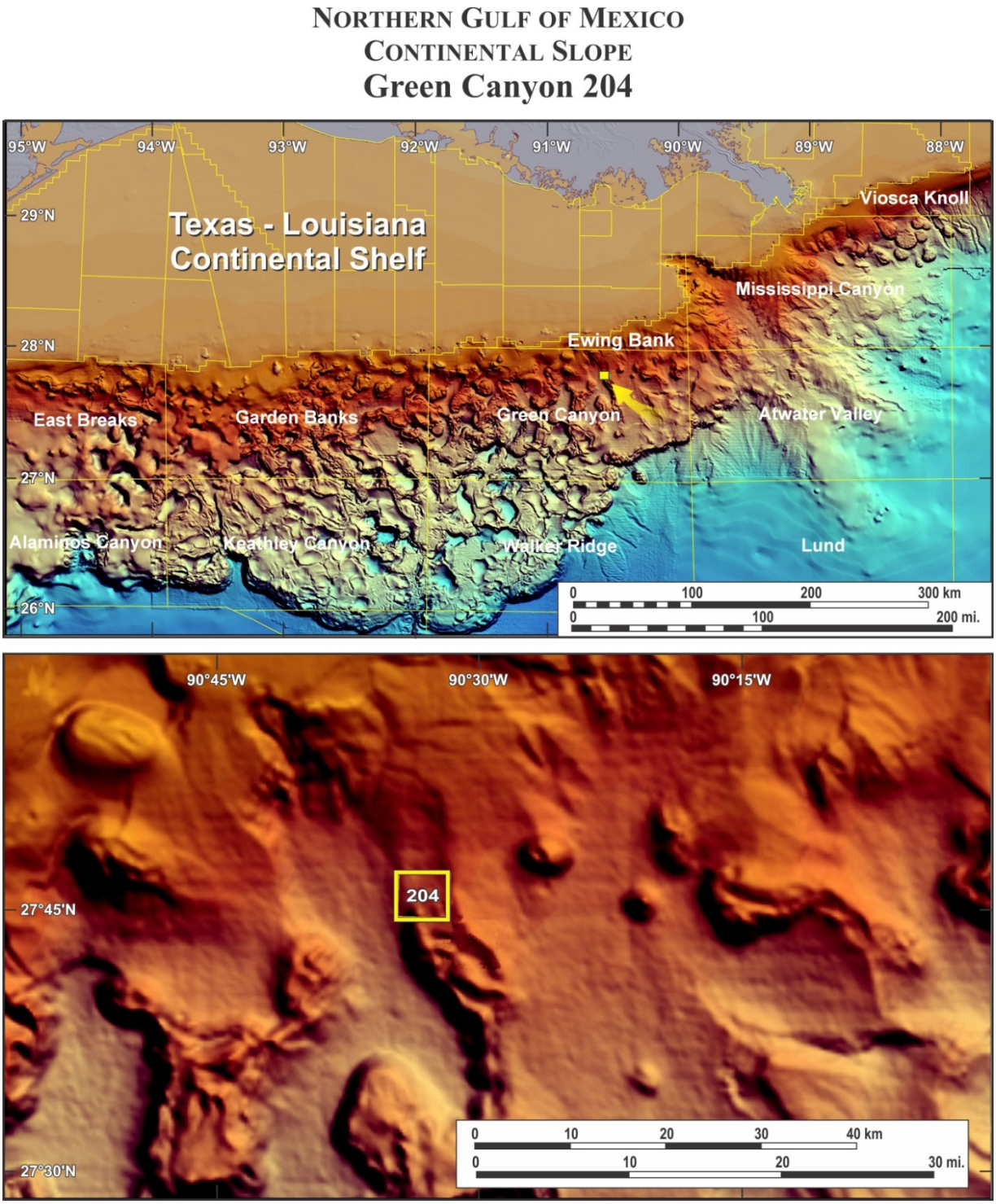

Figure 31. (A) Shaded multibeam bathymetry map of the continental slope of the northern Gulf of Mexico. The yellow arrow indicates the location of Green Canyon Block 204 (GC 204) which contains the features of interest to this study. (B) The enlarged area of the continental slope in the vicinity of GC 204 illustrates location of fluid-gas expulsion centers and associated bathymetric features including sediment flows that were investigated.

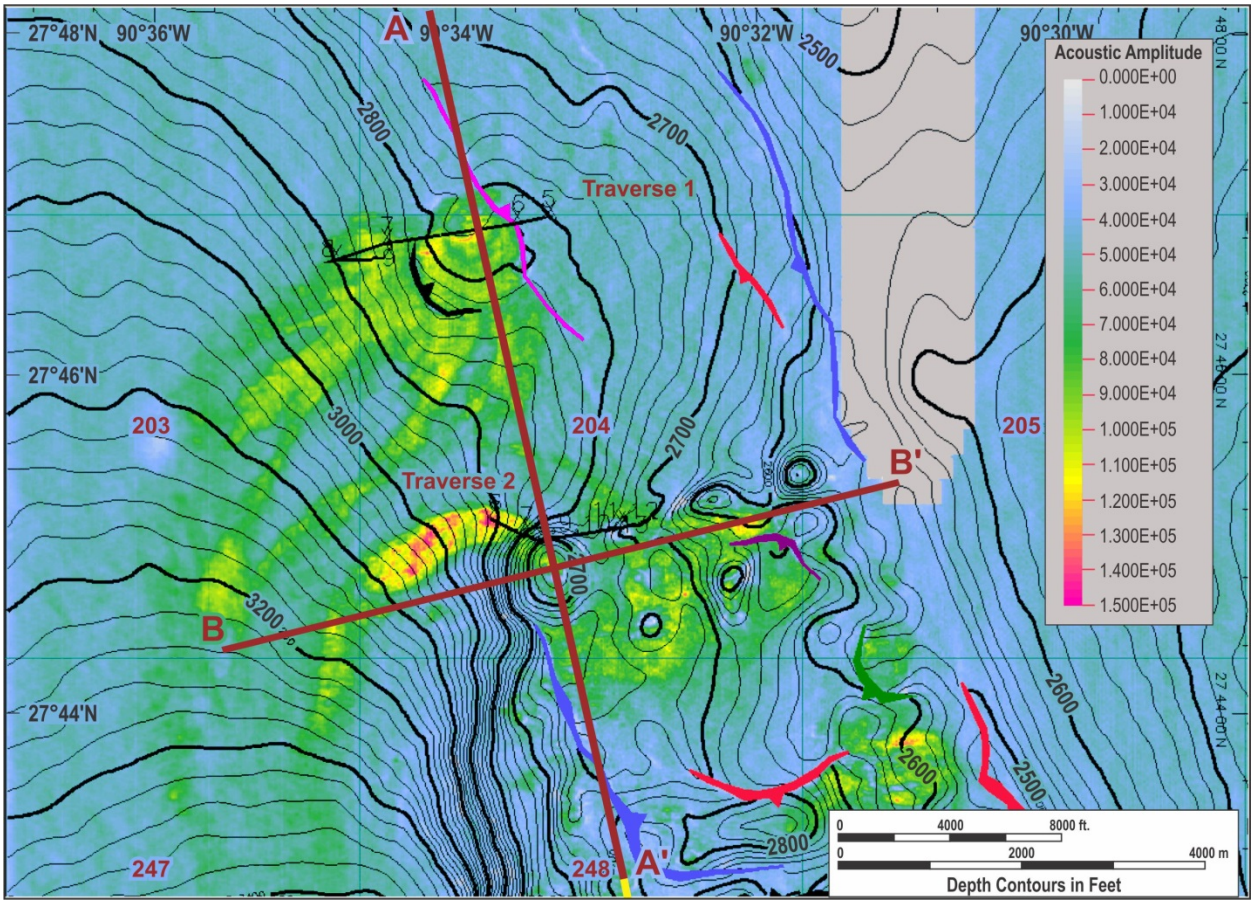

Figure 32. This combined bathymetry and 3-D seismic surface amplitude map clearly identifies the sites of fluid-gas expulsion (low positive to negative surface amplitudes) and the downslope sediment flows emanating from the major expulsion centers that have a high positive 3-D seismic seafloor amplitude signature. The location of seismic profiles A-A´ and B-B´ of Figure 33 are identified.

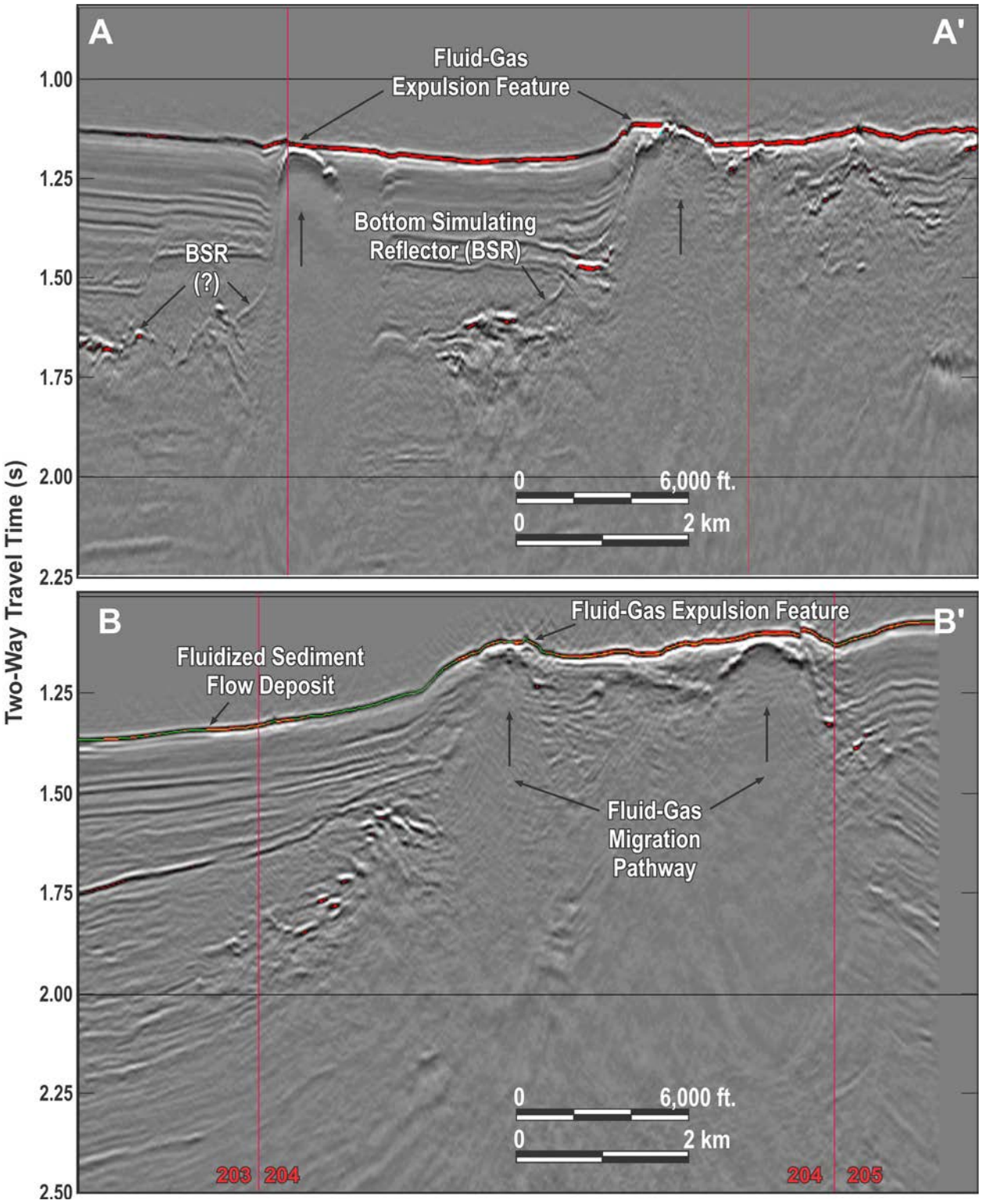

Figure 33. This figure is composed of two seismic profiles that cross the area of interest. (A) North-south profile A-A´ crosses two major expulsion centers, one on the northern boundary of GC 204 and the other near the southern border of GC 204. Both have clearly-defined migration pathways to the sediment-water interface and 'bright'

reflectors beneath the seafloor that appear to be the elevated and gas-rich base of the gas hydrate stability zone. A deep-cutting bottom simulating reflector (BSR) appears to be traceable to the high amplitude reflector just beneath the seafloor, an upward displacement/related to heat exported with fluids (including fluidized sediment) and gas at these sites. (B) The roughly E-W profile (B-B´) shows the same relationships with the subsurface and the expulsion sites at the seafloor as profile A-A´. Acoustic blanking characterizes the migration pathway. Gas and possibly gas hydrate occur in the very shallow subsurface at the expulsion centers.

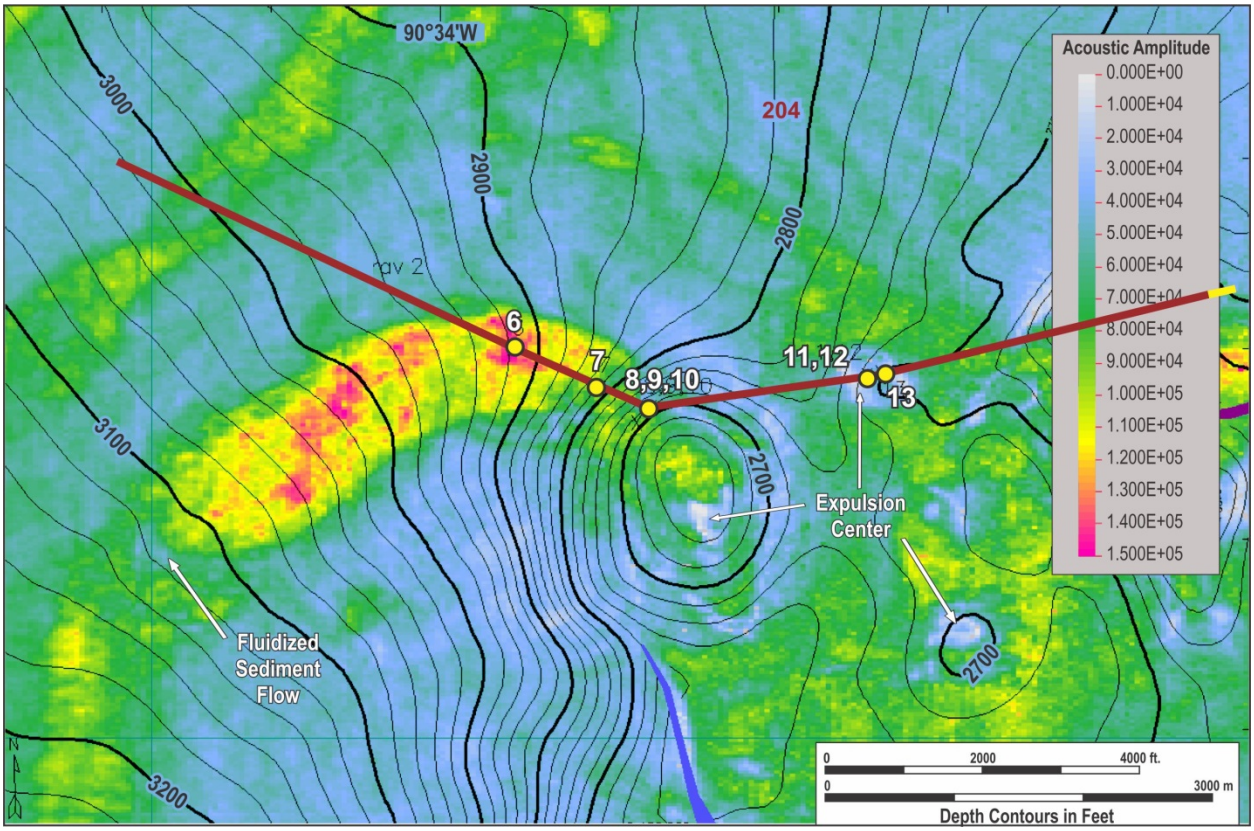

Figure 34. This enlarged map of both bathymetry and 3-D seismic surface amplitude data covers part of the complex's southern expulsion site (see Figure 32) and identifies a dive transect in red that crosses one of the downslope-oriented fluidized sediment pathways. The transect extends over mounded higher ground where several low positive to negative surface amplitude areas identify the gas-charged surface sediments of the expulsion centers. Fix Points 6-13 are sites where key observations were made in order to reference surface amplitude response to bottom characteristics.

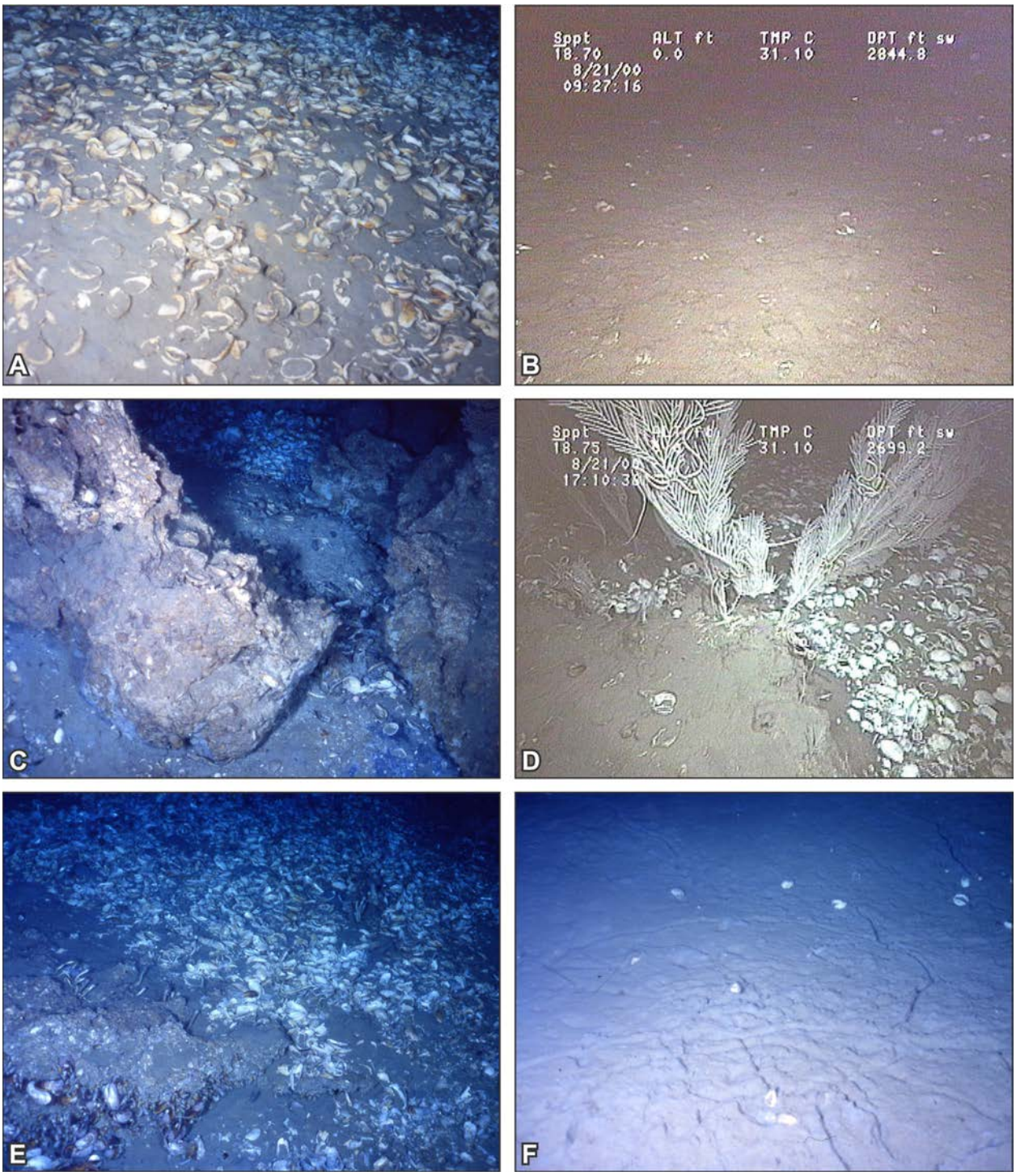

Figure 35. These photographs of the sea floor were taken at or near the fix points shown on the dive transect of Figure 34. (A) The very high positive surface amplitude at Fix Point 6 is associated with the sediment flow originating from an up-slope fluid-gas expulsion center. The amplitude response is related to a "carpet" of lucinid-vesycomyid clam shells. It is thought that stacked horizons of these shells identify multiple major expulsion events. The clams are harvesting the hydrogen sulfide in

the hydrocarbon-laced fluidized sediment. (B) On the flank of the mounded expulsion center small nodular masses of authigenic carbonate and clam shells are scattered over the surface. Surface amplitude response at this site (Fix Point 7) is less than the dense shell-cover over the sediment flow at Fix Point 6. (C) On the upper flank of the expulsion center (Fix Point 8), large slabs and boulder-sized pieces of authigenic carbonate containing numerous clam shells occur scattered over the sea floor. (D) The hard substrates provided by the carbonate outcrops are frequently populated by octacorals (Fix Point 9). (E) Near the expulsion center (Fix Point 10) living mussels occur along with tubeworms that extend beneath exposures of authigenic carbonate. Most of the shells in this photograph are mussel shells. (F) At Fix Point 13, a low reflectivity expulsion center, recently deposited fluidized sediment is being burrowed by scavenging lucinid-vesycomyid clams. This site has a very low positive to negative 3-D seismic surface amplitude response. The cross-photograph field of view dimensions of the sea floor photographs are 2-4 m except for photographs A and C which are approximately 3 ft (1 m).

7.6 Case Investigation: Ewing Bank 1001 (EW 1001)

7.6.1 Location and Geologic Setting

The features of interest that occur in Ewing Bank 1001 (EW 1001) are located just seaward of the continental shelf edge in a water depth of approximately 1800 ft (549 m), Figures 36 and 37. Water depths in lease block EW 1001 range from about 1400 ft (427 m) along the north-central block boundary to about 1960 ft (598 m) in the SW corner of the block. Two prominent down-to-the basin faults that trend roughly parallel to the shelf edge cross the middle portion of EW 1001 (Figure 37).

The locations of two seismic profiles A-A´ and B-B´ are illustrated in Figure 37 and the profiles are presented in Figure 38. A regional extensional setting is the structural framework for this site. There is a well-defined down-to-the-basin fault north of the surface features of interest (Figure 38). A salt body in the subsurface beneath the EW 1001 mounds has a vertical salt weld beneath it and steeply dipping faults and buoyancy-driven migration routes along its margin that are conduits to the mounded expulsion features on the sea floor. The fluid-gas migration pathways are vertically oriented and acoustically blanked. The features of interested are areas of mounded sea floor that have vertically-oriented and clearly defined acoustically blanked fluid-gas migration pathways to the continental slope seabed from the deep subsurface.

7.6.2 Sea Floor Amplitudes and Surface Geology

Figure 37 and Figure 39 illustrate the 3-D seismic sea floor amplitude response in the EW 1001 area. The enlarged area of interest shown in Figure 39 illustrates a broad range of sea floor amplitudes associated with two mounds clearly delineated by the bathymetry of Figures 37 and 39. High positive 3-D seismic surface amplitudes occur primarily on the flanks of the mounds and in association with linear off-mound features that were initially identified as sediment flows. As is common to active mounded fluid-gas expulsion features, the apex areas of the mounds are characterized by very low positive-to-negative acoustic amplitude response. These low positive-to-negative areas of surface amplitudes that are lower than the hemipelagic mud background surface amplitudes for the region generally correspond to surface or near-surface sediments that are soft and contain bubble-phase gas. These areas are frequently sites where gas-charged and fluidized sediment is being forced to the modern sea floor to form positive relief features such as mud volcanoes with associated down-slope sediment flows.

7.6.3 Interpretation of 3-D Seismic Sea Floor Amplitude Using "Ground Truth" Data

Figure 39 illustrates the Johnson Sea-Link submersible transect designed to collect ground-truth observations and physical samples from the mounded areas that were associated with a wide variety of 3-D seismic sea floor amplitude responses. At Fix 1 along the southeastern flank of the largest mound, the seabed was rather featureless mud with numerous tracks and trails plus burrow structures, but no signs of biologic communities or lithification related to hydrocarbon seepage. The 3-D seismic surface amplitude response at Fix 1 was the same as the regional background for the area (Figure 39). However, as the submersible started

upslope toward the mound crest, a small area of tubeworm communities was encountered which was positive evidence of hydrocarbon seepage (Figure 40A). Just the ends of the tubeworms protruded from the sediment as if sediment accumulation rates for the area were keeping up with or perhaps out-pacing tubeworm growth. In addition to tubeworms, this area exhibited small areas of reducing sediment and bacterial mat development. This region of the mound flank exhibited very high positive 3-D seismic surface amplitude values suggesting a hard reflective sea floor. Although no authigenic carbonate pavements were observed, small nodular masses of carbonate were found in the sediment. More substantial carbonate pavements and other types of carbonate outcrops are usually associated with tubeworm communities. In this case, the hard bottom areas may have been buried by what appears to be the high sedimentation rate for the area. Because the surface amplitude signature for any given site is the integration of acoustic reflectivity over the upper 16-25 ft (~ 5-7 m) of the sediment column, hard material does not always appear at the seabed, but it may be buried by a relatively thin layer of sediments.

A transect across the apex of the mound to Fix 4 revealed a newly deposited light grey mud bottom. Upon arriving at Fix 4 an oxidized edge was encountered (Figure 40B). Although the light grey mud exhibited surface structures associated with bioturbation (tracks and trails), the adjacent oxidized muddy seabed was more thoroughly modified with more tracks and trails plus burrows.

From Fix 4 the submersible traveled south to Fix 5 looking for the expulsion point for the apparent newly deposited light grey mud that filled the central depression of the largest mounded feature (Figure 39). At Fix 5 the seabed was highly furrowed, probably by lucinid-vesycomyid clams (Figure 40C). No clam shells are in the photograph of Figure 40C, but scattered clam shells were observed in the area as well as living clams. These clams exploit the hydrogen sulfide in the surface sediments as an energy resource.

Leaving the large mound and transiting toward the smaller mound to the NE, the seabed of the mound flank appeared much the same as the sea floor at Fix 3 without the tubeworm communities. Small white bacterial mats were scattered over the bottom, especially around the openings of burrows. These areas had a high positive 3-D seismic surface amplitude (Figure 39). Like the sea floor at Fix 3, the high positive acoustic amplitude appeared to be related to hard horizons recently buried by sediment and now in the shallow subsurface.

At Fix 9 near the apex of the smaller of the two mounds (Figure 39), newly deposited light gray mud intersected the oxidized and slightly higher edge of the expulsion center (Figure 40D). The oxidized sediment surface was irregular, thoroughly burrowed, and covered with tracks and trails. The light grey mud, interpreted as newly deposited sediment, had a relatively smooth surface and only a few indicators of bioturbation. This crestal area of the small mound exhibited very low positive-to-negative 3-D seismic surface amplitude response (very low acoustic reflectivity), Figure 39.

Along the SE flank of the small mound was an area of very high acoustic reflectivity (high positive 3-D seismic surface amplitude response, Figure 39). The sea floor at Fix Points 10 and 11 in this zone was characterized by small areas of reducing sediment surrounded by white bacterial mats (Figure 40E, F). Nodular masses of authigenic carbonate were found in the sediments of these two sites, but no outcrops or pavements of lithified material were observed.

7.6.4 Summary

The two mounds and surrounding areas of sea floor in EW 1001 are good examples of 3-D seismic sea floor amplitude anomalies. Both mounds have the seismic, physical, and sedimentological characteristics of mud volcanoes. They have positive relief above the surrounding sea floor, a circular plan-view outline, and in seismic profile view, they are surface expressions of acoustically opaque fluid-gas migration pathways from the deep subsurface. The sea floor acoustic amplitude patterns associated with these mounds also support an interpretation that these features are active or recently active centers of fluidized sediment extrusion. The flanks of the mounds have high positive 3-D seismic surface amplitude responses while the mound crests have a very low positive-to-negative acoustic amplitude characteristic. High positive acoustic amplitudes identify sea floor areas of high reflectivity of acoustic energy commonly associated with authigenic carbonates, shell beds such as those produced by abundant lucinid-vesycomyid clams, or a combination of the two. In the case of these two mounds which are interpreted as active expulsion centers for fluidized sediment in EW 1001, rates of sediment accumulation on the mound flanks may be so high that clam shell beds and authigenic carbonates, developed during periods of inactivity in the process of fluid mud expulsion, are buried during the next expulsion event. Observations from high amplitude areas along the submersible track illustrated in Figure 39 confirm the presence of nodular carbonates in surface sediment that indicate lithification is taking place. Scattered clam shells also occur in the high positive surface amplitude areas. These areas also have numerous small, white bacterial mats that indicate active but perhaps slow flux hydrocarbon seepage.

Arcuate trends of high positive sea floor acoustic amplitudes to the W-SW of the largest mound (Figure 39) appear to be sediment flows from the largest mound or expulsion center, although this interpretation was not confirmed by observations from the Johnson Sea-Link submersible. However, these interpreted sediment flows are very similar to those documented from GC 204 where beds of lucinid-vesycomyid clam shells and nodular authigenic carbonates in surface and near-surface sediments account for the acoustic reflectivity of these features.

The apex areas of the EW 1001 mounds exhibit a very low positive-to-negative 3-D seismic surface amplitude response (Figure 39). In seismic profile (Figure 38), these regions are also the sites of phase reversals of the sea floor reflection horizon. This combination of seismic characteristics suggests soft, unconsolidated, and gas-charge surface sediments. Observations and physical samples from the low positive 3-D seismic surface amplitude regions of these mounds confirmed the presence of newly deposited fluidized sediment containing gas.

The two EW 1001 mounds are active mud volcanoes. A lack of hard, reflective sea floor areas (e.g. lithified pavements and shell beds) in the high positive 3-D seismic amplitude zones is attributed to high rates of recent sedimentation from the two expulsion centers. Previous studies (Kohl and Roberts, 1994) have emphasized the episodic nature of fluidized sediment expulsion. The sea floor lithification takes place during periods of non-expulsion or low expulsion periods. During periods of active fluidized sediment expulsion, areas of lithified sea floor or areas with reflective clam shell beds are covered with sediment. These are the processes that seem to explain the 3-D seismic sea floor amplitude patterns associated with the EW 1001 mounds interpreted to be mud volcanoes.

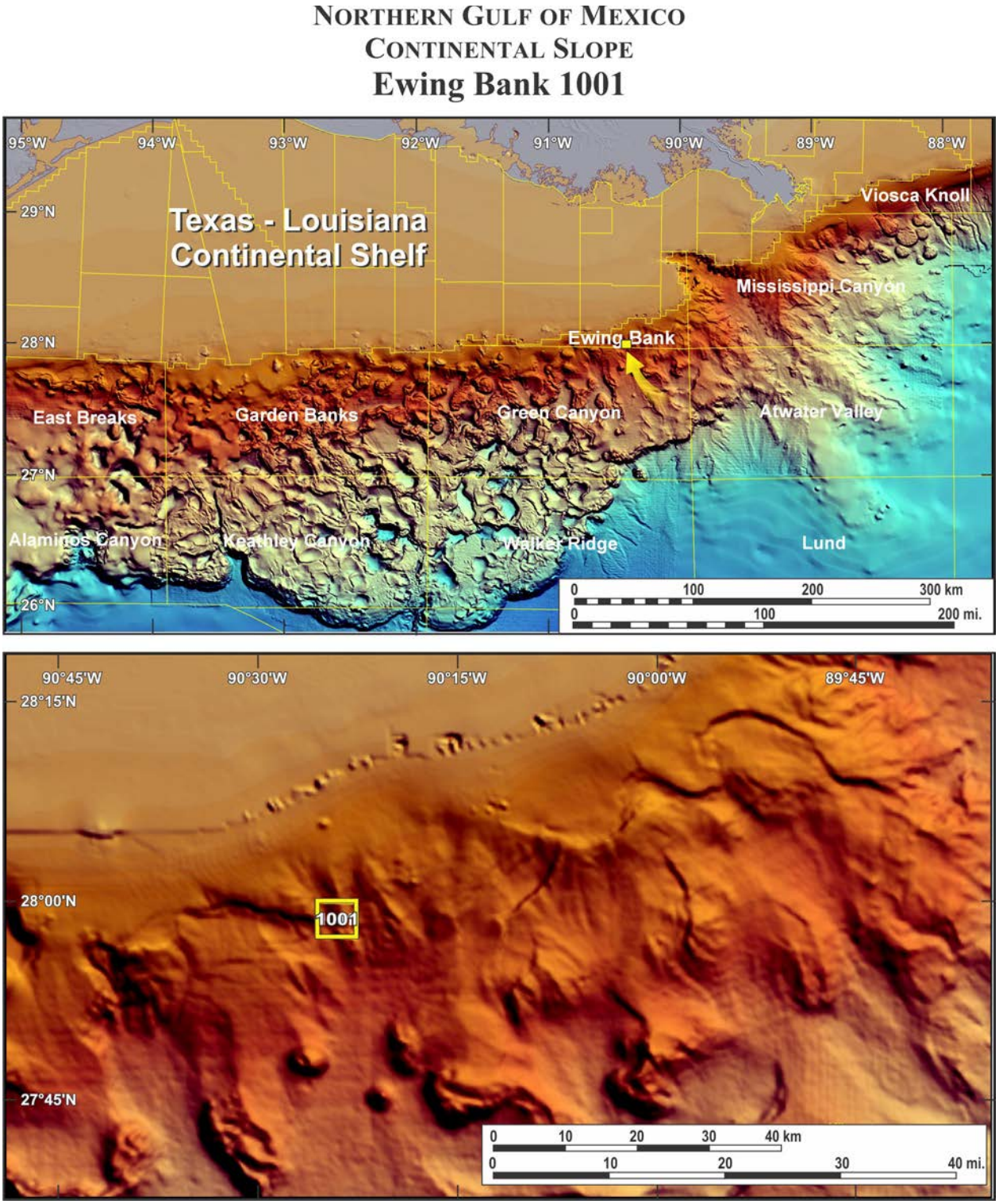

Figure 36. (A) Shaded multibeam bathymetry map of the continental slope of the northern Gulf of Mexico. The yellow arrow indicates the location of Ewing Bank Block 1001 (EW 1001). (B) The enlarged area of the continental slope surrounding EW 1001 illustrates the major bathymetric features within and surrounding the block.

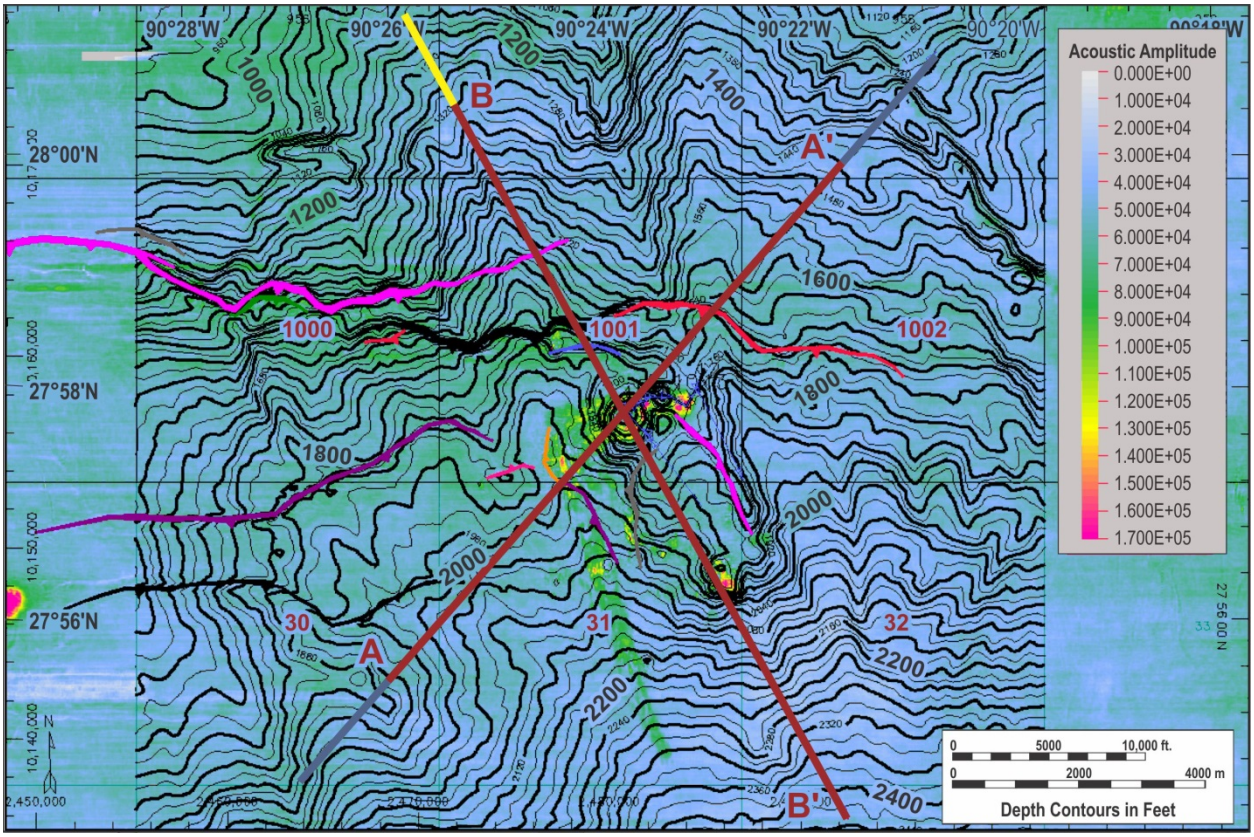

Figure 37. This combined bathymetry and 3-D seismic surface amplitude map illustrates the location of the area of interest and the mounded features within this area. Lines A-A´ and B-B´ represent the locations of SW-NE and NW-SE trending seismic profiles through the mounded features within the study area. The seismic profiles appear in Figure 38.

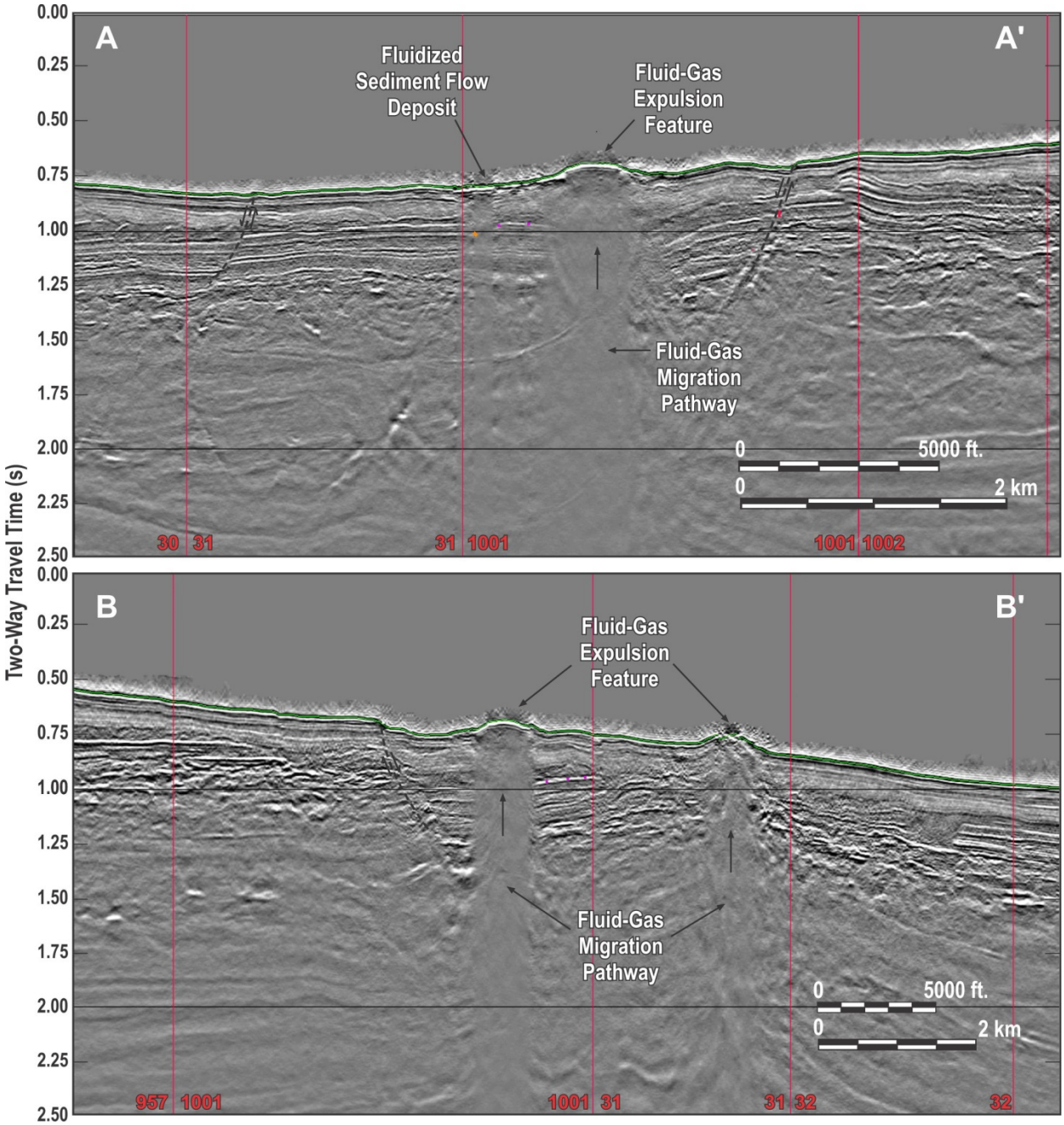

Figure 38. Seismic profile A-A´ (see Figure 37 for location) cuts across a clearly mounded fluid-gas expulsion feature in the SE part of EW 1001. This mound occurs downthrown to a regional E-W trending fault that appears on the seismic profile near the EW 1001 – 1002 boundary. A well-defined migration pathway is identified by acoustic blanking beneath the mound. Seismic profile B-B´ (see Figure 37 for location) is oriented through two fluid-gas expulsion mounds, one in EW 1001 and the other in EW 31. Both have clear migration pathways beneath them and bright surface reflector that demonstrate a phase reversal suggesting gas-charged sediments.

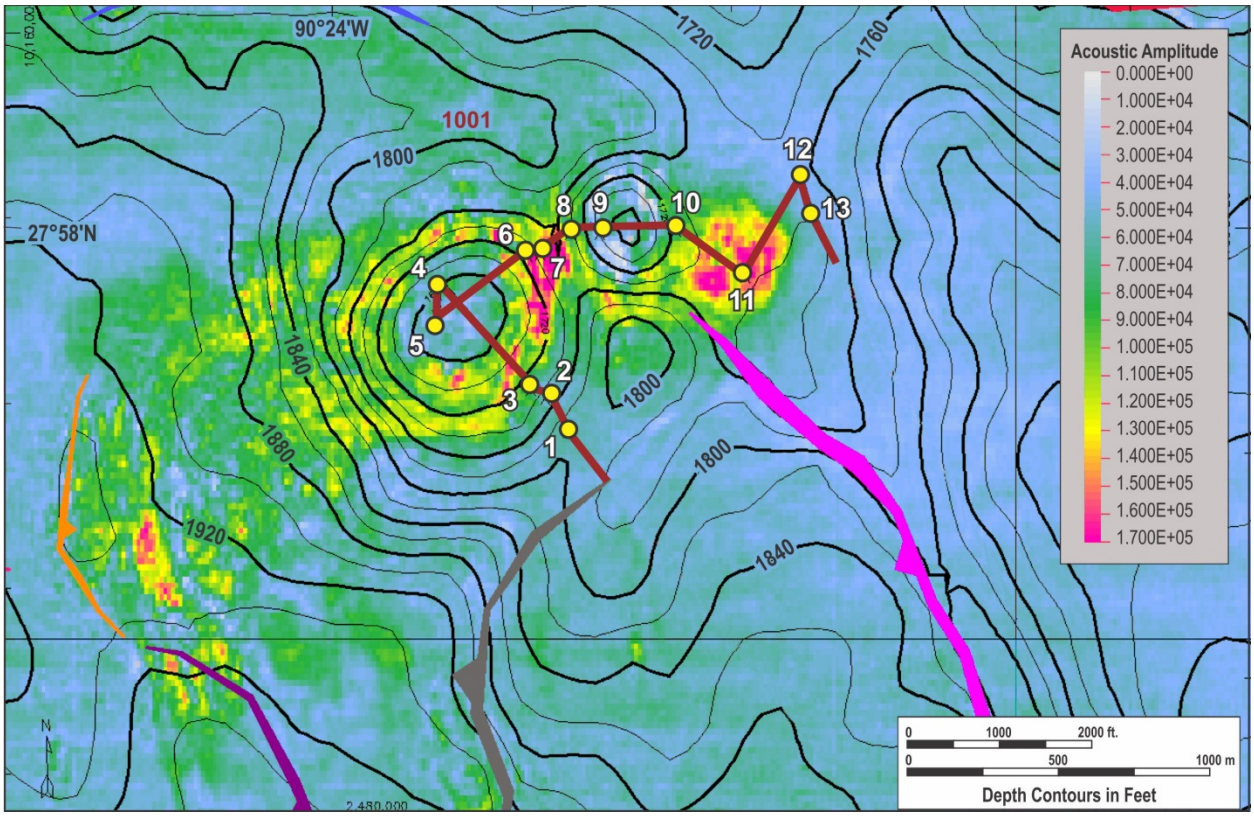

Figure 39. This combined bathymetry and 3-D seismic surface amplitude map of the area of interest in EW 1001 illustrates two distinct mounded features. The dive transect goes through the two mounds that have low positive to negative surface amplitude values. High positive surface amplitudes occur on the flanks of the mounded area and on flows emanating from these features. The fix points along the dive transect cover all of the surface amplitude patterns and values.

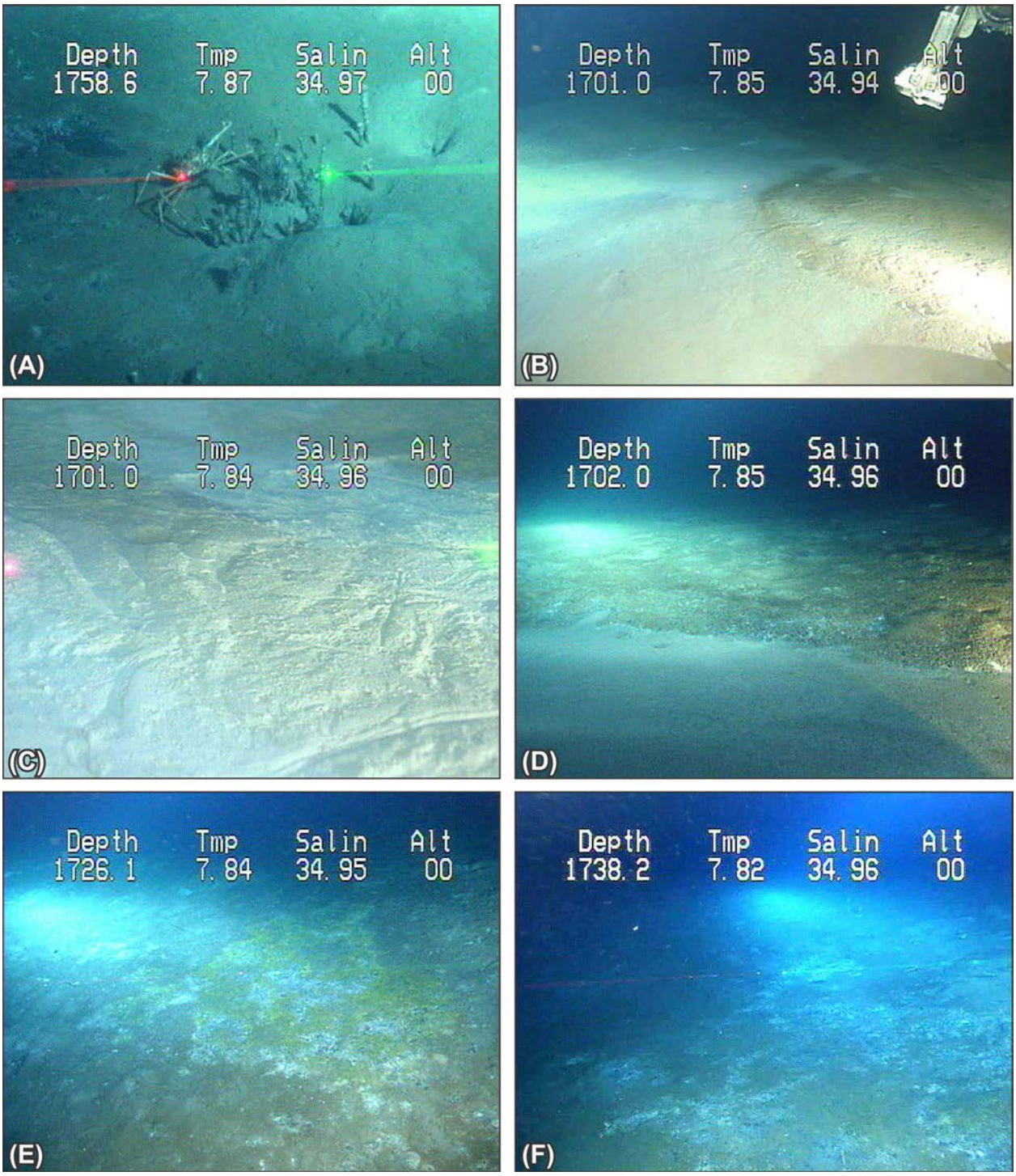

Figure 40. These photographs of the seafloor were taken at or near fix points shown in Figure 39. (A) A crab is present in this picture along with a group of short tubeworms that appear in the process of being buried by sedimentation. This photograph was taken at Fix Point 2 on the flank of the large mound of Figure 39. This site has a surface amplitude response that is slightly more positive than background. (B) At Fix Point 4 near the center of the large EW 1001 mound (see Figure 39) new and unburrowed

fluidized mud (light color) interfaces with older oxidized and burrowed sediments (brown). (C) At the center of the mound where fluidized sediment is being extruded onto the surrounding seafloor (Fix Point 5), the light colored and unoxidized sediment is being actively burrowed by a variety of organisms. A low positive to negative 3-D seismic seafloor amplitude response is characteristic of this site. (D) Fix Point 9 is located near the apex of a smaller-expulsion center (mound) to the NE of the larger mound discussed above. In this photograph, newly extruded mud near the vent site interfaces with older mud deposits that are oxidized and thoroughly burrowed. (E) Along the eastern flank of the smaller of the two mounds in EW 1001, the surface amplitude is much higher than the low reflective zone at the venting area near the mound apex. The photograph shows that the bottom at Fix Point 10 is covered with small bacterial mats with nodular masses of authigenic carbonate forming in the surface sediments. (F) Like Fix Point 10, the end of the dive transect at Fix Point 13 illustrates a seafloor of extruded sediment covered with small bacterial mats. Samples of these sediments contain nodular masses of authigenic carbonate. A moderately positive seafloor amplitude response is associated with this site. The cross-photograph field of view dimensions of all seafloor photographs of this figure are approximately 6-12 ft (2-4 m).

7.7 Case Investigation: Mississippi Canyon 885 (MC 885)

7.7.1 Location and Geologic Setting

Mississippi Canyon 885 is located along the western margin of the distinctive Mississippi Canyon which cuts across the outer shelf and continental slope extending to the deep floor of the northern Gulf (Figure 41). Water depths in the lease block range from slightly greater than 2200 ft (670 m) in the SW corner of the block to approximately 2040 ft (622 m) near the block's center.

The feature of interest is a large, roughly oval-shaped positive relief feature generally defined by the 2100 ft (640 m) isobath (Figure 42). This platform-like regional relief feature is approximately 2.5 mi (4 km) wide in the E-W direction and slightly larger in the N-S dimension. Structurally, the MC 885 surface feature is the result of expulsion processes resulting from the crestal collapse of a salt-cored feature in the subsurface. Faulting focused on high points associated with the underlying salt body and buoyance-driven forces account for the fluid-gas migration to the modern sea floor.

In a regional context, the oval platform in MC 885 exhibits the strongest positive 3-D seismic sea floor amplitudes in this general area of the continental slope (Figure 42). The high amplitudes are concentrated in three slightly higher positive relief areas within the 2100 ft (640 m) isobath. These slightly higher relief areas correlate to the vertically oriented fluid-gas migration pathways in the subsurface beneath the surface of the platform. The seismic profiles of Figure 33 clearly identify the acoustic blanking or wipe-out zones that underlie the high positive acoustic amplitude zones on the MC 885 mound surface (Figure 44). The northern boundary of this low-relief mound-like platform is defined by two distinct faults that tend roughly E-W and NW (Figure 44).

7.7.2 Sea Floor Amplitudes and Surface Geology

The moderate-to-high positive sea floor amplitudes are concentrated in two major areas located in the south-central part of the larger mounded platform-like feature (Figure 44). The western area is roughly kidney shaped while the eastern area is more oval shaped. Both areas rise well over 40 ft (12.2 m) above the general elevation of the larger platform. In addition to these two areas of moderate-to-high positive acoustic amplitude response, two distinct high positive amplitude "spots" occur along the NW margin of the platform. However, these features were not observed or sampled using the Johnson Sea-Link submersible. To the SW of the MC 885 platform a separate and distinct mound with strong positive sea floor amplitudes occurs at the MC 929-928 boundary (Figures 42 and 43B). Johnson Sea-Link dives on this mound found several unusual expulsion features composed largely of barite-rich mud.

Seismically, the area of interest in MC 885 displays strong sea floor reflectivity observed both in the surface amplitude data of Figures 42 and 44 as well as the reflection strength of the sea floor reflector illustrated in the seismic profiles of Figure 43. In the subsurface, reflectors adjacent to the feature trend upward toward the zones of acoustic blanking. The area of interest in MC 885 as well as a large intraslope basin to the west are underlain with salt. Ferry (1999),

from an investigation of high quality industry seismic data, indicates that the top of salt is irregular and faults intersect the high points on the upper surface of the salt. Linking faults to salt underlying the features of interest in MC 885 is difficult because of the acoustic blanking beneath the zones of moderate-to-high positive 3-D seismic surface amplitude response. However, Ferry (1999) suggests that the two distinct migration pathways (Figure 43A) leading to zones of high positive sea floor amplitudes (Figure 42) are quite different in that the western kidney-shaped area is surrounded by low positive amplitudes and has lower molecular weight hydrocarbons associated with sediments from the area. Table 1 illustrates the differences in hydrocarbons extracted from cores collected from the western "kidney shaped" area of surface amplitude anomalies compared to the circular eastern anomaly field.

Submersible dives associated with this study and the one reported by Ferry (1999) indicate that the MC 885 platform top displays impressive and wide-spread areas of lithified sea floor, both individual boulder-sized outcrops and pavements. In the eastern area of concentrated moderate-to-high positive sea floor amplitudes, Ferry (1999) reports the occurrence of a series of ridges radiating from the eastern and southern flanks of the mounded area. These features are interpreted as the expression of faults associated with the mounded area on the SE platform top. In addition, a small active mud vent was found in this area. Gas and crude oil droplets along with muddy sediments were being carried upward into the water column during the period of observation. Fluidized mud ejected onto the sea floor created sheets of light grey mud deposited in bathymetrically low areas by mudflows that ran downslope. The mudflows draped subtle bathymetric features as they traveled downslope to the S-SE from the vent. Active mud venting was not observed in association with the kidney-shaped zone of more moderate sea floor amplitudes toward the western margin of the MC 885 platform. However, a variety of hard ground types (e.g. pavements, slabs, boulder-sized outcrops etc.) inhabited by octacorals, sponges, and other organisms needing a hard substrate were common to this part of the MC 885 platform top.

7.7.3 Interpretation of 3-D Seismic Sea Floor Amplitude Using "Ground Truth" Data

Figure 44 illustrates the Johnson Sea-Link submersible transect across the area of moderate-to-high positive surface acoustic amplitude response in the kidney-shaped mounded area toward the western part of the MC 885 platform top. At the western end of the transect, Fix 1 (Figure 44A), the submersible descended to the seabed on the flank of the platform where 3-D seismic sea floor amplitude response is consistent with background values for the region. At the Fix 1 location the seabed was composed of homogeneous appearing hemipelagic sediments that exhibited evidence of rather extensive bioturbation (small mounds, open burrows, and tracks-trails). No bacterial mats, patches of reducing sediment, brine concentrations, or zones of sea floor lithification suggesting hydrocarbon-brine seepage were observed at this starting point for the submersible transect.

Table 1
Summary of Hydrocarbon Concentrations in Core Samples (MC 885: Note large differences in headspace gas concentration for the two features).*

W Anomaly Field Core No.	Waypoint	Headspace Methane	Gas (ppm) Total C1-C5	Long Chain C15-C22	Alkanes (ppb) C23-C32	Unresolved C15-C22	Complex Mixture C23-C32
4074-1	2	110	114	407	918	7	13
4074-2	3	26	28	148	448	4	11
4074-3	4	1782	1806	384	1798	6	25
4074-4	5	82300	82358	421	993	8	18
4074-5	6			116	349	3	8
4075-1	9			1807	688	19	21
4075-2	12	69	71	312	1087	7	21
4075-3	14	98	103	231	969	6	18
4075-4	15	51	53	153	752	3	9
4075-5	NEAR 15	27	30	176	775	4	12
E Anomaly Field							
4071-1	1						
4076-2	2	50	51	1117	1343	15	24
4076-3	3	9239	9342	1111	1259	13	19
4076-4	4	29979	30110	1459	1840	17	24
4077-1	7	20026	20112	1318	1763	15	22
4077-2	8	64076	64283	1127	1340	13	20
4077-3	9	46536	46699	1106	1023	14	13
4077-4	10	23413	23448	689	987	9	15
4077-6	12	61582	61651	1227	1582	14	20

***Ferry (1999)**

Fix 2 is on the steep western flank of the MC 885 platform. As the submersible started climbing toward the platform edge the character of the seabed changed from hemipelagic sediments with no indicators of hydrocarbon seepage or hard bottom to mud bottom with scattered octacorals. Octacorals require a hard substrate on which to attach. Shells or small nodular masses of authigenic carbonate which form in the near-surface sediments appear to have provided the hard attachment points for the octacorals. Although the muddy sediments of the Fix 2 area were highly bioturbated hemipelagics, there was a definite difference between the Fix 1 area and Fix 2. The sediments at Fix 2 contained hard materials. Because shells, such as lucinid-vesycomyid clam shells, were not observed in the immediate area of Fix 2, small nodular masses of carbonate are interpreted as the attachment points for most of the octacorals.

Approaching the platform top (between Fix Points 2 and 3) the sea floor acoustic amplitude responses shown in Figure 44 change dramatically from background to moderate-to-high positive values. Fix 3 and the surrounding area is in the center of a high positive sea floor amplitude area which correlates to low-relief mounded carbonate features, carbonate pavements, and carbonate slabs with tubeworms protruding from cracks and cavities observed from the submersible. Figure 45C is typical of this region of the MC 885 platform top. In addition to tubeworms associated with the various forms of authigenic carbonates, these hard substrates supported various types of octacorals, sponges, and other organisms requiring hard substrate conditions. Thoroughly burrowed muddy sediments filled the low areas between carbonate outcrops.

Transiting from Fix 3 to Fix 4 (Figure 44) the character of the seabed changed from one dominated by scattered authigenic carbonate slabs and low-relief mounds to flat expanses of sea floor covered with lucinid-vesycomyid clam shells, small nodular carbonates masses protruding from the surface sediments, and scattered octocoral colonies (Figure 45D). The 3-D seismic amplitude response to this type of sea floor indicated less acoustic reflectivity than at Fix 3, but still a moderately positive value (Figure 44).

Toward the SE edge of the western area of surface anomalies at Fix Points 5 and 6, scattered authigenic carbonate slabs and low-relief mounded outcrops as well as tubeworm aggregations and clam shell beds were encountered (Figure 45E, F). Like the seabed at Fix 4, this region produced a moderate positive 3-D seismic surface amplitude response (Figure 44).

7.7.4 Summary

The MC 885 platform is a regional 3-D seismic sea floor amplitude anomaly. Within this large feature a raised area in the SW sector of the platform was selected for direct observation and sampling in support of this project, the focus of which was to build an understanding between surface amplitude response and seabed characteristics, especially in settings where hydrocarbons are either seeping or are being vented to the sea floor.

Data collected from SW of the field of moderate-to-high sea floor amplitude responses on the platform confirmed that off-platform sites are blanketed with soft muddy hemipelagic sediments that are poor reflectors of acoustic energy. These areas (Fix Points 1 and 2 of Figure 44) have a surface amplitude response that is consistent with the regional background and exhibit no indicators of hard bottom or gas-charged sediments.

Submersible-acquired observations and bottom samples from the platform top compared to 3-D seismic seafloor amplitudes of the Fix 3 – 6 area of Figure 44 indicate that moderate-to-high positive surface acoustic amplitude values for the region correlate to an acoustically reflective seabed. Although the seabed in this SW part of the platform top has variable characteristics, much of the area exhibits mounded outcorps, slabs, or scattered nodular masses of authigenic carbonate as well as scattered shell beds. Both bottom types are efficient reflectors of acoustic energy. This region of acoustically reflective sea floor is underlain by a migration pathway that is a vertically-oriented acoustic “wipe-out” zone. It appears that the pathway is following a fault that intersects the top of a shallow subsurface salt body. The occurrence of hydrocarbons in the surface sediments within the anomaly field of the western platform as well as living communities of chemosynthetic organisms, particularly tubeworms, indicate the active flux of hydrocarbon along the acoustically blanked migration pathway to the modern sea floor.

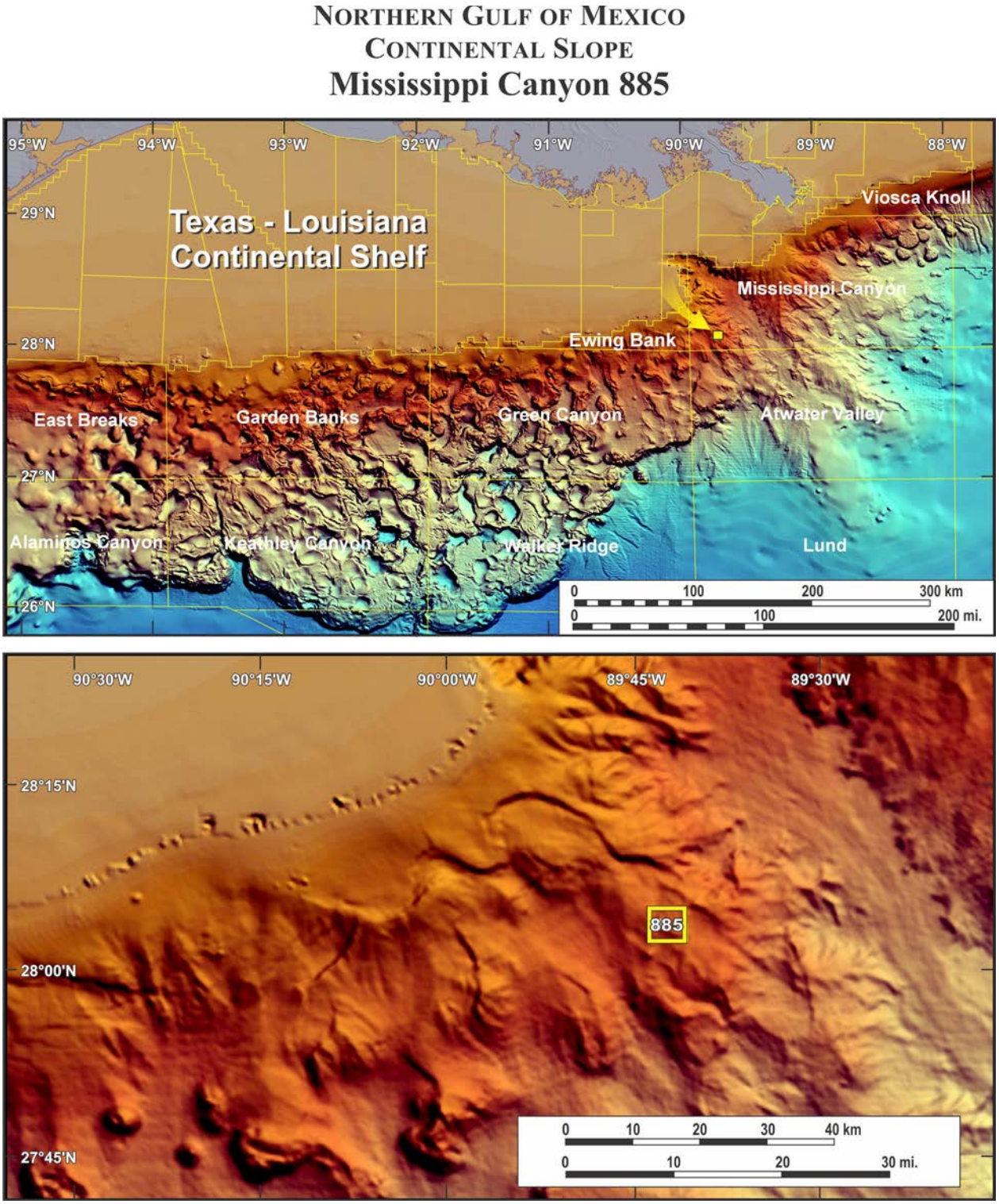

Figure 41. (A) Shaded multibeam bathymetry map of the northern Gulf of Mexico continental slope. The yellow arrow points to the location of Mississippi Canyon Block 885 (MC 885). (B) The enlarged area of the continental slope surrounding MC 885 illustrates the bathymetric features within and surrounding the block.

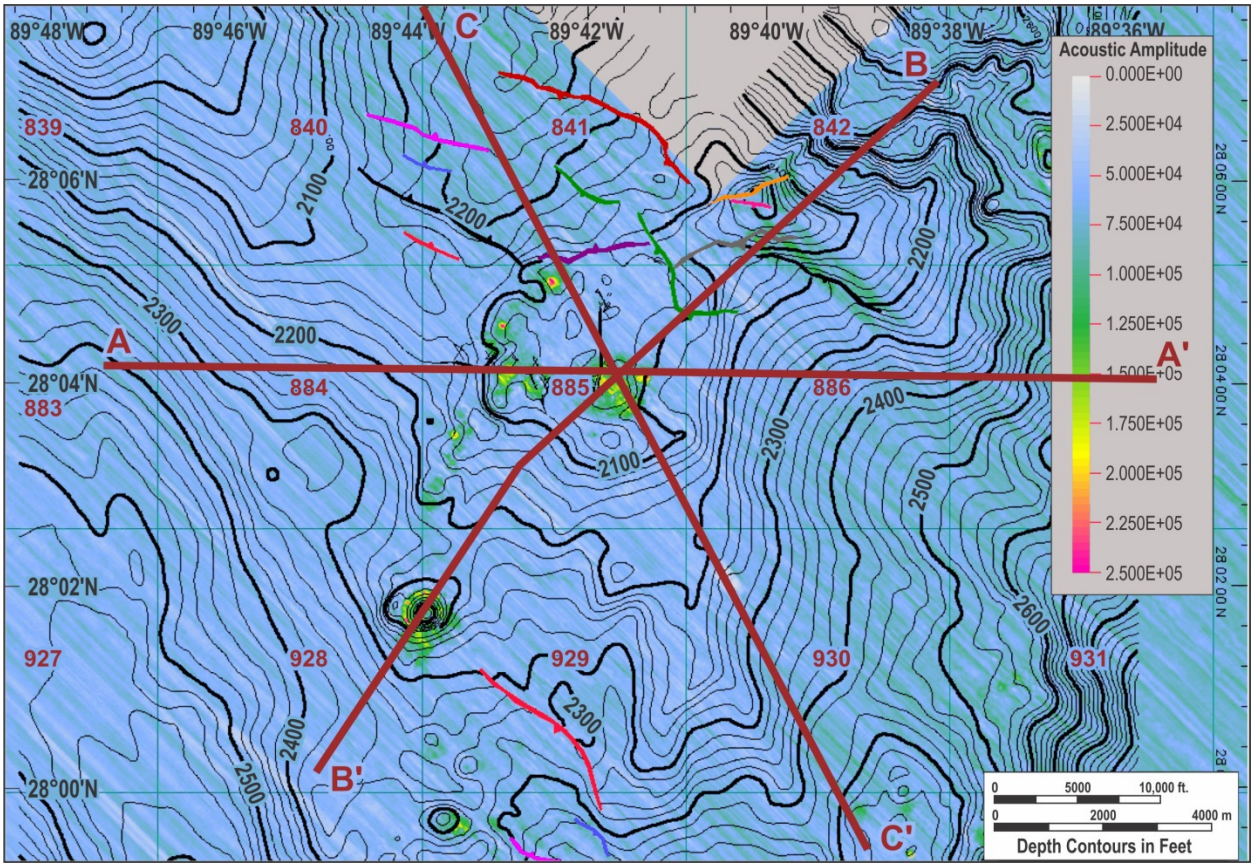

Figure 42. This combined bathymetric and surface amplitude map illustrates the location of the area of interest, a large dome-like relief feature that occupies most of GC 885. The locations of three seismic profiles across this feature are indicated by lines A-A´, B-B´, and C-C´.

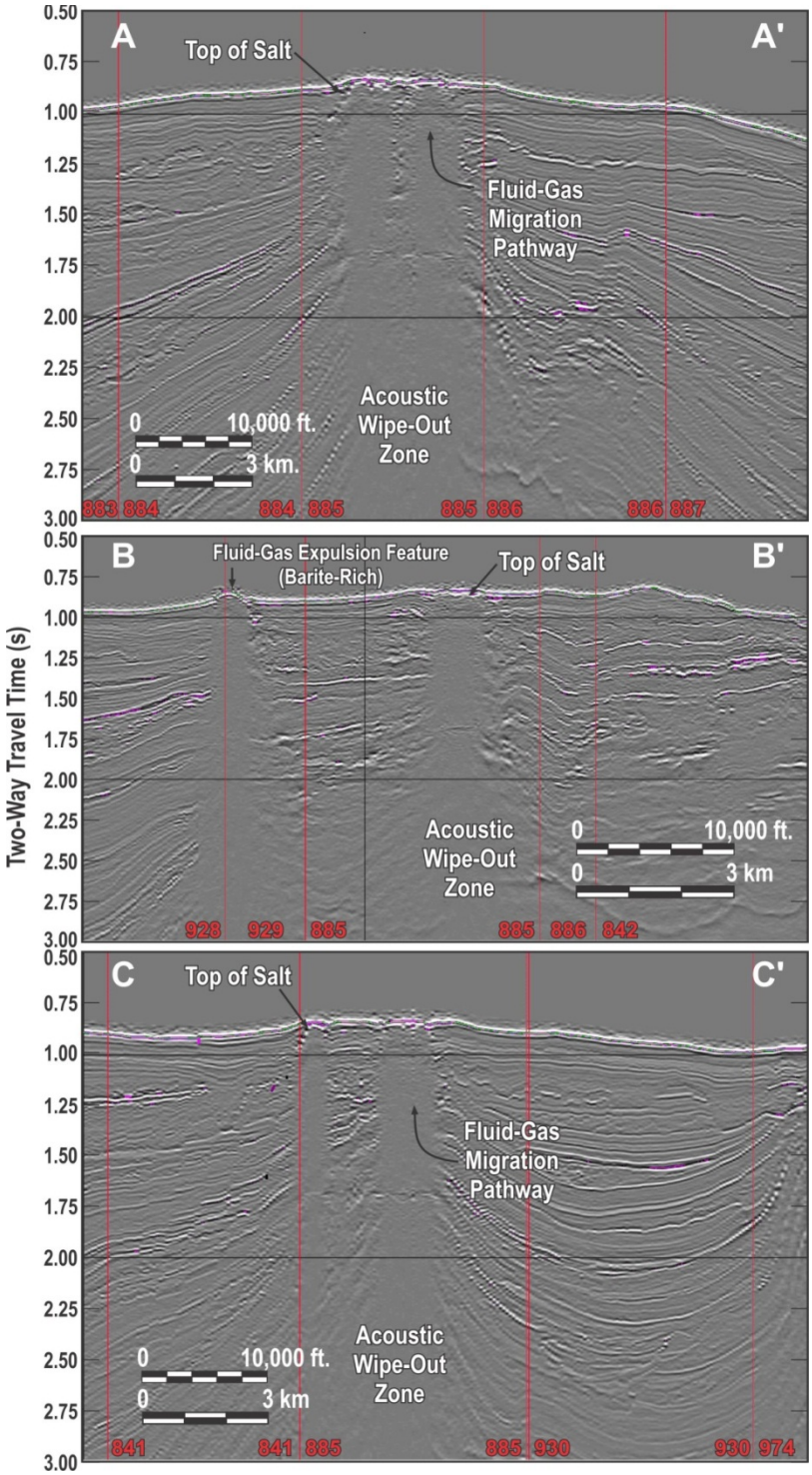

Figure 43. Within the boundaries of the feature confined to MC 885, seismic profiles A-A´ and C-C´ (see Figure 42 for location) show that there are two distinct pathways for fluid-gas migration from the deep subsurface to the seafloor. Profile B-B´ identifies a small but distinct mound on the sea floor to the SW of GC 885 in MC 929. An acoustically blanked migration pathway clearly connects the subsurface to this feature.

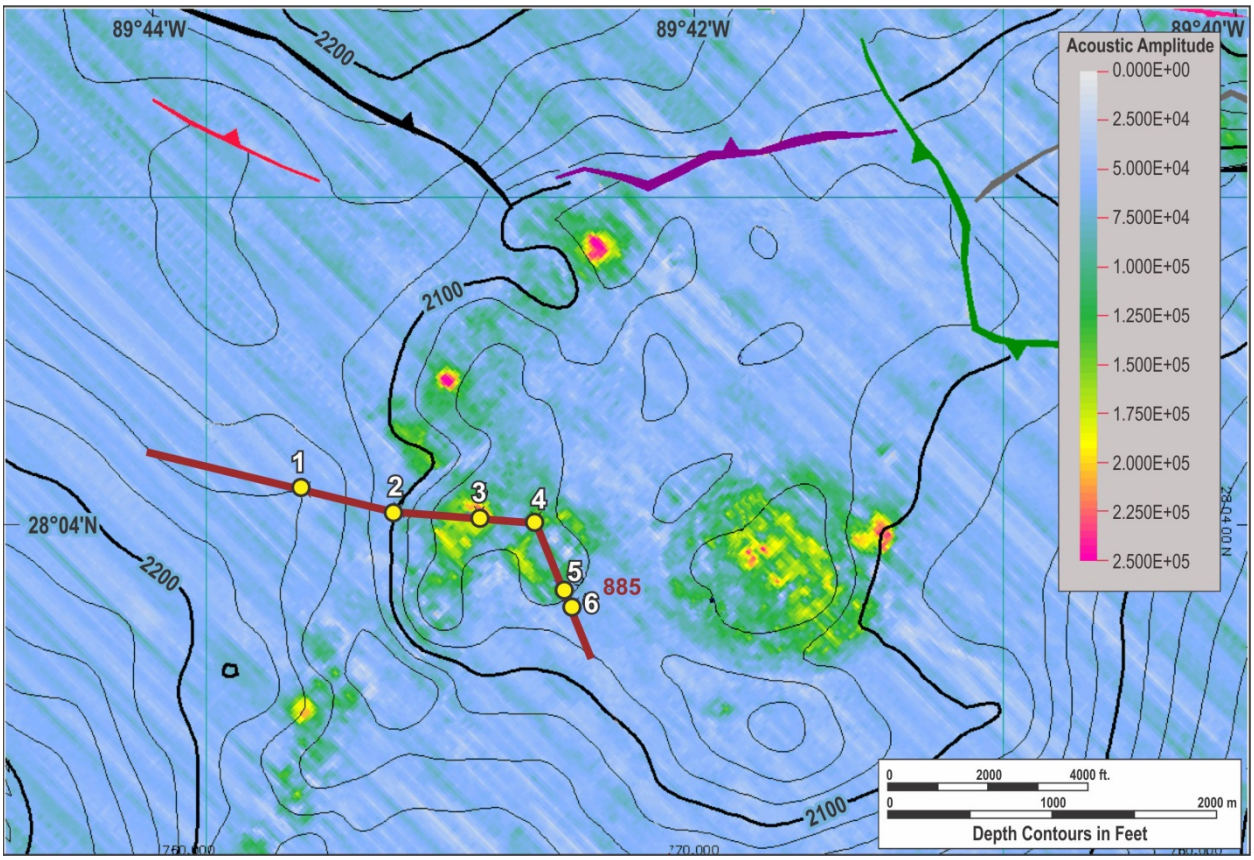

Figure 44. This combined bathymetry and surface amplitude map of the area of interest in MC 885 illustrates the areas of high positive 3-D seismic surface amplitudes and a dive transect with fix points where the character of the sea floor, as determined from submersible observations, is compared to seismic response.

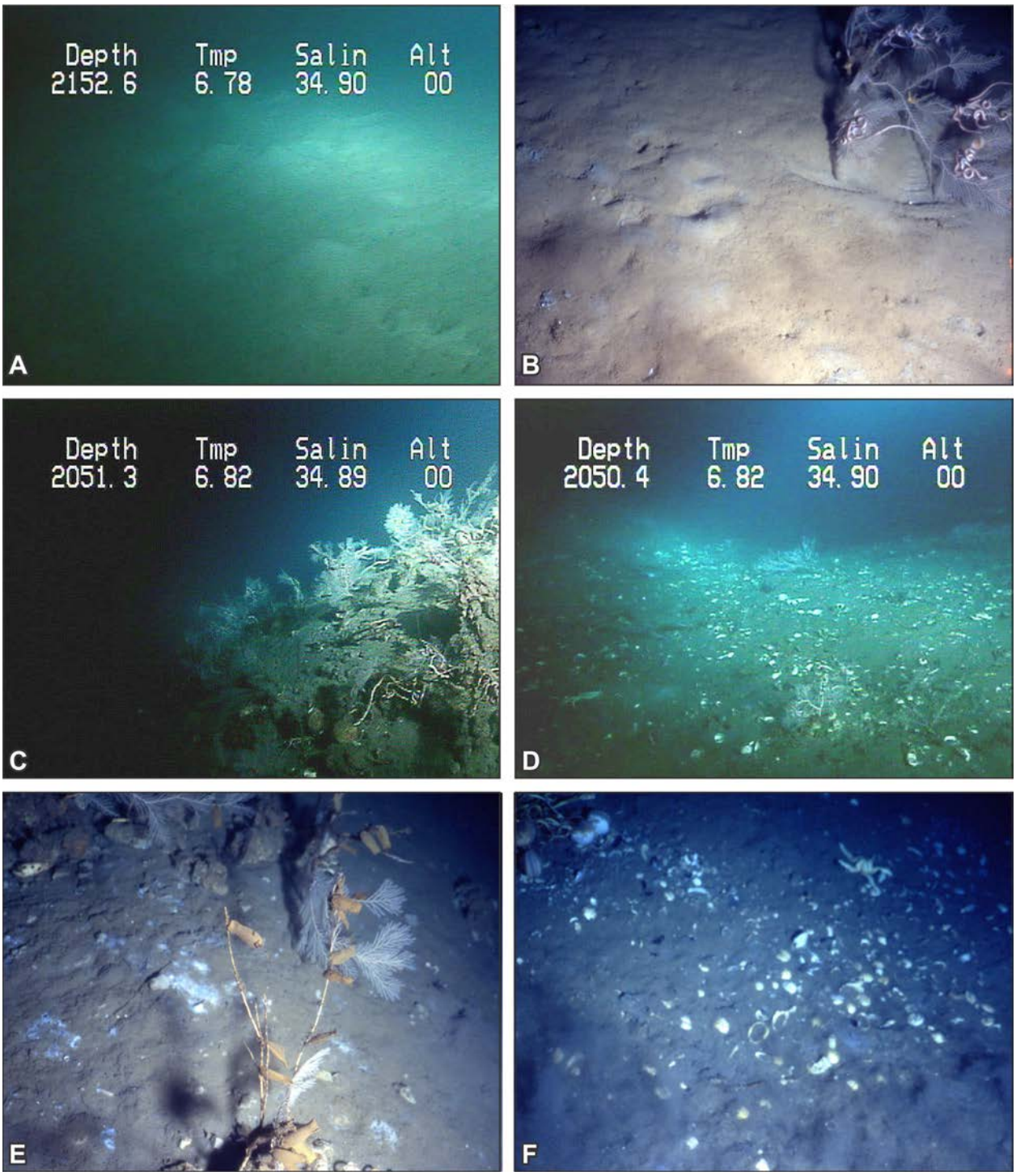

Figure 45. These photographs were acquired at or near the fix points identified on the dive transect of Figure 44. (A) The first fix point on the dive transect occurs on the flank of the large mounded area in MC 885. Burrowed hemipelagic sediments with no indicators of hydrocarbon seepage occur at this site which has a "background" or very low positive 3-D seismic surface amplitude signature. (B) At Fix Point 2, plumes of soft octacorals are attached to a hard substrate below the surface

sediments. The burrowed hemipelagic sediments do not have obvious indicators of hydrocarbon seepage. However, isolated hard substrates, probably shell and/or nodular masses of authigenic carbonate, provide the attachment points for soft corals and other benthic fauna requiring hard bottom conditions. These fauna increase from Fix Point 2 toward the high amplitude area around Fix Point 3. (C) At Fix Point 3, the character of the sea floor changes dramatically from mud-covered bottom to hard bottom composed of authigenic carbonate outcrops covered by soft octacorals, sponges, and small aggregations of tubeworms usually extending from beneath rock ledges and in crevasses. This area of rocky outcrops corresponds to a high positive 3-D seismic surface amplitude response. (D) Between outcrops of authigenic carbonate on top of the mound in MC 885, the bottom is littered with lucinid-vesycomyid clam shells. This site exhibits colonies of soft octacorals seated on both shells and carbonate outcrops scattered throughout the area. (E) At Fix Point 5, the scattered hard bottom elements (carbonates and shells) extend into this area. Small white bacterial mats indicate that slow hydrocarbon seepage is ongoing. This area is representative of a very low hydrocarbon flux environment. (F) Scattered lucinid-vesycomyid clam shells litter the bottom at Fix Point 6. The cross-photograph field of view dimensions of seafloor photographs of this figure are approximately 6-12 ft (2-4 m) except in photographs B and E which are approximately 3-6 ft (1-2 m).

7.8 Case Investigation: Mississippi Canyon 709 (MC 709)

7.8.1 Location and Geology Setting

The feature of interest in MC 709 is an area of elevated sea floor located at the western edge of the Mississippi Canyon (Figures 46 and 47). The prominent cross-slope canyon cuts through the shelf edge and extends downslope to the deep Gulf of Mexico basin floor. This canyon functioned as a sediment conduit for the latest lobe of the Mississippi Fan on the floor of the deep Gulf. The MC 709 mounded zone has distinctive 3-D seismic positive surface amplitude expression. The platform-like feature is located on the apex of a ridge along the highly scalloped canyon margin. This scalloping was created by progressive slumping of the canyon wall (Coleman et al. 1983).

Structurally, the MC 709 feature is related to the crestal collapse of an underlying salt pinnacle that caused extension of the salt and the sediments above it. A crestal fault family developed above the pinnacle-like salt body in the subsurface beneath the MC 709 feature (Figure 48). The stratigraphic interval above the salt is shattered by faulting. Many fluid-gas migration pathways from the relatively deep subsurface exist in this area. Migration is focused by the salt body's pinnacle-like geometry.

The low-relief platform-like feature with positive sea floor amplitude response is located in the SE sector of MC 709 and is generally defined by the 2300 ft (~ 700 m) isobath (Figure 47). This platform is basically oval-shaped in general configuration and is nearly 2 mi (3.2 km) wide in the NE-SE dimension. Two small, but prominent mounds occur on the platform top, the largest of which is located in the SW part of the platform. The second and smallest of the mounds is located near the northern boundary of the platform. Seismic profile A – A' of Figure 47 shows that the platform is underlain by shallow salt, perhaps as shallow as 1 sec (two-way travel time) beneath the sea floor (Figure 48). Numerous faults radiate from the top of salt and offset the shallow subsurface stratigraphy adjacent to and beneath the platform. Acoustic blanking surrounds most of the faults and also occurs in the larger subsurface corridor from the top of salt to various subsurface depths below the platform surface. Stratigraphy beneath the sea floor is chaotic because of the offsets by numerous faults creating discontinuous plus highly reflective segments of once continuous layers.

7.8.2 Sea Floor Amplitudes and Surface Geology

The southern half of the MC 709 platform is the most reflective of acoustic energy and therefore displays the greatest density of scattered patches of moderate-to-high positive sea floor acoustic amplitudes. A well-defined mound bordered by faults on its NE, SW, and SE flanks is the dominant feature in the southern platform sea floor anomaly field. To the SE of this feature, the sea floor slopes gently toward the platform edge, a depth of approximately 2300 ft (~ 700 m). Two low-relief NE-SW oriented ridge-like features occur in this relatively flat part of the MC 709 platform. Very high sea floor amplitudes are scattered throughout this SE platform sector. Faults clearly visible in the shallow subsurface, Figure 48, translate to the seabed and are probably responsible for the ridge-like features dominating the geomorphology of the sea floor in

this part of the platform. The shallowest area associated with the SE sector of the platform generally exhibits a low positive acoustic amplitude or low acoustic energy reflectivity.

7.8.3 Interpretation of 3D-Seismic Sea Floor Amplitude Using "Ground Truth" Data

The NW-SE oriented Johnson Sea-Link submersible transect for collecting photographs and samples of the MC 709 surface amplitude anomaly is shown on Figure 49. The transect begins along the NW flank of the MC 709 platform and extends to the SE platform margin.

The beginning of the transect (Fix 5, Figure 49) starts on the slope leading up to the NW part of the platform top. At this site, the sea floor acoustic amplitude response is slightly above general off-platform background levels, moderate-to-low values. The seabed at this initial part of the transect is basically highly burrowed hemipelagic sediments. It also appears that remnant bed forms are present and have been degraded by bioturbation after their formation. These features suggest that strong currents have impacted the flank of the MC 709 platform in the recent past.

The areas upslope of Fix 5 (Figure 49) exhibit discrete and scattered moderate-to-high acoustic amplitude sites. One of the sites, Fix 8, occurs on the top of the mounded feature in the SW part of the platform top. At this location, scattered high amplitude patterns at the mound crest are surrounded by low positive amplitudes of the mound flanks. Hard substrates of seep-related carbonate were found at Fix 8 and other scattered high amplitude sites in this general area (Figure 50B).

Outside of the high amplitude areas associated with the crest of the mound described above, the sea floor has poor reflectivity (low positive acoustic amplitude) and shows signs of active brine seepage. Escarping gas was observed in several areas of the low positive 3-D seismic surface amplitude field. At Fix Points 9 and 10 brine streams were observed eroding the bottom sediments (Figures 50C, D). These areas supported communities of lucinid-vesycomyid clams and gastropods. In general, the sea floor areas of high positive acoustic amplitude values along the submersible transect shown in Figure 49 were found to be areas of outcropping seep carbonates as illustrated at Fix Points 11 and 12 (Figure 50) and the low positive amplitude were found to be primarily zones of brine seepage and gas-charged sediments.

7.8.4 Summary

The MC 709 mounded platform constitutes a large and an imposing 3-D seismic surface amplitude anomaly along the western margin of Mississippi Canyon. Seismic profile data show that this feature, which is approximately 2500 m (8200 ft) wide in the E-W direction, is supported by salt in the relatively shallow subsurface (approximately 2 sec. two-way travel time below the sea floor). Shallow subsurface seismic data from below the surface of the MC 709 mounded platform reveal a complex faulting pattern that roughly radiates from the top of the underlying salt body. Stratigraphic reflectors are highly chaotic in this zone above the salt and the many faults appear to provide numerous pathways for fluids and gases to migrate from the subsurface to the modern sea floor.

The correlation between 3-D seismic sea floor amplitudes, both high positive and low positive-to-negative values, and the character of the seabed was consistent with most sites analyzed as a part of this investigation. The moderate-to-low positive sea floor amplitudes at the off-feature starting point for the submersible transect is consistent with other areas of the slope where hemipelagic muds drape the sea floor including low relief features. On top of the platform, however, the sea floor acoustic amplitudes range widely from high positive to low positive-negative values. The areas of high positive values were generally correlated with regions where authigenic carbonate outcrops protruded from a mud-rich surface sediment. These outcrops ranged in scope from lithified slabs and crusts to large boulder size and larger features.

The areas that demonstrated low seismic energy reflectivity, or low positive-to-negative acoustic amplitude values most often correlated to areas of brine seepage and soft sediment. At several of these areas crossed during the submersible transect, gas bubbles were observed escaping from the sea bed into the water column.

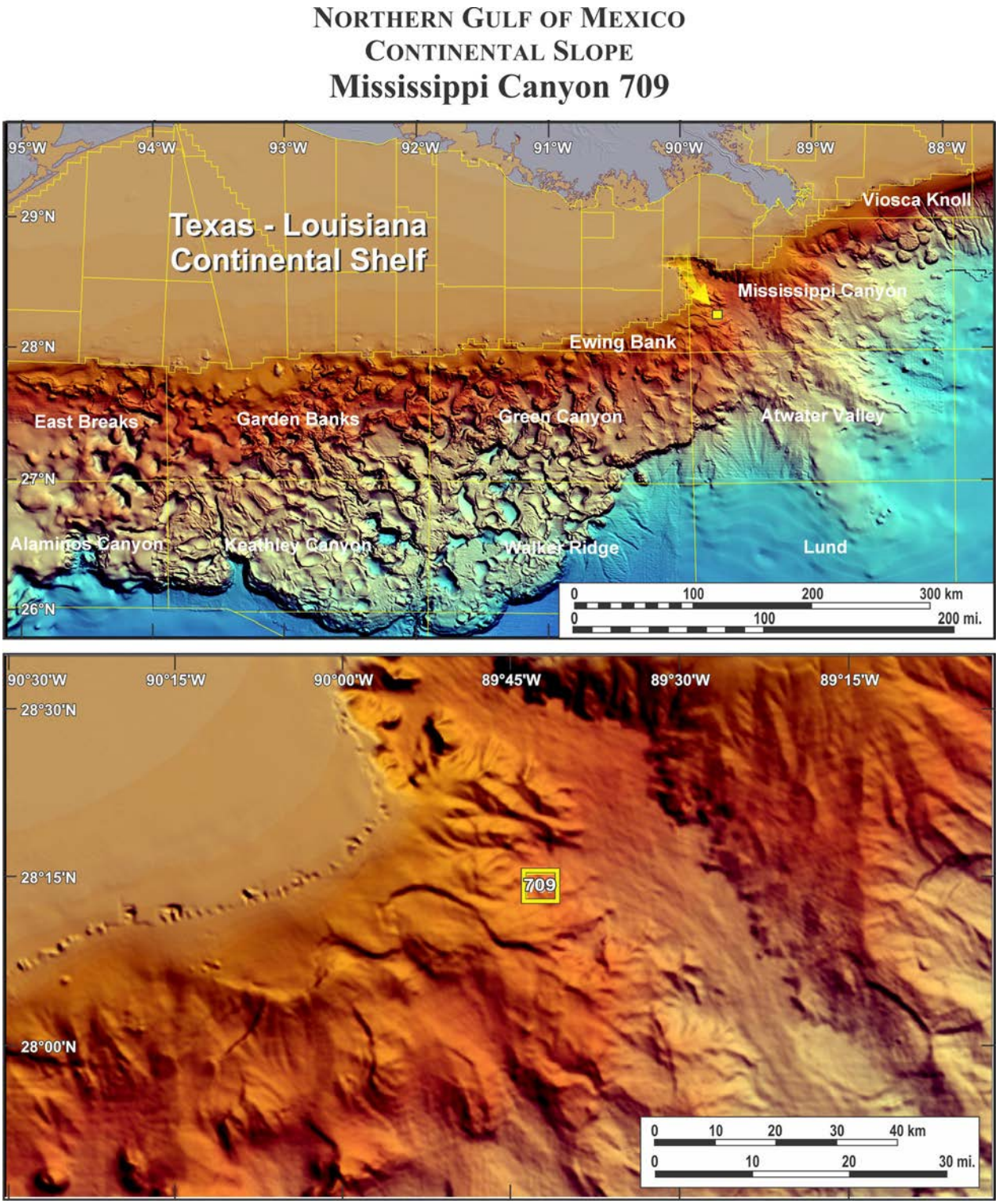

Figure 46. (A) Shaded multibeam bathymetry map of the northern Gulf of Mexico continental slope. The yellow arrow points to the location of Mississippi Canyon Block 709 (MC 709). (B) The enlarged area of the continental slope surrounding MC 709 identifies the bathymetric features within and surrounding the block.

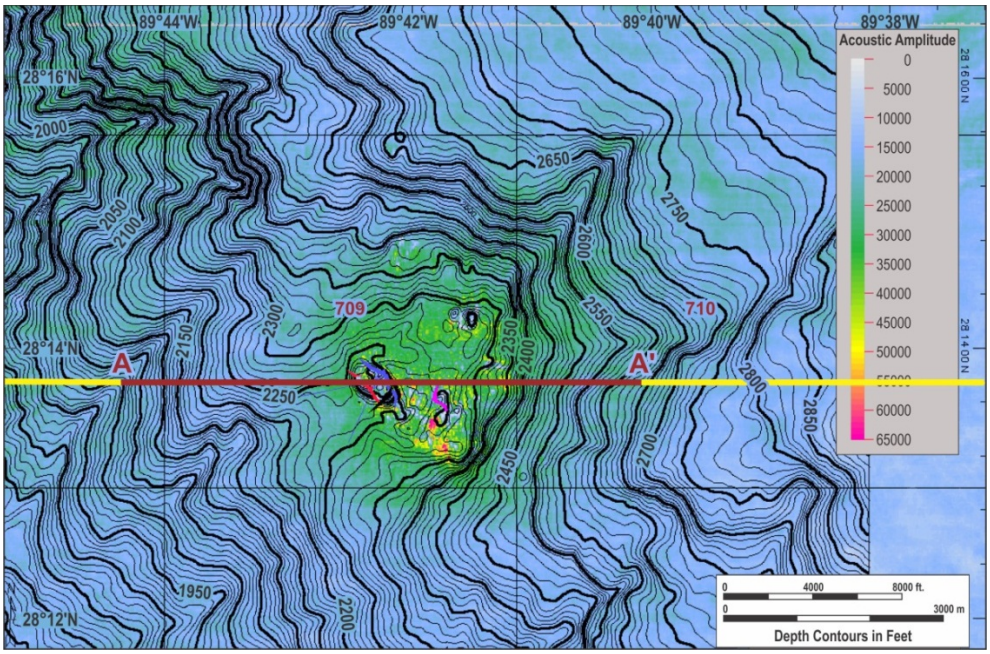

Figure 47. This combined bathymetry and surface amplitude map illustrates the area of interest along the SW part of a large complex mounded area that is supported by shallow subsurface salt in the eastern part of MC 709. Line A-A´ indicates the location of an E-W oriented seismic profile through an area of both low and high surface amplitudes on top of the low-relief MC 709 mound.

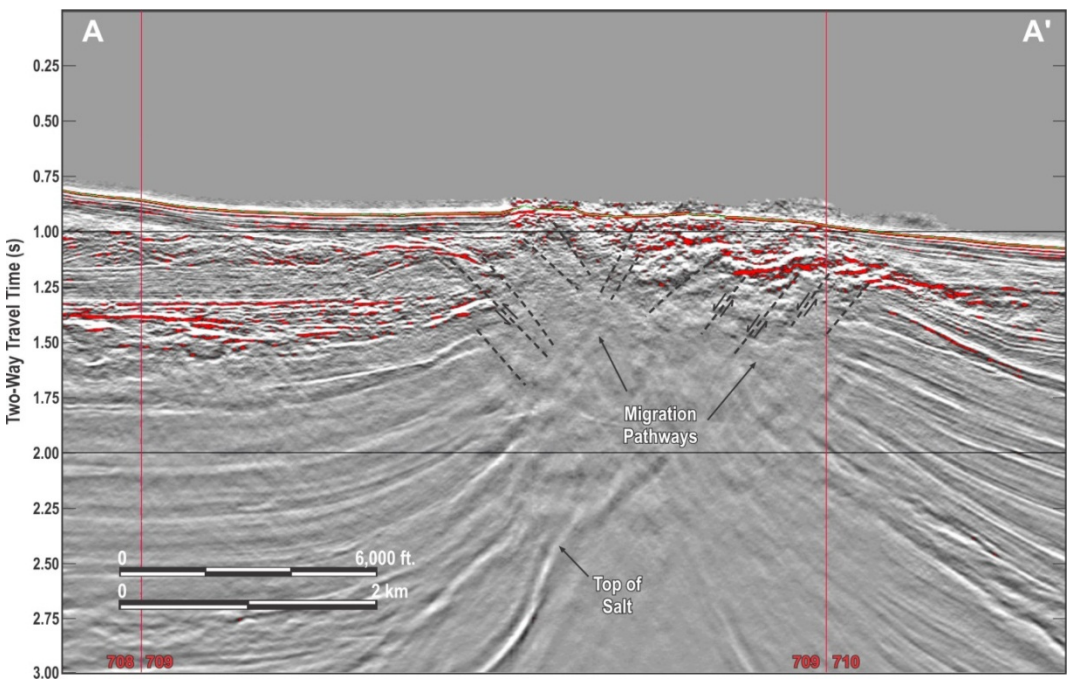

Figure 48. Seismic profile A-A´ shows the subtle relief of the MC 709 mound and the complex network of faults that have the capability of acting as transport pathways for fluids and gases to migrate from the deep subsurface to the sea floor (see Figure 47 for location of seismic profile A-A´). A broad zone of acoustic blanking and acoustic turbidity characterizes the subsurface beneath the surface mound and above the top of salt.

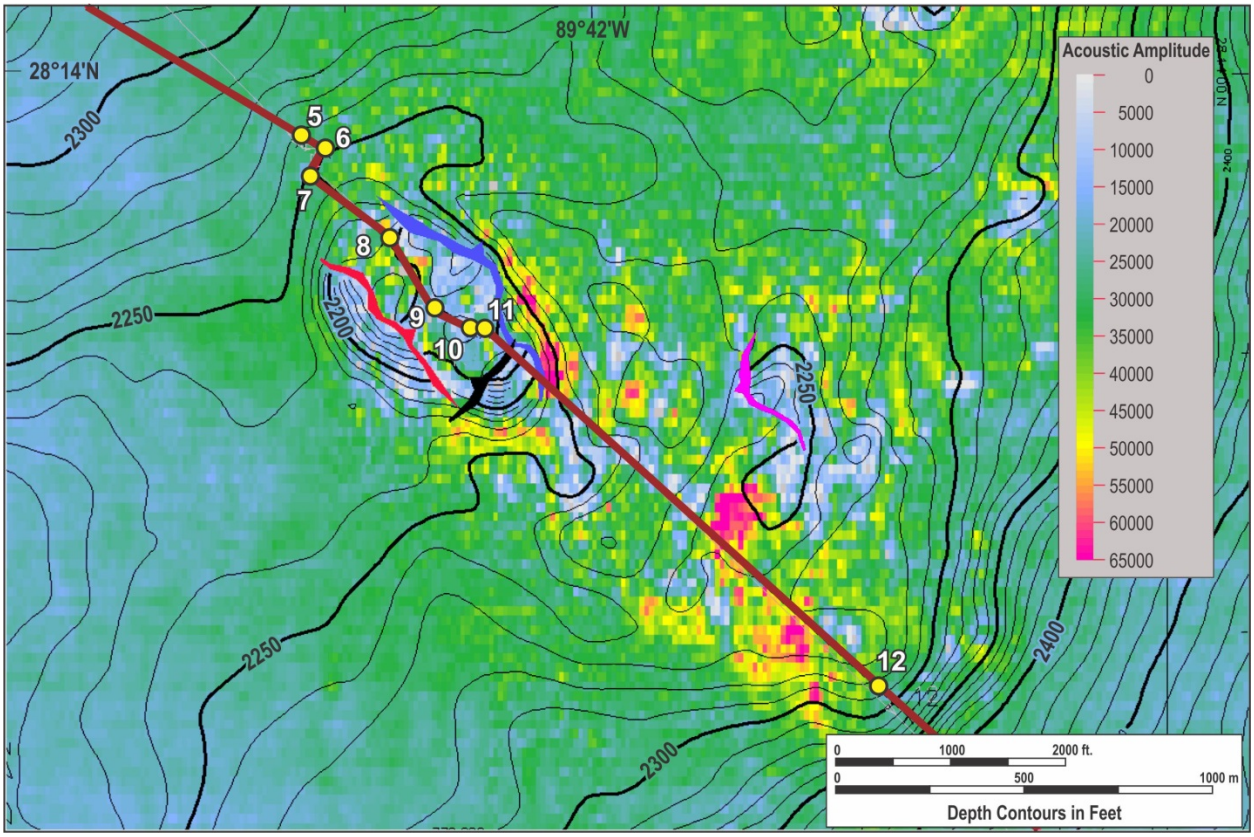

Figure 49. This combined bathymetry and 3-D seismic surface amplitude map illustrates a high level of variability in surface acoustic reflectivity. Surface amplitudes range from low positive amplitudes associated with the elevated and roughly rounded feature in the western part of the MC 709 mound to very high positive amplitudes in the SE sector. The NW-SE trending dive transect concentrates observations on the local mound in the NW sector of the overall area of interest.

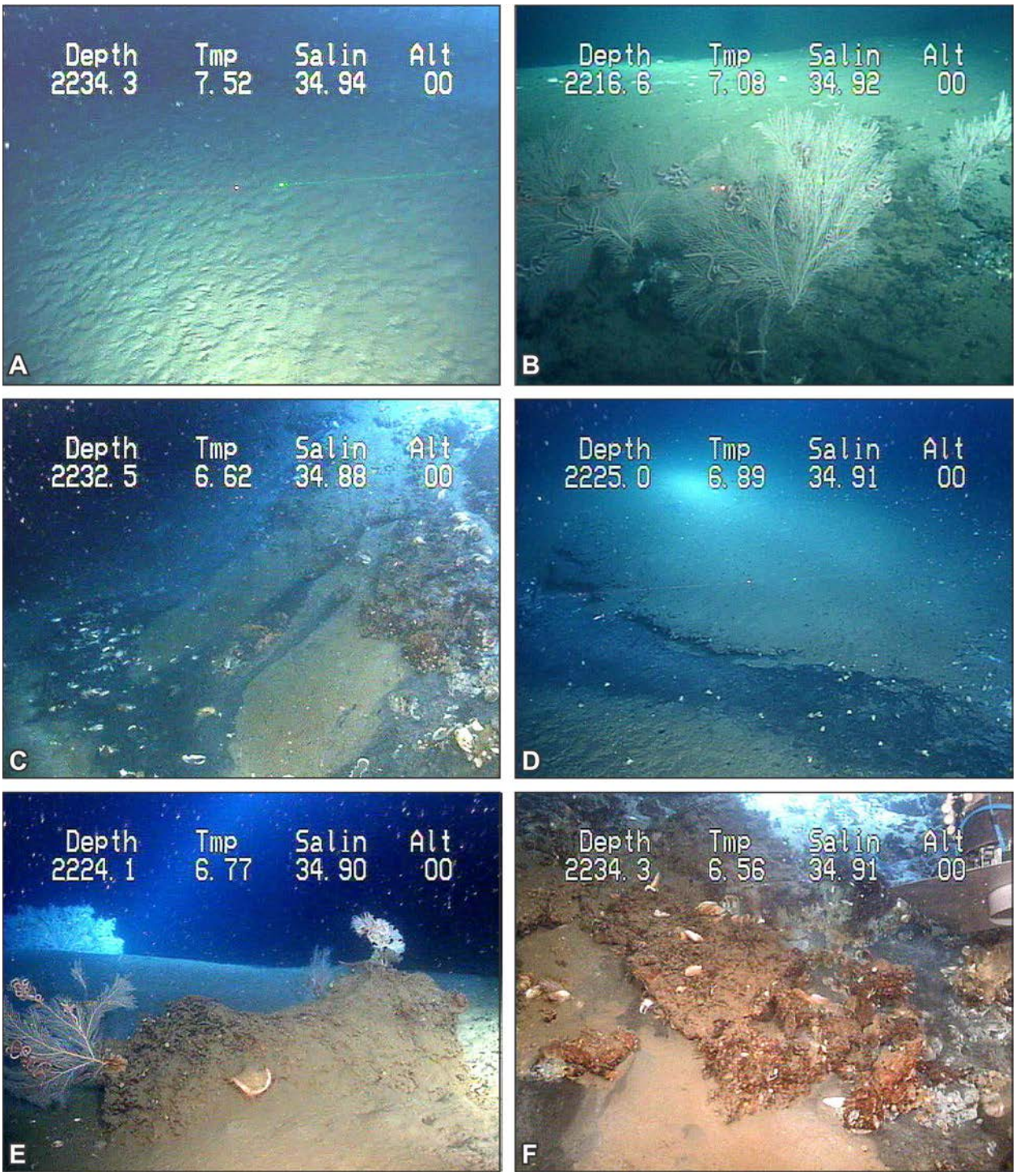

Figure 50. These bottom photographs are typical of various zones of reflectivity along the dive transect shown in Figure 49. (A) At Fix Point 5, the beginning of the dive transect, the surface amplitude map (Figure 49) indicates near background levels, but slightly above background. The bottom photograph of this site identifies muddy sediments, probably hemipelagic sediments, that are thoroughly burrowed and have a few clam shells scattered over the bottom in the background. (B) On top of the mound

localized in the NW part of the general area of interest, surface amplitudes are highly variable (see Figure 49). At Fix Point 8 hard substrate composed of authigenic carbonate is commonly exposed at the sea floor. Soft octacorals inhabit these hardgrounds that provide the necessary substrates for sessile organisms. (C) This photograph taken at Fix Point 9 illustrates an area of brine seepage, localized authigenic carbonate occurrence, and scattered lucinid-vesycomyid clam shells. (D) Like Fix Point 9, Fix Point 10 is at a site of brine seepage. Small gastropod shells are scattered over the bottom in this area. Areas surrounding both fix points have low positive 3-D seismic sea floor amplitude responses. (E) Fix Point 11 is located on a fault that trends NW-SE along the eastern flank of the mounded feature shown in Figure 49. Large carbonate outcrops inhabited by sessile organisms such as soft octacorals are scattered throughout the area. A pattern of variable surface amplitudes characterize this site. (F) Between Fix Points 11 and 12, the surface amplitude response varies from very high positive zones to isolated areas of low positive values. This photograph comes from an area NW of Fix Point 12 that displays a high positive surface amplitude response. Abundant slabs and boulder-sized outcrops of authigenic carbonate cover the seafloor of this area. The cross-photograph field of view dimensions for the sea floor photographs of this figure are approximately 6-12 ft (2-4 m).

7.9 Case Investigation: Mississippi Canyon 118 (MC 118)

7.9.1 Location and Geology Setting

The MC 118 hydrocarbon seepage site was first directly observed and sampled in 2002 on a series of Johnson Sea-Link submersible dives. Location of the feature of interest was accomplished by analyzing regional 3-D seismic datasets held by BOEM in their New Orleans Office. A distinctive 3-D seismic sea floor anomaly occurs in the southern half of the MC 118 lease block. In a regional context, this lease block is located on the upper continental slope approximately 50 miles (~ 80 km) SE of the modern Mississippi River delta (Figure 51). This location is directly downslope of the Lagniappe shelf-edge delta (Kindinger 1989) and the western margin of an upper continental slope area characterized by the occurrence of numerous near-surface tablet-like salt bodies and cross-slope channels.

The 3-D seismic surface amplitude anomaly that constitutes the area of interest in MC 118 is bracketed by water depths between approximately 2900 -3060 ft (884-933 m), Figures 52 and 53. This area of enhanced seabed acoustic reflectivity is on the flank of a NW-SE trending channel-like depression that marks the western margin of a distinctive subrounded shallow salt body (Figures 51 and 52). The MC 118 anomaly is a very low relief and complex sea floor feature directly above an underlying shallow salt body. The seismic profiles of Figure I3 indicate that top-of-salt is located approximately 0.5 s (two-way travel time) from the modern sea floor. A family of faults originating from the top and flanks of the shallow salt body focus migration of hydrocarbons to the sea floor. Fluid-gas migration pathways from the deep subsurface on the salt body flank and above the salt to the seabed are clearly defined by the numerous faults cutting through the stratigraphic interval above the salt. The migration pathways (faults) are very steeply dipping (near vertical). There is no collapse structure above the salt and no regional fault to which the MC 118 feature is related. However, this feature is above a part of the continental slope characterized by deep salt roller terrain (Rowan et al. 1999).

High resolution AUV data from the area of interest reveal a complex sea floor with considerable variability in local relief, strong backscatter in side-scan sonar data, and nearly complete acoustic blanking on chirp sonar profiles of subsurface reflectors beneath the overall feature (Sleeper et al. 2006). These characteristics are in stark contrast to the well-stratified sediments adjacent to the anomaly.

7.9.2 Sea Floor Amplitudes and Surface Geology

The field of elevated sea floor reflectivity in MC 118 has a “pock marked” appearance on the 3-D seismic surface amplitude map of Figure 53. Discrete rounded areas of moderate seismic energy reflectivity are surrounded by higher reflectivity sea floor. A halo of moderately positive sea floor amplitudes surrounds the main area of interest which exhibits isolated areas of very high positive acoustic amplitude response. These high positive areas correlate to the highest relief features associated with the overall seismic amplitude anomaly. Sleeper et al. (2006) identify five separate subcircular high backscatter patterns in the side-scan sonar backscatter data from the MC 118 anomaly. Three of these areas correlate with vent structures identified by Sassen et al. (2006). The seabed is highly irregular on a local scale within the high

backscatter areas. Seismic profiles (N-S and E-W) across the MC 118 anomaly clearly illustrate faults that reach the modern sea floor and are not only avenues for fluid-gas migration, but are largely responsible for the prominent variations in sea floor relief associated with this feature.

7.9.3 Interpretation of 3-D Seismic Sea Floor Amplitudes Using "Ground Truth" Data

The Johnson Sea-Link was used to initially explore the MC 118 sea floor anomaly once it had been identified and thoroughly studied in conjunction with BOEM geoscientists using the 3-D seismic database housed in the New Orleans office. A NW-SE transect across the anomaly illustrated in Figure 54, was conducted in the submersible in order to collect "ground truth" observations and bottom samples to correlate to 3-D seismic surface amplitude data. Figure 55 compiles submersible-acquired photographs of the sea floor along the transect of Figure 54.

At the beginning of the transect, Fix 2 of Figure 54, which was in the halo of moderate acoustic sea floor amplitudes, a rather featureless mud bottom with animal burrows was encountered. However, a few small rock clasts and clam shells were observed in the area. Moving eastward from this site to Fix 3 (Figure 54) the character of the bottom changed considerably. This site, less than 500 ft (152 m) away, had numerous clasts of carbonate rock and clam shells scattered over the surface of hemipelagic muddy sediment (Figure 55B). The bottom character at this site remained essentially the same as the submersible transited upslope to Fix 4 (Figure 54). The 3-D seismic sea floor amplitudes steadily increased upslope to Fix 4 where very high positive values were encountered.

At Fix 4, the local relief on the sea floor became dramatic. Outcrops of authigenic carbonate rock invaded with orange-colored gas hydrate formed the highest relief areas. Figures 55C and D illustrate the carbonate rock outcrops with seams of orange gas hydrate. Each of these outcrops was observed to have free gas escaping through cracks and pores of the carbonate rock producing bubble streams into the overlying water column. Several of these bubble streams can be observed in Figure 55C.

A series of carbonate rock outcrops containing seams of gas hydrate were encountered around the very high acoustic amplitude zone roughly in the middle of the overall MC 118 anomaly (Fix Points 4-7, Figure 54). Small gas seeps resulting in bubble streams were observed throughout this area and they appear to be related to gas hydrate destabilization (Lapham et al. 2010). However, as the submersible transect continued toward the southeast, local topography became less variable and a mud bottom with numerous rocky clasts became the norm. At Fix 8 (Figure 54) bottom topography became hummocky and mud covered. The carbonate clasts mixed into this sediment provided limited substrates for sessile benthic fauna. The transect ended in a zone of moderately high acoustic amplitudes (Figure 54) which probably correlates to the considerable number of carbonate clasts mixed into the surface sediment as well as the possibility of buried carbonate hardgrounds and gas hydrate.

7.9.4 Summary

The area of interest in MC 118 is a large 3-D seismic sea floor amplitude anomaly that is approximately 1.5 mi (2.4 km) in diameter and has a complex of surface amplitude patterns and local relief features. The areas of highest acoustic amplitude or reflectivity were found during ground truth data collection to correlate to areas of mounded authigenic carbonates associated with orange gas hydrate and escaping gas. The gas hydrate invaded the cracks and voids of the carbonate buildups as well as occurred as stand-alone outcrops on the sea floor.

Lateral to these areas of high acoustic amplitude or seismic energy reflectivity, the sea floor changed dramatically from rocky outcrops to mud-covered bottom containing both carbonate clasts and clam shells. This type of bottom and slight variations of it correlated to a moderate acoustic amplitude or reflectivity (Figure 54). Observations at the overall MC 118 anomaly made from the Johnson Sea-Link submersible did not get outside of the anomaly itself where only background hemipelagic sediments would be encountered.

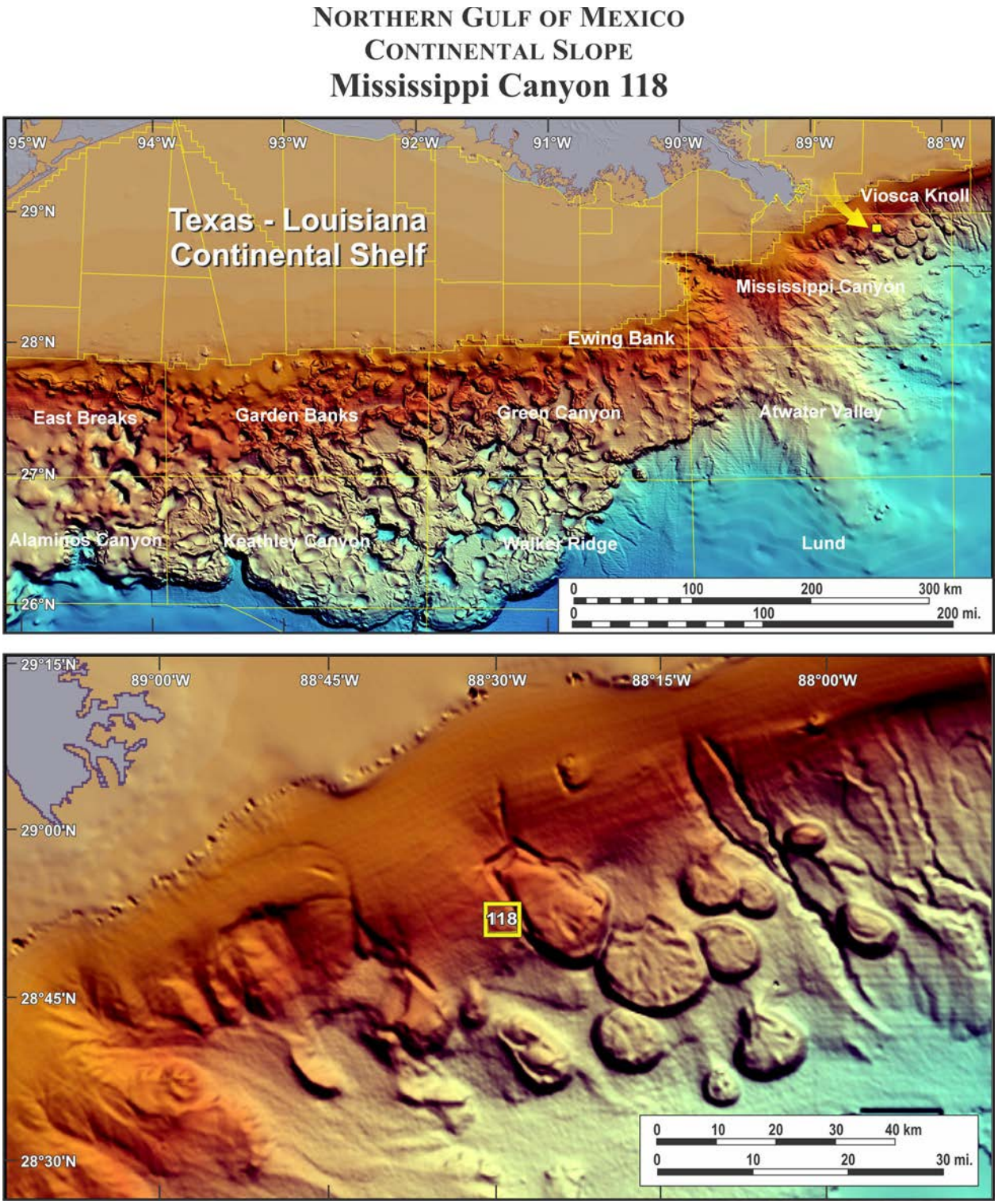

Figure 51. (A) Shaded multibeam bathymetry map of the northern Gulf of Mexico continental slope. The yellow arrow points to the location of Mississippi Canyon Block 118 (MC 118). (B) The enlarged view of the area of the continental slope surrounding MC 118 illustrates the bathymetric features within and surrounding the block.

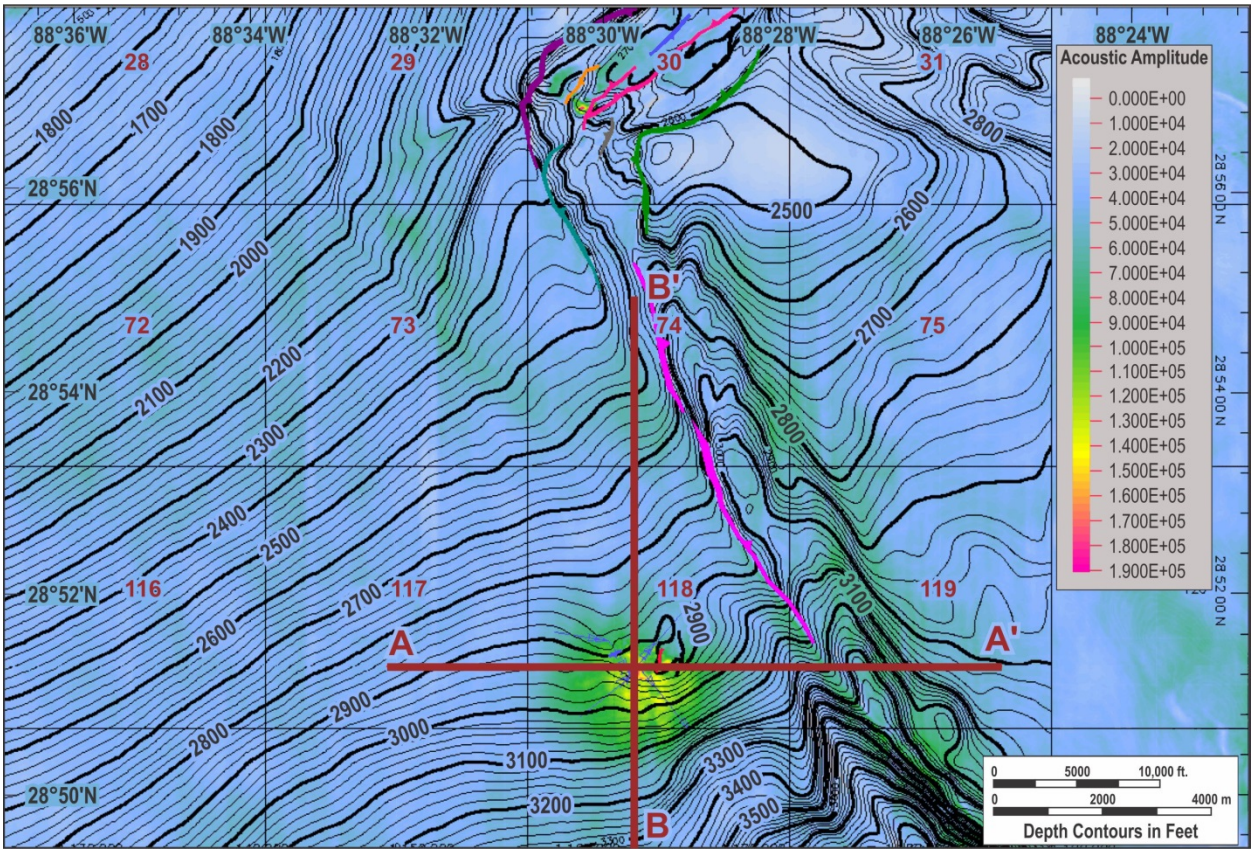

Figure 52. This combined bathymetric and surface amplitude map illustrates the feature of interest in the SW sector of MC 118 where 3-D seismic surface amplitude data indicate a highly reflective seafloor. Lines A-A´ and B-B´ indicate the locations of N-S and E-W. oriented seismic profiles through the zone of highly reflective seafloor.

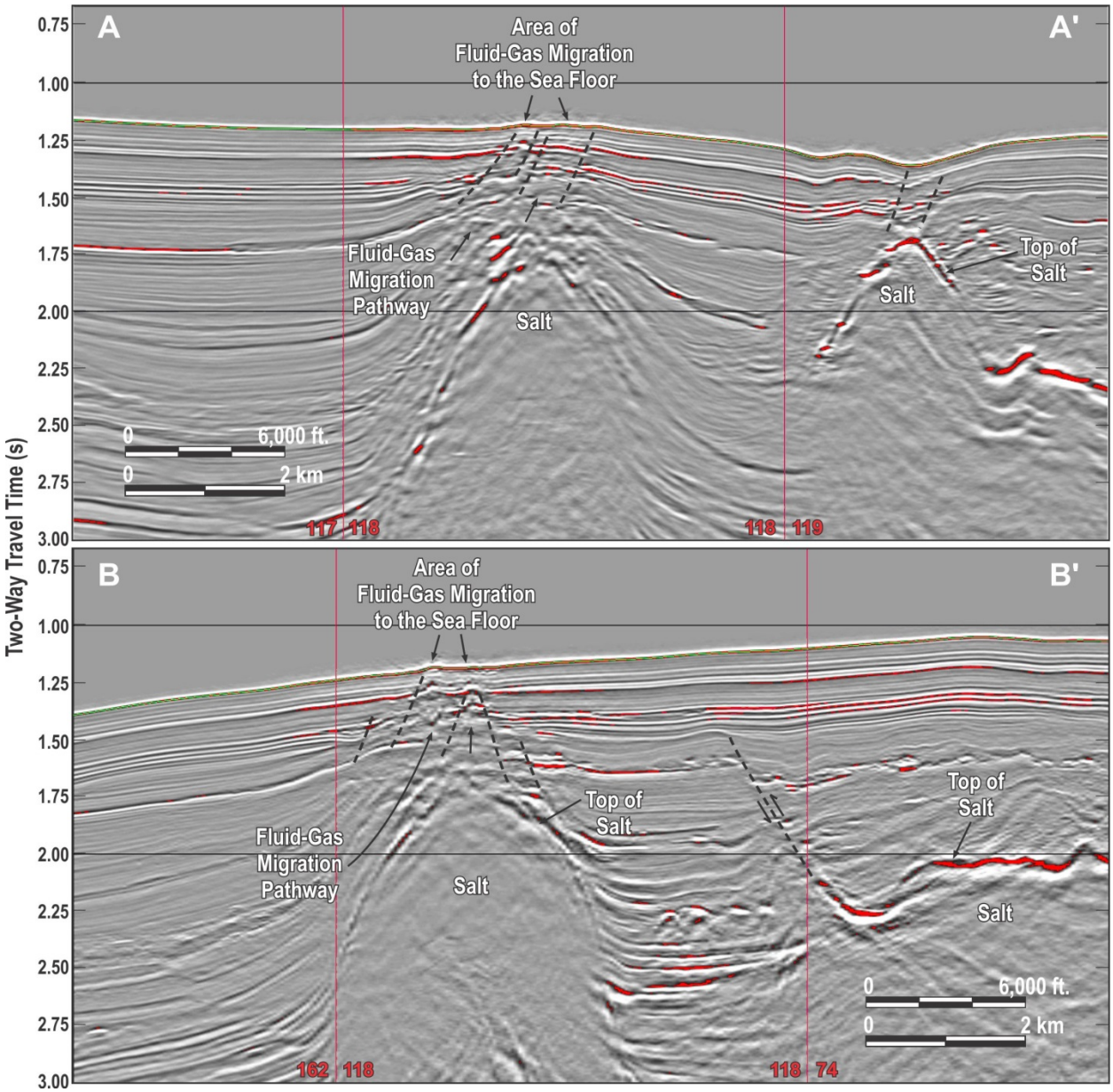

Figure 53. Seismic profile A-A´ (see Figure 52 for location) is an E-W trending seismic cross section through the high amplitude sea floor area in the SW part of MC 118. This profile indicates that the area of interest overlies a faulted zone located above a shallow salt body. Migration pathways for fluid and gas from the deep subsurface to the sea floor are clearly fault-controlled. The NW-SE trending sea floor depression east of the high amplitude zone is a product of faulting at the edge of the shallow subsurface salt body. The N-S trending profile (see Figure 52 for location) reveals the highly faulted sedimentary section below the sea floor area of interest and above the shallow subsurface salt body.

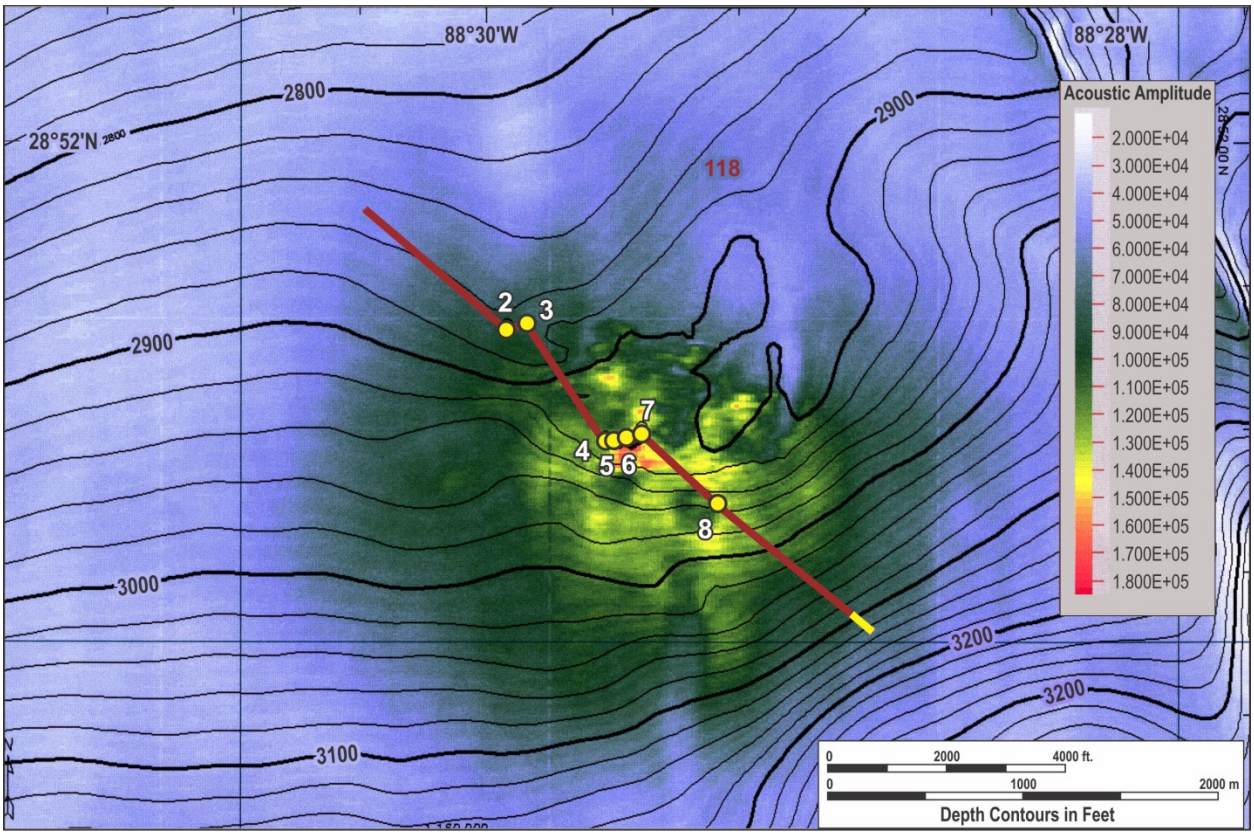

Figure 54. This combined bathymetry and 3-D seismic surface amplitude map of the acoustically reflective area of interest in MC 118 has a dive transect superimposed on it and fix points where bottom observations were made.

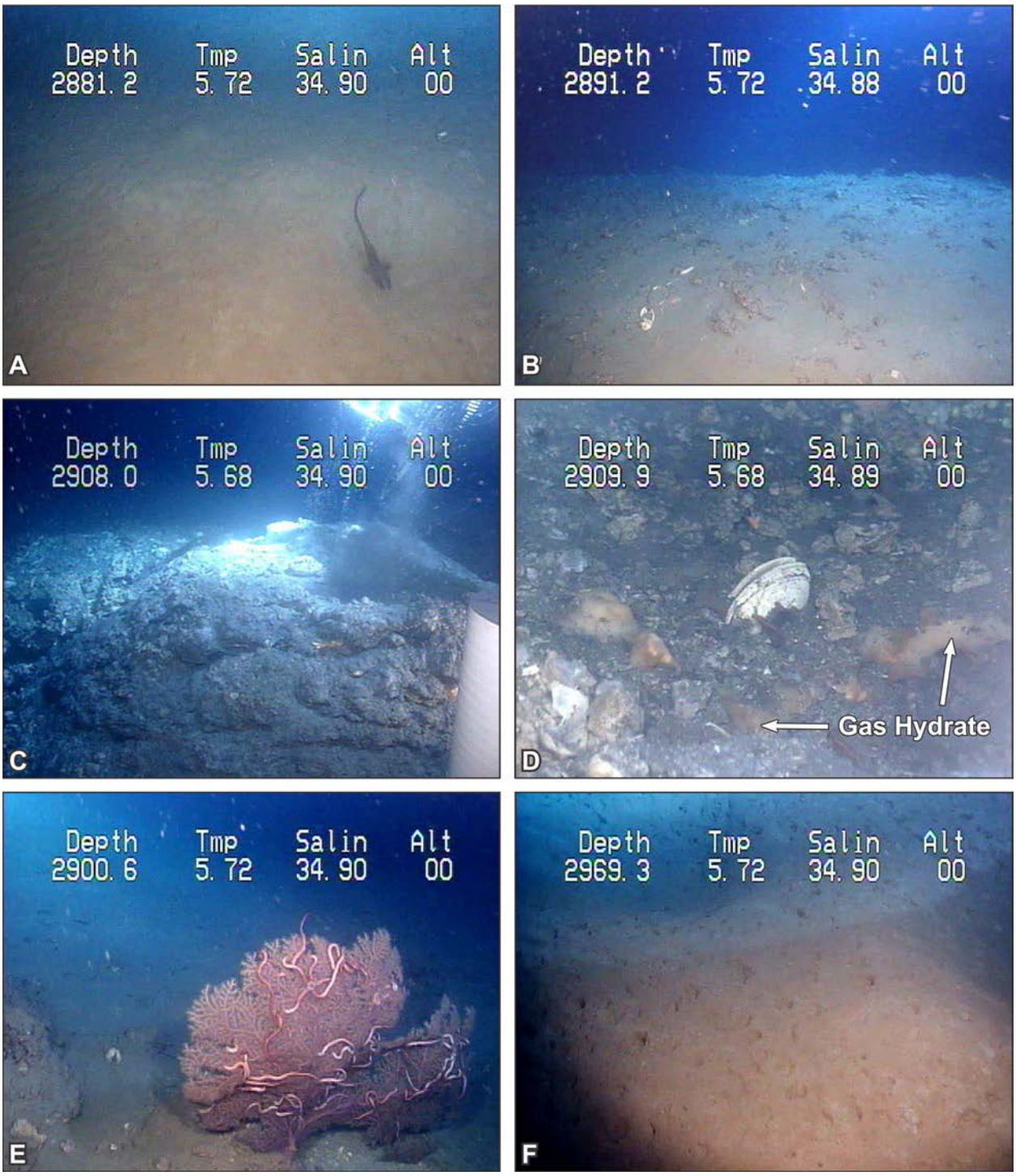

Figure 55. These photographs are representative of sea floor characteristics at or near the fix points identified in Figure 54. (A) At Fix Point 2 near the beginning of the transect, the bottom is mud-covered and burrowed. There is very little evidence of hydrocarbon seepage indicators. (B) Slightly upslope of Fix Point 2 at Fix Point 3, the character of the bottom changes. Scattered lucinid-vesycomyid clam shells and small nodular masses of authigenic carbonate litter the muddy bottom sediments

and reflectivity of the sea floor, as estimated with 3-D seismic surface amplitude data, becomes more positive upslope. (C) At the apex of the MC 118 slightly mounded area, outcrops of authigenic carbonate invaded with gas hydrate are common. At this site (Fix Point 5), gas is escaping from the top of one of these outcrops. (D) A close-up view of a carbonate outcrop containing "seams" of orange gas hydrate and clam shells embedded in the carbonate at Fix Point 6 illustrates the "hard bottom" conditions that correlate to the zones of very high positive 3-D seismic surface amplitude values. (E) Gorgonians and other organisms requiring a hard substrate are common to the areas where authigenic carbonates outcrop at the bottom, like the areas in the vicinity of Fix Point 7. (F) Much like the bottom at Fix Point 3, muddy sediments with isolated nodular masses of authigenic carbonate characterize this sea floor area. The cross-photograph field of view dimensions for all of the above bottom photographs of this figure are in the 6-12 ft (2-4 m) range except for the close-up (6). The lateral dimension of this close-up is < 1.5 ft (0.5 m).

7.10 Case Investigation: Vioska Knoll 826 (VK 826)

7.10.1 Location and Geologic Setting

The feature of interest in VK 826 (Figure 56) is a large mounded area of sea floor located in the SW corner of VK 826 extending into the SE corner of VK 825 and slightly into the northern parts of VK 869 and 870 (Figure 57). The VK 826 mound is on the upper continental slope about 90 mi (144 km) east of the modern Mississippi River Delta and just downslope of the eastern lobe of the late Pleistocene Lagniappe shelf-edge delta (Kindinger 1989; Sydow et al. 1992). As the computer enhanced multibeam bathymetry map of Figure 56 illustrates, VK 826 is located along the eastern margin of a sector of the continental slope distinguished because of its numerous cross-slope channels that start on the upper slope and terminate at the deep basin floor. The VK 826 mound occurs on a comparatively featureless part of the upper continental slope just upslope of the apparent starting point for most of the cross-slope channels.

The southeastern part of the VK 826 mound is defined by a prominent NE-SW trending down-to-the southeast fault. An E-W trending down-to-the-south fault forms the southern boundary of the mound. However, structurally the mound is only related to the very shallow subsurface salt body. The mound occurs in water depths between approximately 1600 ft (488 m) and 2200 ft (671 m) with a crest slightly shallower than 1500 ft (457 m). As the SW-NE and NW-SW oriented seismic profiles of Figures 57 and 58 clearly illustrate, the mound is the product of salt in the shallow subsurface. The top of underlying salt is as close as 0.10s (two-way travel time) from the modern sea floor. The stratigraphic interval between the salt and sea floor has a chaotic character. The discontinuous reflectors in this interval suggest a “shattered” or highly faulted stratigraphy. Well-defined fluid-gas migration pathways occur on the flanks of the salt body. Figure 57 illustrates the primary faults associated with the VK 826 mound.

7.10.2 Sea Floor Amplitudes and Surface Geology

The bathymetric maps of Figures 57 and 59 indicate highly irregular local relief associated with the overall mounded feature that mostly occurs in VK 826. Although the 3-D seismic surface amplitude data from the area of interest displays “stripes” associated with the data acquisition grid, other amplitude patterns relate to the acoustic reflectivity of the surface of the salt-supported mound. Most of the high positive acoustic amplitudes occur on localized areas of the low-sloping flanks of the mound and on the mound’s crest. Although most of the mound surface exhibits either high positive or moderately positive values of acoustic amplitude, some areas have low positive-to-negative values (Figure 59). Most of these areas are associated with steep local slopes and may represent local deflection of acoustic energy resulting in less positive values of surface reflectivity or acoustic amplitude.

The influence of well-defined faults is evident in bathymetry of the VK 826 mound. The NE-SW trending fault on the SE flank of the mound has created a steep slope that appears as an offset of the sea floor reflector on seismic profile B-B´ of Figure 58. Similarly, faulting can be observed along the SW flank of the mound on seismic profile A-A´ of Figure 58. The mound surface, as observed on these seismic profiles, varies considerably in surface reflectivity.

However, much of this surface appears very reflective (red areas of the surface reflector on profiles of Figure 58).

7.10.3 Interpretation of 3-D Seismic Sea Floor Amplitudes Using "Ground Truth" Data

Figure 59 illustrates the roughly W-E transect of the Johnson Sea-Link submersible and fix points where key observations and samples from the sea floor were acquired. At the western end or beginning of the transect, Fix 5 (Figure 59) is located near a highly reflective part of the mound flank, but in an area of moderate-to-low surface reflectivity (acoustic amplitude). The seabed at this site was mud covered and punctuated with brittle stars and sea anemones (Figure 60A). Low relief mounds of sediment and other types of animal burrows as well as tracks and trails sculptured the unconsolidated surface sediments. Although hard substrate materials were not abundant at this site, small pieces of carbonate rock and nodules that appear to have formed in place provided attachment points for the sea anemones. No clear indicators of hydrocarbon seepage were observed at the beginning of the submersible transect.

As the submersible moved upslope to Fix 6, near the very high positive surface amplitude illustrated in Figure 59, the seabed became littered with small patches of hard bottom (authigenic carbonate) and coral "sticks." Scattered living colonies of primarily *Lophelia pertusa* occurred throughout the area (Schroeder et al. 2005). Much of the coral "litter" appeared to result from the collapse of once thriving coral thickets. Upslope of Fix 6, the numbers and sizes of coral colonies increased as well as the frequency of occurrence of carbonate rock outcrops. At Fix 7, much of the bottom was composed of carbonate hardgrounds with pockets of unconsolidated muddy sediment and scattered coral thickets (Figure 60C). The region between Fix Points 6 and 7 comprised one of the highest positive acoustic amplitude areas associated with the VK 826 mound. Carbonate hardgrounds and coral thickets were pervasive throughout this region. At Fix 8, numerous coral thickets were present, but these thickets occurred on a steep slope and the acoustic amplitudes from this and adjacent areas were low-to-moderately positive values. As suggested earlier, much of the incident acoustic energy from this site was probably scattered laterally by the steep slope.

Proceeding upslope from Fix 8 the bottom transitioned from *Lophelia* thickets and a few hardgrounds to a dominance of authigenic carbonate boulders, lower relief hardgrounds, and small mound-like buildups. As illustrated in the photograph of Figure 60E taken at Fix 10, a few tubeworms were observed protruding from the edges of the carbonate slabs and boulders that covered most of the sea floor. Some scattered lucinid-vesycomyid clam shells were also observed in sediment-filled depressions among the carbonate outcrops. The corresponding 3-D seismic sea floor amplitude in this area of the mound was a high positive value, suggesting a hard and very reflective seabed (Figure 59).

Scattered carbonate hardgrounds were common along the eastern end of the submersible transect between Fix Points 10 and 12 (Figure 59). At Fix 12 near the end of the transect, areas of sea floor covered with lucinid-vesycomyid clam shells were encountered. Figure 60F illustrates the density of clam shells at Fix 12. Although these clam beds have been highly reflective at other sites like GC 204, resulting in a high positive acoustic amplitude response, Fix

12 exhibits only moderately positive amplitude values. Again, the steepness of the slope in the area around Fix 12 may be responsible for scattering incident acoustic energy resulting in a moderately positive surface amplitude response.

7.10.4 Summary

The VK 826 3-D seismic amplitude anomaly constitutes a sizeable mounded feature which extends into VK 825 to the west and VK 869 and 870 to the south. Like many other features identified in this study, a salt body is located in the shallow subsurface directly beneath the mounded feature of interest. In general, the correlation between high positive values of 3-D seismic surface amplitudes and hard bottom and low positive values with soft bottom areas was reasonably good. The high positive values were found to represent pervasive carbonate hardgrounds and corals, both thickets of living coral and accumulations of coral "sticks" that appear to represent collapsed thickets.

These areas of high acoustic amplitudes in the mapped surface amplitude data (Figure 59) occur on the low sloping surfaces of the mound flank and crest. However, because of the complex local relief associated with the VK 826 mound surface, it appears the high positive surface amplitudes are underrepresented. For example, beds of clam shells that are highly reflective of acoustic energy in other settings (e.g. GC 204) display only moderate acoustic amplitude values in the VK 826 case. It is suggested that the steep local slopes associated with this mound deflect incident acoustic energy and therefore reduce overall reflectivity of many parts of the mound surface. Regardless, hard bottom areas are clearly distinguished in the 3-D seismic surface amplitude data.

NORTHERN GULF OF MEXICO
CONTINENTAL SLOPE
Viosca Knoll 826

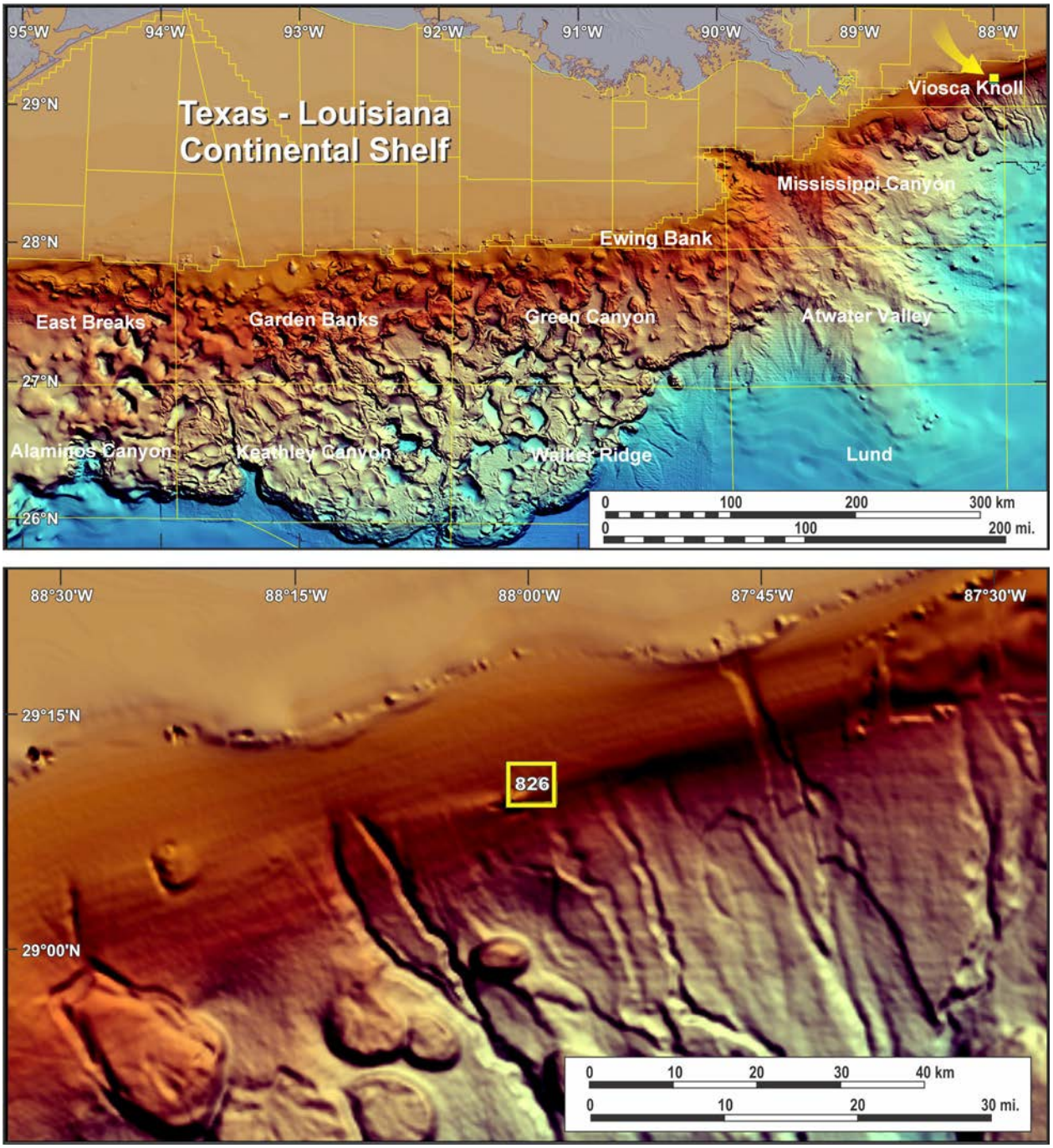

Figure 56. (A) Shaded multibeam bathymetry map of the northern Gulf of Mexico continental slope. The yellow arrow points to the location of Viosca Knoll Block 826 (VK 826). (B) The enlarged view of the area surrounding VK 826 illustrates the bathymetric features within and adjacent to the block.

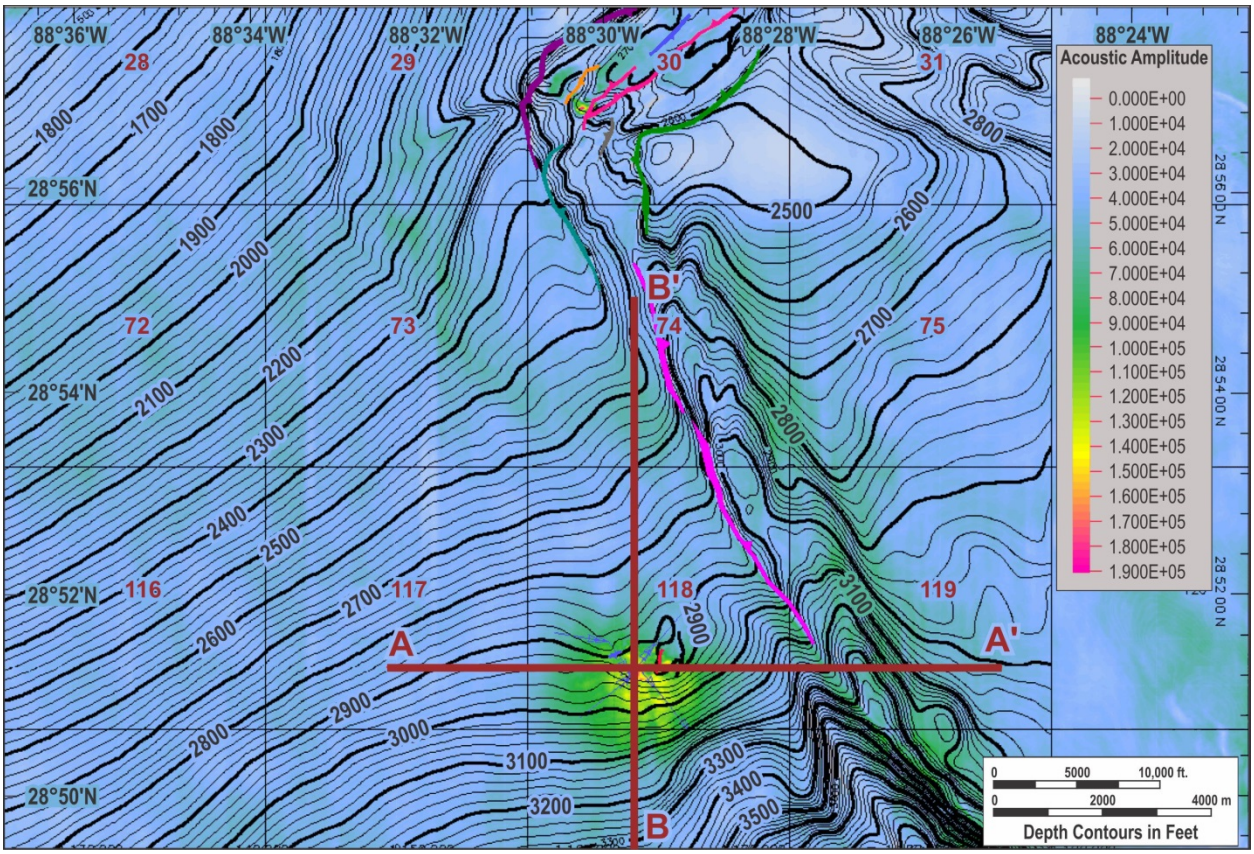

Figure 57. This combined bathymetry and 3-D seismic surface amplitude map illustrates the location of a mounded area in the SE sector of VK 826. A series of NE-SW trending faults form the SE boundary of the mound. The locations of two seismic profiles illustrated in Figure 58 are identified by lines A-A´ and B-B´.

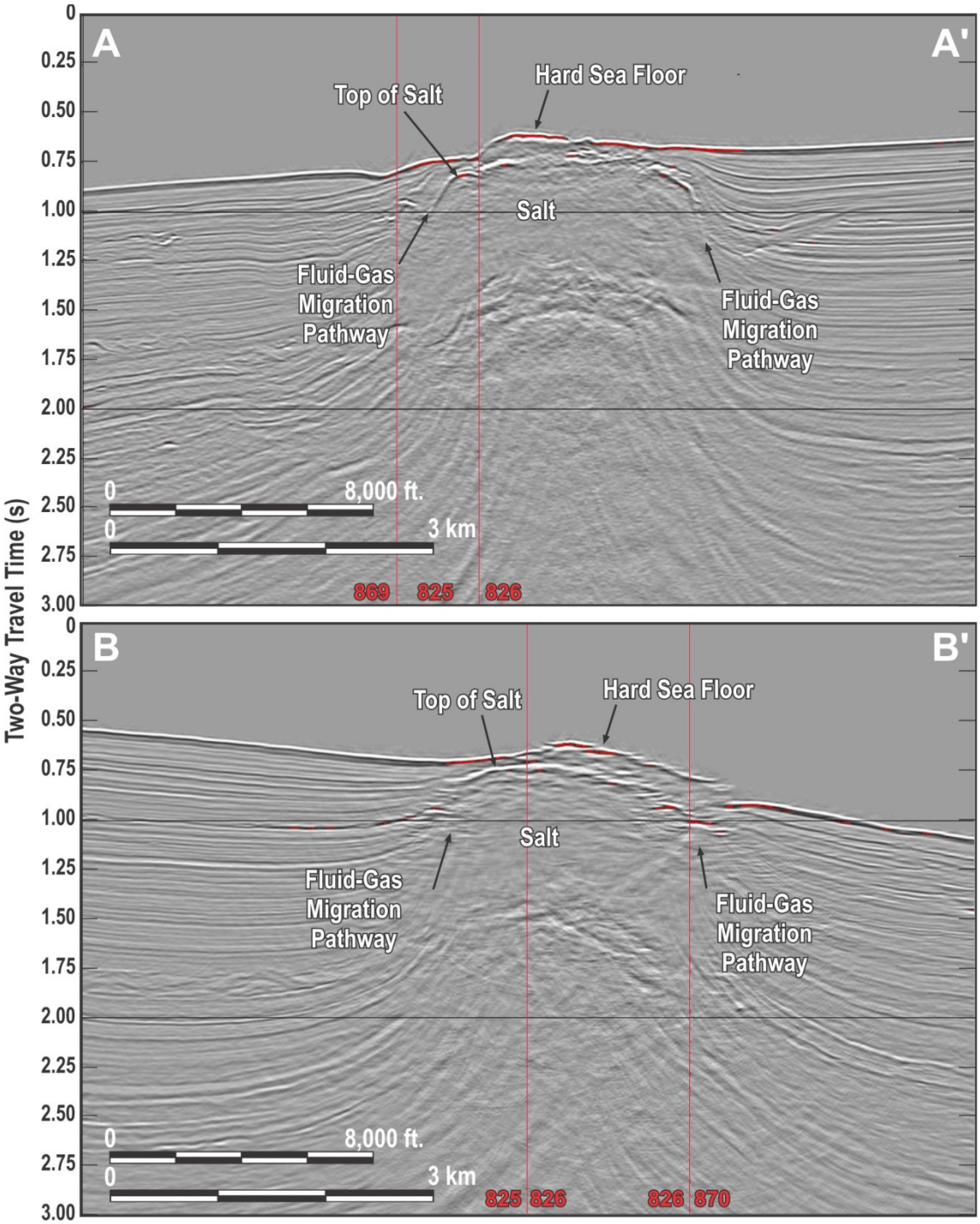

Figure 58. Seismic profile A-A´ is oriented in a SW-NE direction across the broad, mounded sea floor feature primarily located in VK 826. This profile indicates that the top of a salt body is located in the shallow subsurface close to the sea floor. The stratigraphic horizons adjacent to salt are upturned on the flanks of the salt body. The sea floor over salt has a high positive amplitude character with small offsets related to short faults that extend to the top and flanks of salt. Pathways for fluid-gas migration from the deep subsurface occur on the flanks of salt. Seismic line B-B´ (NW-SE) shows the local variability of relief of the sea floor above shallow subsurface salt and the general high positive amplitude (reflectivity) value of the sediment-water column interface.

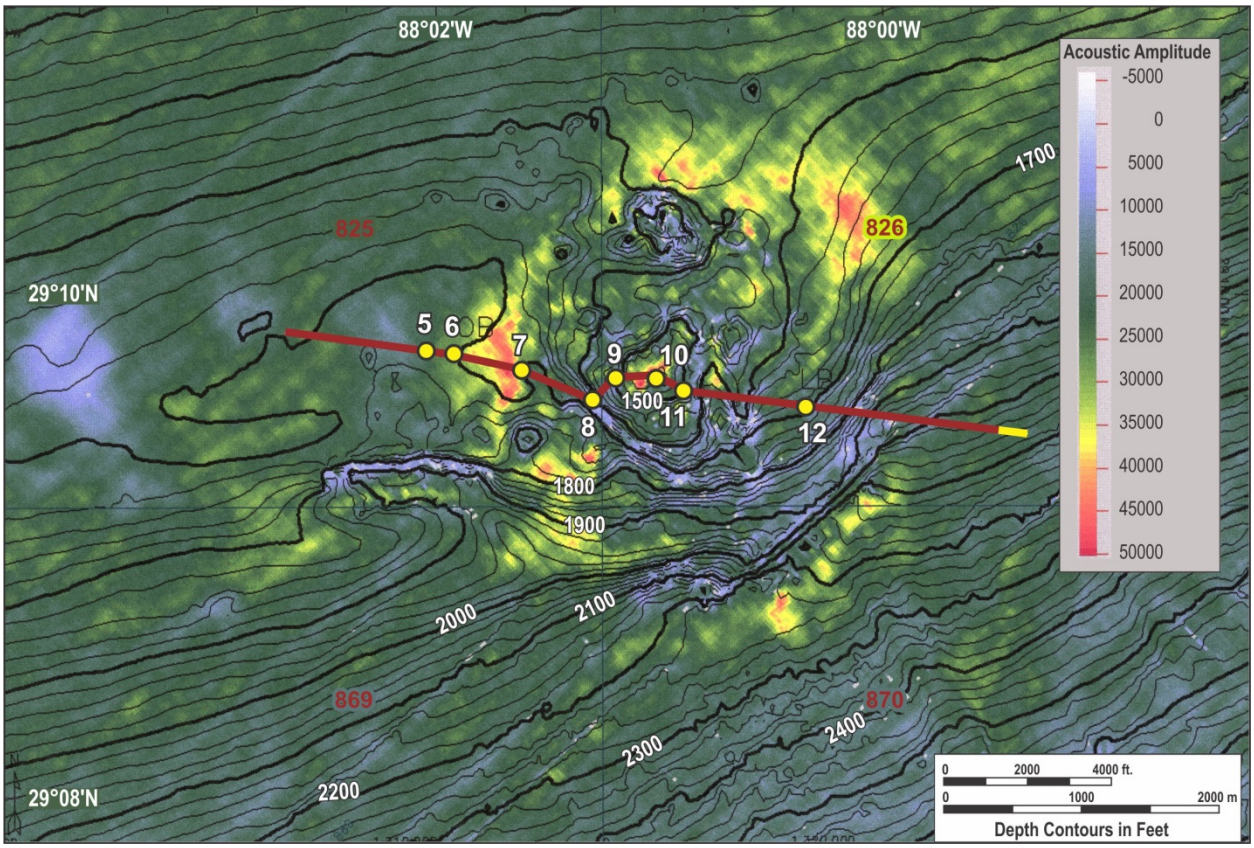

Figure 59. This combined bathymetry and 3-D seismic surface amplitude map is focused on the large mounded feature in the SW sector of VK 826. The W-E trending dive transect across the VK 826 mound identifies fix points where observations about sea floor conditions were made.

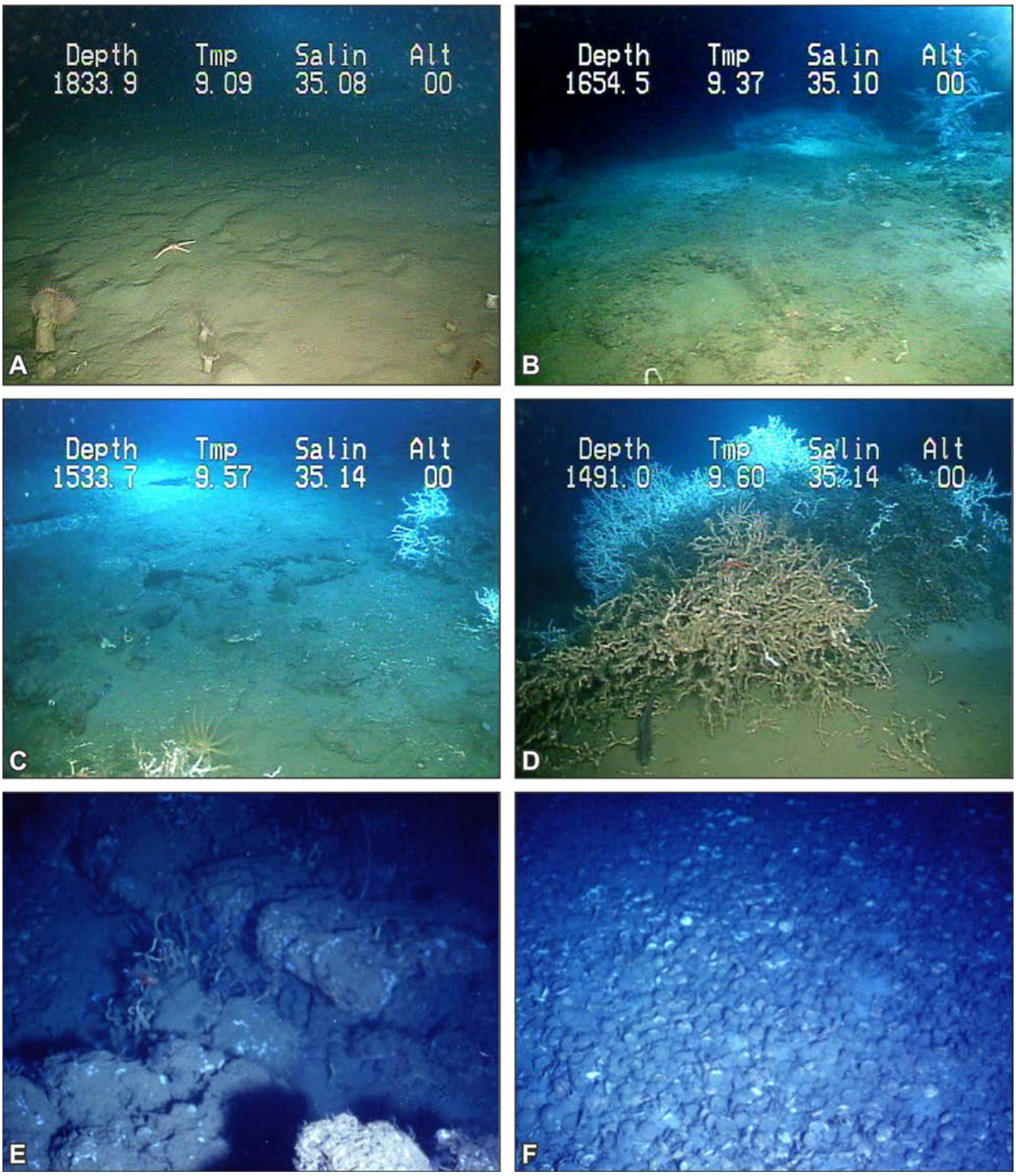

Figure 60. These photographs are typical of the various sectors of the 3-D seismic surface amplitude map illustrated in Figure 59. (A) This bottom photograph was taken at the submersible touchdown point before starting the dive transect shown in Figure 59. At this site the burrowed, mud-covered bottom is punctuated with sea anemones and brittle stars. The sea anemones used a hard substrate on which to attach. Nodular masses of authigenic carbonate scattered throughout the

unconsolidated sediments provide these substrates. A moderate-to-low positive 3-D seismic surface amplitude value is typical of this area. (B) At Fix Point 6, this bottom photograph shows a pervasive cover of hard bottom composed of authigenic carbonate. A coral (*Lophelia*) community in the background has developed on a carbonate outcrop. A high positive 3-D seismic surface amplitude characterizes this part of the dive transect. (C) At Fix Point 7, similar conditions as those found at Fix Point 6 exist. The bottom is dominated by authigenic carbonate outcrops with muddy sediments filling the local low relief areas. *Lophelia* colonies are scattered throughout the bottom photograph. The 3-D seismic surface amplitude response in the Fix Point 7 area is a very high positive value. (D) At Fix Point 8, colonies of *Lophelia* are common. (E) At the apex of the mounded feature in VK 826, a very high positive surface amplitude value reflects an area of carbonate outcrops (see Fix Point 10, Figure 59). Small clumps of tubeworms occur at the edges of some carbonate outcrops. (F) At Fix Point 12, on the eastern flank of the VK 826 mounded feature, a moderate 3-D seismic surface amplitude response is typical of the area surrounding this fix point. The bottom photograph from this area shows a bottom covered with lucinid-vesycomyid clam shells. The cross-photograph field of view dimensions for the six photographs of this figure are approximately 6-12 ft (2-4 m).

8.0 SUMMARY AND CONCLUSIONS

The ten case histories presented in this report are a geographically wide-spread set of representative examples of 3-D seismic surface amplitude anomalies from the northern Gulf of Mexico upper continental slope (water depths less than 3000 ft or approximately 1000 m). The most western of these sites is from the Garden Banks lease area (GB 535) and the easternmost site is from the Vioska Knoll area (VK 826). These ten examples where chosen from many hydrocarbon seep sites remotely identified using 3-D seismic surface attribute data and directly observed-sampled using either a research submersible or remotely operated vehicle (ROV). The ten examples were selected to both demonstrate the utility of 3-D seismic surface amplitude or reflectivity data for finding "hard bottom" areas related to hydrocarbon seepage and also to demonstrate some of the problems in applying this methodology.

All case histories discussed in this report were located on the upper continental slope and in a regional structural framework that is largely dominated by extensional faulting (Rowan et al. 1992). Table 2 summarizes the structural setting for each site and the types of pathways for fluids-gases to migrate from the deep subsurface to the seabed. Seven of the ten sites were in regional structural frameworks clearly defined by extensional faults either at the margins of intraslope basins or as families of faults related to collapse above the crests of shallow subsurface salt bodies. Exceptions to the regional extensional fault framework were the salt weld leading to the distinct surface amplitude anomaly in GC 238 and the salt-focused faults at MC 118 and VK 826. In the latter two cases the salt bodies were located in the shallow subsurface and the sediment column above the salt was broken by numerous faults, but graben-like collapse structures were not present. This type of faulting was especially true of the VK 826 case.

In addition to faults, clearly identified by seismic data, that provide pathways for the migration of hydrocarbons, brines, and formation fluids from the subsurface to the modern seabed, many migration routes are manifested as vertical zones of acoustic blanking (acoustic "wipe-out" zones). Of the ten case histories summarized in Table 2, GC 238, GC 204, EW 1001, and MC 885 exhibit vertical zones of acoustic blanking that are interpreted as buoyancy-driven migration routes. Most of these types of fluid-gas migration pathways occur at the edges of subsurface salt bodies. Except for the GC 238 case, it appears that fluids gases collect on the underside of the salt bodies and then migrate to the margins where they are driven vertically to the surface by buoyancy forces. These vertical migration pathways are characterized by acoustic blanking on seismic profiles. Faults in these cases cannot be completely ruled out as possible additional migration pathways because, if present, they cannot be imaged in the zones of acoustic blanking. In the GC 238 case, buoyancy-driven migration develops from the surface of a fault above a salt weld. The seismic imaging problem generally arises from the scattering of acoustic energy by bubble-phase gas along the migration route. Observations of the sea floor above these buoyancy-driven migration routes usually confirms gas leakage into the water column. Sometimes, fluidized sediment-brine expulsion and gas hydrate formation can be observed. The 3-D seismic surface amplitude response directly above the buoyancy-driven migration pathways is usually low positive (below background for the area). Occasionally, there is a phase reversal of the sea floor reflector in these areas and the presence of fluidized sediment is common.

TABLE 2
Structural Summary

Site	Regional Structural Framework	Migration Pathways
GB 535	Extensional Faults (Crestal Collapse)	Salt-Focused Crestal Collapse Faults and Buoyancy-Driven Vertical Migration
GC 232	Extensional Faults (Crestal Collapse)	Salt-Focused Crestal Collapse Faults
GC 238	Vertical Salt Weld	Salt Weld and Buoyancy-Driven from Fault above Weld
GC 286	Extensional Faults (Margin of Minibasin)	Buoyancy-Driven Vertical Migration from Salt Body Margins
GC 204	Extensional Faults (Crestal Collapse)	Salt Focused Crestal Collapse Faults and Buoyancy- Driven Migration
EW 1001	Extensional Faults (Step-Down Faults)	Buoyancy-Driven Vertical Migration from Salt Body Margins
MC 885	Extensional Faults (Crestal Collapse)	Salt Focused Crestal Collapse Faults and Buoyancy-Driven Vertical Migration
MC 709	Extensional Faults (Crestal Collapse)	Salt Focused Crestal Collapse Faults
MC 118	Salt-Focused Faults	Faults Above Salt Body
VK 826	Salt-Focused Faults	Faults Above and on Flanks of Salt Body

This low reflectivity of the sea bed in areas above well-developed vertical migration pathways defines soft and usually gas-charged sediments. Two sites that clearly demonstrate these relationships are GC 204 and EW 1001. The expulsion centers have a low positive acoustic amplitude signature. However, the flanks of these expulsion centers characteristically display areas of high positive sea floor amplitudes. Direct observation and sampling of these areas reveals hard and acoustically reflective surfaces of either authigenic carbonate (nodular masses, slabs, and boulder-sized or larger exposures) or shell beds (usually lucinid-vesycomyid clam shells).

Areas with well-defined expulsion centers exhibiting low acoustic reflectivity, as described above, commonly have accompanying sediment flows that extend downslope which have a moderate-to-high acoustic reflectivity or positive 3-D seismic surface amplitude. The GC 204 area of interest has very good examples of these sediment flows that originate from well-defined expulsion centers. Ground-truth observations from these flows indicate that the acoustic reflectivity originates from lucinid-vesycomyid clam shell beds. As described previously, clams populate newly deposited flows to exploit the hydrogen sulfide derived from microbial oxidation of hydrocarbons contained in the fluidized sediment. Once the hydrogen sulfide is depleted, the clam population dies leaving disarticulated shells scattered across the surface of the recently deposited sediment flow. After another episode of fluidized sediment expulsion, the process of clam repopulation and exploitation of hydrogen sulfide starts over again, suggesting that within the fairway of downslope sediment transport, flow deposits and accompanying shell layers are

stacked. Therefore, the acoustic reflectivity of these features is probably associated with more than the surficial clam shell layer. Furthermore, sediment sampling of the GC 204 sediment flow, as well as other similar deposits, indicates that nodular masses of authigenic carbonate develop in these sediments and undoubtedly account for some of the acoustic reflectivity of fluidized sediment flow deposits. In all of the other case study sites (GC 232, MC 709, MC 118, and VK 826), faults provide the main fluid-gas migration pathways. Particularly good examples are GC 232, MC 709, and MC 118. These cases clearly demonstrate a direct correlation between faults that intersect the modern sea floor and indicators of hydrocarbon seepage or more rapid venting.

Table 3 summarizes the relationships between 3-D seismic sea floor amplitude response and ground-truth observations of sea floor characteristics. With the exception of one gas-prone and narrow site (GC 232), all sites investigated displayed moderate-to-high positive acoustic amplitudes. The patterns of sea floor amplitudes were quite different, but in each area of interest hard bottom could be interpreted from the seismic data because of the strong acoustic reflectivity or high positive acoustic amplitudes associated with the sea floor reflection horizon. Because the northern Gulf of Mexico continental slope has received vast quantities of terrigenous sediment throughout its Quaternary history, surface-to-near-surface acoustically reflective "hard bottom" areas are limited primarily to salt exposures, sand, and authigenic carbonates formed at the sites of hydrocarbon seeps and vents. The salt exposures are concentrated mostly along the Sigsbee Escarpment. Sands are concentrated in canyons, slope channels, and in slope and basin floor fans. However, most sand deposits interpreted from 3-D seismic sea floor amplitude data are not exposed at the surface, but are covered with a thin deposit of hemipelagic sediments. By far the most numerous and wide-spread hard bottom areas on the northern Gulf's continental slope result from the precipitation of various carbonate minerals at fluid-gas expulsion sites where hydrocarbons, as well as other formation fluids-gases and fluidized sediments, are being fluxed at various rates to the modern sea floor.

Although 3-D seismic sea floor amplitude mapping has become an accepted methodology for identifying sites of hydrocarbon seepage, mainly because of acoustic reflectivity associated authigenic carbonates, the use of these data is not without limitations. The primary purpose of 3-D seismic data is to image the stratigraphic and structural complexities of the subsurface. The frequency content of the seismic energy to accomplish this task does not allow for just the sediment-water interface to be imaged. Therefore, the first reflected return from the sea floor integrates information from approximately the upper 5-7 m (15-25 ft) of the sediment column. Buried hardgrounds, shell layers, sand deposits, salt, and other acoustically reflective materials may therefore be represented in the amplitude of the "sea floor" reflector. The case examples summarized in Table 3 demonstrate this limitation of the 3-D seismic surface amplitude methodology for predicting areas of hard bottom. Although all but one case exhibited areas of moderate-to-high positive 3-D seismic sea floor amplitudes, three of these cases (GB 535, GC 238, and EW 1001) had either no surface evidence of "hard bottom" or very few indicators. In these cases, it is highly suggestive that the acoustically reflective surfaces imaged in the 3-D seismic sea floor amplitude data are in the subsurface covered with sediment. In the EW 1001 case, fluidized sediment expulsion from two separate expulsion centers is burying chemosynthetic communities (e.g. tubeworms) and areas interpreted as lithified zones on the flanks of the mounded expulsion centers.

TABLE 3

Summary of Acoustic Amplitude Response and Sea Floor Characteristics

Site	Sea Floor Acoustic Amplitude Response	Sea Floor Characteristics
GB 535	High-to moderate positive amplitudes spread over the graben floor	Few indicators of hard bottom or hydrocarbon seepage (scattered bacterial mats and clam shells)
GC 232	Low positive amplitudes in zone paralleling regional fault.	Few hard bottom areas. Narrow zone of abundant indicators of hydrocarbon seepage (escaping gas, gas hydrate, chemosynthetic communities).
GC 238	Moderate-to-high positive amplitudes in a well-defined mound-like area.	Moderate indicators of hard bottom conditions. Nodular masses of authigenic carbonate, bacterial mats, and scattered clam shells indicate on-going hydrocarbon seepage.
GC286	Moderate-to-high positive amplitude surround low positive areas interpreted as once active expulsion centers.	Hard bottom areas are abundant and they consist of authigenic carbonate slabs and boulders that incorporate clam shells. Disarticulated clam shell beds are also common.
GC 204	High-to-moderate positive amplitudes with low positive areas interpreted as expulsion centers.	Widespread hard bottom areas consisting of authigenic carbonate blocks and slabs. Concentrations of clam shells are common. Fluidized sediment (mud) in expulsion centers.
EW 1001	Moderate-to-high positive amplitudes surrounding two low positive amplitude expulsion centers.	No hard bottom areas found on the flanks of the expulsion centers. However, many bacterial mats and "buried" tubeworms. Recently deposited fluidized mud in expulsion centers.
MC 885	Moderate-to-high scattered positive amplitudes concentrated along elevated margins of the feature of interest.	Hard bottom areas composed of authigenic carbonate slabs and boulders were scattered throughout the areas of amplitude development. Clam beds were also scattered within these areas.
MC 709	High-to-moderate positive amplitudes are scattered throughout the area of interest.	Hard bottom areas of authigenic carbonate slabs and boulders were scattered throughout the area. Brine seeps and scattered clam shells occur with the field of sea floor amplitudes.
MC 118	High-to-moderate positive amplitudes occur around moderate –to-low rounded "expulsion areas"	Hard grounds of authigenic carbonate invaded with gas hydrate common to high-to-moderate positive amplitude areas. Gas hydrate outcrops and escaping gas present.
VK 826	High-to-moderate positive amplitudes are common to the flanks and crest of the feature of interest.	Extensive hard bottom areas consisting of authigenic carbonate pavements and blocky outcrops are common to the entire feature of interest. Coral thickets and clam beds are scattered over the surface of the feature.

In contrast, six of the cases (GC 286, GC 204, MC 885, MC 709, MC 118, and VK 826) had clear and in some cases extensive hard and acoustically reflective bottom composed primarily of authigenic carbonates and/or clam shell beds. Only the GC 232 site was not represented by high or even moderate positive sea floor amplitudes. At this site, seismic data demonstrated that flux of hydrocarbons from the deep subsurface to the ocean floor was controlled by a steeply dipping regional fault. Direct observations around this fault have indicated that abundant indicators of hydrocarbon seepage such as lush chemosynthetic communities and outcrops of gas hydrate are organized in a narrow zone along the fault. A lack of high positive amplitude response from this zone may be attributed to several factors such as an abundance of bubble phase gas in surface and near-surface sediments, scattering of acoustic energy by the steeply dipping fault, and a general lack of authigenic carbonate hardgrounds in the area of interest.

Conclusions drawn from this study are as follows:

1. The structural frameworks for most of the cases investigated in this study (7 out of 10) were defined by extensional faulting either at the margins of intraslope basin or as families of faults above the crests of shallow subsurface salt bodies. Many of these faults clearly provided pathways for fluid-gas migration from the subsurface. However, nearly half of the sites investigated (4 of 10) displayed vertical buoyancy-driven migration routes, mostly at the edges of salt bodies characterized by acoustic blanking on seismic profiles.

2. The 3-D seismic sea floor amplitude methodology for identifying exposed hard bottom areas on the seabed is very successful. Hard bottom was interpreted and confirmed by "ground truth" observations in 7 of 10 cases considered in this investigation. However, the method is not infallible. In the 3 cases where little or no hard bottom was found by direct observation in areas defined by medium-to-high positive acoustic amplitudes, the acoustically reflective surfaces were interpreted as being covered by unconsolidated sediment. Because of the frequency content of the 3-D seismic data, the sea floor amplitude response is integrated over approximately 5-7 m (15-25 ft) of the sediment column. Therefore, acoustically reflective surfaces can occur anywhere in that interval and result in a positive acoustic sea floor amplitude.

3. Considering the limited options for "hard bottom" on the northern Gulf of Mexico continental slope (shallow sands, salt, and seep-related carbonates), the 3-D seismic sea floor amplitude methodology is well-suited for identifying sites of hydrocarbon seepage or more rapid venting. High positive acoustic amplitudes have the highest probability of correlating to areas of authigenic carbonate development (nodular masses in the sediment, slabs, boulders and large outcrops) and/or lucinid-vesycomyid clam shell beds. Chemosynthetic communities, outcropping gas hydrate, and deep water corals are also frequently encountered in these sea floor areas of moderate-to-high acoustic amplitude response.

4. Patterns of 3-D seismic acoustic amplitudes or acoustic reflectivity from the sea floor are meaningful. For example linear patterns of moderate-to-high acoustic amplitudes are usually sediment flows from mounded expulsion centers with crestal areas of low positive values (below the regional background values). The low positive areas usually represent gas-charged sediment. Small scattered "spots" of high positive acoustic amplitude have been found to represent discrete authigenic carbonate outcrops of low relief separated by unconsolidated sediments.

5. The 3-D seismic sea floor amplitude method is limited and should only be considered a first-level approach to interpreting details of the seabed. However, this methodology has proved to be of immense value in locating probable sites of chemosynthetic communities, deep water corals, and gas hydrates. Furthermore, the methodology has provided a way to efficiently apply more specific and costly methods of collecting detailed data from the sea floor. An ideal investigation would include 3-D seismic sea floor amplitude mapping for identifying areas of interest, high resolution multibeam bathymetry to obtain details of seabed relief, and manned submersibles or ROVs for direct observation and sampling of specific areas within the field of sea floor amplitudes and specific seabed features identified in the multibeam bathymetry dataset.

9.0 REFERENCES

Aharon, P., 2000, Microbial processes and products fueled by hydrocarbons at submarine seeps: *In:* Riding, R.E., and Awramik, S.M., (eds.) Microbial Sediments: Springer-Verlag, Berlin, P. 270-281.

Aloisi, G., I. Bouloubassi, S.K. Heijs, R.D. Pancost, C. Pierre, J.S.S. Damste, J.C. Gottschal, L.J. Forney and J.M. Rouchy, 2002, CH_4-consuming microorganisms and the formation of carbonate crusts at cold seeps: Earth and Planetary Science letters, v. 203, p. 195-203.

Anderson, R.K., Scalan, S., Parker, P.L. and Behrens, E.W., 1983, Seep oil and gas in the Gulf of Mexico slope sediments: Science, v. 22, p. 619-621.

Amery, G.B., 1969, Structure of the Sigsbee scarp, Gulf of Mexico: American Association of Petroleum Geologists Bulletin, v. 53, p. 2480-2482.

Aylor, W.K., Jr., 1998, The role of 3-D seismic in a world-class turnaround: The Leading Edge, v. 17, p. 1678-1681.

Barber, A.J., S. Tjokrosapoetro and T.R. Charlton, 1986, Mud volcanoes, shale diapirs, wrench faults, and mélanges in accretionary complexes, eastern Indonesia: American Association of Petroleum Geologists Bulletin, v. 70, p. 1729-1741.

Baker, C., 1972, Aquathermal pressuring-role of temperature in development of abnormal-pressure zones: American Association of Petroleum Geologists Bulletin, v. 56, p. 2068-2071.

Bennett, S.S. and H.S. Hanor, 1987, Dynamics of subsurface salt dissolution at the Welsh dome, Louisiana Gulf Coast, in Lerche, I., and O'Brien, J.J., eds., Dynamical geology of salt and related structures: Orlando, FL, Academic Press, p. 653-677.

Berryhill, H.L., Jr., J.R. Suter, and N.S. Hardin, 1986, Lake Quaternary facies and structure, northern Gulf of Mexico: Interpretations from seismic data: American Association of Petroleum Geologists, Studies in Geology 23, p. 131-189.

Bouma, A.H. (Ed.), 1981, High resolution seismic profiling and side-scan sonar: Short course Notes, United States Geological Survey office of Marine Geology, Corpus Christi, Texas, 209 p.

Brooks, J.M., M.C. Kennicut II, R.R. Fay, T.J. McDonald and R. Sassen, 1984, Thermogenic gas hydrates in the Gulf of Mexico: Science, v. 226, p. 965-967.

Brooks, J.M., H.B. Cox, W.R. Bryant, M.C. Kennicutt, R.G. Mann and T.J. McDonald, 1986, Association of gas hydrates and oil seepage in the Gulf of Mexico: Organic Geochemistry, v. 10, p. 221-234.

Buffler, R.T., 1991, Seismic stratigraphy of the deep Gulf of Mexico basin and adjacent margins. *In.* Salvador, A. (ed.), The Gulf of Mexico Basin: The Geology of North America, Geological Society of America, V.J., p. 353-38.

Buffler, R.T. and D.S. Sawyer, 1985, Distribution of crust and early history, Gulf of Mexico Basin: Gulf Coast Association of Geological Societies Transactions, v. 35, p. 333-344.

Carney, R.S., 1994, Consideration of the oasis analogy for chemosynthetic communities at Gulf of Mexico hydrocarbon vents: Geo-marine Letters, v. 14, p. 149-159.

Childress, J.J., C.R. Fisher, J.M. Brooks, M.C. Kennicutt II, R. Bidigare and A. Anderson, 1986, A methanotrophic marine molluscan symbiosis: Mussels fueled by gas: Science, V. 233, p. 1306-1308.

Coleman, J.M., D.B. Prior, and J.F. Lindsay, 1983, Deltaic influences on shelf edge instability processes, in (D.J. Stanley and G.T. Moore, eds.) the Shelfbreak: Critical Interface on

Continental Margins: Society of Economic Paleontologists and Mineralogists Special Publication No. 33, p. 121-137.

DeBeukelaer, S.M., I.R. MacDonald, N.L. Guinnasso, Jr., and J.A. Murray, 2003, Distinct side-scan sonar, RADARSAT SAR, and acoustic profiler signatures of gas and oil seeps on the Gulf of Mexico slope: Geo-Marine Letters, v. 23, p. 177-186.

De Jong, A., 1968, Stratigraphy of the Sigsbee Scarp from reflection survey (abst.): Society of Exploration Geophysicists Program, Fort Worth, TX, p. 51.

Diegel, F.A., J.F. Karlo, D.C. Schuster, R.C. Shoup and P.R. Tauvers, 1995, Cenozoic structural evolution and techono-stratigraphic framework of the northern Gulf coast continental margin, *In* M.P. A. Jackson, D.G. Roberts, and S. Snelson, eds., Salt tectonics: a global perspective: American Association of Petroleum Geologists Memoir 65, p. 109-151.

Ferrell, R.E., Jr. and P. Aharon, 1994, Mineral assemblages occurring around hydrocarbon vents in the northern Gulf of Mexico: Geo-Marine Letters, v. 14, p. 74-80.

Ferry, E.J. Jr., 1999, Sea floor amplitude interpretations and their subsurface relationships, northern Gulf of Mexico continental slope: MS Thesis, Department of Geology and Geophysics, Louisiana State University, Baton Rouge, LA., 117 pp.

Fillon, R.H., 2007, Wilcox Depositional architecture in the Gulf of Mexico Basin: A framework for improving deep water exploration and reservoir risk: L. Kennan, J. Pindell, and N.C. Rosen, eds., Gulf Coast Section SEPM Publication (CD-ROM), p. 428-456.

Garcia-Pineda, O., I. MacDonald, B.Zimmer, B. Shedd, and H. Roberts, 2010, remote-sensing evaluation of geophysical anomaly sites in the outer continental slope, northern Gulf of Mexico: Deep-Sea Research II, v. 57, p. 1859-1869.

Geyer, R.A. and C.P. Giammona, 1980, Naturally occurring hydrocarbons in the Gulf of Mexico and Caribbean Sea: Marine Environmental Pollution I., Hydrocarbons, Elsevier Scientific, New York, p. 37-106.

Graebner, R.J., B.A. Hardage and R. Shneider, 2002, 3-D seismic exploration: Society of Exploration Geophysicists Series, No. 22, p. 17-34.

Greenlee, S.M., Gaskins, G.M. and G.M. Johnson, 1994, 3-D seismic benefits from exploration through development: An Exxon Perspective: v. 13, p. 730-734.

Harrison, W.J., and L.L. Summa, 1991, Paleohydrology of the Gulf of Mexico Basin: American Journal of Science, v. 291, p. 109-176.

Hedberg, H.D., 1974, Relation of methane generation to under-compacted shales, shale diapirs, and mud volcanoes: American Association of Petroleum Geologists Bulletin, v. 58, p. 661-673.

Hedberg, H.D., 1980, Methane generation and petroleum migration, *In:* W.H. Roberts, III and R.J. Cordell (eds.) Problems of Petroleum Migration: American Association of Petroleum Geologists, Studies In Geology Number 10, p. 179-206.

Hill, A.W., 1996, The use of exploration 3-D data in geohazard assessment: Where does the future lie? Proceedings Offshore Technology Conference, OTC Paper 7966, p. 113-117.

Hovland, M. and A.G. Judd, 1988, Seabed pockmarks and seepages: Impact on geology, biology and the marine environment: London, Graham and Trotman, 293 p.

Humphries, C.C., Jr., 1978, Salt movement on continental slope, northern Gulf of Mexico, In A.H. Bouma, G.T. Moore, and J.M. Coleman, eds., framework, facies and oil-trapping characteristics of the upper continental margin: American Association of Petroleum Geologists Studies in Geology 7, p. 68-86.

Hunt, I.M., 1990, Generation and migration of petroleum from abnormally pressured fluid compartments: America Association of Petroleum Geologists Bulletin, v. 74, p. 1-12.

Jackson, M.P.A. and W.E. Galloway, 1984, Structural and depositional styles of Gulf Coast Tertiary continental margins: Application to hydrocarbon exploration: AAPG Continuing Education Course Note Series 25, 226 p.

Jackson, M.P.A., and C. Cramez, 1989, Seismic recognition of salt welds in salt tectonics regimes, Gulf of Mexico salt tectonics, associated processes and exploration potential: SEPM Foundation, Gulf Coast Section, 10th Annual Research Conference Program and Extended and Illustrated Abstracts, p. 66-71.

Jackson, M.P.A., and C.J. Talbot, 1989, Salt canopies, Gulf of Mexico salt tectonics, associated processes and exploration potential: SEPM Foundation, Gulf Coast Section, 10th Annual Research Conference Program and Extended and Illustrated Abstracts, p. 72-78.

Jackson, M.P.A. and C.J. Talbot, 1991, A glossary of salt tectonics: The University of Texas at Austin, Bureau of Economic Geology Geological Circular, No. 91-4, 44 p.

Jackson, M.P.A., B.C. Vendeville, and D.D. Schultz-Ela, 1994, Structural dynamics of salt systems: Annual Reviews of Earth and Planetary Science, v. 22, p. 93-117.

Kennett, J.P., K.G. Cannariato, I.L. Hendy, and R.J. Behl, 2002, Methane hydrates in Quaternary climate change: American Geophysical Union, Washington, D.C., 216 p.

Kennicutt II, M.C., J.M. Brooks, R.R. Bidigare, R.R. Fay, T.L. Wade, and T.J. McDonald, 1985, Vent-type taxa in a hydrocarbon seep region on the Louisiana slope: Nature, v. 317, p. 351-353.

Kennicutt, M.C., J.M. Brooks and G.J. Denoux, 1988, Leakage of deep, reservoired petroleum to the near surface of the Gulf of Mexico continental slope: Marine Chemistry, v. 24, p. 39-59.

Kindinger, J.L., 1989, Depositional history of the Lagniappe Delta, northern Gulf of Mexico: Geo-Marine Letters, v. 9, p. 59-66.

Kohl, B. and H.H. Roberts, 1994, Fossil foraminifera from four active mud volcanoes in the Gulf of Mexico: Geo-Marine Letters, v. 14, p. 126-134.

Kohl, B. and H.H. Roberts, 1995, Mud volcanoes in the Gulf of Mexico: A mechanism for mixing sediments of different ages in slope environments: Gulf Coast Association of Geological Societies Transactions, v. 45, p. 351-359.

Lapham, L.L., J.P. Chanton, R. Chapman, and C.S. Martens, 2010, Methane under-saturated fluids in deep-sea sediments: Implications for gas hydrate stability and rates of dissolution: Earth and Planetary Science Letters, doi:10.1016/j.espsl.2010.07.016, p. 1-11.

McBride, B.C., 1998, The evolution of allochthonous salt along a megaregional profile across the northern Gulf of Mexico Basin: American Association of Petroleum Geologists Bulletin, v. 82, p. 1037-1055.

McBride, B.C., M.G. Rowan, and P. Weimer, 1998a, The evolution of allochthonous salt systems, Ewing Bank and northern Green Canyon, northern Gulf of Mexico Basin: AAPG Bulletin, v. 82, p. 1013-1036.

McBride, B.C., P. Weimer and M.G. Rowan, 1998, The effect of allochthonous salt on the petroleum systems of northern Green Canyon and Ewing Bank (offshore Louisiana), northern Gulf of Mexico: American Association of Petroleum Geologists Bulletin, v. 82, p. 1083-1112.

MacDonald, I.R., N.L. Guinasso, Jr., R. Sassen, J.M. Brooks, L. Lee and K.T. Scott, 1994, Gas hydrate that breaches the seafloor on the continental slope of the Gulf of Mexico: Geology, v. 22, p. 699-792.

MacDonald, I.R., W.W. Schroeder, and J.M. Brooks, 1995, Chemosynthetic Ecosystems Studies Final Report: U.S. Department of the Interior, Mineral Management Scrvice, New Orleans, LA., 338 p.

MacDonald, I.R., D.B. Buthman, W.W. Sager, M.B. Peccini, and N.L. Guinasso, 2000, Pulsed oil discharge from a mud volcano: Geology, v. 28, p. 907-910.

MacDonald, I.R., I. Leifer, R. Sassen, P. Stine, R. Mitchell, and N. Guinasso, Jr., 2002, Transfer of hydrocarbons from natural seeps to the water column and atmosphere: Geofluids, v. 2, p. 95-107.

MacDonald, I.R., R. Arvidson, R.S. Carney, C.F. Fisher, N.I. Guinasso, Jr., S. Joye, P. Montagna, J.W. Morse, D.C. Nelson, E. Powell, W. Sager, R. Sassen, S. Schaeffer, G.A. Wolff, 2002, Stability and change in Gulf of Mexico Chemosynthetic Communities: Final Report, U.S. Dept. Interior, Minerals Management Service, Gulf of Mexico OCS Region, Contract 14-35-001-31813, New Orleans, LA., p. 498.

Nestvold, E.O., 1992, 3-D seismic: Is the promise fulfilled? The Leading Edge, v. 11, p. 11-19.

Newton, R.S., R.C. Cunningham and C.E. Schubert, 1980, Mud volcanoes and pockmarks: Seafloor engineering hazards or geologic curiositics? Proceedings 12th Annual Offshore Technology Conference, Paper OTC 3729, p. 425-435.

Neurauter, T. W. and W.R. Bryant, 1990, Seismic expression of sedimentary volcanism on the continental slope, northern Gulf of Mexico: Geo-Marine letters, v. 10, p. 225-231.

Neurauter, T.W. and H.H. Roberts, 1992, Seismic and visual observation of seepage-related structures on the continental slope, northern Gulf of Mexico: Proceedings Offshore Technology Conference, 24th, Houston, Texas, p. 355-362.

Neurauter, T.W. and H.H. Roberts 1994, Three generations of mud volcanoes on the Louisiana continental slope: Geo-Marine Letters, v. 14, p. 120-125.

Orcutt, B.N., S.B. Joye, S. Kleindient, K. Knittel, A. Ramette, A. Reitz, V. Samarkin, T. Treude, and A. Boetius: Deep-Sea Research II, v. 57, p. 2008-2021.

Paull, C.K., J.P. Chanton, C. Neumann, J.A. Coston, C.S. Martens and W. Showers, 1992, Indicators of methane-derived carbonates and chemosynthetic organic carbon deposits: examples from the Florida Escarpment. Palaios, v. 7, p. 361-375.

Peel, F.J., C.J. Travis and J.R. Hossack, 1995, Genetic structural provinces and salt tectonics of the Cenozoic offshore U.S. Gulf of Mexico: a preliminary analysis, in M.P.A. Jackson, D.G. Roberts, and S. Snelson, eds., Salt tectonics: a global perspective: American Association of Petroleum Geologists Memoir 65, p. 153-175.

Post, P., D.L. Olson, K.T. Lyons, S.L. Palmes, P.F. Harrison and N.C. Rosen (eds.), 2004, Salt-Sediment Interactions and Hydrocarbon Prospectivity: Concepts, Applications, and Case Studies for the 21st Century: Gulf Coast Section Society of Economic Paleontologists and Mineralogists Foundation Bob F. Perkins 24th Annual Research Conference, 1174 p.

Ritger, S., Carson, B., and Suess, E., 1987, Methane-derived authigenic carbonates formed by subduction-induced pore-water expulsion along the Oregon/Washington margin: Geological Society of America Bulletin, v. 98, p. 147-156.

Roberts, H.H, 2001a, Improved geohazards and benthic habitat evaluations: Digital acoustic data with ground truth calibrations: OCS Study MMS2001-050, U.S. Department of the

Interior, Minerals Management Service, Gulf of Mexico OCS Region, New Orleans, LA, 116 p.

Roberts, H.H., 2001b, Fluid and gas expulsion on the northern Gulf of Mexico continental slope: Mud-prone to mineral-prone responses: *In:* Paull, C.K. and W.P. Dillon (eds.), Natural Gas Hydrates: Occurrence, Distribution, and Detection, Geophysical Monograph 124, p. 145-161.

Roberts, H.H., 1992c, Reefs, bioherms, and lithoherms off the northern Gulf of Mexico: The important role of hydrocarbon seeps: Proceedings of the Seventh International Coral Reef Symposium, Guam, v. 2, p. 1121-1128.

Roberts, H.H., R. Sassen, R. Carney, and P. Aharon, 1989, Carbonate buildups on the continental slope off central Louisiana: Proceedings 21st Annual Offshore Technology Conference, OTC Paper 5953, p. 655-622.

Roberts, H.H., D.J. Cook and M.K. Sheedlo, 1992a, Hydrocarbon seeps of the Louisiana continental slope: Seismic amplitude signature and sea floor response: Transactions 42nd Annual Gulf Coast Association of Geological Societies Convention, p. 349-362.

Roberts, H.H. and P. Aharon, 1994, Hydrocarbon-derived carbonate buildups of the northern Gulf of Mexico continental slope: A review of submersible investigations: Geo-Marine Letters, v. 14, p. 135-148.

Roberts, H.H. and R.C. Carney, 1997, Evidence of episodic fluid, gas, and sediment venting on the northern Gulf of Mexico continental slope: Economic Geology, v. 92, p. 863-879.Roberts, H.H., R. Sassen, R. Carney and P. Aharon, 1989, Carbonate buildups on the continental slope off central Louisiana: Proceedings 21st Offshore Technology Conference, OTC Paper 5953, p. 655-662.

Roberts, H.H., B. Kohl, D. Menzies and G.D. Humphrey, 1999, Acoustic wipe-out zones – A paradox for interpreting sea floor geologic/geotechnical characteristics (An example from Garden Banks 161): Proceedings Offshore Technology conference, OTC Paper 10921, p. 1-12.

Roberts, H.H., B.A. Hardage, W.W. Shedd, and J. Hunt, Jr., 2006, Seafloor reflectivity – An important seismic property for interpreting fluid/gas expulsion geology and the presence of gas hydrate: The Leading Edge, Society of Exploration Geophysicists, v. 25, p. 620-628.

Roberts, H.H. and D. Feng, 2010, Cold-seep carbonates of the middle and lower continental slope, northern Gulf of Mexico: Deep-Sea Research II, v. 57, p. 2040-2054.

Roberts, H.H., W. Shedd, and J. Hunt, Jr., 2010a, Geologic framework and seafloor impacts of fluid-gas expulsion sites on the middle and lower continental slope, northern Gulf of Mexico: Special Issue, Deep Sea Research, v. 57, p. 1837-1858.

Roberts, H.H., W. Shedd, and J. Hunt, Jr., 2010b, Dive site geology: DSV ALVIN (2006) and ROV JASON II (2007) dives to the middle-lower continental slope, northern Gulf of Mexico: Deep-Sea Research II, v. 57, p. 1837-1858.

Rowan, M.G., 1994, A systematic technique for the sequential restoration of salt structures: Tectonophysics, v. 228, p. 331-348.

Rowan, M.G., 1995, Structural styles and evolution of allochthonous salt, central Louisiana outer shelf and upper slope, *In* M.P.A. Jackson, D.G. Roberts, and S. Snelson, eds., Salt tectonics: a global perspective: American Association of Petroleum Geologists Memoir 65, p. 199-228.

Rowan, M.G., 1997, Allochthonous salt systems (abs.): AAPG Annual Meeting Program and Abstracts, v. 6, p. A100.

Rowan, M.G. and P. Weimer, 1998, Salt-sediment interaction, northern Green Canyon and Ewing Bank (offshore Louisiana), northern Gulf of Mexico: American Association of Petroleum Geologists Bulletin, v. 82, p. 1055-1082.

Rowan, M.G., M.P.A. Jackson and B.D. Trudgill, 1999, Salt-related fault families and fault welds in the northern Gulf of Mexico: American Association of Petroleum Geologists Bulletin, v. 83, p. 1454-1484.

Salvador, A., 1991, Introduction. *In:* Salvador, A. (ed.) The Gulf of Mexico Basin: The Geology of North America, Geological Society of America, v. J, p. 1-12.

Samuel, B.M., 2004, A comparison of high-resolution survey and a three-dimensional seismic survey in a feature-rich region of the Green Canyon Area, Gulf of Mexico: MS thesis, Department of Geology and Geophysics, Louisiana State University, Baton Rouge, LA, 102 p.

Sassen, R., H.H. Roberts, R. Carney, A.V. Milkov, D.A. Defreitas, B. lanoil and C. Zhang, 2004, Free hydrocarbon gas, gas hydrate, and authigenic minerals in chemosynthetic communities of the northern Gulf of Mexico continental slope: Relation to microbial processes: Chemical Geology, v. 205, p. 195-217.

Sassen, R., H.H. Roberts, W. Jung, C.B. Lutken, D.A. DeFreitas, S.T. Sweet, and N.L. Guinasso, 2006, The Mississippi Canyon 118 gas hydrate site: A complex natural system: offshore Technology Conference Proceedings, OTC 18132, Houston, TX p. 1-6.

Schroeder, WW., S.D. Brooke, J.B. Olson, B. Phaneuf, J.J. McDonongh III, and P. Etnoyer, 2005, Occurrence of deep-water *Lophelia pertusa* and *Madrepora oculate* in the Gulf of Mexico: *in* (A. Freiwald and J.M. Roberts, eds.) Cold-Water Corals and Ecosystems: Springer-Verlag, Heidelbert, p. 297-307.

Schuster, D.C., 1995, Deformation of allochthonous salt and evolution of related salt-structural systems, eastern Louisiana Gulf Coast, *in* M.P.A. Jackson, D.G. Roberts, and S. Snelson, eds., Salt tectonics: a global perspective: AAPG Memoir 65, p. 177-198.

Sheriff, R.E., 2002, Encyclopedic Dictionary of Applied Geophysics, fourth Addition: Society of Exploration Geophysicists, Talsa, Oklahoma, 429 p.

Sleeper, K., A. Lowrie, A. Bosman, L. Macelloni, and C.T. Swann, 2006, Bathymetric mapping and high resolution seismic profiling by AUV in MC 118: Offshore Technology Conference Proceedings, OTC 18113, Houston, TX, p. 1-6.

Sloan, E.D., 1990, Clathrate Hydrates of Natural Gases: Marcol-Dekker, Inc., New York, 664 p.

Sumner, H.S., B.A. Robison, W.K. Dirks and J.C. Holliday, 1990, Morphology and evolution of salt/minibasin systems: lower shelf and upper slope, central offshore Louisiana (abs.): Geological Society of America Annual Meeting, Programs with Abstracts, Dallas, Texas, p. 48.

Suter, J.R. and H.L. Berryhill, Jr., 1985, Late quaternary shelf margin deltas, northwest Gulf of Mexico: American Association of Petroleum Geologists Bulletin, v. 69, p. 77-91.

Sydow, J.C., H.H. Roberts, A.H. Bouma, and R. Winn, 1992, Constructional subcomponents of a shelf-edge delta, northeast Gulf of Mexico: Gulf Coast Association of Geological Societies Transactions, v. 42, p. 717-726.

Sydow, J.C., H.H. Roberts, 1994, Stratigraphic framework of a Late Pleistocene shelf edge delta, northeast Gulf of Mexico: American Association of Petroleum Geologists Bulletin, v. 78, p. 1276-1312.

Tanner, M.T. and R.E. Sheriff, 1977, Application of amplitude, frequency, and other attributes to stratigraphic and hydrocarbon determination. *In*: C.K. Payton 9ed.) Seismic Stratigraphy: Application to Hydrocarbon Exploration: American Association of Petroleum Geologists Memoir 26, p. 301-327.

Talbot, C.J., 1993, Spreading of salt structures in the Gulf of Mexico: Tectonophysics, v. 228, p. 151-166.

Travis, C.J., B.C. Vendeville, H. Harrison, F.J. Peel, M.R. Hudec and B.F. Perkins (eds.), 1995, Salt, Sediment, and Hydrocarbons: Gulf Coast Section Society of Economic Paleontologists and Mineralogists Foundation 16th Annual Research Conference, Houston, TX., 308 p.

Vendeville, B.C. and M.P.A. Jackson, 1993, Rates of extension and deposition determine whether growth faults or salt diapirs form: Gulf Coast Section Society of Economic Paleontologists and Mineralogists Foundation Annual Research Conference, 14th, Houston, Texas, December 5-8, 1993, Proceedings, p. 268-268.

Vendeville, B.C. and M.P.A. Jackson, 1992, The rise of diapirs during thin-skinned extension: Marine and Petroleum Geology, v. 9, p. 331-352.

Weimer, P., P. Varnai, Z.M. Acosta, F.M. Budhijanto, R.E. Martinez, A.F. Navarro, M.G. Rowan, B.C. McBride and T. Villamil, 1994, Sequence stratigraphy of Neogene turbidite systems, northern Green Canyon and Ewing Bank, northern Gulf of Mexico: Gulf Coast Section Society of Economic Paleontologists and Mineralogists Annual Research Conference, 15th, Houston, Texas, 1994, Proceedings, p. 383-396.

Worrall, D.M. and S. Snelson, 1989, Evolution of the northern Gulf of Mexico, with emphasis on Cenozoic growth faulting and the role of salt, *In* A.W. Bally and A.R. Palmer, eds., The geology of North America: an overview: Geological Society of America Decade of North American Geology, v. A, p. 97-138.

Wu, S.A., A.W. Bally, and C. Cramez, 1990, Allochthonous salt, structure and stratigraphy of the northeastern Gulf of Mexico, part II: Structure: Marine and petroleum Geology, v. 7, p. 334-370.

10.0 APPENDIX A: 2000 DIVE LOG SUMMARY

APPENDIX A

Logs From Each Dive Conducted as a Part of the BOEM Project Designed to Improve the Predictive Capability of 3-D Seismic Surface Amplitude Data

During each dive, a representative from the research team occupied a position on the bridge of Harbor Branch Oceanographic Institute's support ship fro the John Sea-Link where communication between the submarine and the ship was centralized. This person kept a time-based log of submersible activities and observations and collections being made. Important sample sites as well as observation sites were spatially located by the ship-submarine navigation system and given a latitude, longitude, and water depth. These data as well as a short descriptions of the type of samples being acquired or characteristics of the sea floor environment were included in the dive logs. The observational data are relayed to the surface ship by an acoustic link between the submarine pilot and a member of the submersible crew manning the communication and navigation station during the dive. In the project discussed in this report, a predetermine set of bottom locations, based on locations associated with 3-D seismic surface amplitude maps, were given to the submersible crew prior to the dive. These predetermined sites were designed to "field verify" surface reflectivity patterns. The submarine was guided to these sites by the Sea-Link crew member operating the ship-board communications and navigation station. These logs for each dive made under the canopy of this BOEM-supported project are archived in Appendices A and B.

Dive Log Summary
Johnson Sea Link 1 Submersible Cruise
August 17-30, 2000

Dive 4231:

Traverse 1, GC 286/287/331

August 20
Dan Boggess, Harry Roberts – front
Frank Lombardo, Jim Coleman – rear

08:01	Launch
08:50	On bottom, Fix 5: 27:39.6373 N, 90:47.9751 W, depth 2980 ft., Temp. 4.5C.
09:00	1st Bacterial mat, Fix 6: same as above, course 245°. Seep Fix 7: 27:39.6300 N, 90:47.9458, depth 2847 ft.
09:35	Clam bed, depth 2802 ft., Fix 8: 27:39.3900 N, 90:48.5000 W.
09:49	Competent Rocks and clams, depth 2780 ft.
10:13	Burrowed Sediment, depth 2772 ft., Fix 9: 27:39.31 N, 90:48.70 W. "Stonehenge".
10:30	Calcium carbonate sample, depth 2901 ft., Fix 10: 27:39.25 N, 90:48.93 W.
10:44	Grab sample, depth 2972 ft. Fix 11: 27:39.19 N, 90:49.05 W (barite seep).
10:48	Leave bottom

Dive 4232:

Traverse 2, GC 286/287/331

August 20
Dan Boggess, Jesse Hunt – front
Frank Lombardo, Kerry Campbell – rear

15:57	Launch
16:45	On bottom, depth 2804 ft., Fix 6: 27:40.55 N, 90:50.19 W, temp. 4.5C.

17:17	Carbonate boulder, depth 2766 ft., Fix 7: 27:40.62 N, 90:49.99 W. under way, course 080°.
17:29	course correction to 070°.
17:46	Clam mound 2, depth 2748 ft., Fix 8: 27:40.69 N, 90:49.67 W.
18:00	Clam hole, Fix 9: 27:40.6682 N, 90:49.6758 W. depth 2752 ft.
18:06	Large expulsion crater with fractured carbonate crust around rim. Depth 2753 ft., Fix 10: 27:40.6436 N, 90:49.6494 W. Grab sample, then gas sample taken, underway heading 070°.
18:38	Leave bottom, depth 2733 ft. Fix 11: 27:40.6604 N, 90:49.5376 W.

Dive 4233:

Traverse 2, GC 204,249

August 21
Ken Obrien, Jim Coleman – front
Roger Sassen, Ben Chiong – rear

08:00	Launch
08:44	On bottom, depth 2860 ft., temp. 4.9C, Fix 5: 27:46.9941 N, 90:33.4326 W. begin transect at 260°.
08:53	Starting upslope
09:00	Depth 2839 ft., white shell has area with escarpments.
09:06	Still in striated clam hash, level bottom.
09:23	Still in dead clam field, depth 2843 ft.
09:27	Ridge-swale area, depth 2844 ft., Fix 7: 27:46.8660 N, 90:34.5123 W., new bearing 255°.
09:33	Back underway at 255°.
09:34	Leaving clam shell area.
10:13	Stop transect, Fix 8: 27:46.7743 N, 90:34.8315 W, back to clam field at bearing 083°
10:38	Leave bottom, depth 2903 ft., Fix 9: 27:46.7822 N, 90:34.5156 W.

Dive 4234:

Traverse 3, GC 204

August 21
Ken Obrien, Harry Roberts – front
Ben Chiong, Larry Cathles – rear

15:29	Launch
16:14	On bottom, depth 2960 ft., temp. 4.5C, Fix 6: 27:45.2335 N, 90:33.8408 W, underway bearing 110°.
16:23	Starting upslope on small pinnacle, depth 2908 ft.
16:34	Depth 2819 ft., Fix 7: 27:45.1460 N, 90:33.6260 W.
16:44	Up mound, depth 2742 ft., Fix 8: 27:45.0945 N, 90:33.5469 W.
16:48	Old mud vent, depth 2726 ft., Fix 9: 27:45.0944 N, 90:33.5513 W.
16:54	Taking grab sample of old clams, Fix 10: 27:45.0864 N, 90:33.5034 W.
16:58	Underway bearing 090°.
17:06	Change course to 080°.
17:45	Coming up on mound, old mussels with some live ones. Depth 2727 ft.
17:47	At Waypoint 3, Fix 11: 27:45.1527 N, 90:32.9956 W
17:54	Large carbonate area, depth 2761 ft., Fix 12: 27:45.1519 N, 90:32.9956 W.
18:22	Leave bottom, depth 2658 ft., Fix 13: 27:45.1497 N, 90:32.9736 W.

Dive 4235:

Traverse 1, GC 260/304

August 23
Dan Boggess, Harry Roberts – front
Frank Lombardo, Mary Boatman – rear

09:05	Launch
09:49	On bottom, depth 1441 ft., temp. 8C, Fix 6: 27:42.8511 N, 91:58.1768 W. bearing 300°.
09:59	New heading 310°.
10:05	At a fault, depth 1435 ft., Fix 7: 27:42.9763 N, 91:58.3228 W.
10:15	Hard ground area, depth 1835 ft., Fix 8: 27:42.9879 N, 91:58.4033 W. heading 060°.
10:24	Past point 2. Heading 060° to Point 3.

10:32	Change course to 030°.
10:34	At point 3. Heading 330° to Point 4.
10:35	Course correction to 300°.
10:43	Sediment plain, depth 1415 ft., Fix 9: 27:43.1105 N, 91:58.5498 W.
10:44	Course change to 285°.
10:51	At point 4, continue at heading 300°.
11:18	Depth 1573 ft., Fix 10: 27:43.3071 N, 91:58.9961 W.
11:21	Leave bottom, depth 1574 ft., Fix 11: 27:43.2955 N, 91:59.0557 W.

Dive 4236:

Traverse 2, GB 260

August 23
Dan Boggess, Harry Roberts – front
Frank Lombardo, Bill Shedd - rear

15:36	Launch
16:03	On bottom, depth 1507 ft., temp. 8C, Fix 7: 27:42.3350 N, 91:58.9985 W. Underway at 100° to Point 1.
16:05	At waypoint 1, new bearing 035°, depth 1855 ft.
16:13	Pock mark, depth 1479 ft., Fix 9: 27.42.3691 N, 91:58.8994 W.
16:28	Boulder field, depth 1470 ft., Fix 10: 27:42.5447 N, 91:58.8267 W. 16:31 Heading 050°.
16:34	Numerous small vents and seeps. 3 m. diameter brine pool. Fix not possible, GPS off line. Fix 11: 27:42.5914 N, 91:58.7793 W.
16:36	New heading 035° to waypoint 3.
16:44	Mud bottom, depth 1442 ft., Fix 12: 27:42.6682 N, 91:58.7329 W.
17:03	Flat, depth 1417 ft., Fix 13: 27:42.8723 N, 91L58.5547 W.
17:08	At waypoint 3, depth 1413 ft.
17:17	At waypoint 4.
17:18	Sample slab of carbonate, depth 1378 ft., Fix 14: 27:43.0271 N, 91:58.4390 W.
17:24	New heading 035°.
17:37	Carbonate field, depth 1391 ft., Fix 15: 27:43.0667 N, 91:58.3892 W.
18:10	Leave bottom, depth 1355 ft., Fix 16: 27:43.4059 N, 91:58.0068 W.

Dive 4237:

GC 354

August 24
Ken Obrien, Mary Boatman – front
Allan Fuller, Mike Smith – rear

08:11	Launch
08:49	At bottom, depth 2434 ft., temp. 5C., Fix 5: 27:35.4330 N, 91:48.9670 W., underway upslope at heading 325°.
09:38	First signs of carbonate.
09:39	Course correction bearing 005°, Fix 7: 27:35.7310 N, 91:49.4468 W.
09:53	Small mat of orange *Beggiatoa*, depth 1800 ft.
09:55	Collected tube worm sample, Fix 8: 27:35.9181 N, 91:49.4185 W.
10:00	Underway.
10:02	Large carbonate rocks with tube worms, depth 1770 ft., Fix 9: 27:35.9310 N, 91:49.3840 W.
10:10	Underway after video work.
10:12	Fan city! Depth 1746 ft., Fix 9: 27:35.9624 N, 91:49.3921 W.
10:17	Carbonate rocks, sea fans, and tube worms.
10:20	Leaving carbonate rocks, back into mud. At point 2.
10:22	Mud flow, depth 1713 ft., small pockets with gas.
10:31	Major mud flow, depth 1773 ft. Fix 10: 27:36.0885 N, 91:49.3916 W.
10:46	Depth 1747 ft., Fix 11: 27:36.1984 N, 91:49.4805 W.
10:48	Leave bottom.

Dive 4238:

Traverse 2, GC 354

August 24
Ken Obrien, Bill Shedd – front
Alan Fuller, Greg Boland – rear

15:36	Launch
16:10	On bottom, depth 1909 ft., temp. 6.7C., Fix 8: 27:36.3033 N, 91:48.8555 W.
16:13	Starting transect at heading 245°.

16:19	Up slight slope barren of geological features
16:23	Small colony of tubeworms.
16:31	First carbonate rocks with sea fans, depth 1800 ft., Fix 9: 27:36.1752 N, 91:49.1499 W.
16:33	New heading 230°.
16:35	Small patch of red *Beggiatoa*. Course correction to 240°.
16:45	Collect some tubeworms.
16:50	Heading upslope.
16:52	Mud flow area, depth 1705 ft., Fix 10: 27:36.0682 N, 91:49.4028 W.
16:57	Underway at heading 190°.
16:59	Going over several mud flows with powdery white silt.
17:03	Out of the mud flow area and into carbonate area.
17:05	Stop to collect tubeworms, depth 1745 ft., Fix 11: 27:35.9871 N, 91:49.4180 W.
17:12	Back underway.
17:13	Change course to 230°.
17:14	In an area of carbonates with small tubeworm colonies.
17:16	Crossed large outcropping of carbonates with tubeworms
17:24	Area of large carbonates with tubeworms, depth 17:45 ft.
17:26	Course change to 225°.
17:27	Large outcropping of carbonates, Fix 12: 27:35.9108 N, 91:46.5518 W.
17:32	Underway at heading 225°.
17:36	Passing over large carbonate rocks, depth 1720 ft.
17:48	Area of large carbonate buildups, depth 1752 ft.
17:54	Small mat of *Beggiatoa.*
17:56	Large carbonate buildup, mat of *Beggiatoa.* Depth 1799 ft.
18:04	More carbonates.
18:20	Leave bottom, Fix 14: 27:36.6379 N, 91:49.9399 W.

Dive 4239:

Traverse 1, GB 543

August 25
Craig Caddigan, Bob Woolsey – front
Frank Lombardo, Vernon Asper – rear

08:02	Launch
08:31	On bottom, depth 1885 ft., temp. 7C, Fix 6: 27:26.8624 N, 93:10.5513 W. Mud bottom, slight uphill. Underway at heading 305°.
08:36	Still on mud bottom, heading upslope, depth 1890 ft.
08:41	Mud bottom with a few small rocks and boulders, depth 1874 ft., Fix 7: 27:26.9182 N, 93:10.6450 W.
08:43	Passing over small white bacterial mat.
08:51	Bacterial mats, first small bushes of tubeworms, depth 1844 ft.
08:54	Past point 2, depth 1860 ft., past another bacterial mat and small tubeworm clump.
09:01	Lower port thruster flooded.
09:05	Down a small ridge, mud bottom with singular tubes sticking out (not tubeworms).
09:13	Mud bottom with occasional small bacterial mats, depth 1875 ft.
09:17	Up on ridge, depth 1873 ft., down the other side.
09:24	Small carbonate field with bushes, boulders and bacterial mats, depth 1846 ft., Fix 9: 27:27.2764 N, 91:11.2173 W.
09:27	Starting up another ridge.
09:29	Area of small bacterial mats and tubeworm clumps, depth 1800 ft., still going upslope.
09:31	On top of ridge, mud volcano with flows, searching for gas seep, depth 1746 ft., Fix 10: 27:27.3665 N, 93:11.3579 W.
09:33	Mud flows running 300°.
09:35	Back to course 140°.
09:39	At the other side of where the flow runs off, no gas vent sighted, returning to course 300°.
09:42	Another pass, featureless, no gas eruptions marks, back underway at course 305°.
09:44	Chimney protruding from mud bottom, 1 ft. high and 8” across, Fix 11: 27:27.3296 N, 93:11.3867 W.
09:45	Finished shooting video and stills, underway at course 305°.
09:57	Tried to sample chimney, too soft, got grab sample of it.
09:58	Over a hump in the bottom 15-20 ft. across, depth 1754 ft.
10:00	Onto a rocky bottom, scattered rocks.
10:02	More rocks, big areas of exposed plates with individual rocks.
10:06	Change course to 315.
10:12	Out of area of big slabs and rocks and back into mud bottom, depth 1771 ft., Fix 12: 27:27.5134 N, 93:11.6187 W.

10:15	Depth 1782 ft., heading downslope.
10:19	Change course to 090, Fix 13: 27:27.5619 N, 93.11.6743 W., depth 1782 ft.
10:28	Leave bottom, depth 1783 ft., Fix 14: 27:27.5680 N, 93:11.6152 W.

Dive 4240:

Traverse 1, GB 543

August 25
Ken Obrien, Barry Kohl – front
Frank Lombardo, Dick Fillon – rear

15:42	Launch
16:14	On bottom, depth 2128 ft., temp 7C, at point 1. Fix 5: 27:25.6432 N, 93:08.2520 W.
16:17	Underway, burrowed hemipelagic mud.
16:22	Grab sample, depth 2093 ft., Fix 6: 27:25.6868 N, 93:08.3511 W.
16:31	Depth 2073 ft., small ridge with patch of *Beggiatoa* with small tube worms
16:34	Fix 7: 27:25.6819 N, 93:08.4092 W. Underway at 305°
16:49	Depth 2064 ft., take rock sample, Fix 8: 27:25.7616 N, 93:08.5259 W.
16:49	Back underway, heading 300°.
16:50	Starting to see some small carbonate rocks sticking up. Fix 9: 27:25.8179 N, 93:08.5239 W.
16:51	Change course to 290°.
16:56	Across an area of outcropping rock, linear pattern. Depth 2047 ft., Fix 27:25.7874 N, 93:08.5781 W.
16:58	Change course to 300°.
17:03	New heading of 270°.
17:03	Crossing area of limestone and small patches of white *Beggiatoa.*
17:05	Depth 2032 ft., limestone pieces concentrated, Fix: 27:25.8586 N, 93:08.6060 W.
17:06	Heading 305°
17:11	New heading of 310°.
17:12	Seeing more patches of *Beggiatoa* and limestone clumps. Fix: 27:25.8175 N, 93:08.6772 W.
17:25	Change course to 270°.

17:29	Small tubeworms. At waypoint 2, Fix 9: 27:25.8912 N, 93:08.7798 W.
17:36	Heading out of limestone and *Beggiatoa* area, up small slope.
17:39	Depth 2013 ft, still going upslope.
17:40	Change course to 310°.
17:41	Definitely out of limestone, now regular soft mud bottom.
17:45	Stop for a grab sample. Depth 1990 ft., Fix 10: 27:25.9323 N, 93:08.9116 W. Back underway at 310°.
18:02	Hemipelagic mud with burrows.
18:06	*Beggiatoa* mats.
18:12	Just past waypoint 3.
18:13	Depth 2089 ft., going upslope.
18:16	Stop for a grab sample. Depth 2017 ft., Fix 11: 27:26.1693 N, 93:09.2988 W.
18:29	Leaving bottom. Depth 2040 ft.

Dive 4241:

Traverse 1, GB 535

August 26
Dan Boggess, Vern Asper – front
Alan Fuller, John Herries – rear

08:03	Launch
08:31	On bottom, depth 1932 ft., temp. 6C, Fix 6: 27:26.3535 N, 93:36.2749 W. Underway at course 125°.
08:34	Landed in soft sediment. Coming up on small rise, bottom type appears to be changing.
08:37	Starting to see small bacterial mats and a series of little ridges and trenches about 15 ft. wide. Ridges seem to be oriented N-S (crossing them at about 45° on heading of 125°).
08:42	Bacterial mats with individual clam shells scattered with 1 or 2 per square meter.
08:49	Area of small clumps of tube worms, depth 1881 ft.
08:52	Change course to 090, depth 1876 ft., 800 ft. to point 2
09:08	At point 2, change course to 125°, depth 1875 ft. mostly loose mud with some bacterial mats

09:42	Depth 1914 ft., reached a downslope, course change to 100°.
09:51	Depth 1959 ft., leveled off and hit shallow upslope – 10° at most.
09:54	Orange and white bacterial mat, depth 1964 ft., Fix 7: 27:25.7141 N, 93:35.4126 W.
10:01	Back underway at 080°, change course to 090°, 300 ft. to Point 3.
10:02	Depth 1964 ft. Two clumps of tube worms with bacterial mats. Take a sample, Fix 8: 27:25.7352 N, 93:35.3774 W.
10:21	New heading of 115°.
10:34	Finished collection and getting underway at course 125°.
10:39	Depth 1948 ft., at 35° upslope. Fix 9: 27:25.7100 N, 93:35.0160 W.
10:43	At 1878 ft., and still rising. Bottom type loose sediment with fine burrows.
10:46	Leveled out at depth 1860 ft.
10:47	Back to steep upslope, about 45°, depth 1853 ft., Fix 10: 27:25.6586 N, 93:35.2861 W. Into slope is 160 degrees, proceeding upslope.
10:55	Still going upslope, just past 1800 ft.
10:56	Leave bottom, depth 1789 ft., Fix 11: 27:25.6248 N, 93:35.2856 W.

Dive 4242:

Traverse 2, GB 535

August 26
Dan Boggess, Greg Boland – front
Alan Fuller, Mary Boatman – rear

15:49	Launch
16:17	On bottom, depth 1923 ft., temp. 6C,. 125 ft. SE of start position, course 170° to point 2.
16:28	Still on course 170 – Mud with lot of *Beggiatoa* mats
16:31	Depth 1915 ft., end of bacterial mats. Fix 6: 27:26.4292 N, 93:35.2207 W.
16:38	Course change to 245°.
16:39	Lost GPS.
16:40	New course 250°, Fix 7: 27:26.2772 N, 93:35.2422 W.
16:42	Depth 1928 ft., grab sample at top of small sand dune, Fix 8: 27:26.2662 N, 93:35.2148 W.

16:48	Resuming course at 250°.
16:56	Series of little ridges, almost right angles. Gullies between ridges are almost 6 ft. deep and getting shallower.
17:09	Change course to 240°.
17:12	Request moving fix. Clam shells, depth 1877 ft., Fix 9: 27:26.2079 N, 93:35.6431 W.
17:16	Depth 1873 ft., request fix for clam bed. Fix 10: 27:26.1553 N, 93:35.8670 W.
17:18	Back underway at course 290°.
17:28	At waypoint 3, change course to 220° for waypoint 4.
17:35	Request running fix, continuing clam beds, Depth 1873 ft., Fix 11: 27:25.5500 N, 93:36.2670 W.
17:40	Area of small ridges, depth 1872 ft.
17:42	Continuing at course 220°.
17:55	Sediment mounds continuing but smaller.
18:03	Fix 13. Strong ridges.
18:09	Fix 14. Depth 1899 ft., gorgonian field.
18:14	Leave bottom, depth 1906 ft.

Dive 4243:

Traverse 2, GB 460/461

August 27
Ken Obrien, Harry Roberts – front
Frank Lombardo, Nate Usher – rear

07:57	Launch
08:31	On bottom, depth 2623 ft., Temp 4.5C. Fix 9: 27:30.2806 N, 92:56.5820 W.
08:32	Getting underway at course 240°
08:36	Lost tracking.
08:38	Got tracking back, past point 1, New bearing 070°, hemipelagic mud bottom.
08:47	Lost tracking.
08:48	Depth 2600 ft.
08:51	Still trying to acquire tracking.
08:55	Course correction to 030°, 730 ft. to point 3

08:59	Depth 2577 ft., heading uplsope.
09:03	Change course to due N, 200 ft. to point 3, still going upslope.
09:06	Change course to 330°. Continue to top of mound.
09:07	Will make course adjustment to run directly upslope. Course 030°. Bottom type is hemipelagic mud with burrows.
09:16	Depth 2295 ft., At top of mound, lot of dead clam shells. Will look around. Fix 10: 27:30.9009 N, 92:56.3994 W, temp. 4.5C.
09:25	Taking grab sample, depth 2296 ft.
09:26	Heading of 110, 1000 ft. to waypoint, getting underway.
09:29	Downslope, depth 2320 ft.
09:44	Depth 2955 ft.
09:46	Depth 2562 ft. Course of 105.
10:01	Course correction to 060°, heading upslope. Tracking lost again.
10:11	Showing sub on the numbers for point 6, still going upslope, will continue to the top.
10:16	Depth 2370 ft., still going upslope at 030°.
10:23	Depth 2325 ft., request fix at top of mound. Fix 11: 27:30.7848 N, 92:55.7686 W., bottom is hemipelagic mud with very few clams.
10:31	Taking grab sample. Depth 2334 ft., Fix 12: 27:30.7910 N, 92:55.7578 W.
10:44	Leave bottom, depth 2389 ft., Fix 13: 27:30.8057 N, 92:55.2886 W.

Dive 4244:

Traverse 1, GB 460/461

August 27
Ken Obrien, Harry Roberts – front
Frank Lombardo, Mike Cassik – rear

15:34	Launch
16:11	On bottom, depth 2692 ft., temp. 4.5C, Fix 9: 27:31.6144 N, 92:56.7827 W., underway at course 270°.
16:14	Course change to 300°.
16:16	At point 1, course 110 1200 ft. to next point.
16:20	Lost tracking.
16:27	Change course to 060°, going upslope, depth 2643 ft.

16:38	Depth 2555 ft., at top of a mound, Fix 10: 27:31.4968 N, 92:56.5835 W., Hemipelagic mud bottom with occasional shells
16:52	Still taking photos and looking around. Took grab sample.
16:54	Underway at course 100°.
16:59	Heading downslope, depth 2575 ft.
17:00	Depth 2600 ft.
17:05	Depth 2667 ft., at the base of mound. Fix 11: 27:31.4159 N, 92:56.3745 W.
17:09	Underway at course 105°.
17:16	Depth 2676 ft., still hemipelagic bottom.
17:28	Tracking bad, depth 2676 ft.
17:35	Appears at point 6
17:59	Depth 2664 ft.
18:09	Depth 2655 ft.
18:10	At point 7.
18:13	Leave bottom, Fix: 27:31.0673 N, 92:55.5103 W.

Dive 4248:

Traverse 1, EW 873

August 30
Ken Obrien, Harry Roberts – front
Frank Lombardo, Nate Usher – rear

07:55	Launch
08:11	On bottom, depth 672 ft., temp. 13.5C, visibility 20 ft. Fix 7: 28:06.9492 N, 90:12.7759 W.
08:12	Course to point 2 is 065°.
08:19	Changing course to 120°, upslope.
08:23	Depth 646 ft., in middle of a small mud vent. Fix 8: 28:06.9232 N, 90:12.6401 W.
08:29	Bearing to top of large vent is 020°.
08:39	Close to the numbers for top of vent, depth 614 ft.
08:45	Change course to 050°.
08:53	Depth 605 ft.
08:56	Still heading upslope, hard bottom with sea fans and gorgonians.

09:02	Depth 619 ft., small vent. Taking grab sample. Fix 9: 28:07.1193 N, 90:12.3359 W.
09:10	Will look around the area.
09:14	Underway heading 050°.
09:18	GPS out
09:23	GPS back, adjust course to 090°.
09:25	1300 ft. to waypoint 2.
09:31	Headed downslope, depth 645 ft.
09:35	Adjust course to 110, depth 700 ft.
09:49	New course due N.
09:53	Fix 10: 28:07.1117 N, 90:12.1372
10:00	Problems with tracking.
10:01	All stop.
10:02	Depth 686 ft.
10:04	New heading 100°, 1000 ft. to point 3.
10:07	Heading up a slope.
10:11	Depth 643 ft., Vent field, Fix 11: 28:07.3326 N, 90:12.1338 W.
10:18	Taking grab sample.
10:24	Abort dive due to weather. Depth 648 ft., Fix 12: 28:07.2965 N, 90:12.1382 W.

11.0 APPENDIX B: 2002 DIVE LOG SUMMARY

Dive Log Summary
Johnson Sea Link Submersible 2002 Cruise

Friday, May 17:

Load at Gulfport, cold front blew through. Stayed at the dock Sat. and Sun.

Sunday, May 19:

Depart Gulfport and steamed overnight to be on station at VK 826.

Monday, May 20:

Too rough to dive. By 2:00pm, decided to return to Gulfport to repair lower deck A/C unit and ship's freezer. Departed Gulfport at 11:30 pm for VK 826.

Tuesday, May 21:

Hove to all day on VK 826. Still too rough to dive.

Wednesday, May 22:

Hove to all day. Decided to abort the site and head west in search of better weather. Ran west overnight.

Thursday, May 23:

Hove to at MC 885 all day.

Friday, May 24:

MC 885, Dive 4392

Crew: Front, Craig Caddigan, Mike Smith
Rear, Frank Lombardo, Susan Childs

Purpose: Survey traverse and find and recover thermistor.

Attempted to dive, but had to abort due to weather. Hove to all day, and decided to run west to GC 185 (Bush Hill). Arrived at Bush Hill, attempted to trip acoustic release on current meter array. Did not release.

Saturday, May 25:

GC 185, Dive 4393

Crew: Front, Craig Caddigan, Harry Roberts
Rear, Frank Lombardo, Eric Guilbeau

Purpose: Free current meter, collect bubbleometers, deploy rabbit chow.

7:58 Boom out
8:01 Launch
8:02 Permission to dive, problem with a contact in the sub. Depth 250 ft.
8:08 Resurface, recovered sub. Water in a breaker tripped it.
8:13 Recovered sub and began repairs.

GC 185, Dive 4394

Same crew.
Same purpose.

9:23 Boom out
9:25 Launch
9:26 Permission to dive. Launch at 27-46.8031N 91-30.3743W
9:30 Returning to surface. An alarm was getting louder.
9:36 Surface, repaired sub.

GC 185, Dive 4394

Same crew, same purpose.

15:56 Launch, permission to dive 27-46.8652N 91-30.4087W
16:09 Depth 1000 ft.
16:19 Near bottom, mooring 20 ft. in front of sub.

16:22 On bottom, depth 1793 ft., 0.1 kt. of current from W, temp. 7.40 c. Released mooring.
16:24 Mooring on the way up.
16:27 Deploy a bucket of rabbit chow at 27-46.0931N 91-30.4081W
16:30 Heading due West
16:32 Current meter array on the surface.
16:34 Deployed bucket #2 on bearing of 345° (no fix) approx. 27-46.9437N 91-30.4550W.
16:37 Within 50 ft. of the numbers, searching for instruments.
16:38 Instruments in sight
16:40 Will deploy bucket #1 just North of where Harry's gear was, Just down from Junk yard, Depth 1783 ft.
16:49 At the first funnel, trying to get the can off the side.
17:00 Can is in the basket, but can't close the lid, will try to fit the funnel on top.
17:10 Funnel onboard, moving away from the time lapse camera.
17:16 Don't know how the funnel will ride. Request permission to leave bottom. Must go back and look at something.
17:20 By Ian McDonald's time lapse camera, looking at thermistors. Will take water samples.
17:23 Depth 1772 ft., Permission to leave bottom. 27-46.9763N 91-30.4724W.
17:47 Done with water samples at 2000 ft. Permission to surface.
17:51 On surface.

GC 185, Dive 4395

Crew: Front, Craig Caddigan, Harry Roberts
Rear, Frank Lombardo, Duofu Chen

Purpose: Retrieve gear and conduct acoustics experiments (night dive)

20:38 Launch, permission to dive, 27-46.9850N 91-30.4715W
20:50 Showing bottom at 1800 ft. on ship.
20:53 Range 100 ft. bearing 174° to landing site.
20:55 Ship showing bottom at 1775 ft.
20:57 Target at 100 ft. at 165°.
21:00 Bottom in sight
21:01 On bottom, 1780 ft., Temp. 7.33, visibility 45 to 50 ft., 0.1 kt. of current from due North. Next to Ian's cameras, getting video at 27-46.9530N 91-30.4178W.

21:19 Got the other funnel on board, will go back and do some video.
21:31 Depth 1763 ft., took video, request permission to leave bottom
27-46.9529N 91-30.4865W
21:55 On surface.

Sunday, May 26

GC 185, Dive 4396
Crew: Front, Don Liberatore, Harry Roberts
Rear, Hugo Marrero, Rex Poling

Purpose: Locate and retrieve tripod and thermistor string, target mud vent, and shoot stills of the bottom.

07:03 Launch and permission to dive 27-46.0511N 91-30.3480W
07:04 Ship showing bottom at 1858 ft.
07:15 Range to target 459 ft. at 339°.
07:16 Range 600 ft. at 340°.
07:17 Ship showing bottom at 1852 ft.
07:19 Ship showing bottom at 1844 ft., sub at 1200 ft.
07:22 Range 350 ft. at 325°, sub at 1400 ft.
07:29 Sub depth 1800 ft.
07:30 Range 400 ft., bearing 345°.
07:31 Bottom in sight.
07:34 Range 150 ft., Bearing 350°.
07:36 Range 100 ft., Bearing 290°.
07:37 Sighted bacterial mat, probably coming into mud vent site.
07:41 Range 90 ft., Bearing 120°. Unable to locate site.
07:46 Range 150 ft., Bearing 350°, Unable to locate site.
07:49 Currently searching for site, bottom (from ship) 1862 ft.
07:54 Range 250 ft., Bearing 040°, searching for site.
07:55 Sub underway at 040°.
07:59 At the mud vent.
08:02 Found something on mud vent, probably old thermistor. Harry confirms this is the thermistor.
08:03 Sub depth 1876 ft.
08:06 See the ADCP, do not see the auger with the thermistor string.

08:09 Sitting at the tripod, depth 1878 ft., temp. 7.14, visibility 25 ft., current 0.1 kt. at 090°.
08:11 Will move around and look for the auger and come back and retrieve the tripod.
08:24 Unable to locate the auger and thermistor, heading back to retrieve the doppler current meter from tripod.
08:31 Unable to lift instruments, will back off and try again. T-handle at top is broken off (Harry doesn't remember that problem during deployment). At 27-46.1579N 91-30.4132W.
08:40 Unable to dislodge doppler instrument, regrouping and waiting for sediment to clear.
08:45 Trying to tip the tripod and get the doppler exposed for easier access.
08:58 Tried pulling on it and still unable to dislodge it, waiting for sediment to settle.
09:18 Grabbed the doppler and blew the ballast tanks, failed to dislodge. Standing by.
09:27 Leaving the mud vent site and heading for Bush Hill site.
09:29 Underway due east, depth 1880 ft., taking water samples at 27-46.1970N 91-30.3672W
09:31 Changed course to north, following mud flow to investigate.
09:33 New vent observed at 1873 ft., 27-46.1975 N 91-30.3589W
09:35 At top of the vent, observing bubble stream. Top at 1875 ft.
09:43 Permission to leave bottom at depth 1875 ft.
09:44 Leaving bottom at 27-46.2018N 91-30.3587W
10:08 On surface.

GC 238, Dive 4397

Crew: Front, Don Liberatore, Mike Smith
Rear, Hugo Marrero, Charles Billups

Purpose: Survey Traverse 1 and record observations. If time permits, collect two push cores and 1 carbonate sample.

13:19 Launch, permission to dive at 27-44.3886N 91-03.0461W. Punch cores are OK.
13:21 Ship showing bottom at 2276 ft.
13:24 Depth 295 ft., going through murky layer of sediment laden water.
13:36 Range 700 ft. Bearing 280°.

13:42 Ship showing bottom at 2325 ft.
13:45 Sub at 2000 ft. and descending
13:49 Sub at 2200 ft., ship shows bottom at 2335 ft.
13:52 Bottom in sight.
13:53 On bottom, depth 2343 ft., temp. 6.23, visibility 35-40 ft., current 0.1 kt. at 300°, 27-44.4453N 91-03.0470W
13:56 WP1 range 950 ft., bearing 140°.
13:58 Underway at 140°.
14:00 Coming up on slight slope at 4° to 5°, on way to WP1.
14:06 Range 250 ft., bearing 110° to WP1. Depth 2294 ft., Lots of bacterial mats, mounds, shells (mussels and clams). Most shells observed are dead, possibly active area at one time. Seeing chemo biota.
14:08 27-44.3441N 91-03.0025W, traveling to WP1.
14:14 Sending sub to WP2, Range 400 ft. bearing 270°.
14:15 More shells, big depressions, smooth bottom, no bacterial mats present.
14:16 Dan instructs sub to stand by, checking on incorrect bearing of 270°.
14:17 WP2 is at 450 ft., bearing of 150°.
14:18 Sub at 2276 ft., ship showing 2273 ft.
14:21 New heading of 175°, depth 2274 ft. Big craters with bacterial mats at the base, approximately 3m across.
14:23 Changing bottom, more bacterial mats, anemones, mussels.
14:24 Depth 2274 ft., anemones only on slope sides.
14:27 New heading of 150°, depth at 2278 ft.
14:30 On way to WP3, Range 750 ft., bearing 140°.
14:32 Change in bottom, hundreds of starfish, small shallow depressions, occasional hard bottom. Depth 2283 ft. 21-44.1256N 91-02.8683W
14:35 Depth 2282 ft., “Starfish City”.
14:36 Back in larger depression, no starfish.
14:37 Investigating location of bacterial mat for punch core sample.
14:44 Due east to WP3, depth 2290 ft., taking punch core in bacterial mat at 27-44.0516N 91-02.8310W
14:49 Soft sediment, push core went in and came out half full, underway due east.
14:50 Range 200 ft. to WP3.
14:51 090°, underway due east.
14:52 Crossing over small furrow 1 to 1.5 ft. across running N-S.
14:54 Course change, bearing 140°, range 1300 ft.

14:56 Depth 2310 ft., underway at 140° to EOL.
14:57 Headed downslope
15:02 Depth 2390 ft., changing video tapes, 27-43.9884N 91-02.6707W
15:07 Course change to due S.
15:11 At EOL. Depth 2415 ft., bottom is smooth and homogeneous, no mats.
15:16 Shooting video of starfish.
15:17 Depth 2417 ft., request permission to leave bottom, 27-43.8256N 91-02.6217W.
15:40 On surface.

GC 238, Dive 4398

Crew: Front, Don Liberatore, Susan Child
Rear, Hugo Marrero, Bob Hardage

Purpose: Survey and photodocument Traverse 2

19:03 Launch, permission to dive, 27-43.9001N 91-02.8074W
19:08 Going through a layer of murky water at 300 ft., looks like sediment in the water column.
19:16 Depth 1000 ft.
19:21 Target range 300 ft., bearing 220°, getting underway.
19:26 Drop straight down, depth 1770 ft.
19:32 Depth 2200 ft.
19:37 On bottom, depth 2389 ft., 27-43.9072N 91-02.8360W
19:48 Going upslope
19:50 Course change to 355°, range 350 ft.
19:51 Small craters with bacterial mats, depth 2310 ft.
19:57 Bigger craters with some rock, will take sample, also clams and mussels, took push core and grab sample 27-44.0266N 91-02.8252W
20:11 Completed push core, some hard substrate, will look around for several minutes.
20:15 Came across battery box tracks, get underway at 005°, range 1800 ft., depth 2280 ft.
20:17 Huge chunk of coral about 4 ft. across, will sample 27-44.0772N 91-02.8232W
20:26 Back underway, small piece of coral in the basket, course 005°, range 1700 ft.

20:28 back in big field of starfish
20:31 Two more big mounds of coral, all dead.
20:38 Out of area of depressions and mats, now even seafloor 27-44.2089N 91-02.8226W
20:43 Depth 2295 ft. Changing video tapes, 27-44.2635N 91-02.7774W
20:44 Feature in the bottom like a tow fish or cable drug across, runs N-S.
20:46 Change course to 330°.
20:56 Waypoint 2, change course to 230°, range 1060 ft., overshot WP2, course change 27-44.4021N 91-02.8822W. Depth 2372 ft.
21:06 Change course to 230°, 27-44.3691N 91-03.0352W
21:10 Course change to due S., crossing over battery box tracks again.
21:11 Big depressions with bacterial mats, depth 2294 ft., 27-44.3671N 91-03.0629W
21:15 Back on line, course change to 260°, range 1600 ft. 27-44.3039N 91-03.0455W
21:24 Depth 2297 ft., shallow depressions with bacterial mats. 27-44.2969N 91-03.1792W. course change to 240°, range 800 ft., fix 27-44.2701N 91-03.3665W, depth 2280 ft., taking water sample, permission to leave bottom.
21:43 depth 2288 ft.
22:12 On surface.

Monday, May 27

GC 257, Dive 4399

Crew: Front, Dan Boggess, Bill Shedd
GC 257, Dive 4399 (cont.)
Rear, Frank Lombardo, Melissa Lobegeier

Purpose: Survey and photodocument 8200 ft. Traverse, depressional seafloor.

07:58 Launch and permission to dive. Ship shows depth of 2887 ft. 27-42.403N 90-07.223W
08:25 Depth 2000 ft., ship shows bottom at 2914 ft.
08:25 Underway at 271°, range 700 ft.
08:32 On the numbers, drop straight down, bottom shows at 2880 ft.

08:39 Bottom in sight.

08:42 On bottom, depth 2894 ft., temp 5.42, visibility 35-40 ft., current less than 0.1 kt. from 010°. 27-42.443N 90-07.272W, bottom soft muddy, small deep slope craters, but mostly soft mud.

08:45 Bearing 050°, range 1400 ft.

08:48 Fairly sharp ridge line in sight.

08:48 Fix 27-42.473N 90-07.166W, taking video of ridge and associated bottom.

08:51 Flat spot at depth of 2895 ft.

08:53 Depth 2910 ft., steep drop off, terracing down at 60° angle. Heading of 050°, ridge lines running perpendicular, 5 to 8 m wide.

08:55 Leveled off, same soft sediment with some shell hash, depth 2933 ft.

08:56 Mussel shell clumps along heading.

08:58 Depth 2928 ft., gentle slope.

08:59 Depth 2926 ft., small bacterial mat.

09:00 More small bacterial mats.

09:02 Visibility 30-35 ft., turbidit increasing and decreasing, fog-like, possible proximity to mud vent, within 140 ft. of WP1.

09:03 Depth 2915 ft., very gentle slope, very smooth bottom, no big mounds or large depressions.

09:05 Depth 2911 ft., taking punch core sample within 40 ft. of WP1, trying to find vent, following flow back to vent, found a big lake , got fathometer trace showing plume in water column, 27-42.609N 90-06.997 W.

09:12 Depth 2910 ft., gas coming up, also sediment. Visibility low and slight increase in currents. Bubbles are about a mm in diameter.

09:21 Could not tell where flow is originating, no visibility and not enough current.

09:22 Course 055°, range 900 ft. to WP2. Back at flow and trying to take samples again, Harry says to take grab sample. Sample in bucket 12. 27-42.609N 90-06.997W (sample lost over the side.)

09:30 Have grab sample and underway.

09:32 More flows, smooth, new looking flows, several inches thick. Taking still shots.

09:33 Bill thinks they are at the vent site, 27-42.648N 90-07.006W, now heading to WP2.

09:42 Pock marks, observing loose scattering of mussels and clams, not much relief.

09:45 Coming up on ridge line, carbonate structures, mussels. 27-42.692N 90-06.860W, within 100 ft. of WP2.

09:49 Very steep upslope, within 80 ft. of WP2.

09:50 Following slope up, then head on new course of 190°.

09:51 Depth 2938 ft., heading to top of slope and took punch core, will send S (190°) at top of slope.

10:01 Depth 2911 ft., came up on terrace, seems to be the top, heading 190°, 27-42.716N 90-06.797W

10:03 Depth 2925 ft., coming up on drop off of about 25 ft.

10:05 Depth 2941 ft., slight drop off, WP2.

10:14 Depth 2934 ft., taking another mat sample (push core), need to go 045° to 050°, get underway, no more samples.

10:17 Depth 2942 ft., getting underway.

10:19 Coming up on very steep slope, very soft bottom.

10:22 Depth 2919 ft., near top of slope (15° slope).

10:25 Depth 2912 ft., large depression about 1m across, 600 ft. due E from WP2.

10:30 Depth 2898 ft., All stop, coming up on a slight slope, changing course to 260°, range 1000 ft., 27-42.720N 90-06.691W

10:32 underway at 260°.

10:34 Depth 2905 ft., passing large crater about 3m diameter, very round.

10:39 Depth 2925 ft., now on downslope, observed small mats along the terrace. Slightly north of previous transect.

10:42 Depth 2938 ft., observed carbonate structure, will grab carbonate sample, 27-42.715N 90-06.855W. Could not get basket to close, had to abandon grab sample of carbonate.

11:00 Regrouping and plan to get underway at 260°. Observed gorgonians.

11:02 Depth 2923 ft., observing mussels and clams.

11:08 Depth 2912 ft., observing area of possible old flows, heading 260°, flow is at least 50 ft., unable to find the end.

11:10 Reach the edge of the flow field, approximately 120 ft. wide.

11:13 Battery getting weak on sub. Will transect at least 5 minutes. Harry-probably 200 ft. from site, 500 ft. west of WP1.

11:15 Depth 2920 ft., now on mussels and clams, appear to be alive.

11:22 Depth 2930 ft., mounds, about 1.5 m across, small craters.

11:24 Very soft mounds, like mud vents.

11:26 Depth 2915 ft., 10°-15° upslope.

11:27 70° slope about 40 ft. tall, instructions to look for carbonates.

11:28 Depth 2873 ft., At top of slope, no carbonate. End of transect, leaving bottom. 27-42.607N 90-07.207W

12:08 On surface.

EW 1001, Dive 4400

Crew: Front, Dan Boggess, Larry Cathles
Rear, Trainee Jimmy Nelson, Frank Lombardo

Purpose: Run transect, collect carbonates and push cores.

16:34 Launch and permission to dive. 27-57.644N 90-23.477W, Ship shows bottom at 1770 ft.
16:40 Bearing 270°, range 450 ft., bottom showing at 1775 ft.
16:50 Depth 1000 ft., bottom showing at 1760 ft.
16:55 Bearing 270°, range 150 ft.
16:58 Dropping straight down.
17:05 Bottom in sight.
17:07 On bottom, depth 1794 ft., temp. 7.73, visibility 35-40 ft., current 0.1 kt. from N. 27-57.686N 90-23.538W, light sediment covering bottom.
17:09 Bearing 320°, range 1600 ft., getting underway to WP1.
17:13 45°-50° slope about 25 ft. high, 27-57.731N 90-23.574W, depth 1790 ft.
17:15 Depth 1740 ft., on top of feature.
17:17 Depth 1720 ft., another slope, 55°-60°, 27-57.744N 90-23.593W
17:24 Depth 1693 ft., continuing on gentle upslope.
17:26 Depth 1689 ft., going over *beggiatoa* mat.
17:27 Bearing 295°, range 325 ft.
17:30 Depth 1683 ft., going over area with gorgonians, with encrusting sponges and small *beggiatoa* mats. Took sample of *beggiatoa* 27-57.925N 90-23.780W, 300 ft. to WP1.
17:39 Bearing 156°, range 350 ft. underway to WP1.
17:41 Depth 1675 ft., could be going over gas vent, suspended particles look like they are coming from the east.
17:42 Depth 1675 ft., Turning easterly to hunt for origin of suspended sediments.
17:48 Depth 1679 ft., change course to 060°, range 2100 ft. to WP1. 27-57.8888N 90-23.7754W
18:01 Depth 1729 ft. noticed gentle downslope.
18:03 Depth 1741 ft., change video tape 27-57.994N 90-23.6032W, heading 065° and getting underway.
18:04 *Beggiatoa* and small tube worms.

18:07 Depth 1758 ft, sampling a *beggiatoa* mat (bucket sample) 27-58.0014N 90-23.5835W, 0.3 kt. Current at 090°.

18:18 Sample finished, underway at 070°.

18:22 Depth 1758 ft., going up a 30° slope, 750 ft. from WP2.

18:27 Observed light sediment plume as approaching a ridge, 650 ft. from WP2.

18:29 Depth 1718 ft., top of small ridge and is starting downslope 27-58.0309N 90-23.5211W, bearing 070°, range 600 ft.

18:36 Change course to 030°, at WP2, 27-58.0273N 90-23.4440W.

18:37 Depth 1715 ft., heading 030°.

18:39 Depth 1710 ft., sub stopped, getting course to WP3.

18:40 Bearing 110°, range 1500 ft. to WP3.

18:41 Depth 1704 ft., came up on old mud vent, coming up on slope of mud volcano.

18:45 Depth 1701 ft., taking grab sample of mud, same coordinates (active area on fathometer image).

18:49 Good scoop in Bucket #5, underway on 110°.

19:03 Depth 1735 ft., changing tape in video camera, 27-58.0267N 90-23.3011W

19:06 heading 110

19:13 Depth 1748 ft., large mat of beggiatoa, white and yellow deposits as well, extensive, goes at least 30 ft. to N, new heading 160°, range 180 ft.

19:15 Underway heading 160°

19:17 Depth 1729 ft., new heading of 040°, 27-57.9503N 90-23.1674W

19:23 Course correction 029°.

19:31 Passed over cable trench perpendicular to sub track.

19:33 Depth 1757 ft., stopped at EOL, 27-58.1166N 90-23.0572W, going over more beggiatoa, no significant relief, soft silty sediment cover over sticky sand. Heading 200° upslope.

19:44 Depth 1726 ft., stop, permission to leave bottom.

19:44 Depth 1729 ft., leaving bottom, 27-58.0423N 90-23.0430W

18:15 On surface.

Tuesday, May 28

Port day at Fourchon to change scientific crews.

Wednesday, May 29

GC 232, Dive 4401

Crew: Front, Craig Caddigan, Roger Sassen
Rear, Hugo Marrero, Tom McGee

Purpose: Locate, videotape and sample hydrates, take cores in the area.

08:03 Launch and permission to dive, 27-44.4825N 91-19.0562W.
08:28 Bottom in sight.
08:30 On bottom, depth 1870 ft., temp. 7.6, visibility 30-40 ft., 0.1 to 0.2 kts. current, mud bottom with white bacterial mats, taking water sample. 27-44.5112N 91-19.0757W, within 70 ft. of target.
08:34 Heading 310°.
08:36 Depth 1869 ft., stopping to take tube worm samples, 27-44.5227N 91-19.0916W
08:39 Getting back underway.
08:40 Range 80 ft., due S
08:42 Course change to 130°.
08:42 Lost main control box that controls camera, arc lamp, pilots box, etc. Check main connector on back of pilots box.
08:45 Bottom connection loose, tightened it and all came back.
08:48 Depth 1868 ft., small tube worm bushes and bacterial mats.
08:50 Setting down to sample bacterial mat, punch core #1, 27-44.5721N 91-19.0737W.
08:54 Back underway.
08:55 Heading NE of site and searching
08:56 100 ft. N of target
09:06 Good plume, 075° about 200 ft. away.
09:07 Good sized piece of exposed hydrate, depth 1866 ft., 27-44.5173N 91-19.0828W.
09:12 Taking sample, gas escaping from bottom of hydrates, tried to take sample but hundreds of small pieces broke off.
09:23 Took grab sample with tube worms in it.
09:26 Moved left of hydrate, will take 4 punch cores, depth 1865 ft., tubes #2,3,4&5. 27-44.4974N 90-19.0687W
09:37 Will now do suction sample.

09:58 Another exposed hydrate sample about 15 ft. from the other, depth 1865 ft., doing last punch core. 27-44.5165N 91-19.0866W. Pin came out of bucket, cannot rotate anymore.
10:03 Finished with push cores and will cruise around and look for more hydrates.
10:11 Hydrates just downhill from landing, did small circle, will get underway at 310° to see what else is there.
10:17 Large area of tubeworms, appears to have exposed carbonate, depth 1867 ft. 27-44.5009N 91-19.0915W.
10:26 Setting down to take couple of small rocks. 27-44.5108N 91-19.0879W.
10:29 Back underway.
10:46 Fix #12 27-44.4907N 91-19.0457W, depth 1870 ft., exposed carbonate and tube worms, carbonate sampled.
10:52 Fix #13 27-44.4924N 91-19.0765W, depth 1868 ft., exposed gas hydrates with tube worms and mussels.
10:57 Permission to leave bottom. 27-44.4856N 91-19.0849W.
11:23 On surface.

GC 232, Dive 4402

Crew: Front, Craig Caddigan, Dan McConnell
Rear, Hugo Marrero, Mark Brausse

Purpose: Push cores, grab samples, and gas samples adjacent to hydrates.

15:34 Launch and permission to dive. 27-44.5190N 91-19.0066W
15:37 Sounded like a bucket imploded at about 150 ft.
15:40 Abort dive to repair bucket, depth 300 ft.
15:43 180 ft., permission to surface.
15:45 On surface, repaired imploded bucket.

GC 232, Dive 4403

Crew: same

Purpose: same

16:03 Launch and Permission to dive. 27-44.5134N 91-19.0792W.

16:21 Bearing 150°, range 400 ft., depth now 1000 ft.

16:21 Range 100 ft., bearing 130°, depth now 1600 ft.

16:26 Bottom in sight.

16:30 On bottom, depth 1871 ft., temp. 7.71, visibility 30-35 ft., current 0.1 kt. from 310°, 27-44.4992N 91-19.0751W, target 60 ft. at 180°.

16:39 Range 150 ft., bearing 110°.

16:46 Range 250 ft., bearing 340° to 1st hydrate mound.

16:56 At hydrate mound. Will go behind to punch cores with tubes #1, 2, and 3.

16:59 Sitting on slope of hydrate mound, will take 3 punch cores in that location. 27-44.5053N 91-19.0812W.

17:02 GPS down.

17:07 Finished with punch cores #1, 2, and 3. Will now move over and take the other 3.

17:08 GPS back on line.

17:08 Will take the other 3 punch cores on back side of tube worm patch. Mud bottom with a little bacteria, will space cores about 3 ft. apart.

17:17 Will go to the other side for a gas sample.

17:22 25 ft. from the vent this morning, still bubbling a little. Will try for a gas sample. Depth 1862 ft. 27-44.4998N 91-19.0852W

17:30 Abort gas sampling because gas is coming out too slowly.

17:31 Bearing 130° to WP6, large exposed hydrate mound.

17:33 Fix 10, small bacterial mats. Getting 2 grab samples. Depth 1866 ft. White and orange bacterial mats.

17:52 Left bacterial mat site to look for gas vent.

17:54 Suction sample of bacterial mat, depth 1870 ft., 21-44.4728N 91-19.0789W.

17:58 Back underway.

18:00 Bearing 010°, range 190 ft. to hydrates and mussels.

18:03 Change course to 310°.

18:07 Change course to due N.

18:18 Depth 1867 ft., mussels and tube worms with encrustations, will sample each, 27-44.4977N 91-19.1010W.

18:36 On back side of the hydrate mound found this morning. Will try for a gas sample, 27-44.4947N 91-19.0866W.

18:56 Definitely at the hydrates found this morning, gas coming out but not as much.

19:02 Depth 1867 ft., permission to leave bottom, 27-44.4977N 91-19.0922W.

19:24 Depth 200 ft., permission to surface.

19:26 On surface.

Thursday, May 30

GC 232, Dive 4404

Crew: Front, Don Liberatore, Alexi Milkov
Rear, Frank Lombardo, Tyler Hodges

Purpose: Collect hydrate samples, cores, grab samples and water samples.

08:16 Launch and permission to dive 27-44.4904N 91-19.0068W
08:19 Weird caution light on both videos, "Caution C31". Took the tape out and put it back in and fixed the problem.
08:36 Get underway bearing 330°, range 180 ft.
08:40 Change course to 030°.
08:43 All stop, go straight down.
08:45 Bottom in sight.
08:47 On bottom, depth 1866 ft., temp. 7.4, visibility 30-35 ft., current 0.1 kt. at 035°. 27-44.5230N 91-19.0936W
08:48 Bearing 140°, range 80 ft. to hydrates.
08:50 Sandy area with tube worm bushes, will scout around.
08:53 Coming up on exposed hydrate, will take still shots for a few minutes.
08:56 Hydrates. 27-44.5109N 91-19.0789W
09:01 Seeing fogging in camera (condensation on the lens).
09:03 Emptied air from the gas sampler, going in to collect gas sample.
09:22 Got a gas sample. Will take more still shots.
09:31 Shot still shots all around the mound. Will settle in and try to break a piece of hydrate off to put in pressure bomb.
09:41 Broke off a big piece of hydrate. Stayed in. Waiting for silt to clear to put the lid on.
09:49 Can't get the lid all the way down. Last quarter inch won't go. Will take the lid off and try to vacuum the threads and try again.
10:02 Think they have the lid down, will proceed.
10:10 Moved over to a small depression. Have iceworms in the hydrates. Will attempt to sample ice worms with the suction and take photos.
10:19 Tried to sample iceworms. Broke off a piece and got it in bucket #5. Don't know if we got a worm or not.

10:21 Getting in position to take push core between 2 hydrate sites. Depth 1865 ft. 27-44.5112N 91-19.1028W.
10:32 Question for Roger: 1st site from yesterday, would you like to break off a big chunk and bring it up in the basket? Leave it alone or try to bring it up? Leave it alone in case we need another sample.
10:35 Bearing 180°, range 100 ft. to other hydrate zone. May be able to break off a piece there.
10:38 Found an orange bacterial mat. Will stop and take a suction sample. Depth 1867 ft., Also took photos and video. 27-44.4765N 91-19.0891W.
10:47 Want push cores or suction samples? Harry – take suction sample, push cores are for Jeff.
10:51 Quite a bit of sponge. Will get another sample. Depth 1865 ft., 27-44.4773N 91-19.0634W
10:59 Take 2nd push core by the tube worm bush.
11:08 Will take push core and grab sample of tube worms. Depth 1866 ft., 27-44.4701N 91-19.0777W
11:21 Got samples. Now looking for orange bacterial mat for one more suction sample.
11:29 Time to wrap it up.
11:30 Depth 1862 ft., permission to leave bottom.
11:50 On surface.

GC 232, Dive 4405

Crew: Front, Don Liberatore, Laura Laham
Rear, Frank Lombardo, Jeff Chanton

Purpose: Collect pore water samples, and other samples.

15:49 Launch, permission to dive. 130 ft. from station, depth showing 1855 ft. 27-44.5214N 91-19.0677W
16:09 Bearing 210°, range 130 ft.
16:15 Bearing 090°, range 280 ft. Getting underway to E.
16:17 Bottom in sight.
16:19 Getting close to target. Tube worm bushes in sight.
16:21 On bottom at target site, depth 1862 ft., temp. 7.77, visibility 30-35 ft., current 0 to 0.1 kt. at 140°, 27-44.5142N 91-19.0893W
16:26 At exposed hydrates. Going to deploy the pore water sampler. Fix 6: 27-44.5136N 91-19.0893W Depth 1867 ft.

16:29 One of the valves is closed, putting it into the bottom.
16:31 Sampler is in the bottom. Seafloor is very soft.
16:33 Got sampler triggered, waiting for 30 minutes.
17:00 Two minutes to go. Then they will take the pore water sampler out of the soft soil. When the sampler is on the sub, will trigger the valves.
17:02 Pick up probe and sampler.
17:06 Got sampler on sub.
17:18 Closed all valves. Took push core #4 right next to pore water sampler location. Fix 7 27-44.5059N 91-19.0784W Depth 1867 ft.
17:29 Second push core taken next to first one. Moving in to take another sample near bubble stream.
17:41 Collecting a gas sample in the same location as the 2nd push core.
17:50 Grab sample of sediment above the gas hydrate.
18:06 Took push core next to the hydrate mound. Shook the push core to get the sample out.
18:12 Took third push core at the same location (redid the previous one).
18:21 Took scoop sample, moving on bearing 140°, range 90 ft. Target location is large exposed hydrate.
18:29 Picked up rock sample at depth of 1864 ft., could not find hydrate mound. Range 40 ft. to exposed hydrates.
18:31 Picked up scoop sample, Fix 8 27-44.4899N 91-19.0785W, depth 1864 ft.
18:41 Sword fish in sight.
18:44 Fix 9 27-44.4960N 91-19.0766W, depth 1864 ft., took scoop sample of orange material.
18:52 Still have not found second hydrate mound, time to wrap dive up.
18:56 Permission to leave bottom, depth 1867 ft.
19:16 Depth 200 ft., permission to surface.
19:18 On surface.

Friday, May 31

GC 234, Dive 4406

Crew: Front, Dan Boggess, Roger Sassen
Rear, Hugo Marrero, Kelley Peeler

Purpose: Take hydrate samples, cores, and grab samples.

08:01 Launch and permission to dive. 27-44.7543N 91-13.3406W
08:16 ottom showing at 1730 ft., get underway due S for 200 ft.

08:23 Adjust heading to 200°.
08:25 Change course to 100°.
08:28 Bottom in sight.
08:31 On bottom, depth 1711 ft., temp. 8.66, visibility 40-45 ft., current 0.1 kt. from 070°, 27-44.7422N 91-13.4194W. Bearing 090°, range 400 ft.
08:37 Area with lots of tube worms, will sit down and take grab sample of orange mat, bucket #8, depth 1762 ft. 27-44.7766N 91-13.3613W
08:45 Done with sample. Underway due E.
08:47 At marker "TX", small float to left, depth 1772 ft.
09:00 Moving toward marker "V", depth 1778 ft. Think they found hydrate.
09:01 Will try for a gas sample, 27-44.7587N 91-13.3101W.
09:57 took gas sample, getting hydrate sample.
10:36 Dropped chipper off platform, recovering it and still trying to get hydrate sample.
11:02 Still trying to get hydrate sample, got some pieces, depth 1778 ft.
11:10 Directed to wrap up operation.
11:17 Permission to leave bottom.
11:18 Left bottom, 27-44.7448N 91-13.3201W
11:43 Depth 200 ft., permission to surface.
11:45 On surface.

GC 234, Dive 4407

Crew: Front, Dan Boggess, Jeff Chanton
Rear, Hugo Marrero, Howard Manlovitz

Purpose: Observe hydrates, take video and stills, take push cores and grab samples.

16:06 Launch and permission to dive. 27-44.7614N 91-13.3365W
16:23 Course change to 050°, range 400 ft.
16:25 Stop, drop straight down, bottom showing at 1735 ft.
16:31 Bottom in sight.
16:34 On bottom, depth 1756 ft., temp. 8.1, visibility 35-40 ft., current 0 to 0.1 kt. from 130°. Fix 27-44.7906N 91-13.3467W. Landed in tube worms, no markers, will look around.
16:35 Found Marker "T2"
16:37 Depth 1763 ft., will sample orange mat, will do mesh bag #9 first, then screen.

16:38 Platform is stuck. Bucket #9 is the one stuck under the funnel. Will forget that spot and try to find hydrate mound.
16:50 Moving, using gas sampler to push down on lid of bucket. Worked, and platform will rotate again.
16:56 Taking suction sample of red mat into fine mesh bucket, Fix 27-44.7882N 91-13.3426W.
17:12 At 1767 ft., at marker "A1", also at marker "TX" again. Should be on hydrate.
17:16 Went straight over a tub worm bush at "TX", has flat tile with "12" on it, upslope are 2 floats, perhaps near hydrates.
17:17 Moving in on hydrates now at marker "B".
17:20 Taking tube #1 push core. Depth 1777 ft., 5 ft. from hydrate mound. Fix 27-44.7531N 91-13.3119W.
17:30 Take cores 1 & 2 on side of hydrate mound. Take core 3 to left of tube worm bush about 10 ft. away.
17:37 Tube core 4 will be taken there also (about 15 ft. to west of core 3 location).
17:47 Depth 1784 ft., Taking push core 5 downslope from thermistor site. Fix 6: 27-44.7661N 91-13.2936W.
18:02 Have Ion pump device deployed, going back to collect mussels.
18:03 Back on mussel bed, same place they took the gas sample this morning. Will take another gas sample.
18:15 Done at hydrate mound, depth 1776 ft. Will now go look for rocks for Harry.
18:24 Depth 1768 ft., Put one piece of rock in bucket #12, will try to suction bacterial mat in Bucket 11, which has mesh. Didn't work out.
18:26 Will grab another rock. Fix 27-44.7723N 91-13.3104W. Rock is in the basket, will try for another bacterial mat.
18:29 Depth 1771 ft., Found orange bacterial mat, will attempt to sample.
18:35 Moved over a ridge. Will try to sample another orange bacterial mat.
18:42 Have bacterial mat sampled.
18:57 Depth 1792 ft., Request permission to leave bottom (no fix available).
19:15 Permission to surface.
19:15 Surface in sight, surface clear.
19:17 On surface.

Saturday, June 1

MC 885, Dive 4408

Crew: Front, Craig Caddigan, Dick Fillon
Rear, Frank Palumbo, Barry Kohl

Purpose: Survey preselected traverse, collect still shots, video and samples.

08:01 Launch and permission to dive. Fix 28-04.0497N 89-43.2765W
08:26 Course 085 degrees, range 200 ft. Depth showing 1800 ft.
08:32 Bottom in sight.
08:34 On bottom, depth 2160 ft., temp 6.79, visibility 20-30 ft., current 0,4 kt. from 030°. Fix 1: 28-04.0403N 89-43.3787W. Core sample 1.
08:40 Head on course 100°. Bottom is basically mud. Bearing of 100° is taking sub diagonally up a gentle slope.
08:50 Depth 2134 ft., Bottom is the same.
08:56 New heading of 040°, depth 2117 ft., bottom is the same.
08:59 At WP1, All stop, look for thermistor.
09:07 New heading of 100° to WP2.
09:11 Underway at 100°, bottom is the same.
09:15 Depth 2100 ft.
09:17 Depth 2080 ft., Starting to see rocks with crinoids.
09:19 Took long push core, Fix 2: 28-03.9712N 89-43.0429W Punch core #5.
09:20 Just lost forward horizontal thruster.
09:26 Coming to small drop off, one big boulder there with coral on it. Going down, then back up again.
09:28 Area of small rocks and small gorgonians, depth 2065 ft.
09:30 Going over a series of ridges, current up to 0.5 kts.
09:31 Back over clean mud bottom.
09:31 Lots of shell hash with gorgonians.
09:32 New heading of 070°.
09:39 Change to video tape #2.
09:40 Tube worms with clams on top.
09:46 New heading of 035°.
09:47 Underway at 025°.
09:49 Bottom covered with dead clams.
09:52 All stop. Took long punch core. Fix 3: 28-03.9611N 89-42.7557W. Depth 2037 ft. Be advised forward horizontal is coming on by itself. Punch core only penetrated 2 or 3 inches, took grab sample.
09:59 New course of 080°, range 1000 ft.
10:07 Next time clams are seen, take sample.

10:08 Came across fiberglass pole sticking out of bottom.
10:09 Starting to see series of small ridges.
10:11 New heading of 060°.
10:14 New heading of 035°.
10:21 WP3 is due N range 100 ft.
10:23 On WP3, depth 2066 ft., clean bottom with some shell hash. Took punch core #4. Fix 4: 28-03.9564N 89-42.5319W.
10:28 New heading of 150° to EOL.
10:33 New heading of 120° (current set)
10:38 Changing to video tape #3.
10:42 Be advised, sub going sideways more than forward.
10:46 New heading of 200°.
10:49 WP due N about 100 ft.
10:50 Stop and take punch core.
10:50 Depth 2575 ft., clean mud bottom, punch core #3, Fix 5: 28-03.664N 89-42.4005W.
10:55 Head back to WP 3, due N.
11:01 Getting swept up slope.
MC 885, Dive 4408 (cont.)
11:02 Go up slope, about 330°.
11:04 At top of slope, depth 2061 ft., turning to head back into current.
11:08 Bottom is featureless mud with burrows.
11:09 Will take grab sample. Fix 6: 28-03.7227N 89-42.4090W, Depth 2063 ft.
11:10 Request permission to leave bottom. Total distance covered 6493 ft.
11:36 On surface.

MC 885, Dive 4409

Crew: Front, Craig Caddigan, Bob Woolsey
Rear, Frank Palumbo, Tyler Hodges

Purpose: Survey traverse 2 and sample, take stills and video.

15:40 Lunch and permission to dive. Fix 1: 28-04.5120N 89-43.3480W
15:57 Start heading on course of 320°.
16:01 New heading of due N, bottom showing at 2060 ft.
16:04 New heading of 020°.
16:06 Bottom in sight, new heading of 060°.

16:08 On bottom, depth 2087 ft., temp. 6.82, visibility 20-25 ft., current 0.3 to 0.4 kts. at 030°. Fix 2: 28-04.6908N 89-42.8598W Same bottom as this morning, flat muddy bottom. Underway at 060°.

16:13 New heading of 150, SOL.

16:17 Depth 2068 ft., bottom is the same.

16:22 New heading of 155°.

16:23 Came across first outcropping of rocks with gorgonians on them, Fix 3: 28-04.5735N 89-42.7919W.

16:26 Bottom featureless again, depth 2063 ft.

16:28 Coming into more gorgonians, will sample. Fix 4: 28-04.4861N 89-42.7767W.

16:36 Got sample of small rock with egg sacks on it, will take punch core. Depth 2055 ft.

16:39 Back underway at 155°.

16:44 Depth 2067 ft. Crossed small rocks, then barren bottom, starting to see shell hash.

16:45 New heading of 220°, range about 100 ft.

16:46 Small rocks with shell hash.

16:48 Near WP1, heading of 150° to WP2.

16:57 Depth 2056 ft., Barren bottom, gently rolling up and down maybe 10 ft.

17:01 Came down a slope to 2104 ft., now going back up.

17:07 Depth 2056 ft. On clean bottom.

17:11 Depth 2049 ft. Getting back into shell hash.

17:13 Shell hash getting thicker, also occasionally seeing gorgonians.

17:16 Shell has thicker, depth 2041 ft. Will do 1 long push core and 1 short push core. Fix 5: 28-03.9911N 89-42.7551W

17:22 Punch core 1, punch core 4. Sent to WP3 on bearing of 200°, range 1700 ft.

17:32 Small gorgonians, rocks, and shell hash.

17:40 Going slightly upslope. Depth 2057 ft. Have now left shell covered bottom and now on burrowed mud.

17:44 Back in shell covered bottom, rocks, and gorgonians. Going back upslope.

17:46 Depth 2064 ft. Top of a little ridge, took punch core #5.

17:49 Have punch core and getting underway bearing 195°.

17:52 Change course to 170°.

17:55 Change course to 160°.

17:57 Change course to 090°.

18:01 Near WP3. Take long push core.
18:03 Setting down, depth 2061 ft., sitting atop a silt covered rock formation. Fix 6: 28-03.7116N 89-42.8518W.
18:11 Got core, had to move slightly.
18:11 Proceed approximately 80 ft. at 280°.
18:12 Course change, 50 ft. due south.
18:15 Course change 110°.
18:23 Looking around for thermistor, heading 110°.
18:24 Found the thermistor. Fix 7: 28-03.6917N 89-42.8765W, Depth 2052 ft., Taking video and will recover thermistor.
18:30 Have thermistor on platform, won't go in the basket.
18:54 Permission to surface.
18:56 Surface in sight, surface clear.
18:57 On surface.

Sunday, June 2

VK 826, Dive 4410

Crew: Front, Don Liberatore, Harry Roberts
Rear, Hugo Marrero and trainee Curt Patterson

Purpose: Survey traverse 1, take stills, video and samples.

08:00 Launch and permission to dive. Fix 1: 29-10.5088N 88-00.9544W, bottom showing at 1599 ft.
08:03 Going through layer of turbid water, coming up on depth of 200 ft.
08:14 Get underway at 060°.
08:19 Course change to 080°, range 400 ft. Depth showing at 1400 ft.
08:22 Bottom in sight.
08:25 On bottom, depth 1581 ft., temp 9.67, visibility 25-30 ft., current 0.2 kts. at 090°. Fix 2: 29-10.4874N 88-00.0064W. Bottom flat, soft sediment, and lots of small fish.
08:29 At SOL, new course of 170°, range 1600 ft.
08:33 Came over a ridge, now heading down slope.
08:37 Depth 1600 ft., Slope increasing, no difference in bottom type.
08:40 Depth 1640 ft., Looks like slope is 30° or more.

08:41 Bottom starting to flatten out, same type, mud.
08:42 Continues on down. Will follow. Appears course of 230°.
08:43 Course of 220°, depth 1700 ft.
08:45 Request estimated depth of hole. Appears to be 1800 to 1850 ft. deep. At 1728 and still going down.
08:46 Depth 1750 ft.
08:48 Still going down, now at 1775 ft.
08:56 At 1838 ft., not flat but slight slope, waiting for sediment to clear. Fix 4: 29-10.3128N 88-00.9993W
08:59 Bottom looks flat.
09:07 Motored around a bit, depth 1837 ft., will take punch core #6. WP2 is at course of 170°, range 4000 ft.
09:15 Found a gorgonian with a clam growing on it.
09:22 Depth 1700 ft.
09:26 Depth 1637 ft., looks like top of the slope. Fix 5: 29-10.2464N 88-01.0481W. Bottom change, harder with gorgonians, anomenes, etc.
09:27 Down slope slightly, back into soft sediment.
09:31 Working back up a shallow slope.
09:39 Leveled out at 1580 ft.
09:40 Ridge with gorgonians and small rock.
09:41 Depth 1573 ft., Fix 6: 29-10.0951N 88-01.0672W, back underway at 170°.
09:43 Lost tilt function on video, still have pan.
09:44 More of hard bottom with gorgonians.
09:47 Going back upslope.
09:50 Course change to 150°, range 1400 ft. At the top of a little hill, depth 1590 ft.
09:51 Series of ridges, couple of meters high with shell hash, etc.
09:52 Lot of shell hash, mostly dead stuff.
09:56 Coming across Lophelia coral, depth 1532 ft., (photo of fathometer plume) Fix 7: 28-09.7827N 88-01.0395W. Large field of lophelia.
09:58 Depth 1538 ft. Will sample coral.
10:02 Back underway on course of 150°.
10:03 Course change to 165°, range 700 ft.
10:06 Getting out of coral area and into broken bottom with shell hash.
10:07 Hard bottom, broken material and shell hash.
10:08 Just spotted 1st tube worms, course change to 145°.
10:10 Up a mound of thick coral, carbonate mound.
10:11 Course change to 120°, range 180 ft. to WP2.

10:15 New course of 040°, 80 ft. Will stop and grab rock sample. Fix 8: 29-09.6482N 88-01.0060W. Got rock sample, will continue on 030° 120 ft.
10:24 At WP2, bearing 185°, range 1800 ft. to EOL. Depth 1465 ft.
10:39 Back into coral field, depth 1529 ft., course change to 160°.
10:42 Depth 1546 ft., will take scoop sample of clams and little sediment.
10:51 Very rocky bottom, coral and gorgonians.
10:54 Depth 1580 ft., down slope at a steep angle.
10:56 At EOL, will mosey around and look for something interesting.
10:58 See a few clams on coral, will take samples. Fix 9: 29-09.3803N 88-01.0239W, tilt now working again.
11:07 Got 2 clams, heading upslope, depth 1526 ft.
11:14 Depth 1565 ft., permission to leave bottom. Fix 29-09.4147N 88-01.0255W.
11:33 Surface in sight, surface clear.
11:34 On surface

VK 826, Dive 4411

Crew: Front, Don Liberatore, Barry Kohl
Rear, Hugo Marrero, Mark Brausse

Purpose: Survey traverse 2, take stills, video and samples, get 2 background cores for Jeff.

15:32 Launch and permission to dive. 29-09.7557N 88-01.8910W
15:58 Bottom in sight.
15:58 On bottom, depth 1708 ft., temp. 8.80, visibility 25-30 ft., current 0.1 kt.
16:02 Instructed to take 2 background push cores for Jeff.
16:05 Have push core #1.
16:08 Have push core #2. Bearing 100°, range 1400 ft. to WP1. Bottom is featureless soft sediment with pock marks. Fix 6: 29-09.7528N 88-01.9246W
16:21 Course change to 090°, range 400 ft. Featureless, small pock marks. (Moderately high amplitude on map)
16:23 Different bottom type, shells, but not hard bottom.
16:24 Depth 1696 ft., on hard bottom with gorgonians (corresponds to high amplitude on map). At WP 1, ridge with some tubeworms.

16:26 Course 100°, range 3500 ft. to WP2.
16:27 Flat mud bottom, depth 1700 ft.
16:31 Huge shark spotted, trying to get video.
16:34 Chasing shark, coming on hard bottom and gorgonians.
16:35 Rock outcrop, depth 1708 ft., gorgonians and tubeworms.
16:36 Bigger bushes of tubeworms. Depth 1703 ft.
16:37 Over small ridges, rough outcrop.
16:39 Over soft bottom.
16:39 Small patches of hard bottom among flat sand.
16:41 Depth 1684 ft., bottom change upslope and shell hash.
16:43 Crossing isopods, a lot more than before.
16:44 Depth 1661 ft., rocky bottom.
16:44 Going to find rock sample.
16:46 Rock sample at depth of 1654 ft., Fix 7: 29-09.6671N 88-01.3772W.
16:47 Bearing 100°, shark following.
16:49 No sign of gas or any hydrate so far.
16:52 Depth 1600 ft., gorgonians, sponges and more hard ground.
16:53 Slope about 20°, *Lophilia* more dominant.
16:57 Large carbonate structures, depth 1560 ft., many gorgonians and black coral. Fix 8: 29-09.6497N 88-01.2705 W.
17:04 Transition to deep soft sediment, depth 1519 ft.
17:06 Back in coral area, depth 1487 ft.
17:07 Carbonate structure under *Lophelia* bushes, lots of shell hash among boulders.
17:08 Horizontal slabs of carbonate rock (corresponds to high ampltude). 600 ft. west on line from WP 2
17:10 Coral, tubeworms, stopping to take video. Fix 9: 29-09.6290N 88-01.1307W.
17:15 Back underway at 100°.
17:19 Course 090°, 0.4 to 0.5 kts. of current.
17:24 Depth 1453 ft., now going downslope.
17:25 Now at WP 2, new course 100°, range 5000 ft.
17:27 Softer bottom with shell hash, depth 1474 ft.
17:28 Depth 1480 ft., going back upslope.
17:29 On top of ridge, now going back downslope, depth 1474 ft.
17:30 Depth 1480 ft., grab sample. Fix 10: 29-09.6108N 88-00.9787W
17:35 Now have grab sample.
17:37 Back underway.

17:38 Seeing battery track marks, depth 1479 ft., 0.6 kts of current at 100°, going against sub.
17:45 Stopping to take push core, Fix 11 29-09.6006N 88-00.8949W, push core tube #3. Depth 1517 ft.
17:55 Depth 1565 ft., downslope, sharp break downslope.
17:57 Urchins, smooth sediment bottom, depth 1600 ft.
18:00 Flat bottom with anemones, depth 1638 ft. Stopping for grab sample at depth of 1640 ft.
18:17 Heading downslope, depth 1587 ft.
18:20 Arrived at bottom of slope, depth 1660 ft.
18:32 Bottom a little more local relief.
18:34 Area looks disturbed (perhaps anchor drag). Will take grab sample in flat area at depth of 1702 ft.
18:41 Grab sample (Fix 13) acquired, and leaving bottom. 29-09.5233N 88-00.3467W

Monday, June 3

MC 709 Dive 4412

Crew: Front, Dan Boggess, Roger Sassen
Rear, Frank Lombardo, Jeff Chanton

Purpose: Survey Traverse 1, take stills, video and samples, and select site for pore water sample.

07:58 Launch, permission to dive.
08:21 Get underway at 330°.
08:24 Change course to 300°, range 400 ft.
08:27 Bottom in sight.
08:31 On bottom, depth 2262 ft., temp. 5.99, visibility 25 ft., current 0.1 kt. at 220°. Soft brown pock marked mud. New course of 275° to SOL.
08:34 All stop. At SOL, get underway at 140°, range 1800 ft. to WP 1. Fix 28-13.8670N 89-42.4670W.
08:38 Across wide drag marks, 3 ft. wide, not very deep.
08:39 Soft mud bottom with pock marks, up shallow slope. Depth 2254 ft.
08:41 Light shell hash and bacterial mats.

08:48 Edge of depression, old mud volcano. Has shell hash and bacterial mats. Fix 28-13.8469N 89-42.4109W.

08:53 Another wide track mark, 1m wide, 0.5m deep, crossing perpendicular to sub track., back into regular pock marked mud.

08:56 Small terrace about 2 m wide, another about 10 m. wide, heading down, depth 2213 ft.

08:56 Fix (ship) 28-13.82N 89-42.44 W(tracking problems, fix from ship).

09:02 Punch core sample of bacterial mat in tube #1, Fix 28-13.7296N 89-42.3210W, depth 2223 ft.

09:09 Forget punch core, silted in. no visibility, back underway at 140°.

09:12 Course change, heading 040° (tracking now working). Setting down for core, push core tube #2. Depth 2232 ft., Fix 9: 28-13.6284N 89-42.2415W

09:17 Getting underway course 035°.

09:20 New course of 130°, range 1200 ft.

09:28 Found small depression, will try to sample mussels and bacterial mat. Fix 10: 28-13.6011N 89-42.1661W, depth 2232 ft.

09:38 Suction sample of clams and mussels, Fix 11: 28-13.6050N 89-42.1433W, depth 2225 ft. (Photo of fathometer – oil seep).

09:53 Two push cores, short push Core (#3), also taking a carbonate sample. The two initial push cores were long ones, no numbers given. No carbonate sample taken.

09:58 Underway bearing 140°.

10:00 Pockmarks, bacterial mats, and scattered shells (can't get fix).

10:03 Underway at 150°, stopped to sample holothurian, but encouraged to get back underway. (Photo of plume on fathometer).

10:12 At WP 2, Course 125°, range 700 ft. to WP 3.

10:18 Going downhill, depth 2269 ft., change course to 115°.

10:20 Coming over the edge of a large circular depression about 30 m in diameter., shell hash and possibly a brine pool, depth 2280 ft.

10:28 Change course to 100°.

10:30 At WP 3, new course of 130°, range 2255 ft. to EOL.

10:31 Bottom small pock marked fine mud, shallow upslope, depth 2258 ft.

10:33 Coming over a big hole with steep sides, 30 m diameter and 5 m deep.

10:41 Depression between 2 ridges, now slight upslope of about 15°, every 15 or 20 m are small depressions with nothing inside.

10:44 Depth 2267 ft., small mud vent.

10:49 Course change to 115°.
10:52 Depth 2292 ft., been on a shallow downslope.
10:54 Depth 2302 ft., on 15° downslope. Change course to 090°.
10:56 At bottom of slope, depth 2332 ft.
10:58 All stop, geotechnical punch core, depth 2329 ft., Fix 28-13.0739N 89-41.4570W.
11:03 Lost up and down on arm.
11:05 Permission to leave bottom.
11:38 On surface.

MC 709, Dive 4413

Crew: Front, Dan Boggess, Harry Roberts.
Rear, Frank Lombardo, Laura Laham

Purpose: Find vent site, install and retrieve pore water sampler, survey and take stills, video, grab samples and push cores. Will launch at WP 1 on Traverse 1 and search for vent.

15:38 Launch, permission to dive. Fix 1: 28-13.6669N 89-42.2072W
15:43 Murky layer at about 250 ft.
15:53 Get underway at 075°.
15:56 Change course to 060°.
15:58 Lot of turbidity in water at 1400 ft.
16:00 Change course to 030°.
16:04 Drop straight down.
16:11 Bottom in sight.
16:14 On bottom, depth 2231 ft., temp. 6.85, visibility 30-35 ft., current 0.2 kt. from N, Fix 2: 28-13.6530N 89-42.2089W Landed at brine seeps. Punch core tube #4.
16:25 Got punch core, heading of at 030°.
16:29 Haven't found seep site, found tube worms, mussels, depth 2329 ft., Deploying pore water sampler.
16:39 Tripped handles, closed 1st. Sitting for 28 more minutes.
17:07 30 seconds to go, will move in, pick up pore water sampler and bring back on board. Fix 4: 28-13.6837N 89-42.1965W
17:22 Have sampler back on board, closing valves.

17:34 Got scoop of sediment in bucket #3, will head off into current (330°), will take punch core sample. (Plume on fathometer, but appears to be sub and not seep, took photo), Fix 28-13.64N 89-42.22W.
17:41 Heading to plume, 300 ft. at 200°.
17:56 Depth 2228 ft., stopped to sample carbonate rock, Fix 28-13.6661N 89-42.1850W. Did not sample.
18:00 Bearing 225°, range 140 ft. to plume.
18:03 On site, will look around.
18:08 Sample rocks and clams, fix 28-13.6448N 89-42.2209W, depth 2230 ft.
18:24 Will stop and take grab samples of mussels and clams, depth 2232 ft., fix 28-13.6531N 89-42.2707W
18:45 Time to wrap it up, attempting to sample rock.
18:47 Depth 2231 ft., request permission to leave bottom, fix 28-13.6540N 89-42.2664W
19:13 Permission to surface.
19:15 Surface in sight, surface clear.
19:16 On surface.

Tuesday, June 4

MC 118, Dive 4414

Crew: Front, Craig Caddigan, Harry Roberts
Rear, Hugh Marrero, Tyler Hodges

Purpose: Survey Traverse 1, sample.

07:57 Launch, permission to dive. Fix 1: 28-51.3198N 88-29.8819W
08:04 Going through layer of turbid water at 400 ft.
08:11 Get underway at 340°.
08:22 Course change to 030°, range 650 ft.
08:29 Course change to 040°, range 260 ft., bottom showing at 2200 ft.
08:31 Course change to due N, range 180 ft.
08:34 Drop straight down, within 50 ft.
08:38 Bottom in sight
08:39 On bottom, depth 2869 ft., temp. 5.74, visibility 20-25 ft., current 0.3 to 0.4 kts. at 050°. Fix 2: 28-51.4457N 88-29.9005W.

08:40 Get underway on course of 080°, range 300 ft. to SOL. Bottom is featureless mud with creature depressions

08:46 At SOL, Depth 2873 ft., same bottom, much suspended sediment in water column, get underway at 140°, Fix 3: 28-51.4516N 88-29.8469W.

08:55 Depth 2885 ft., bottom same.

09:03 Depth 2915 ft., down slight slope, visibility worse (15 to 20 ft.), course change to 120°, range 1300 ft.

09:09 Course change to 100°.

09:12 Depth 2914 ft., bottom same.

09:13 Course change to due E (090°).

09:14 Starting to see a few dead shells, starting up slope slightly, depth 2900 ft.

09:15 Starting to see a few small rocks, depth 2898 ft., will take sample. Fix 4: 28-51.1394N 88-29.5820W. Grab sample in bucket #4.

09:19 Getting back underway at 090°.

09:20 will follow up slope, about 080°.

09:21 Just over a small rise, now dropping back down (photo of plume on fathometer).

09:24 At bottom of the feature, more shell hash.

09:24 Will set down for punch core, depth 2912 ft., Fix 5: 28-51.1319N 88-29.5502W. 2 punch cores and 1 grab sample. Oil coming out of bottom of 2nd punch core.

09:37 Found small crater, gas seep with hydrates in the side at depth of 2915 ft. Fix 5: 28-51.1409N 88-29.5361W. Will attempt to sample gas. (Photo of fathometer).

09:55 Gas sample successful, also got punch core and small rock, will look around for more hydrates.

09:56 Lost camera, lights out, green light blinking. No pan and tilt.

10:00 Got camera back.

10:02 Depth 2902 ft., stop for gorgonian and rock sample.

10:13 Range 200 feet, bearing 200° to middle of anomaly.

10:14 Depth 2898 ft., taking push core through bacterial mat. Fix 7: 28-51.1615N 88-29.4769W.

10:21 Course 130°, range 1500 ft. to WP 2.

10:28 Depth 2922 ft., out of shell hash and back onto mud bottom.

10:30 Course change to 120°, range 900 ft. depth 2932 ft., visibility 15-20 ft.

10:36 Course change to 110°, range 400 ft.

10:38 Course change to 090°.

10:40 Stopping at 2968 ft. to collect sea cucumber.
10:41 Back underway at 070°, range 300 ft.
10:43 Depth 2974 ft., starting upslope.
10:47 At WP 2, circular weak amplitude, depth 2970 ft., fix 28-50.9608N 88-29.2729W
10:48 Permission to leave bottom.
11:25 Permission to surface, depth 175 ft.
MC 118, Dive 4414 (cont.)
11:27 Surface in sight, surface clear.
11:27 On surface.

MC 118, Dive 4415

Crew: Front, Craig Caddigan, Harry Roberts
Rear, Hugo Marrero, Howard Manlovitz

Purpose: Will start at EOL and proceed to WP 1 (amplitude), then search for vent site. Won't try for EOL.

15:29 Launch, permission to dive. Fix 1: 28:51.2402N 88-29.2909W
15:45 Get underway at 330°, range 300 ft.
15:51 Drop straight down.
16:07 Bottom in sight.
16:08 On bottom, depth 2907 ft., temp. 5.75, visibility 15-20 ft., current 0.2 to 0.3 kts. at 080°. Fix 28-51.4325N 88-29.3064W. Get underway at 200°, range 2000 ft. Lost pan and tilt on camera. Seeing clams and bacterial mat.
16:14 Got camera back.
16:17 Depth 2903 ft., will stop for grab sample. Bottom is plain mud. Fix 28-51.3682N 88-29.3491W. Sample in Bucket #9.
16:22 Back underway at 200°.
16:25 Back in plain old mud, depth 2908 ft.
16:30 Depth 2908 ft., Starting to see a few clam shells.
16:38 Depth 2899 ft., Some clam shells and small bacterial mats.
16:39 Just passed over site that looks like they worked this morning.
16:40 Starting to see small rocks.
16:40 Depth 2895 ft., Fix 28-51.1585N 88-29.5148W, going down into a crater.

16:45 Depth 2908 ft., found gas vent with hydrates and a lot of oil. Will take sample. Fix 28-51.1377N 88-29.5170W.
16:59 Got gas sample. Trying to get hydrate sample. Tough to break.
17:04 Repositioned and kicked up a bunch of silt. Will sit a wait for it to clear.
17:17 Unable to get hydrate sample. Got one small piece in jaws, but couldn't get it into container.
17:23 Lost arm. Shutting down to see if breakers kick back in.
17:28 Got arm back.
17:41 Lost arm again, waiting to reset breakers.

MC 118, Dive 4415 (cont.)

18:09 Got lid on and valve closed, will take grab sample and rock sample.
18:13 Course 195°, 100 ft. from WP 1, bearing 210°. 2800 ft. to EOL, getting underway.
18:17 Depth 2910 ft., sea fans and gorgonians.
18:20 Will take 2 punch cores. Time to wrap it up. Depth 2926 ft., Fix 28-51.0942N 88-29.5805W.
18:29 Permission to leave bottom.

The Department of the Interior Mission

As the Nation's principal conservation agency, the Department of the Interior has responsibility for most of our nationally owned public lands and natural resources. This includes fostering sound use of our land and water resources; protecting our fish, wildlife, and biological diversity; preserving the environmental and cultural values of our national parks and historical places; and providing for the enjoyment of life through outdoor recreation. The Department assesses our energy and mineral resources and works to ensure that their development is in the best interests of all our people by encouraging stewardship and citizen participation in their care. The Department also has a major responsibility for American Indian reservation communities and for people who live in island territories under US administration.

The Bureau of Ocean Energy Management

As a bureau of the Department of the Interior, the Bureau of Ocean Energy (BOEM) primary responsibilities are to manage the mineral resources located on the Nation's Outer Continental Shelf (OCS) in an environmentally sound and safe manner.

The BOEM Environmental Studies Program

The mission of the Environmental Studies Program (ESP) is to provide the information needed to predict, assess, and manage impacts from offshore energy and marine mineral exploration, development, and production activities on human, marine, and coastal environments.